

Building Technology Graduation project:

Composite Structural Module out of srPP Facings and a PET-Bottle Core

P5 Assessment_Telesilla Bristogianni

Building Technology Graduation project:

Composite Structural Module out of srPP Facings and a PET-Bottle Core

P5 Assessment

Student: T. Bristogianni, 4116704

Mentors: Dr.ir. F.A. Veer (1st),
Ir. A. Borgart (2nd),
Dipl.ing. F. Heinzelmann (3rd)

External Examiner: Ir. Alexander de Ridder

27th of June 2012

Faculteit Bouwkunde TU Delft

Table of Contents

A. Introduction 3
1. Thesis subject 3
2.1. Problem statement 3
2.1.1. The unbearable heaviness of structures 3
2.1.2. Disadvantages of polymeric sandwich structures 5
2.1.3. Immoderate use of materials and the paradox of the plastic litter problem 8
2.2. Purpose of the design 10
3. Design principles 11

B. Research 12
1. Research structure 12
1.1. Topics for investigation 12
1.2. Methodology 12
2. Research and results 13
2.1. PET bottle 13
2.1.1. Material properties and geometry 13
2.1.2. Structural behaviour of internally pressurized bottles 16
2.1.2.1 Overview 16
2.1.2.2 Properties of solid CO_2 16
2.1.2.3 Experimental procedures 18
2.1.2.4. Conclusions 45
2.1.3. Capped non-pressurized bottle 45
2.1.3.1 Overview 45
2.1.3.2. Experimental procedures 46
2.1.3.3. Conclusions 55
2.2. PET-bottle core for a FRP composite module 56
2.2.1. Alternative scenarios proposal and assessment 56
2.2.2. Design proposal chosen for further development 66
2.2.3. Prototype building and testing 72
2.2.3.1 Process 72
2.2.3.2 Experimental procedures and results 75
2.2.3.3 Comparison of experimental results and hand calculations 101
2.2.3.4. Estimation of PET-bottle core properties 107
2.3. FRP facings 111
2.3.1. Design proposal to be further developed 111
2.3.1.1. Criteria 111
2.3.1.2. Proposal description 112
2.3.2. Material selection 122
2.3.2.1. Criteria and material choice 122
2.3.2.2. PURE® self-reinforced Polypropylene composite material 123
2.3.3. Aspects susceptible to redesign 129
2.4. Composite module out of srPP facings and a PET-bottle core 130
2.4.1. Scenarios for a foldable composite module and design to be further developed 130
2.4.2. Assembly method and connection between modules 135
2.4.3. Manufacture process 136
2.4.3. After-Life 138
2.5. Integral building system 138
2.5.1. Components and assembly on-site 138
2.5.2. Shipping 142
2.4.4. After-Life 145
2.6. Application possibilities 146

C. Conclusion and reflection 149

Acknowledgements 150
References 151
Literature 152

A. Introduction

1. Thesis subject

The research work to be presented in this thesis deals with the design of a lightweight and low-cost composite structural module, out of a self-reinforced Polypropylene (srPP) skin and a core of Polyethylene Terephthalate (PET) bottles.

In the following chapters the incentives and intentions for the development of this module will be explained and the design principles guiding the design will be stated. Then the steps of the research will be described and thus the design process will be followed, from the understanding of the PET bottle's structural behaviour up until the design of an integral building system. In the end, the final design product and its application possibilities will be presented.

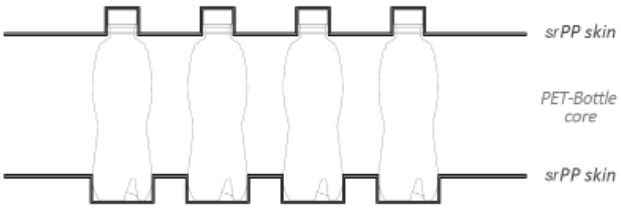

Figure 1. Concept for a composite structure

2. Incentives and intentions in designing a lightweight, low-cost composite module

2.1. Problem statement

2.1.1. The unbearable heaviness of structures

From antiquity up until today, features such as heaviness, solidity and sturdiness have been unconsciously attributed to buildings. Massive structures are linked to strength and stiffness, thick walls express security and durability, and large cranes and heavy equipment are pictured together with construction sites, where non-muscular people have no place.

This perception regarding the reliability of buildings, deeply enrooted in peoples' minds, is sustained by the building sector and especially by the concrete and steel industries, that regenerate their dominant position in the market and leave little room for innovation and drastic change. Current regulations also impediment the change in the way we think and design buildings, by complicating procedures such as the safety guarantee of new materials.

Therefore, although in other fields, such as the automotive and aerospace industry or the consumer goods industry, the constant quest for lighter structures and components is observed, leading to tremendous progress in the design of the objects, similar development is not found in the construction field. The technology does exist however, to realise structures that can be 50% lighter and more efficient [1]. Then, given the fact that the construction industry is responsible for 25% of the road traffic and 35% of the national refuse dump [2], reducing the mass of buildings drastically improves their environmental behaviour.

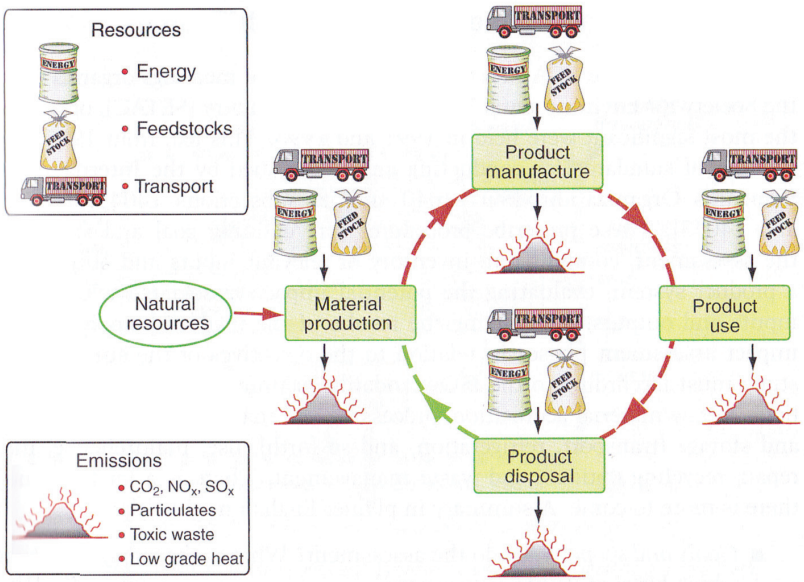

Figure 2. The material life cycle. In each phase materials and energy are consumed and waste and emissions are generated

Source: ASHBY, M.F. Materials and the Environment Eco-informed Material Choice

As cheap energy and material resources are becoming scarce, the issue of lightness and minimum energy consumption is starting to gain value. In addition, the way of living evolves, creating a demand for reconfigurable, non-permanent, transportable or floating structures. While buildings gradually start to become hybrids between cars, boats and transportable goods, the fact that a yacht the size of a house is 90% lighter [3], starts to become a concerning issue.

Raising the cost of buildings is of course undesirable but also unnecessary. By the use of lightweight materials that are properly shaped and combined together, efficient structures can be achieved. This shift in the design approach, although challenging and demanding, is imperative for creating a more sustainable future.



Figure 3. Deflated Bridge by M. Billow, T. Klein, T. Ebbert, W. Blondeel, A. Borgart, TU Delft 2006. The design utilises lightweight materials and the concept of vacuum-supported membrane structures, to achieve a light yet rigid bridge

Source: KNAACK, U., TILLMANN, K., BILOW, M. Imagine 02 Deflatables



Figure 4. Tensairity demonstration bridge with 8 m span and 3.5 tons maximal load. The combination of lightweight materials (in this case airbeam and steel girders) and engineering can lead to surprising results

Source: PEDRETTI, M. Tensairity®

2.1.2. Disadvantages of polymeric sandwich structures

Polymeric Sandwich Structures are characterised by their good strength-to-weight ratio and are a popular choice in the transport industry as their use leads to lightweight structures and important material savings. In the construction field, they can contribute not only to the reduction of the structure's mass, but also speed up the construction process, as large finished building components can arrive on-site, to be assembled. The use of these polymeric composites is also starting to become appealing among the designers, as they can be easily shaped into free form structures.



Figure 5. The Futuro House (1968)

Source: http://ecolocalizer.com

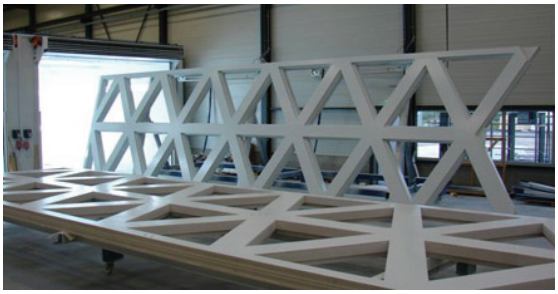

Figure 6. Fabrication of facade modules for 'Building X', Windesheim University, Zwolle (nl)

Source: Holland Composites



Figure 7. Louisiana Pavilion by 3XN (2010)

Source: http://3xn.dk

Fig. 5-7. Aspects of the polymeric sandwich materials that make them appealing in the construction field

Before discussing the advantages and disadvantages related to the use of polymeric sandwich structures it is first necessary to mention a number of key aspects related to the theory and their properties.

Basic principle of any sandwich structure is the combination of thin and strong face sheets with a lightweight core. It is characteristic that, although the components by themselves can be weak, when combined into a coherent unit, they acquire outstanding stiffness and strength while still resulting in a very lightweight structure. This occurs since the stiff facings are placed at the maximum distance from the neutral axis of the structure, increasing the moment of inertia and thus the flexural rigidity of the sandwich component.

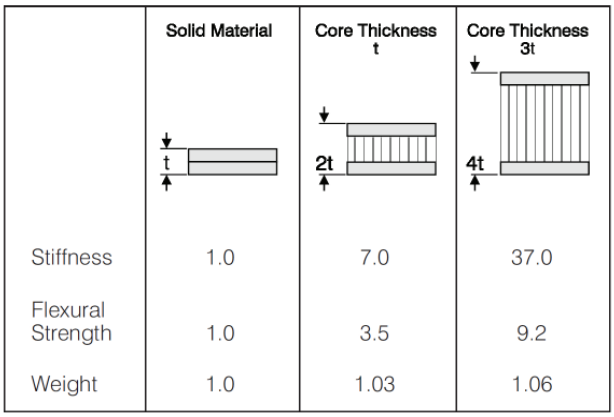

Figure 8. Basic principle of sandwich structures

Source: Sandwich Panel Fabrication Technology Hexcel Composites

The high strength-to-weight ratio linked with the composite structures, and especially with the Polymer Matrix Composites (PMC), is what is making them so appealing and therefore widely used in automotive, aerospace and marine applications. Other advantages of PMC over other materials is their ability to be engineered- in order for their reinforcement to respond to the direction of the loads- and their resistance to harsh environmental conditions [4].

Since the late 80's, polymeric composites appear in civil infrastructure [5], with bridges being one of the most common applications. As recent life-cycle assessments comparing FRP bridges to concrete ones show the significantly smaller CO_2 footprint of the first ones [6], the environmental behaviour of polymeric composites is brought again into discussion. In antithesis to opinions labelling for decades plastics as unsustainable materials, FRP (Fibre Reinforced Polymer) structures are starting to be considered as eco-friendly solutions, since their reduced weight minimises the CO_2 emissions during the transportation and assembly of the components on site and results in overall lightweight structures that require lighter foundations. Their high strength, on the other hand, leads to significant reduction of material use. In that sense, the application of polymeric sandwich structures in architecture is progressively investigated.



Figure 9. High-gloss free-form components can be produced in large series, making the use of composites attractive among the contemporary designers

Source: Photograph taken at the facilities of Poly Products BV



Figure 10. Standard core materials for polymeric sandwich structures include PU foam and aluminium honeycomb

Source: Photograph taken at the facilities of Holland Composites Industrials BV

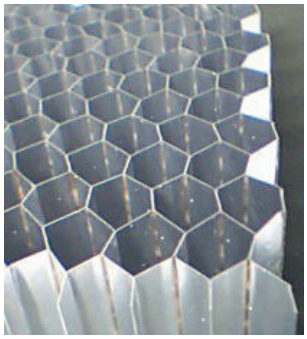

Source: http://www.tootoo.com

Despite the above mentioned advantages of these structures, there are a few disadvantages that need to be specified, mostly related to the core materials commonly used in the current prevailing products. More precisely, in the case where foam materials are chosen, such as Polyurethane Foam (PU, PIR), not only questions arise regarding their environmental footprint, but also regarding the after-life of the sandwich component. Separating the foam core from the FRP skin is a demanding procedure that is avoided and thus the recycling of the core- even when this is theoretically possible, for example when PET foam is used- hardly occurs.

Considering the case of the honeycomb core, important disadvantages are linked to the high cost and to the labour intensive and energy consuming production technique of some of the most common honeycomb products. In addition, the use of strong adhesives to bond the honeycomb to the facings, complicates the separation of the sandwich components and their recycling.

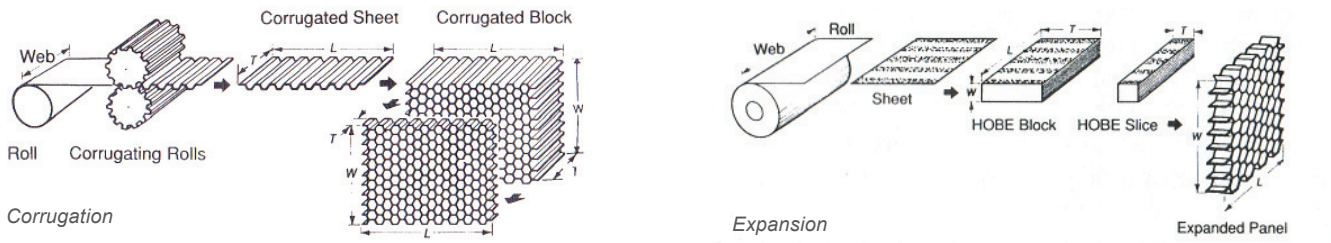

Figure 11. Manufacturing processes of honeycomb products

Source: BITZER, T. Honeycomb Technology Materials, Design, Manufacturing, Applications and Testing

Yet, even if the problem of separating the core from the skin is overcome, the fibre reinforce skin itself is most of the times not recyclable. Currently, 90% of polymers used in composites are thermosets, mainly because their lower than thermoplastics viscosity make them easier to be processed [7] and due to their permanent rigidity even at high temperatures. However, it is not possible to melt down these composite materials in order to separate the matrix from the fibres and recycle them. Downcycling in the form of grounding them and using them as filler seems to be the only possibility [8].



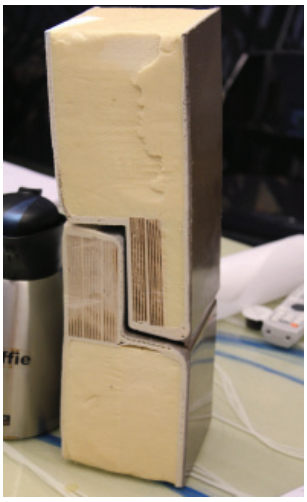

Source: Photographs taken at the facilities of Holland Composites Industrials BV

Figure 12. Once the layers of glass fibres, felt and PIR are impregnated with polyester and curing of the polymer takes place, the separation of the materials is not possible

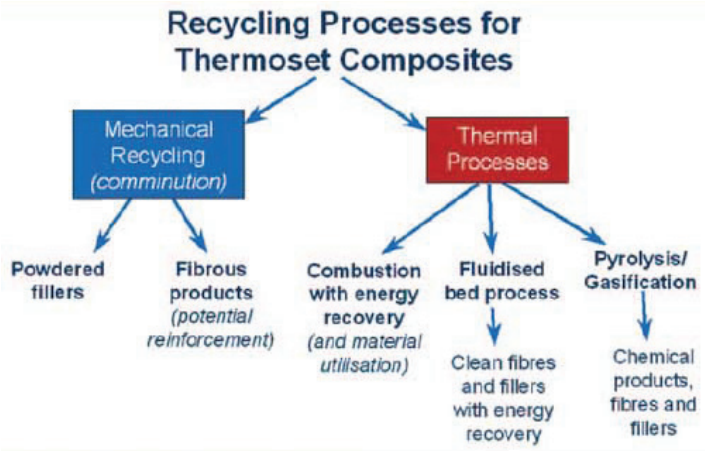

Figure 13. Mechanical recycling and thermal processes related to thermoset composites

Source: PICKERING, S. University of Nottingham, http://www.jeccomposites.com

2.1.3. Immoderate use of materials and the paradox of the plastic litter problem

For many, the fact that material resources are scarce is an issue not yet realised. This lack of awareness in not confined within the boarders of the construction industry but is much more general, generating a serious environmental problem, as it influences how quickly and how easily a product is to be considered waste. Then it also determines the fate of this product after it reaches the end of its life.

According to M.F. Ashby, products not always reach their end of life because simply they stop working but other causes may be involved such as the loss of desirability, the advances in technology making it obsolete or changes in legislation. Nowadays products tend to be rejected more rapidly compared to an era where objects where obtained to last for a lifetime and be passed on to next generations [9]. This attitude results in quality products to be discarded without having reached the end of their physical or functional life. What is more, due to the lack of environmental awareness, the considered as waste product, rarely finds use in other applications, or reaches a recycling or combustion plant, but rather ends up in landfills or the oceans.

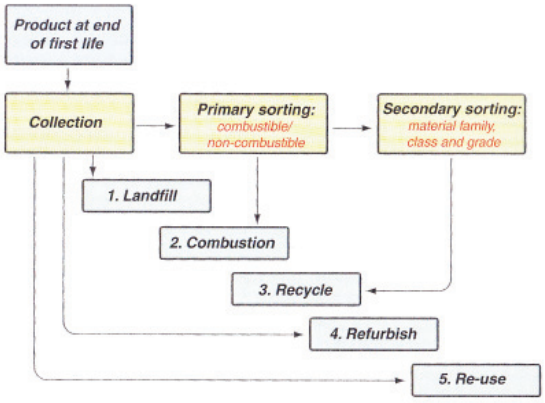

Source: ASHBY, M.F. Materials and the Environment Eco-informed Material Choice

Figure 14. End of life options. Great deal of products, however, do not pass level 1, due to the lack of awareness of the consumers, and absence of state initiatives and regulations

The above described problem becomes much more evident when it comes to plastics, a material that finds widespread use and therefore accounts for 12% of the municipal solid waste (in the U.S.) [10]. The largest category of plastics is found in the packaging sector and packaging makes up about 18% of the household waste [11]. PET bottles, in particular, are at a great extent responsible for the global problem of plastic litter, which is defined by the same paradox: tons of high-quality plastic products, designed to withstand rough handling and environmental conditions, are often regarded, after brief use, as waste, even though they are still at their peak performance.

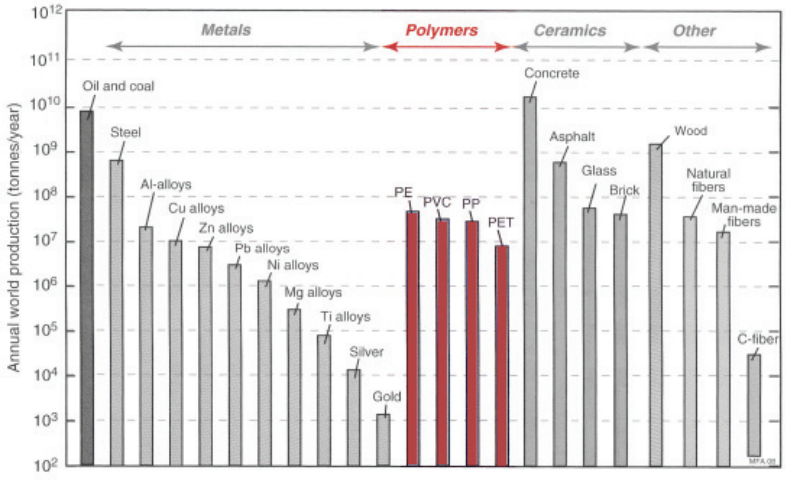

Figure 15. Annual world production of materials. Polymers are an important category
Source: ASHBY, M.F. Materials and the Environment Eco-informed Material Choice

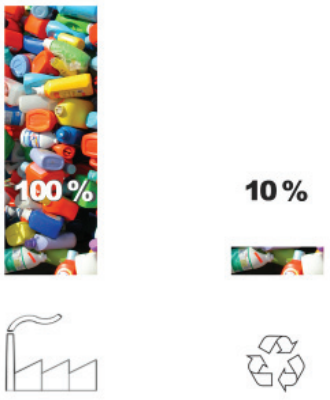

Figure 16. From the 300 million tons of plastic globally produced each year, only 10% is recycled (Data source: NYT)

The fact that only a small percentage of the produced plastics is reused or recycled once having completed its original purpose is not only related to state initiatives and the level of public awareness. More importantly it has to do with the existence of an enlarged market at the end of the re-use and recycling path, able to absorb the reincarnated materials. In the case of PET bottle recycling, it is characteristic that even in the Netherlands, that is performing significantly better than the U.S. (12.500 plastic bottles are consumed in the United states every 8.3 seconds according to The New York Times, and only 27.8 percent of the produced bottles were recycled in 2009) in terms of waste management, 95% of the big PET bottles are recycled while only 18% of the small (0,5L) bottles are reaching the recycling plants [12]. The absence of a deposit-refund system applied to the small bottles is mainly causing this percentage drop. The Plastic Heroes campaign, which alerted the citizens about the seriousness of the problem, managed of course to raise the amount of gathered PET bottles the past few years, but still this is not enough. The lack of motivation induced by an enlarged market that demands the recycled PET material is in the end what is keeping this percentage at a low level. Many PET bottle companies still prefer to use virgin PET, afraid that recycled PET will lower the quality of the bottle or affect the taste of the product, and because it is cheaper [13], while other industrial fields that use recycled PET, like the clothing industry, require only a small amount in relation to the total amount of PET products produced.

Stepping-in at this point, the construction industry, by being one of the biggest industries in the world, can effectively contribute to the utilisation of this waste. Plastic objects can be recovered to be re-engineered/ upgraded or reused in structures, or designers can prefer products resulting from recycled plastics, since the products have not reached the end of their physical life and can effectively function, if properly applied. A good proof of the functionality of these products can be found in cases where money or material resources are limited. In the developing world people reach for available materials- or “waste”- to construct their shelters. Many examples of houses or schools built out of sand-filled PET bottles exist. Once contemporary designers change their perception of waste, a broad pallet of building materials will be at their availability, leading not only to material, energy and money savings but also to aesthetically interesting results.



Figure 17. Shelters built out of PET bottles



Source: http://fabgreen.com

Figure 18. F*reestanding water wall created from 17,400 half-liter plastic bottles (Morimoto Restaurant NY by T. Ando)*

2.2. Purpose of the design

This thesis initiates from the addressed problematic issues. With the list of advantages and disadvantages of the polymeric composite structures as a starting point, the idea of a composite module out of FRP and PET bottles is formulated. The design aims to benefit from the positive aspects of the composites, such as the high bending stiffness and the low weight, but also to provide alternative solutions that avoid their disadvantages.

By locating some of the most important disadvantages to the choice of the core material and the bonding method used to adjust it to the facings, a cheap, sustainable and low-tech core is proposed, out of reclaimed PET bottles. Initial ambition is to design a core out of waste material that can be as -or more- efficient as other standard foam core materials. Then, objective is to develop a sandwich module where the components that consist it can be easily separated at the end of its life and thus reused, recycled or shredded accordingly.

The material choice and assembly method of the proposed component are the key aspects in achieving an “eco-friendly” module. Lightness in combination with the optimised structural performance of the system reduce its CO_2 footprint, whereas, by transforming waste polymer products into suitable building materials, not only resources and energy are saved, but also the ability of the building sector to absorb a significant amount of discarded plastic products, which would otherwise end up in the landfills and our oceans, is demonstrated. In fact, through this design, the big paradox related to the growing problem of plastic litter- that tons of high-quality plastic products, designed to withstand rough handling and environmental conditions, are still regarded, after brief use, as waste, even though they are at their peak performance- is highlighted. Propelling belief behind this research is that by exploring the potential of these well designed objects- which we regularly utilise in everyday life but rarely relate to the building sector- we may not only reach positively surprising results, but also form a sustainable, “low-tech” approach for producing architecture, and broaden the range of materials available to the contemporary designer. In addition, by keeping in mind during the design phase the “distraction” of the module, the recovery of the used materials can be possible and its environmental impact after the end of its service life can be reduced.

An other issue to be examined in this thesis, is the possibility to shift from a thermoset to a thermoplastic composite technology, that enables the recycling of the skins of the sandwich module.

Finally, the advantages of such a lightweight dismantable module are explored, by looking at its possible application in the area of rapidly erectible, non-permanent structures, such as emergency shelters for victims of natural disasters.



Figure 19. Adding value to products means appreciating the materials they are made off and the energy consumed for their production. In that sense, what is generally considered as waste can still have great potentials and applications in several fields, including the building sector



Figure 20. By the reuse of waste materials, sustainable and cheap structures can be achieved

3. Design principles

Taking into account the previously mentioned objectives, a set of design principles is formulated to be used as a guideline and assessment tool throughout the design process. In short, the final product should be:

- Lightweight
- Low-cost
- Low-tech and simple in its detailing

In addition, considering its production, application and after-life, it is intended to:

- Minimise the production time and costs
- Provide the possibly of wide range of standard sizes
- Facilitate its assembly and disassembly on site
- Allow an effortless separation of its components and the recovery of the used materials

B. Research

1. Research structure

1.1. Topics for investigation

For the design of the sandwich module out of FRP facings and a PET-bottle core, first issue that needs to be clarified is the properties and structural behaviour of the PET bottles consisting the core. This research section starts with the understanding of the strengths and weaknesses of the PET bottle and explores the possibility of improving its structural performance by internally pressurising it with the addition of dry ice (solid CO_2). The conclusions derived from this part of the research lead to the second phase of this investigation, which focuses on defining the structural behaviour of the closed, un-pressurised bottles.

The data selected from the work conducted in the first section enable to proceed to the second section of this research that deals with the relationship of the bottles with the facings. At this section, the structural behaviour of the composite module, as a result of the above bottle-to-skin cohesion, is identified.

Then, in the third section, the material choice for the facings is investigated leading to the final design of the module, in section 4. At this chapter, the manufacturing and assembly method of the module are defined.

The last two sections of this research are concerned with the design of an integral building system, based on the developed composite module, and its application possibilities.

Thus, the research will be presented in the structure seen below:

i. PET bottle: properties and structural behaviour
ii. PET-bottle core for a FRP Composite module
iii. FRP facings
iv. Composite module out of srPP facings and a PET-bottle core
v. Integral building system
vi. Application possibilities

1.2. Methodology

The research is significantly based on the results acquired from physical experiments and full scale prototypes. In many cases that it is necessary to prove the feasibility of the assumed concept, the tactic is to start experimenting with means available at local stores before concluding to the most suitable engineering solutions.

Equally important in developing a feasible proposal is the contact and collaboration with companies related to the manufacturing of PET bottles or Polymer Composite Structures.

The data obtained guide the design process which is constantly assessed by the set of design principles, described in the introduction of this thesis. The simplification process of the detailing is constant.

Throughout the research the question of what is possible and what is sufficient keeps returning, and balance is sought between the two situations, in order for the developed module to meet the design criteria.

2. Research and results

2.1. PET bottle

2.1.1. Material properties and geometry

A look into the PET bottle technology draws attention to issues that are relevant to the process of bottle selection and insightful regarding the areas of weakness of the bottles. In short it should be mentioned that:

•Bottles for soft drinks (CSD) have different design specifications from bottles for non-carbonated products

Usually CSD bottles are heavier to increase the bottle's strength, and reduce permeation of CO_2 and creep (expansion of the bottle due to internal pressure). The base is formed in a petaloid structure of 5 feet that prevents deformation and allows the bottle to stand upright when filled with the carbonated beverage. Barriers are applied to reduce the permeation rate of gases and vapour and to prolong the shelf-life of the products. Finally, the bottle's neck has an additional twist.

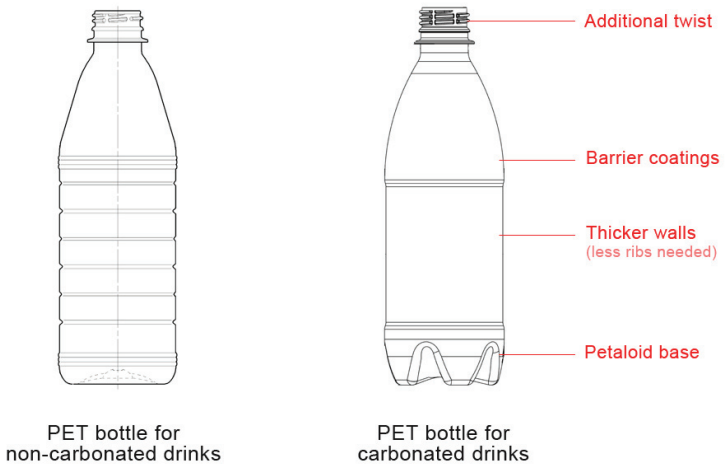

Figure 21. Fundamental differences between bottles for carbonated soft drinks (CSD) and for non-CSD

•Mechanical degradation in the form of crazes and cracks is induced in the material when modest levels of stress are applied over long periods of time

Ductile plastics show a long-term transition from ductile to brittle behaviour. This process can be accelerated with the increase in temperature and the contact with chemical environments. Thus, the time-dependent creep rupture strength of the PET bottles used in the construction needs to be defined.

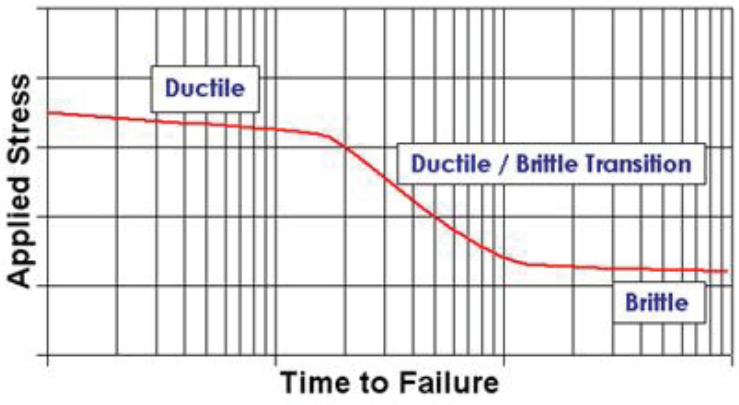

Figure 22. Time-dependent behaviour of polymers under constant stress
Source: www.rapra.net

•*Pet bottles are prone to Environmental Stress Cracking*

Environmental Stress Cracking (ESC) is the premature cracking and embrittlement of a plastic due to the simultaneous action of stress and strain, and the contact with specific chemical environments (including water). The variables during the production of the bottle by stretch blow molding also affect its crack resistance. ESC mostly occurs in the bottle's base as the sharp angles of its geometry become stress concentrators.

This highlights the weakest point of the bottle and where problems are to be expected.

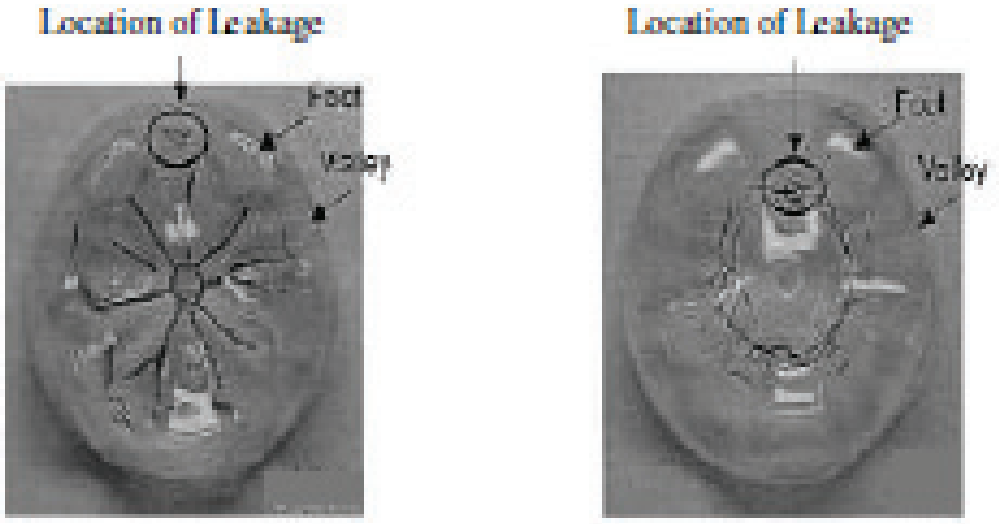

Figure 23. Usual configuration of cracks in radial and circumferential direction of the PET bottle's petaloid base

Source: [DEMIREL 2008]

•*Pet bottles show poor resistance to high temperatures and embrittle at low temperatures*

Maximum service temperature of PET is 71 C and thus, by passing this limit, the PET bottle will start to distort. Minimum service temperature is around -40 C and lower temperatures will cause the bottle to embrittle.

The above data cannot be neglected during the experiments otherwise the bottle may be subjected to its limit temperatures. Heat sealing of the cap, contact with warm water or contact with dry ice (-79 C) may soften or embrittle the specimen.

•*Pet bottles are permeable to gases and water vapour*

Plastics are not perfect gas and vapour barriers and therefore CO_2 can escape and O_2 can ingress over time. In fact 80% of the CO_2 content is lost through the bottle's wall and only 5-10% is lost through the base and the closure. Smaller bottles present higher loss rate due to the relation between the surface areas of the bottle and the liquid volume it contains. It is expected that a typical 0,5L PET bottle will show a 15% CO_2 loss within 8 weeks of bottling. Myltilayer or coated PET bottles with barrier resins delay this process.

Attention is drawn to the permeability of the PET bottles and the pursuit of effective solutions is imperative.

Figure 24. Properties of PET (unfilled, amorphous)
Source: CES EduPack database

PET (unfilled, amorphous)

General properties

Density	1.29e3	-	1.39e3	kg/m^3
Price	1.19	-	1.31	EUR/kg

Composition overview

Composition (summary)
(CO-(C6H4)-CO-O-(CH2)2-O)n

Base	Polymer
Polymer class	Thermoplastic : amorphous

Mechanical properties

Young's modulus	* 2.8	-	3	GPa
Compressive modulus	* 2.76	-	4.14	GPa
Flexural modulus	2.41	-	3.09	GPa
Shear modulus	* 0.994	-	1.49	GPa
Bulk modulus	* 4.94	-	5.19	GPa
Poisson's ratio	* 0.381	-	0.396	
Shape factor	5.7			
Yield strength (elastic limit)	* 50	-	55	MPa
Tensile strength	55	-	60	MPa
Compressive strength	* 50	-	60	MPa
Flexural strength (modulus of rupture)	50	-	60	MPa
Elongation	280	-	320	% strain
Hardness - Vickers	* 2	-	5	HV
Hardness - Rockwell M	28	-	30	
Hardness - Rockwell R	* 45	-	50	
Fatigue strength at 10^7 cycles	* 19.3	-	29	MPa
Fracture toughness	* 4.75	-	5.25	MPa.m^0.5
Mechanical loss coefficient (tan delta)	* 0.00966	-	0.0145	

Impact properties

Impact strength, notched 23 °C	6.19	-	6.83	kJ/m^2
Impact strength, unnotched 23 °C	* 190	-	200	kJ/m^2

Thermal properties

Glass temperature	60	-	84	°C
Heat deflection temperature 0.45MPa	70	-	74	°C
Heat deflection temperature 1.8MPa	68	-	72	°C
Maximum service temperature	* 55	-	65	°C
Minimum service temperature	* -58	-	-38	°C
Thermal conductivity	0.138	-	0.151	W/m.°C
Specific heat capacity	1.15e3	-	1.25e3	J/kg.°C
Thermal expansion coefficient	115	-	119	µstrain/°C

Absorption, permeability

Water absorption @ 24 hrs	0.14	-	0.18	%
Water vapor transmission	0.464	-	0.707	g.mm/m².day
Permeability (O2)	1.2	-	2.77	cm³.mm/m².day.atm

Durability: flammability

Flammability	Highly flammable

Durability: fluids and sunlight

Water (fresh)	Excellent
Water (salt)	Excellent
Weak acids	Acceptable
Strong acids	Unacceptable
Weak alkalis	Acceptable
Strong alkalis	Limited use
Organic solvents	Limited use
UV radiation (sunlight)	Good
Oxidation at 500C	Unacceptable

2.1.2. Structural behaviour of internally pressurized bottles

2.1.2.1 Overview

This part of the research investigates the assumption that PET bottles filled with solid CO_2 can exhibit higher compressive strength than typical foam materials possess, through physical prototypes and experiments. First the bottles' specifications for optimal performance are defined, then their compression and creep rupture strength is investigated. Throughout the experimental process, the main aspect to be dealt with is the permeation of gases and vapour via the PET walls and screw cap. Alternatives including barrier films and structural adhesives are tested and rejected due to unsatisfactory results.

2.1.2.2 Properties of solid CO_2

Dry ice, also referred to as "Cardice", is the solid form of carbon dioxide (CO_2). A block of dry ice has a surface temperature of -78.5°C. When it is placed in normal atmospheric conditions it changes directly from solid to gas without going through a liquid stage. This process is called sublimation and its result is a tremendous increase of the material's volume [14].

Dry ice is a recycled product made from pure carbon dioxide that is a by-product of other industrial processes such as the manufacture of ethanol. It is characteristic that the demand for dry ice is low and many industrial ethanol plants simply release the CO_2 waste to the atmosphere because the process of selling it is economically unfeasible [15].

The use of this gas to achieve pressurised structures in architecture proposes another field of application for this material and contributes to the reduction of the greenhouse effect.

To define the relationship between the mass of dry ice inserted in a bottle of particular volume and the internal pressure expected to be generated we can use the Van der Waals equation, which is a revised version of the ideal gas equation, used to more accurately describe the behaviour of real gasses:

The Van der Waals equation:

$$\left(\mathbf{P} + \frac{\mathbf{n^2} * \boldsymbol{a}}{\mathbf{V^2}}\right) * (\boldsymbol{V} - \boldsymbol{n} * \boldsymbol{b}) = \boldsymbol{n} * \boldsymbol{R} * \boldsymbol{T}$$

Where:

P = pressure *(atm)*

n = number of moles *(mol)*

a = van der Waals constant that depends on the number and distribution of electrons, which relates to the complexity of a particle and the strength of its interparticle attractions *($atm*L^2/mol^2$)*

b = van der Waals constant that relates to particle volume *(L/mol)*

V = Volume *(L)*

R = ideal gas constant *(atm*L/mol*K)*

T = temperature *(K)*

Also we have:

$$n = \frac{m}{MW}$$

Where:

m = mass *(g)*

MW = molecular weight *(g/mol)*

For CO_2 we have the following values:

a = 3,59 $atm*L^2/mol$

b = 0,0427 *(L/mol)*

V = Volume *(L)*

R = 0,0821 *atm*L/mol*K*

MW = 44,01 *g/mol*

Thus:

$$P = \frac{n*R*T}{(V-n*b)} - \frac{n^2*a}{V^2} \quad \rightarrow \quad P = \frac{\left(\frac{m}{44,01}\right)*0,0821*T}{\left(V-\left(\frac{m}{44,01}\right)*0,0427\right)} - \frac{\left(\frac{m}{44,01}\right)^2*3,59}{V^2}$$

Therefore, if, for example, we have a PET bottle of V=0.5L and room temperature T= 20° C +273= 293K, then 3gr of dry ice are going to produce 3.23atm pressure.

According to design specifications, a PET bottle for carbonated products can hold up to 13,6 atmospheres of pressure before it bursts. This level of pressure can be reached if 13,3 grams of powdered dry ice are inserted in the bottle.

The maximum level of pressure that a bottle can hold depends of course on the thickness of the PET vessel (ex. 0.5 liter Sprite PET bottle, 0,45 mm thick has burst pressure =13.6atm) and the configuration of the bottle (ex. a five-footed bottle base gets less distorted than a four-footed base). Nonetheless, 13gr of dry ice can be the starting value for the experiments.

	Height (mm)				Fill Height (mm)				Brimful (mm)			
specimen	20g 4ft	20g 5ft	22g 4ft	22g 5ft	20g 4ft	20g 5ft	22g 4ft	22g 5ft	20g 4ft	20g 5ft	22g 4ft	22g 5ft
1	215.5	215.6	215.4	215.3	506.1	501.6	503.5	498.7	526.3	522.1	524.1	519.4
2	215.5	215.5	215.4	214.4	506.1	501.1	503.6	499.3	526.8	521.4	524.3	519.5
Mean	215.5	215.6	215.4	215.4	506.1	501.4	503.6	499.0	526.6	521.8	524.2	519.5

	Base weight (g)				Panel weight (g)				Burst test (psi)			
specimen	20g 4ft	20g 5ft	22g 4ft	22g 5ft	20g 4ft	20g 5ft	22g 4ft	22g 5ft	20g 4ft	20g 5ft	22g 4ft	22g 5ft
1	4.3	4.3	5.0	5.1	5.7	5.6	6.6	6.6	152	148	199	196
2	4.1	4.3	5.1	5.1	5.7	5.6	6.6	6.5	154	154	199	200
Mean	4.2	4.3	5.1	5.1	5.7	5.6	6.6	6.6	153	151	199	198

Figure 25. Performance of 20g and 22gr 0,5L bottles in 4- and 5-foot base variations

Source: Raising the bar in PET bottle lightweighting - WRAP

2.1.2.3 Experimental procedures

i. Burst strength of various types of PET bottles

Process

In order to define the most suitable PET bottle type for the construction, a series of new and reused PET bottles of different volumes and design qualifications (for CSD/ non CSD products) were subjected to burst and tension tests.

Regarding the burst tests, at first extreme dosages of dry ice (solid CO_2 / -79° C) were inserted into the bottles, to determine their limit point, and then the dosage was gradually lowered to observe the rigidity of the bottles, the areas of weakness and the deformation they would obtain when subjected to different amounts of pressure. To avoid frosting of the PET surfaces from contact with the dry ice, and to accelerate the sublimation of the dry ice, the specimens where placed in warm water once filled with solid CO_2.

The distinct behaviour of bottles with the same wall thickness and induced levels of internal pressure led to a series of tension tests. Strips of 10mm*100mm were cut of *Type 2* (0,5L, Ducona/Juice) and *Type 4* (0,5L, Sprite) bottles and were stressed under tension at different test rates until they broke. Comparing the results with the performance of *Type 3* (0,5L, Coca Cola) bottles was not achieved as the specimens were slipping from the cross members of the machine.



Figure 26. A specific amount of dry ice is inserted in the sample



Figure 28. The sample is sealed and the sublimation of the inserted dry ice starts to take place



Figure 29. During the process of sublimation frost may appear on the bottle's surface



Figure 30. To avoid the frosting of the base and to accelerate the sublimation, samples are inserted in hot water, once sealed

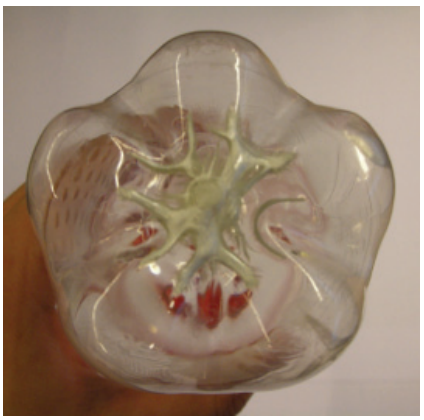

Figure 27. Damage at *Type 3* bottle's base due to bursting under 24atm int. pressure

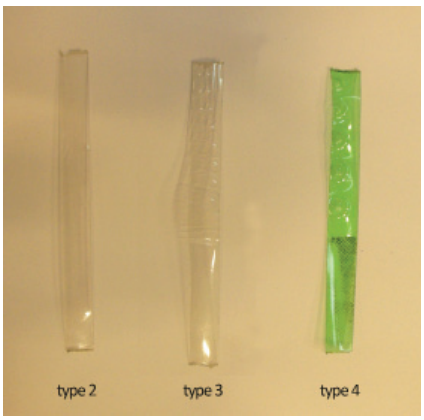

Figure 31. Strips from *Types 2-4* to be tested in tensile strength

Results

During the tests, significant differences between the performance of the CSD bottles versus the non-CSD bottles were noticed. More specifically, the CSD bottles showed a limit of 13atm internal pressure, over which bursting occurred. At this state, the bottles would plastically deform yet they would still be able to stand upright, which was not the case for the non-CSD bottles. The latter could not withstand even half of the CSD bottles' limit pressure and their caps, designed with 1-start thread, were ejected.

Considering the CSD bottles, the areas most prone to cracking were the base and the neck, and then the seams caused by the stretched blow molding of the bottles. At 13atm internal pressure the bottles showed impressive rigidity, yet the level of damage was high, especially at the base, and their condition was unstable, meaning that abrupt impacts could lead to rupture. Under the value of 7atm there were no damages observed (leastwise they were not visible at a macroscopic level) but passing the point of 3atm, the bottles' rigidity was significantly lowered.

An important issue brought to attention was the conditions during the sublimation of the inserted dry ice. The contact of blocks of solid CO_2 (-79° C temperature) with the PET walls and particularly with the bottles' base, was causing frost and embrittlement of the exposed surfaces. This is alarming since the minimum service temperature of PET is around -40 C [16]. Moreover, placing the samples in hot water during sublimation can lead to absorption of water particles from the surface and the swelling of the bottle [17]. Water gradually plasticises the polymer and reduces its yield strength (Environmental Stress Cracking), making the bottle prone to the formation of crazes [18].

Finally, it was shown that the consistency of the PET walls was affecting the behaviour of bottles of same wall thickness, fact also proven through the conducted tension tests.

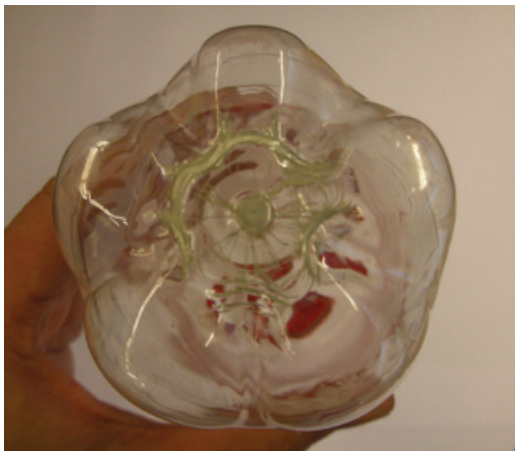

Figure 32. Damage at the base (*Type 3*, *0,5L* CSD, 32atm)



Figure 33. Plastic deformation along the seams (*Type 3*, *0,5L* CSD, 32atm)



Figure 34. Unexpected deformation at base (*Type 3*, *0,5L* CSD, 12atm)



Figure 35. Plastic deformation at base (*Type 6, 0,5L* non-CSD, 20atm)



Figure 36. Standard vs tested bottle (*Type 1, 0,5L* non-CSD, 13atm)



Figure 37. Standard vs tested bottle (*Type 3, 0,5L* CSD, 14atm)

No.	Test no.	8	9	10	11	12	13	14
Sample data	Photo							
	Type code	6	6	14	3	4	10	3
	Product	Tea	Tea	Still	CSD	CSD	CSD	CSD
	Weight (gr)	27,34	27,34	49,49	24,96	27,8	27,21	24,96
	Thickness (mm)	0,35	0,35		0,255	0,3		0,255
	Volume (L)	0,5	0,5	0,5	0,5	0,5	0,5	0,5
	Cap diameter (mm)	40,5	40,5	40,7	30,4	30,4	30,3	30,4
	Cap closure	0,5-start thread	0,5-start thread		3-start thread	3-start thread		3-start thread
Test details	Seal	Teflon around threads	Teflon around threads	Teflon around threads	Teflon around threads	Teflon around threads	Teflon around threads	Teflon around threads
	CO_2 inserted (gr)	20	9,5	10	6	13	13	4,6
	Int. pressure (atm)	19,8	9,9	10,4	6,4	13,3	13,3	4,9
Results	Status	cap ejected	cap ejected	rigid	rigid	rigid/ bursted after impact	rigid/ bursted after impact	rigid
	% Leakage per week	-	-	1,22	0,45	-	-	3,14
	Defects							

Figure 38. Comparative chart, samples 8-14

ii. Reducing the CO_2 permeation rate of the bottles

1st Research Phase
Process

Throughout the experiments the tested samples were weighed, to determine their mass reduction over time. The issue of CO_2 loss was categorised into two parts- the one related with the leakage from the screw cap and the other with the permeation of CO_2 from the PET walls- and different alternatives were examined to retard the permeation rate observed.

For minimizing the cap leakage, first Teflon tape was applied along the bottles' threads. Then, a second series of samples was sealed by applying structural epoxy adhesive (Araldite 2013) around the threads of the cap.

Regarding the permeation rate of gases and vapour from the PET walls, first it was attempted to be reduced by wrapping the samples with aluminum foil, transparent LDPE film, or a combination of both. After 3 days the samples were unwrapped and a selection of them was covered with Parafilm M, a self-sealing film barrier out of polyolefins and paraffin waxes. The permeation rate of the covered samples was compared to that of similar, exposed samples.



Figure 39. Teflon tape along *Type 3* bottle's threads

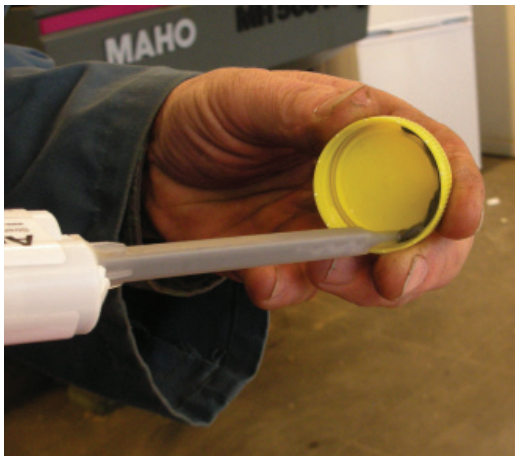

Figure 40. Applying structural epoxy adhesive inside the cap

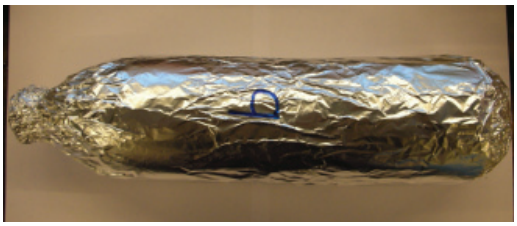

Figure 41. Sample covered with aluminum foil

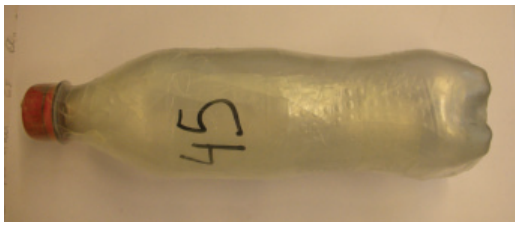

Figure 42. Wrapped sample with Parafilm M film

Results

To begin with the leaking from the cap, applying Teflon tape along the threads was unsuccessful. The permeation rate was scarcely diminished and when high internal pressure was created, CO_2 could easily escape from the cap, preventing the bottle from bursting. Especially during the compression tests, as the bottles' neck was deforming, the gaps between the bottle and the cap were increasing, cancelling the contribution of the Teflon tape and facilitating the leakage of CO_2 until the bottles lost their rigidity and failed. The application of epoxy adhesive around the threads of the cap showed better results regarding the behaviour of the bottles during the compression tests. Proof is that none of the tested samples leaked and the only failure noted was due to bursting. Yet, the permeation rate of the bottles was not satisfactorily reduced and other alternatives should be examined that should include the sealing of the cap from the exterior as well.

Regarding the permeability of the PET walls, it was noticed that by increasing the internal pressure, the percentage of leakage was also increasing. In addition to this, the leakage was gradually decreasing over time. The most abrupt reduction of mass was observed during the sublimation of the inserted dry ice and the compression test. The above observations can be easily explained by Fick's law [19], relating the gas concentration with the flux:

$$J = -D\frac{\partial \varphi}{\partial x}$$

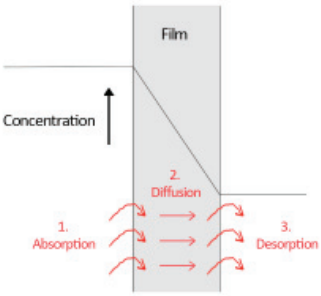

Where:

J is the diffusion flux: the amount of substance per unit area and time $\left(\frac{\text{mol}}{\text{m}^2 \cdot \text{s}}\right)$

D is the diffusion coefficient $\left(\frac{\text{m}^2}{\text{s}}\right)$

φ is the concentration $\left(\frac{\text{mol}}{\text{m}^3}\right)$

x is the length (m)

The above equation can also be expressed as:

$$\frac{\text{Quantity of gas}}{\text{Time}} = \frac{\text{Solubility coefficient} * \text{Diffusion coefficient} * \text{Pressure difference} * \text{Area}}{\text{Thickness}}$$

From this equation the factors that influence the permeation rate are made evident. In short these include the properties of the gas, the temperature and humidity levels, the pressure difference, the area and thickness of the surface, and the structure of the surface (density, arrangement of polymer chain, multiple layers and barrier coatings).

Thus, by wrapping the samples with barrier films or foils, the thickness of the surface is increased and the diffusion coefficient is lowered, and so the permeation rate of the samples is expected to be lower.

Yet, wrapping the samples with LDPE film or aluminum foil did not significantly reduce the permeation rate and once unwrapping the specimens, they showed a higher permeation rate than the similar unwrapped samples. In total, the leakage of the wrapped and then unwrapped bottles was the same with that of the untreated bottles. Apparently, the foil or film on the samples' surface, as it was not in perfect contact with it, allowed for gases to get trapped between the foil/film and the surface. The gases easily escaped once the foil/film was discarded. Another issue is that thin films and aluminum foils often contain minute pinholes that make them less impermeable to gases and vapour [20]. Parafilm M, by establishing better contact with the bottle presented better results, but nevertheless its performance is not sufficient for extending the life span of the module.

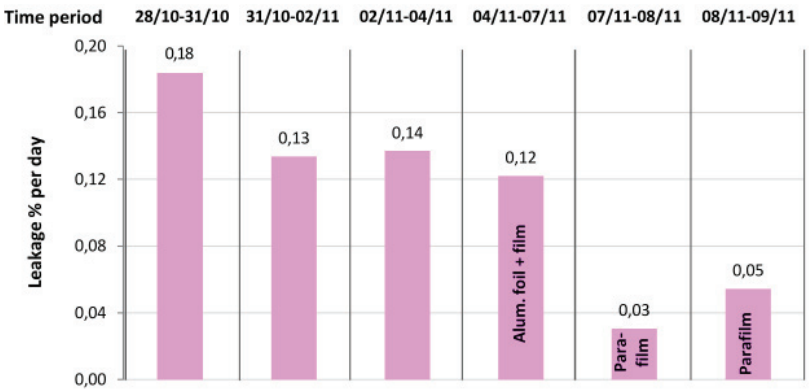

Figure 43. Leakage per day graph, *Type 3* (6atm, adhesive) showing the effectiveness of Parafilm M in reducing the CO_2 permeation rate

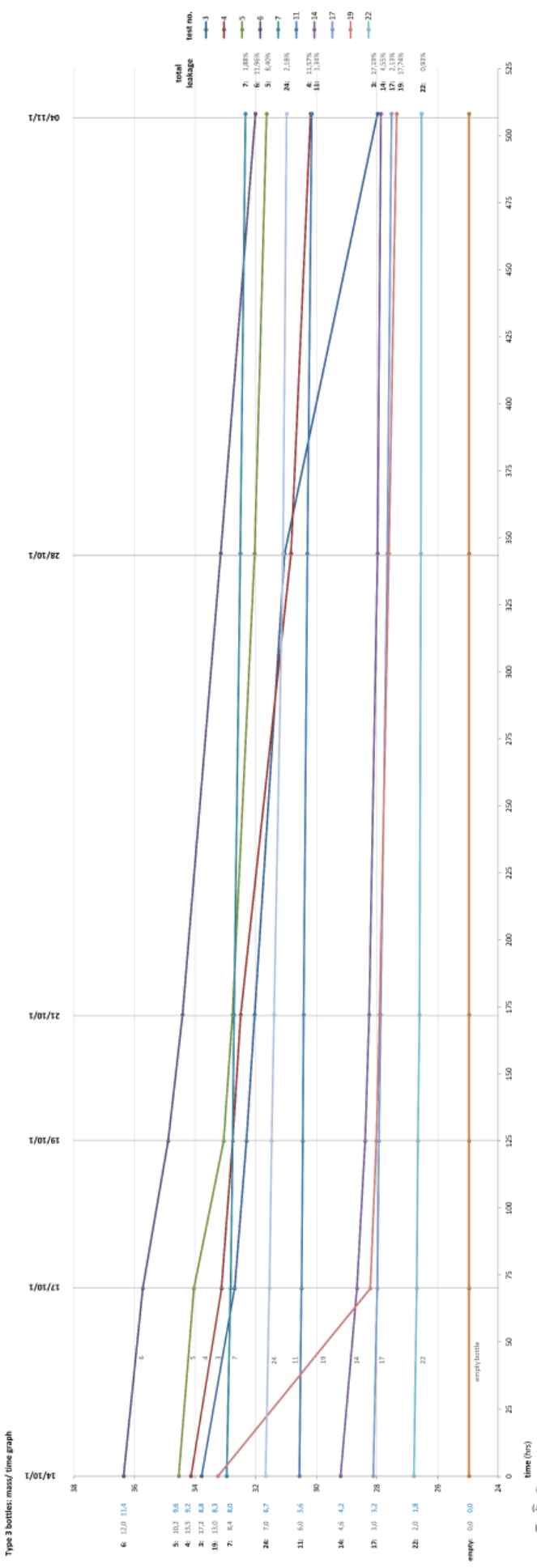

TYPE 3	MASS MEASUREMENT (gr)						LEAKAGE				CO_2 LOSS		CO_2 CONTENT	
DATE	14/10	17/10	19/10	21/10	28/10	04/11	1st Week leakage % 14-21 Oct.	2nd Week leakage % 21-28 Oct.	3rd Week leakage % 28 Oct.-04 Nov.	Weekly leakage %	Total leakage %	Total mass loss (gr)	CO2 loss (gr) per day	Inserted CO_2 (gr)	1st measurement CO2 (gr)
TIME LINE (hrs)	0	70	125	172	344	508									
Test no															
3	33,79	32,7	32,31	32,04	31,05	27,98	5,06	3,02	9,89	5,69	17,19	5,81	0,27	17,20	8,83
4	34,14	33,13	32,76	32,5	30,84	30,19	4,69	4,99	2,11	3,83	11,57	3,95	0,19	13,50	9,18
5	34,54	34,04	33,06	32,77	32,04	31,64	5,01	2,18	1,25	2,78	8,40	2,90	0,14	10,20	9,58
6	36,36	35,73	34,89	34,42	33,16	32,01	5,21	3,58	3,47	3,96	11,96	4,35	0,21	12,00	11,40
7	32,96	32,83	32,76	32,72	32,51	32,34	0,71	0,63	0,52	0,62	1,88	0,62	0,03	8,40	8,00
11	30,56	30,49	30,45	30,42	30,3	30,15	0,45	0,39	0,50	0,44	1,34	0,41	0,02	6,00	5,60
14	29,2	28,66	28,39	28,26	27,98	27,87	3,14	0,97	0,39	1,51	4,55	1,33	0,06	4,60	4,24
17	28,12	27,99	27,94	27,88	27,66	27,52	0,83	0,77	0,51	0,71	2,13	0,60	0,03	3,00	3,16
19	33,25	28,22	28,02	27,92	27,61	27,35	15,66	1,08	0,94	5,87	17,74	5,90	0,28	13,00	8,29
22	26,78	26,69	26,65	26,6	26,55	26,53	0,66	0,18	0,08	0,31	0,93	0,25	0,01	2,00	1,82
24	31,67	31,55	31,48	31,4	31,1	30,98	0,83	0,93	0,39	0,72	2,18	0,69	0,03	7,00	6,71

Figure 44. Graph and table depicting the mass loss for type 3 bottles (Teflon sealing method) filled with different amount of dry ice. Leakage is increasing when internal pressure is higher and it is decreasing over time

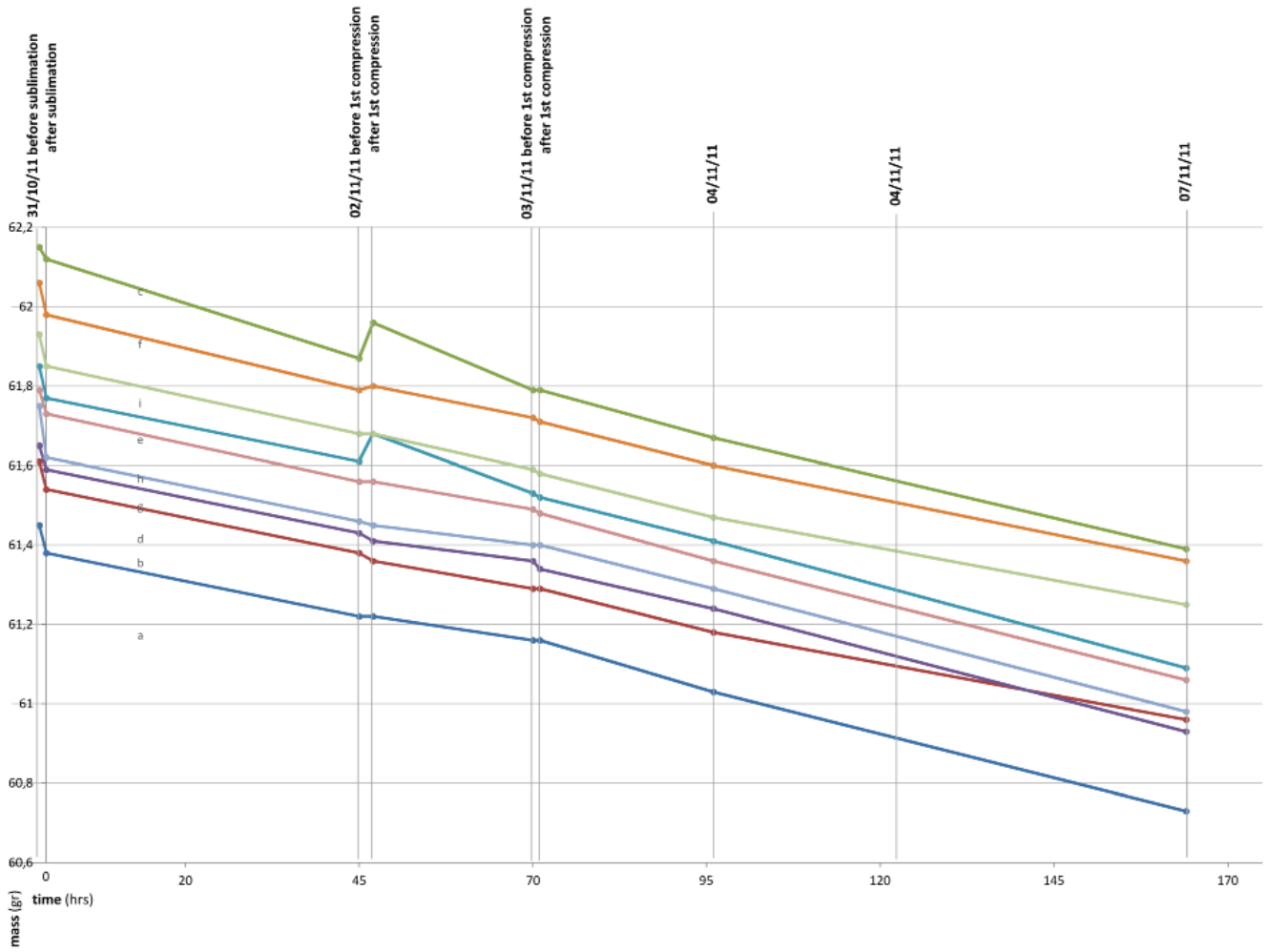

Figure 45. Mass over time graph, *Type 27* (6atm, adhesive). Gradual reduction of mass is noted, which is intensified during the sublimation of the inserted dry ice and when the samples are subjected to compression loads. Some samples, however, present opposite behaviour during these two periods

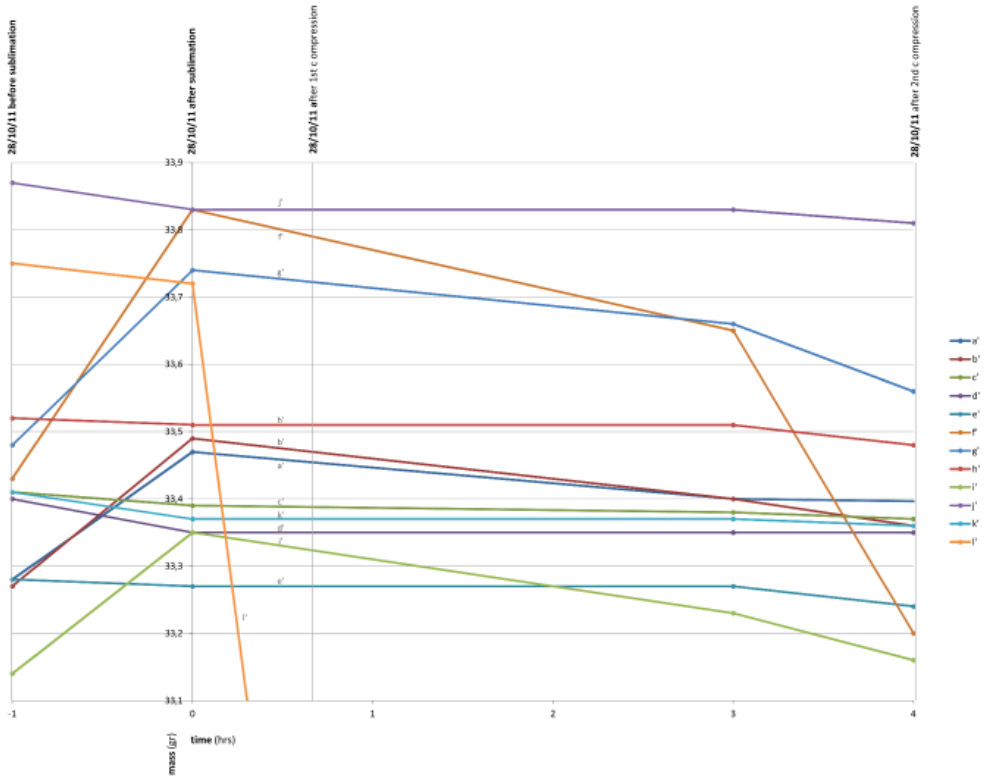

Figure 46. Type 3 a'-l' (adhesive). Behaviour of samples during sublimation

Regarding the thickness of the PET wall, it should also be mentioned that damages on the PET surface, even if they do not penetrate the wall, they reduce its total thickness and accelerate leakage. This was evident when 6 bottles of *Type 28* (0,5L, River Bitter Lemon) that were crushed when collected from the recycling bin, were filled with dry ice and measured over one week period. The bottles, designed for CSD, showed leakage rates that were significantly exceeding those of similar types of CSD bottles. An additional disadvantage related with the use of discarded bottles for the modules is that barrier coatings that may have been applied at the bottles' exterior and interior substrate could have been scratched off or delaminated [21] while the bottles were crushed and thrown in the bin. Furthermore, cracks tend to absorb more fluid than the rest of the material, especially under stress [22], a process already described to be encouraging Environmental Stress Cracking.

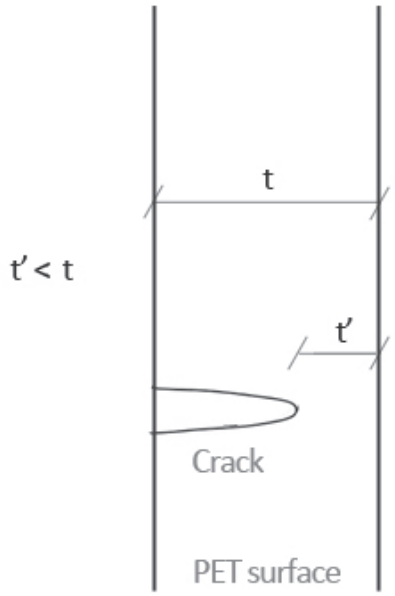

Figure 47. Scheme showing a section of the PET wall and the reduction of its thickness due to crazes



Figure 48. Condition of Type 28 bottles before their filling with dry ice

The matter of H_2O absorption, in this case from the environment and during the sublimation period, seems to be also related with the abnormal increase of mass during sublimation or compression loading, noticed in some of the samples. It is possible that the samples absorb water during the sublimation of the dry ice and their PET surface swells. Moreover, during the compression tests, water vapour from the environment may be forced to insert the PET surface due to the extreme applied pressure.

2nd Research Phase
Process

Regarding the sealing of the cap, the method of wrapping Teflon tape around the threads, the use of epoxy adhesive, and their combination, were again tested with two different bottle Types (31, 32), sponsored by *Ducona Holland BV*. PCO 28mm caps with and without a pilfer-proof ring attached were tested along with new series of bottles. Attempts were made to heat-seal the bottles with a heat blower or seal them with Paraffin wax that has a fast solidification, to reduce the leakage during the sublimation process. Finally, some samples were wrapped with Parafilm around the lid or coated with thick waterproofing roof coatings. To depict the leakage from the cap and the effectiveness of the different solutions, Type 2 bottles were used, with 38mm 3-start thread caps. These samples, unsuitable to withstand the amount of pressure applied, were instantly leaking and explicitly indicating the problems that were undetected in the other samples.

To reduce the gas permeation from the PET surface, different coating solutions were examined in favour of barrier films and foil, since previous results proved the inadequate performance of the later. The materials tested for their barrier properties were paraffin wax, roof waterproof coating, nylon spray and latex. These products were evaluated on their ability to reduce the CO_2 permeation rate and their susceptibility to punctures and delamination. The difference of externally or internally applying a coating layer at the bottle's wall was viewed, not only at a theoretical level but also with tested samples. Only after the completion of the experiments it was discovered that the tested samples (Types 31, 32) are not coated with barrier resins and that are in fact designed for a shelf life of 3 to 4 months. Simultaneously to the experiments, research was conducted on the barrier properties of polymers and elastomers and on the applications used in the food-packaging industry. The possibility to replace CO_2 with a gas of higher molecular weight that would more difficultly escape the bottle, was assessed.

Results and conclusions

Starting with the issue of CO_2 leakage from the cap, the leakage tests performed with Type 31 (0,5L, champagne base, PCO finish) and Type 32 bottles (0,5L, petaloid base, PCO finish) showed reduced percentage of leakage in comparison with previously tested types that had a good performance (ex. Type 3). The fact that in the latest experiments the caps were applied for the first time on the bottles, and thus still contained their pilfer-proof ring attached on them, played a significant role for the reduction of the leakage rate.

Different sealing methods and combinations were tested with the above series of bottles leading to the same conclusion that Teflon tape around the threads, with or without epoxy adhesive inside the cap, would retard the most the gas escape, while simply sealed bottles, with the pilfer-proof ring of the cap cut, would show the worst performance.

To make these differences explicit, bottles from both types were over-pressurised (17gr dry ice inserted) and sealed with different methods. The test showed that epoxy adhesive until the moment it cures (30' after application) is not capable of holding the pressurised gas in. Teflon tape on the other hand, retards the leakage during the CO_2 sublimation but also affects the connection between the cap and the bottle's neck, facilitating the injection of the cap (Type 32, sample 7).

Monday 28-11-11							
No. of Test	Sample Code	Sealing method	CO_2 inserted (gr)	Total mass before sublimation (gr)		Total mass after sublimation (gr)	Expected int. Pressure (atm)	Leakage % btw subl.
7	31	normal sealing	16,9	b+i+c=	51,61	51,15	16,98	0,89
8	31	epoxy adhesive around threads	17,3	b+i+c+e=	53,23	45,61	17,35	14,32
9	31	teflon tape around threads	17,24	b+i+t+c=	52,18	51,85	17,30	0,63

Wednesday 14-12-11							
No. of Test	Sample Code	Sealing method	CO_2 inserted (gr)	Total mass before sublimation (gr)		Total mass after sublimation (gr)	Expected int. Pressure (atm)	Leakage % btw subl.
7	32	teflon tape around threads	16,99	b+i+t+c=	47,84	47,53	17,07	0,65
9	32	normal sealing	16,84	b+i+c=	47,38	47	16,93	0,80

Figure 49. Table showing the performance of Type 31 and 32 bottles under internal overpressure, and the effectiveness of different cap sealing methods

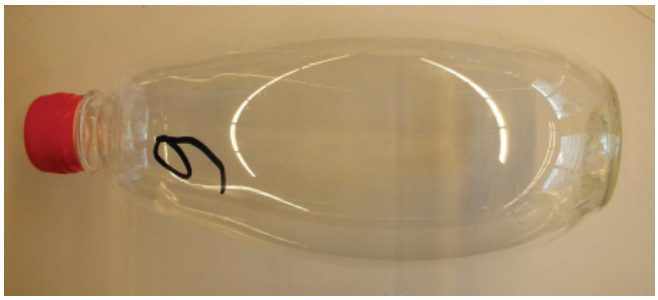

Figure 50. Type 31 presented irregular deformation, the base was stretched and could not stand straight



Figure 51. Type 32, as it is designed for carbonated products, had an even expansion of its volume

The compression tests during Q1, proved that epoxy adhesive should remain in the interior of the caps to prevent exactly this risk of cap injection, so it seems as the combination of Teflon tape and epoxy adhesive is the optimal. The problem however is that until it is cured, it allows the escape of CO_2 from the bottle. This is noticeable when the epoxy adhesive is applied at the exterior of the bottle, around the pilfer-proof ring. Even more, when looking at Type 2 bottles (0,5L, champagne base, 38mm 3-start finish) that abruptly leak after being filled, we can notice minute holes created in the epoxy paste, indicating a passage of gas through this point. This is alarming as it indicates that even when the epoxy is cured, these small holes remain, facilitating the gas leakage. These diodes most probably exist also at the case where epoxy is applied at the interior of the cap.



Figure 52. Combination of Teflon tape around the bottle's threads with epoxy adhesive at the finish of the bottle and the cap

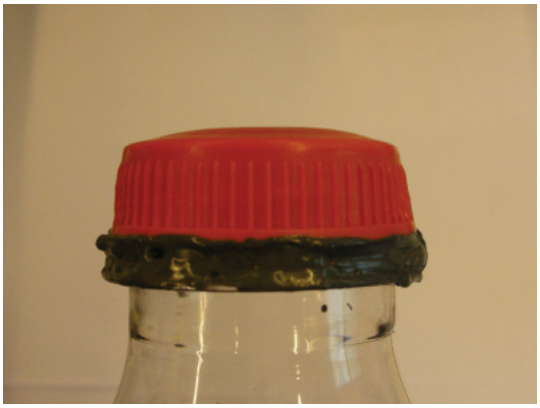

Figure 53. Holes penetrating the epoxy adhesive, created when it was not yet cured, by the escaping gas

Letting the epoxy adhesive cure (for almost 25 min) on the cap, before sealing the bottles is not improving the situation. As it is more difficult to screw the cap, the quality of the sealing is poor (Type 31, Sample 30 showed significant leakage).

In an attempt to accelerate the curing time of the adhesive, the caps were heat-sealed after the application of the glue. The concentrated heat had a negative effect as it deformed the caps and therefore their contact with the bottles' necks was affected.

When parafilm around the cap was combined with epoxy adhesive in the interior, the reduction of the leakage was apparent. To depict the contribution of parafim to this reduction, again Type 2 bottles were used. After the sublimation of the dry ice, the exerted gas was trapped between the exterior part of the cap and the parafilm membrane. Yet, the effect of the parafilm layer is temporary, as the membrane itself is also relatively permeable to gases.



Figure 54. Type 31 bottle sealed with epoxy adhesive inside and outside the cap, and with a layer of Parafilm M wrapped around the cap



Figure 55. Type 2 bottle with a layer of Parafilm M wrapped around the cap. CO2 is temporarily trapped due to the Parafilm M layer

A material that instantly solidifies when applied around the pilfer-proof ring of the cap can be the solution to the problem. In addition it should be capable of resisting the pressure of CO_2 trying to exert. It is necessary to avoid, in other words, the situation observed when melted paraffin wax is applied around the cap of Type 2 bottles. Again minute holes appear at the surface of the sealer.

If we look more carefully at the design of the PCO finish, we notice the appearance of gaps perpendicular to the threads. These pathways- required in order to prevent the injection of the cap when the user is opening a bottle containing a carbonated soft drink- may be related with the problem of leakage that is faced.



Figure 56. Type 31, Sample h2. Epoxy adhesive was applied inside the cap and its curing was accelerated using a heat blower. The cap deformed due to the concentrated heat

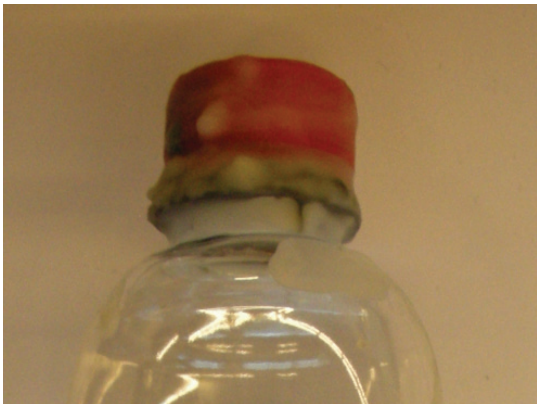

Figure 57. Type 31, Sample 33. Epoxy adhesive was applied inside and outside the cap and after the adhesive was cured, paraffin wax was dripped around the cap

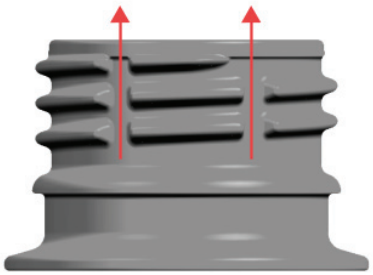

Figure 58. Scheme of typical PCO bottle finish, showing the gaps between the threads to allow the release of CO2 when the bottle is opened

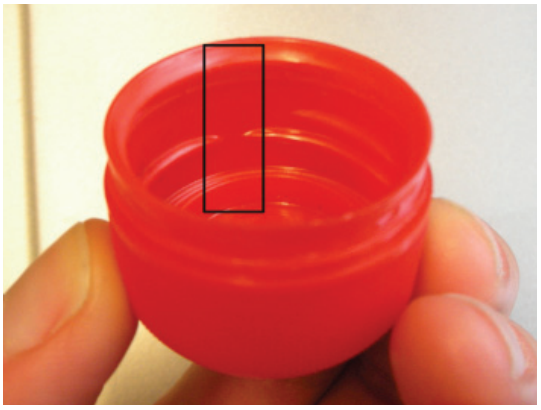

Figure 59. Aspect of PCO cap and indication of the position of the gaps between the threads



Figure 60. Heat Induction Sealing retards the leaking but cannot be combined with PCO caps



Figure 61. The ring indicated in the picture does not allow the addition of a heat induction sealing pad at the finish of the bottle

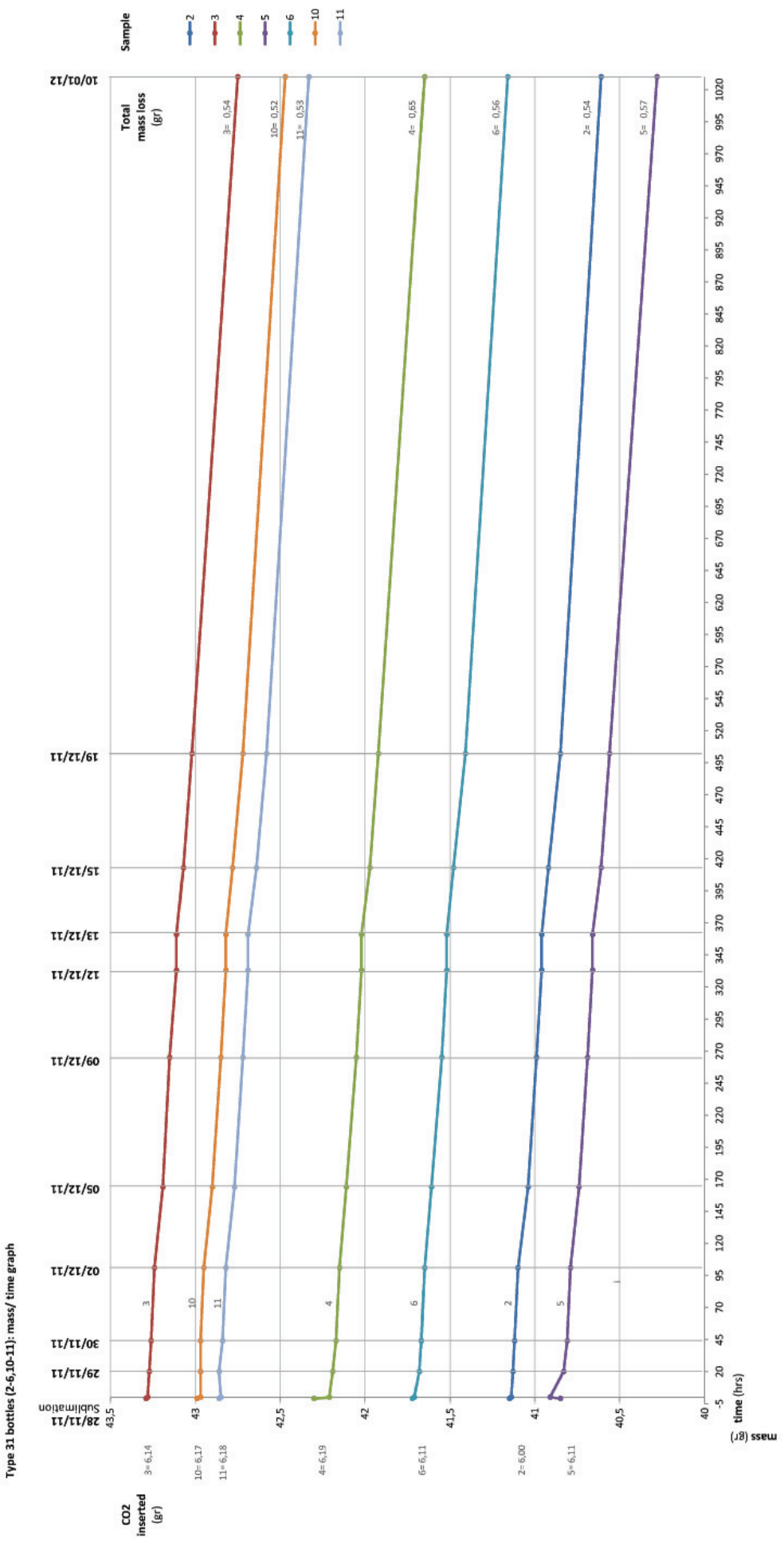

TYPE 31		MASS MEASUREMENT (gr)											LEAKAGE				
DATE		28/11	28/11	29/11	30/11	02/12	05/12	09/12	12/12	13/12	15/12	19/12	10/01	Leakage % during sublimation	Leakage % from 28Nov. to 19Dec.	Leakage % per day 28Nov-19Dec.	Leakage % from 19Dec. to 10Jan.	Leakage % per day 19Dec-10Jan	Total leakage % (43 days)
TIME LINE (hrs)		-1	0	20	44	101	164	265	333	361	413	502	1030						
Code	Description																		
2	5gr/ pilfer-proof ring, teflon on threads	41,35	41,34	41,13	41,12	41,1	41,04	40,99	40,96	40,96	40,92	40,85	40,61	0,02	0,70	0,03	0,59	0,03	1,31
3	6gr/ p-p ring, epoxy adhesive in	43,29	43,28	43,27	43,26	43,24	43,19	43,15	43,11	43,11	43,07	43,02	42,75	0,02	0,60	0,03	0,63	0,03	1,22
4	6gr/ p-p ring, epoxy adhesive out	42,3	42,21	42,19	42,17	42,15	42,11	42,05	42,02	42,02	41,97	41,92	41,65	0,21	0,69	0,03	0,64	0,03	1,33
5	6gr/ normal sealing (2nd time)	40,85	40,91	40,83	40,81	40,79	40,74	40,69	40,66	40,66	40,61	40,56	40,28	-0,15	0,86	0,04	0,69	0,03	1,54
6	6gr/ p-p ring, epoxy adhesive out	41,72	41,71	41,68	41,67	41,65	41,61	41,55	41,52	41,52	41,48	41,41	41,16	0,02	0,72	0,03	0,60	0,03	1,32
10	6gr/ p-p ring, teflon+epoxy adhesive in	42,99	42,97	42,97	42,97	42,95	42,9	42,85	42,82	42,82	42,78	42,72	42,47	0,05	0,58	0,03	0,59	0,03	1,16
11	6gr/ p-p ring, teflon+epoxy in(top)-out	42,86	42,85	42,86	42,84	42,82	42,77	42,72	42,69	42,69	42,64	42,58	42,33	0,02	0,63	0,03	0,59	0,03	1,21

Blue line indicates that sublimation occurred between measurements

Figure 62. Graph and table depicting the mass loss for type 31 bottles (6gr dry ice) sealed with different methods

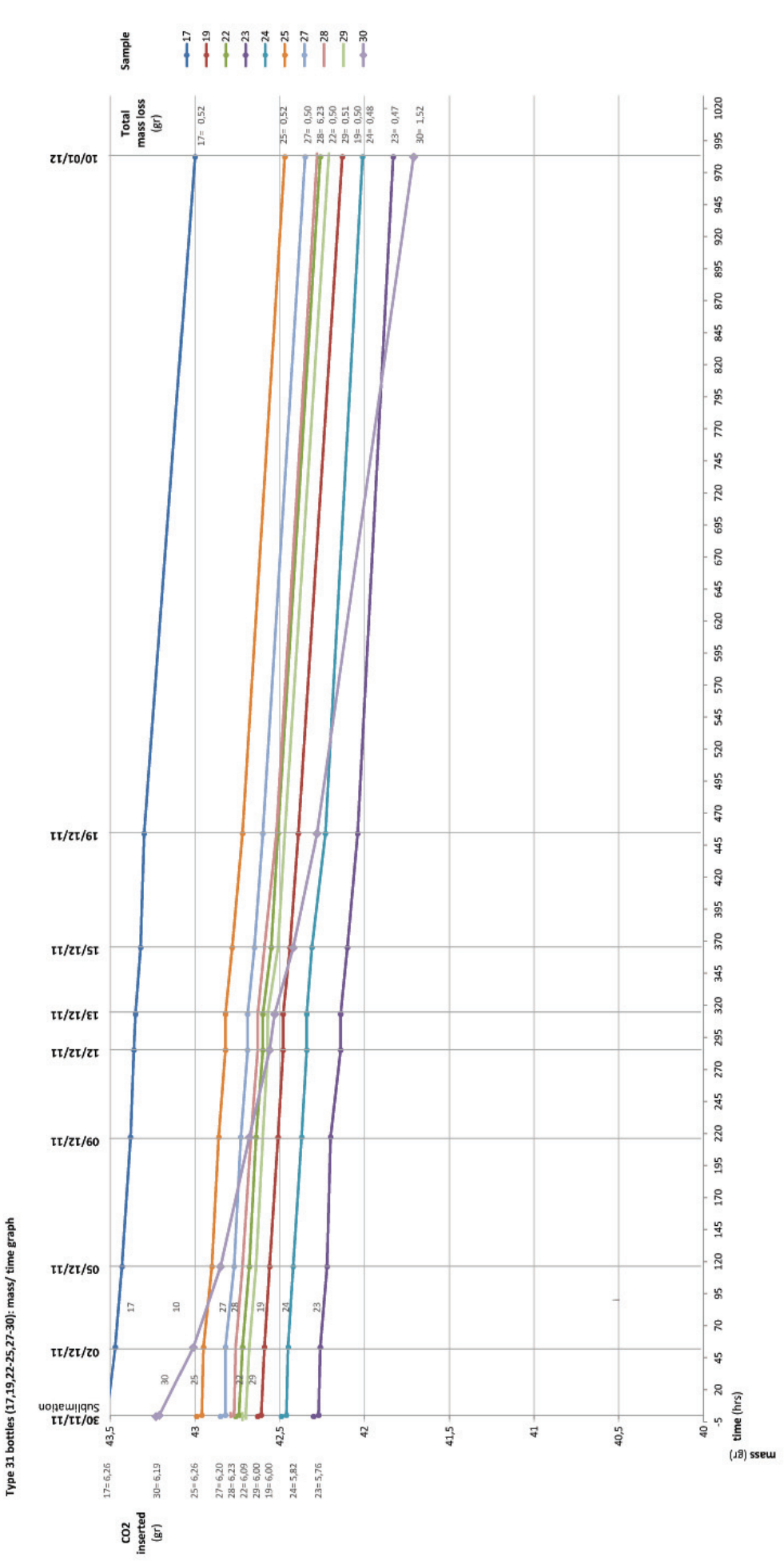

TYPE 31		MASS MEASUREMENT (gr)									LEAKAGE				
DATE		30/11	30/11	02/12	05/12	09/12	12/12	13/12	15/12	19/12	10/01	Leakage % during sublimation	Leakage % from 30Nov. to 19Dec.	Leakage % per day 30Nov-19Dec	Leakage % from 19Dec. to 10Jan.	Leakage % per day 19Dec-10Jan	Total leakage % (41 days)
TIME LINE (hrs)		-1	0	53	116	217	285	313	365	494	982						
Code	Description																
17	6gr/ p-p ring, epoxy in, parafilm (cap)	43,52	-	43,47	43,43	43,38	43,36	43,35	43,32	43,3	43	-	0,51	0,03	0,69	0,03	1,19
19	6gr/ p-p ring, teflon, epoxy in+out	42,63	42,61	42,59	42,56	42,51	42,48	42,48	42,44	42,39	42,13	0,05	0,52	0,03	0,61	0,03	1,17
22	6gr/p-p ring, epoxy in+out, parafilm (cap)	42,76	42,74	42,72	42,68	42,64	42,6	42,6	42,55	42,51	42,26	0,05	0,54	0,03	0,59	0,03	1,17
23	6gr/p-p ring, epoxy in+out, parafilm (cap)	42,3	42,27	42,26	42,22	42,2	42,14	42,14	42,1	42,04	41,83	0,07	0,54	0,03	0,50	0,02	1,11
24	6gr/p-p ring, epoxy in+out, parafilm (cap)	42,49	42,46	42,45	42,42	42,37	42,34	42,34	42,31	42,23	42,01	0,07	0,54	0,03	0,52	0,02	1,13
25	6gr/p-p ring, epoxy in+out, parafilm (cap)	42,99	42,96	42,95	42,9	42,86	42,82	42,82	42,78	42,72	42,47	0,07	0,56	0,03	0,59	0,03	1,21
27	6gr/p-p ring, epoxy in+out, parafilm (cap)	42,85	42,82	42,82	42,77	42,73	42,69	42,69	42,65	42,6	42,35	0,07	0,51	0,03	0,59	0,03	1,17
28	6gr/p-p ring, epoxy in+out, parafilm (cap)	42,79	42,77	42,76	42,72	42,67	42,63	42,63	42,59	42,52	42,28	0,05	0,58	0,03	0,56	0,03	1,19
29	6gr/p-p ring, epoxy in+out, parafilm (cap)	42,72	42,7	42,68	42,64	42,6	42,57	42,57	42,51	42,47	42,21	0,05	0,54	0,03	0,61	0,03	1,19
30	6gr/p-p ring, epoxy in (25°)+out, parafilm (cap)	43,23	43,21	43,01	42,85	42,68	42,56	42,53	42,42	42,28	41,71	0,05	2,35	0,11	1,35	0,06	3,52

Blue line indicates that sublimation occurred between measurements

Figure 63. Graph and table depicting the mass loss for type 32 bottles (6gr dry ice) sealed with different methods. Sample 30 shows greater leakage because the epoxy adhesive around the threads was almost cured when the bottle was sealed

Regarding the CO_2 permeation through the PET walls, different coatings were tested but the reduction of the permeation rate was not significant. Three reasons could be related to this result: the barrier properties of the applied coat were not high, the adhesion of the material on the PET surface was not optimal, or/and the leakage from the cap was extensive so as not to allow for minor differences in the permeation rate from the wall surface to be detected.

It should be noted however, that Type 32 bottles presented so far the best results, although-as it was later discovered- they are not coated with any kind of barrier resin or gliding agent. This is related to the thickness of the bottles as well as to their design (petaloid base). Type 31 bottles have the same neck finish with Type 32 but leak significantly more (this can be noticed at the over-pressurised samples T.31, S. 7-9/ T.32, S. 7, 9) because of base failure.

When roof waterproof coating and nylon spray were applied at the exterior surface of Type 31 samples, minute punctures would appear after the coatings were hardened and pieces would peel off, cancelling the effect of the barrier layer. Into a larger extent this was observed with the application of paraffin wax as an exterior coating. At first, the permeation rate was impressively diminished, yet, because of the brittleness of the material, the coating was easily chopped off. During the compression test with 9 Type 3 bottles, externally coated with paraffin wax, the damage that can be caused to such a brittle coating was evident. In the case of paraffin wax, applying it in the interior of the bottle, to further protect it, also did not prevent it from being detached from the PET surface.

The paraffin wax example was very useful as it made explicit what is occurring to the externally applied coatings, when friction forces between the bottles are developed. The damage, while not visible, is not prevented and therefore an internal coating would be more suitable. Also, by coating the bottles from the inside, we delay the permeant gas from reaching the PET surface, and thus the gas remains longer in the bottle, pressurising its surface.



Figure 64. Type 31, Sample 20 was coated with paraffin wax



Figure 65. After the compression test, most of the paraffin wax applied on this Type 3 bottle was detached



Figure 66. Interior application of the paraffin wax coating barely reduces the problem



Figure 67. Pieces from the roof waterproof coating were detached, cancelling its barrier effect

Considering the above, another approach is to use an elastic coating, that would less easily delaminate. The idea was tested by applying latex either at the exterior or at the interior of Type 31 bottles. The experiments were unsuccessful due to the high CO_2 permeation rate that latex shows. Even more, in the case of the interior coating, when the pellet of dry ice was inserted, it pushed and detached the latex coating from the bottle. In addition, minute pinholes appeared at the surface of the latex layer.

TYPE 31			MASS MEASUREMENT (gr)							LEAKAGE	
DATE: 28 Nov. - 10 Jan.		TIME LINE	Mass before sublimation (gr)	Mass after sublimation (gr)	Time sublimation-coating (hr)	Mass before coating (gr)	Mass after coating (gr)	Time until last measur. (hr)	Final mass (gr)	Leakage % per day before coat	Leakage % per day after coat
Code	Description	External coating									
3	6gr/ p-p ring, epoxy adhesive in	-	43,29	43,28	-	-	-	1030	42,75	0,029	-
a	6gr/ p-p ring, epoxy adhesive in	-	42,07	42,06	-	-	-	413	41,85	0,030	-
g	6gr/ p-p ring, epoxy adhesive in	-	42,53	42,5	-	-	-	413	42,28	0,034	-
a'	6gr/ p-p ring, epoxy adhesive in	-	41,89	41,86	-	-	-	115	41,83	0,030	-
f'	6gr/ p-p ring, epoxy adhesive in	-	41,88	41,86	-	-	-	115	41,83	0,025	-
12	6gr/ p-p ring, epoxy adhesive in	parafilm	42,34	42,33	0	42,33	51,75	1006	51,25	-	0,023
13	6gr/ p-p ring, epoxy adhesive in	roof waterproof coating	42,37	42,45	77	-	48,55	930	46,59	-	0,104
14	6gr/ p-p ring, epoxy adhesive in	vinyl spray (except cap)	41,64	41,69	0	-	48,13	1007	44,17	-	0,196
15	6gr/ p-p ring	paraffin wax (cap before subl.)	42,56	42,55	0	42,55	55,44	983	54,35	-	0,048
16	6gr/ p-p ring, epoxy in+out	paraffin wax	42,74	42,71	0	42,65	73,33	983	72,84	-	0,016
20	6gr/ p-p ring, teflon, epoxy in+out	paraffin wax	42,64	-	0	-	69,86	983	69,38	-	0,017
26	6gr/p-p ring, epoxy in+out, parafilm (cap)	latex	42,98	42,97	246	42,87	58,43	668	58	0,025	0,026
27	6gr/p-p ring, epoxy in+out, parafilm (cap)	-	42,85	42,82	-	-	-	982	42,35	0,029	-

* Expected C02 loss through bottle wall is 0,04gr per week for 0,5L PET bottles
Blue line indicates that sublimation occurred between measurements
Green line indicates external coating was applied between measurements

Figure 72. Table showing the mass loss of coated and uncoated Type 31 bottles





Figure 68. Process of externally coating a Type 31 bottle with latex





Figure 69. Process of internally coating a Type 31 bottle with latex

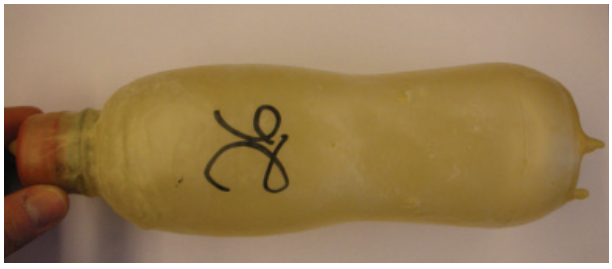

Figure 70. Type 31 bottle externally coated with latex (3 layers)



Figure 71. Type 32 bottle internally coated with latex (2 layers)

Consulting the theory related to the permeability properties of plastics and elastomers and researching on the barrier solutions applied by the food-packaging industry, it was concluded that Ethylene Vinyl Acetate (EVA) resins present the highest barrier properties and then Nylon (especially MXD6, its semi-crystalline form) follows [23]. Yet, although MXD6 has better adhesion to PET than EVA and is more resistant to delamination, it has a melting point at around 240° C [24], which makes it impossible to be processed in the lab for the permeation experiments (and even if it was possible, applying such a hot liquid on the PET surface, that has a maximum service temperature at 71° C, would completely deform the bottle's wall). EVA, on the contrary, can be found in grades with a melting point between 54 to 63° C [25], and different melting indexes, and should be tried out in the following experiments. Also wax blends with EVA additives (EVA adds flexibility to the wax blend, which normally shows excellent barrier properties but is brittle) should be tested.

Material	**Oxygen permeability** ($cm^3.mm/m^2.day.atm$ at 23 °C)	**Moisture vapour transmission rate (MVTR)** ($g.mm/m^2.day$ at 95% relative humidity (RH))	
		at 38 °C	**at 23 °C**
Amorphous PET	3	3	
Oriented PET bottle grade	1.8 to 2.1	1.5	0.23
PEN	0.4	0.8	
PETG	10	3	0.77
Rigid PVC bottle grade	3 to 4	0.8 to 1.1	0.27
HDPE - 0.96 density	42	0.08	0.02
LDPE - 0.92 density	184	0.2	0.08
Polypropylene	38 to 58	0.08 to 0.11	0.02
ABS	42	4.2	0.77
Polystyrene	172	4.2	0.77
PAN - Barex	0.4	2	0.57
MXD6 Nylon	0.1		0.27
Amorphous nylon – 0% RH	0.75		
Amorphous nylon – 100% RH	0.25		
Nylon 6 & 66 - dry	0.4		
Nylon 6 & 66 - wet	2.7	2 to 4	
EVOH (32-mole % ethylene) - dry	0.008		
EVOH (32-mole % ethylene) - 50% RH	0.08		
EVOH (32-mole % ethylene) - 100% RH	0.4	2.3 to 2.7	
EVOH (44-mole % ethylene) - dry	0.04 to 0.08		
EVOH (44-mole % ethylene) - 50% RH	0.2		
EVOH (44-mole % ethylene) - 100% RH	0.8	1.5 to 2	
Blox 0000 Thermoplastic epoxy	0.3	1.47	
Blox 4000 Thermoplastic epoxy	0.04	1.52	

Figure 73. Oxygen and moisture vapour permeability of various polymers

Source: HANNAY, F. 2002. Rigid Plastics Packaging - Materials, Processes and Applications

Other effective solutions used in the food-packaging industry, such as the deposition of silicon oxide coating, require a specific application procedure with industrial equipment, and therefore are not suitable in our case [26].

Given the fact that the tested bottles are uncoated, by using a multi-layer barrier bottle (usually designed for beer) we would achieve a dramatic reduction of the CO_2 permeation rate. This specification however complicates the production of the modules.

Finally, speculating upon the choice of $C0_2$ as a means to pressurise the bottles, and not of a gas with a higher molecular weight (that would permeate less from the bottle), it was concluded that dry ice is the appropriate gas to be used in our case. Other heavier gases (at room temperature) [27] are either dangerous, banned as greenhouse gases, very expensive, or cannot be sublimated into the bottles. On the contrary, dry ice is not only cheap, safe and easily applicable, but is also a recycled product (by-product) resulting from the industrial manufacture of ethanol and other processes.

iv. Defining the structural performance of the pressurised bottles

Process

In total five compression tests took place, with altered variables the number of tested bottles (9/ 12), the bottles' volume (0,5L/ 1,5L), design specifications (for CSD/ non- CSD), condition (used/ new), cap sealing method (Teflon/ Adhesive) and distribution (hexagonal/ orthogonal array).

The internal pressure of the bottles was kept constant for all samples, at a level of 6 atm, in order for the results to be comparable. The level of deformation of the samples and their mass loss were rated after the tests, and the factors leading to failure were analysed.

Thereafter, two series of 3 CSD bottles (0,5L/ 1,5L), with 6atm internal pressure and adhesive applied on their cap were subjected to creep testing. The 0,5L *Type 3* bottles were under a load of 10KN for 68h and the *Type 17* (1,5L, Spa fruit) were loaded with 15KN for 24h. After testing, the samples were examined for leakage and possible crazes and cracks.

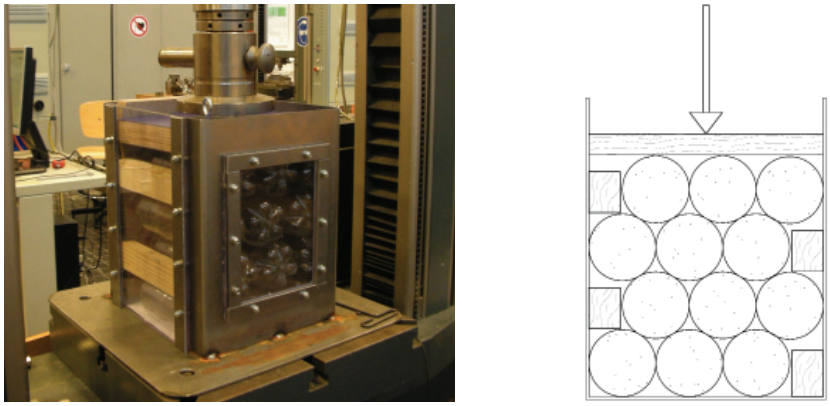

Figure 74. 1st compression test with 12 *Type 3* (0,5L CSD) bottles

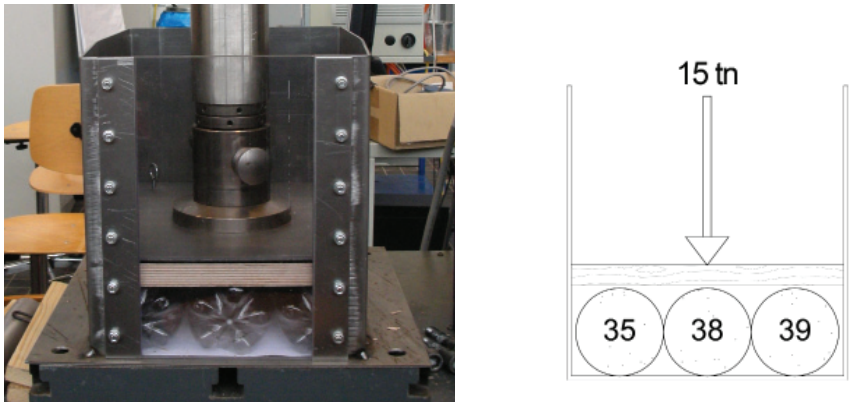

Figure 75. 2nd creep test with 3 *Type 17 (*1,5L CSD) bottles

Results

As previously mentioned, the samples sealed with Teflon tape showed inferior performance during the compression tests, than that presented by the bottles sealed with adhesive. Even more, the *Type 1* bottles (non-CSD), showed the least compressive strength of all samples, severe deformation at 6 out of 9 bottles and an average mass loss of 0,31% for the bottles that remained rigid. All samples presented fissures at the base, which in most cases was stretched. These fissures were usually perpendicular to the direction of the force. Nevertheless, none of the samples bursted, as CO_2 could easily exert from the deformed bottles' neck.

Apart from the sealing method regarding the first two experiments, the experiment itself needed to be revised as the orthogonal shape of the wooden elements inserted to keep the bottles into a hexagonal array, was the cause of concentrated stresses at the surfaces of the peripheral bottles.

The third compression test was performed with a dozen new *Type 3* bottles sealed with epoxy adhesive. Regarding the testing method, this was optimised by replacing the wooden pieces that generated concentrated stresses on the previous two experiments with pvc tubes cut in half.

The group of bottles withstood 2,1tn before failure occurred in one of the samples. In antithesis with the Teflon sealed bottles that failed due to CO_2 leakage from their caps, this bottle bursted at its base. From the tested samples, 9 bottles that presented the least damage and mass loss were subjected to an additional compression test.

During the fourth test, and although the bottles were by 3 less, the compression load reached the value of 7tn. The system presented 140mm of displacement so that the bottles could no be seen from the front Plexiglas opening. At that point, the test was stopped for safety reasons (the Plexiglas sheet on the corner of the safety container started bending outwards) but until then there was no bursting noted nor significant leaking that would lead to rigidity loss. After releasing the load, the bottles returned to their previous shape and remained rigid. All samples presented plastic deformation at the base in the form of pleats on the petaloid's surface.

The 9 *Type 27* bottles withstood 8tn of loading and were displaced by 160mm. In this case, as well, the test was stopped for security reasons and no bursting or serious leaking was detected. The bottles after unloading returned to their previous shape but their base contained damages.

The results from the last two tests are very encouraging, yet more tests should be conducted so that safe conclusions can be drawn.

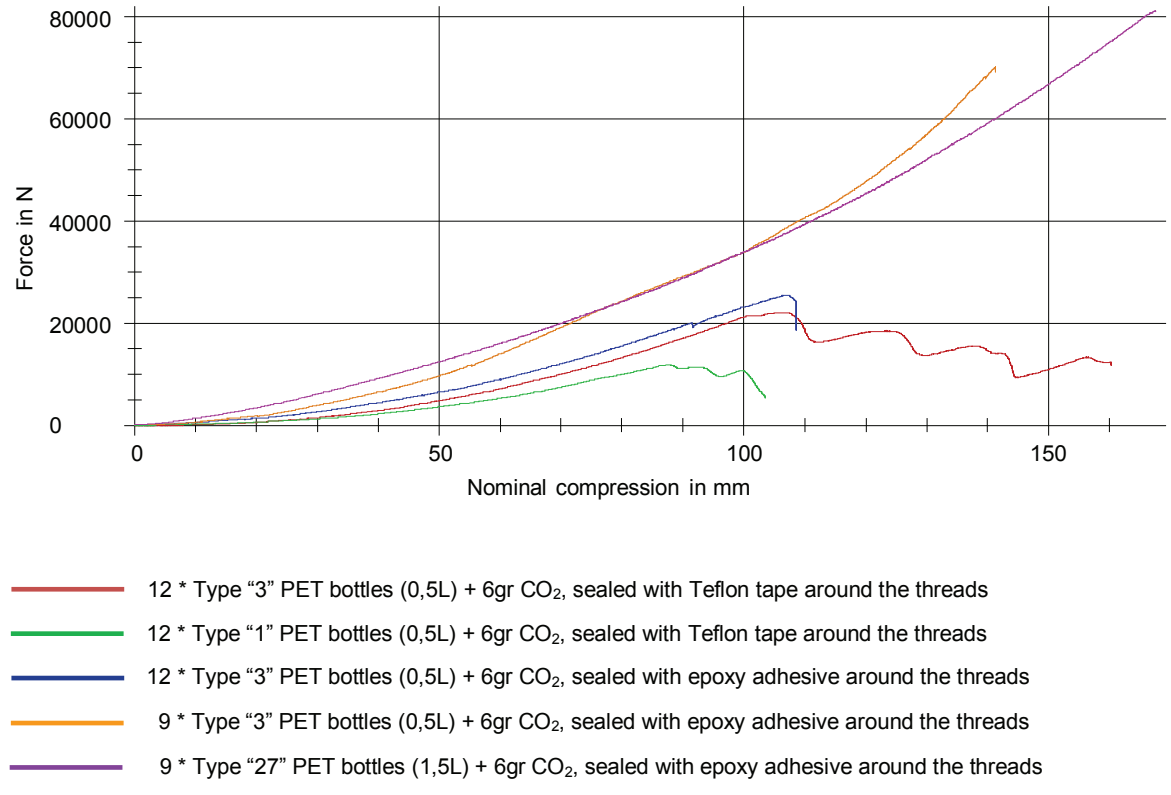

Figure 76. Force over displacement graph presenting the results of the conducted compression tests

Figures 33-38 show samples tested under compression. On the left side, we have Type 1 (0,5L non-CSD) samples and on the right Type 3 (0,5L CSD). All samples were filled with the same amount of dry ice (6gr)

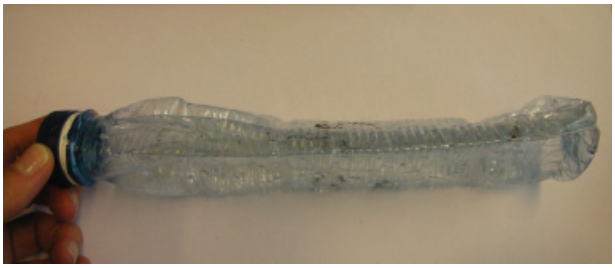

Figure 77. Sample lost its rigidity due to CO_2 leakage and failed



Figure 78. Sample was crushed. Leakage of CO_2 from the cap due to the applied pressure made the bottle lose its rigidity and not be able to withstand the forces. However, the sample did not burst.

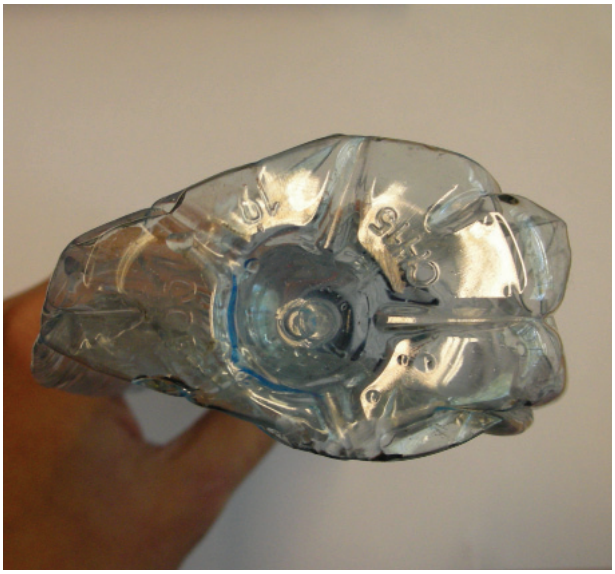

Figure 79. Deformation due to contact with wood insert

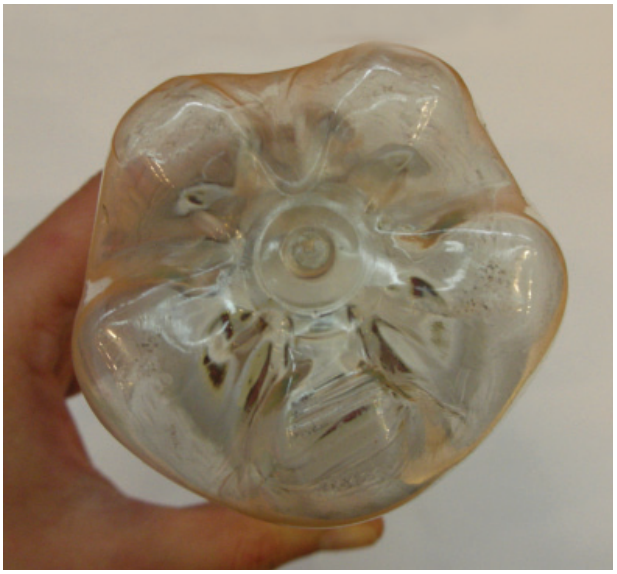

Figure 80. Permanent deformation at base



Figure 81. The most damaged bottles were located at the periphery and in contact with the wooden pieces that kept the bottles into a hexagonal array



Figure 82. In antithesis with the Teflon sealed bottles (a-l) that failed due to CO2 leakage from their caps, sample l', sealed with adhesive, bursted at its base.

In order to better understand the behaviour of the bottles under constant compression load over time, and how the $C0_2$ permeation rate of the bottles is affected by the constant stress, a selection of bottles was also subjected to a creep test. The samples were weighed before and after the test and their leakage was compared with that of equal samples that were not subjected to stress.

The graph deriving from the test results can be explained when taking into account the viscoelastic behaviour of the samples. By applying a load, first we have an instantaneous elastic response and then a viscous retarded response. The deformation they show when stress level is maintained constant is therefore time-dependent and is related to the attempt of the material to relieve stress [28]. This means that the chains of molecules untangle and slip relative to one another to achieve stress relaxation [29] or in other words the bottles change from a round to an ellipsoid shape to better accommodate the pressure. When the load is removed, the bottles recover their original shape.

This type of testing should be repeated, with different applied loads and at different temperatures. The viscoelastic creep data that will be obtained are necessary given that the designed structure will bear long-term loads. Moreover, as viscoelastic materials may have considerably different creep behaviour at different temperatures, it is important to define the performance of the pressurised bottles at changing temperature.

Nr	Specimen identifier	$dL_{(tbefore)}$ mm	$dL_{(tafter)}$ mm	dL_z mm	dL_1 mm	dL_2 mm	dL_3 mm	dL_4 mm	dL_5 mm	t s
1		17,56	19,48	1,92	17,73	17,81	17,86	17,90	17,94	244802,55
2		18,40	19,77	1,37	18,55	18,60	18,63	18,65	18,67	86400,95

Series graph:

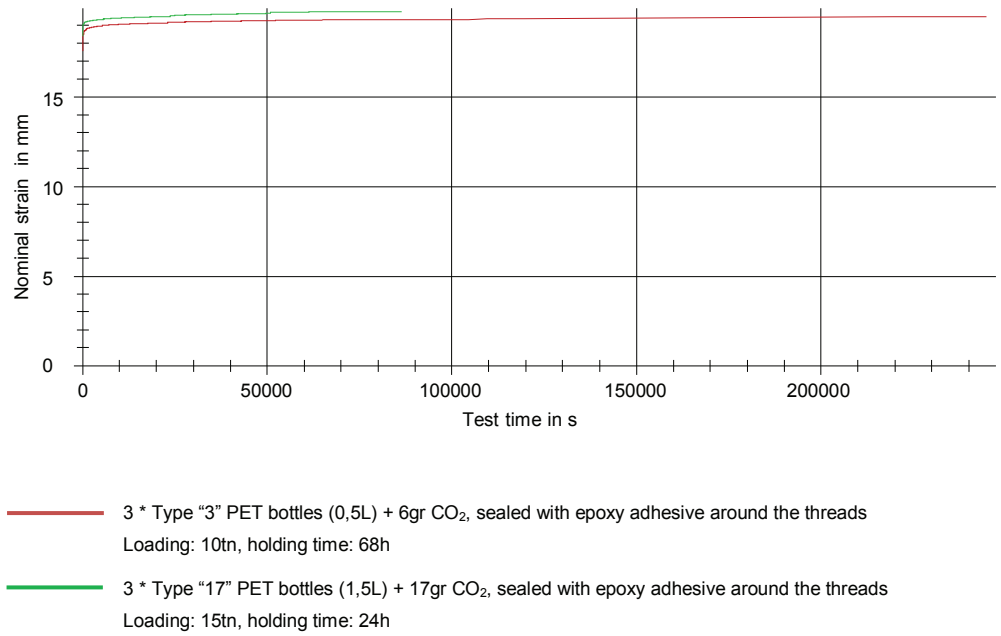

Figure 83. Strain over time graph, depicting the results from the conducted creep tests

v. Investigating the structural performance of the pressurised bottles regarding different bottle-packing methods and boundary conditions

Process

The process of defining the structural properties of the pressurised bottles started with a repetition of the previously conducted compression tests, to test the new series of sponsored bottles Type 31 and 32. Then, Type 3 bottles, entirely coated at their exterior surface with paraffin wax, were tested under the same conditions, to visualise the behaviour of the coating when subjected to friction. Groups of bottles, with lower levels of internal carbonation (4,5 atm, 2,5 atm) were tested in order to verify the choice of 6- 6,5 atm as the appropriate pressure level. Furthermore, tests were conducted with layers of PU foam (with different levels of impact resistance) surrounding the bottles. A first test of the idea of the vacuum bag, joining the bottles into one working element, was conducted, using a “space saver storage bag” out of layers of polyethylene and nylon. Also the idea of filling the gaps between the bottles with Polyurethane spray foam was examined, not only regarding its potential to increase the surface area in contact with the compressive forces but also to reduce the stresses concentrated on the vacuum bag around the caps and bases of the bottles.

Another issue investigated was the proper way of stacking the bottles together (base to base vs. base to cap configuration). Moreover, a group of bottles was tested under axial compression loads, with layers of PU foam placed at the bottom and the top of the safety container.

Figures 67-69 show some of the bottles’ configurations and boundary conditions that were tested:



Figure 84. Type 32, 9 bottles (a-i), 6gr $C0_2$. Test settings: top and bottom protective bubble foil, half pvc tubes between boundary samples

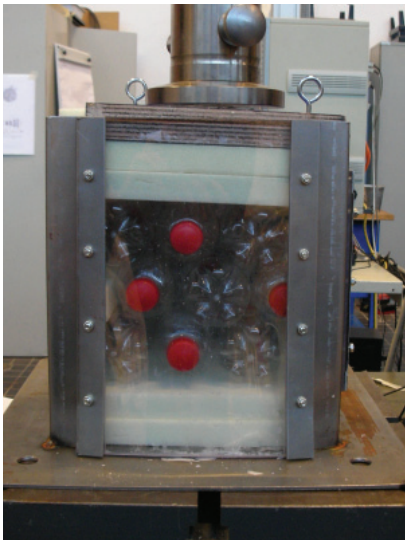

Figure 85. Type 32, 9 bottles (a’’’-i’’’), 6gr $C0_2$. Test settings: top and bottom double layer of PU foam (low tear resistance), foam strips between boundary samples, Interchanging configuration (base-cap-base)



Figure 86. Type 33, 9 bottles (a-i), 6gr $C0_2$. Test settings: top and bottom layer of PU 50mm thick foam (medium tear resistance), 20mm thick side layer of PU foam, PUR between samples, samples placed upright

Results and conclusions

Opening with some general remarks about the new series of tested bottles (Type 31, 32), although their performance regarding CO_2 permeation and leakage is superior than that of previously tested types (ex. Type 3), they are not able to withstand the same amount of load reached with Type 3 bottles, during the compression tests. The bottles were more susceptible to permanent deformations and some of the samples bursted. The later is most probably related to the better sealing of the bottles' caps that reduces the CO2 leakage from the cap during compression and therefore causes additional stress at the base of the bottles. Specifically Type 31 is considered unsuitable due to base failure that may occur when the bottle is subjected to compression. In fact, the inability of the base to hold the amount of inserted CO2 starts to appear, in the form of stretches, from the moment the dry ice is sublimated. Type 32 bottles may not have reached the level of Type 3 bottles, but even so they still withstood a great amount of load.

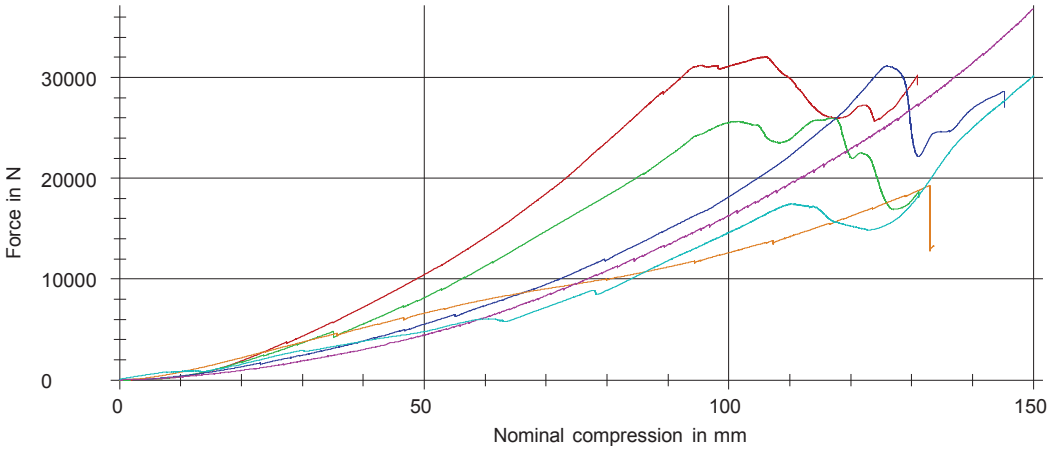

Sample: 9 * Type "32" (a-i) 0,5L + 6gr CO_2
Cap sealing: pilfer-proof ring, epoxy inside
Test settings: top and bottom protective bubble foil, half pvc tubes between boundary samples

Sample: 9 * Type "32" (a'-i') 0,5L + 4gr CO_2
Cap sealing: pilfer-proof ring, epoxy inside
Test settings: top and bottom protective bubble foil, half pvc tubes between boundary samples

Sample: 9 * Type "32" (a''-i'') 0,5L + 2gr CO_2
Cap sealing: pilfer-proof ring, Teflon tape, epoxy inside (end +top)
Test settings: top and bottom protective bubble foil, bottles' bases placed away from wood edges, half pvc tubes between boundary samples

Sample: 9 * Type "32" (a'''-i''') 0,5L + 6gr CO_2
Cap sealing: pilfer-proof ring, Teflon tape, epoxy inside (end +top)
Test settings: top and bottom double layer of PU foam, foam strips between boundary samples, Interchanging configuration (base-cap-base)

Sample: 9 * Type "33" (a-i) 0,5L + 6gr CO_2
Cap sealing: Teflon tape, epoxy inside (end +top)
Test settings: top and bottom single layer of PU foam, foam strips between boundary samples

Sample: 9 * Type "31" (a'-i') 0,5L + 6gr CO_2
Cap sealing: pilfer-proof ring, epoxy inside
Test settings: PU spray foam between and around samples, interchanging configuration (base-cap-base), vacuum bag surrounding samples

Figure 87. Force over displacement graph presenting the results of the compression tests



Figure 88. Type 31, sample f showed significant deformation at the base and could not stand straight



Figure 89. Type 31, sample b bursted during the compression test



Figure 90. Type 31, sample f showed significant deformation at the base



Figure 91. Type 31, sample b bursted during the compression test

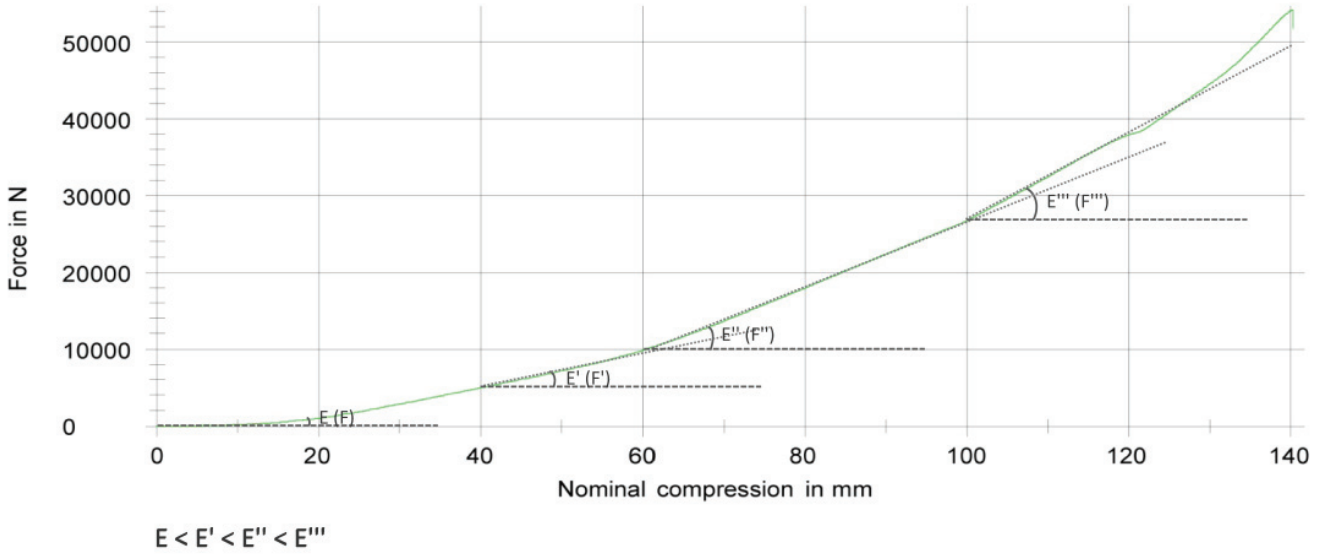

Figure 92. Type 3, 9 bottles (a''-i''), 6gr $C0_2$, cap sealing: epoxy in+out, coating: exterior, paraffin wax, test settings: half pvc tubes between boundary samples. The graph shows the gradual stiffening of the system, as the force increases

Another comment to be made, applicable to all compression tests, is that the tested groups of bottles are stiffening with the increase of force. Looking at the Force/ Nominal compression graphs, we notice the variations in the slope of the curve and the gradual increase of the later (Young's modulus (E) of the system increases). The explanation is that as the system is being compressed, the area of contact between the bottles increases, and in fact, the bottles optimise their position and shape to better transfer the loads.

Regarding the settings of the compression tests, the first tests were conducted with no protective layers applied between the safety container and the group of bottles. As the concentrated stresses at the first and last row of bottles were causing the failure of the later, the test conditions were gradually optimised, first by applying bubble foil between the metal/ wood surfaces and the bottles, then by applying PU foam of low tear strength, and in the end by using stronger PU foam plates. These steps resulted in the efficient protection of the bottles, and proved the importance of introducing foam plates between the rigid FRP skin and the bottles, in the modules. Simultaneously, the problems of combining foam with a rigid object like a PET bottle were depicted. Under extreme loading, the foam can not resist the point loads from the caps and bases of the bottles, which eventually can penetrate it, sometimes even all the way through its thickness (in the case of the caps).

The addition of foam to the system affects its performance during the compression tests. The displacement is noticeably larger, because of the lower Young's Modulus of the foam- and in some cases we observe an increase in the deformation although the force remains constant. The last phenomenon is due to the failure of the foam, and should be avoided. Possible solutions would be to fill the gaps between the bottles with a spray foam material or to introduce a thin rigid layer between the foam and the caps. In addition, using a foam with higher puncture resistance, such as PET foam, will improve the behaviour of the system.

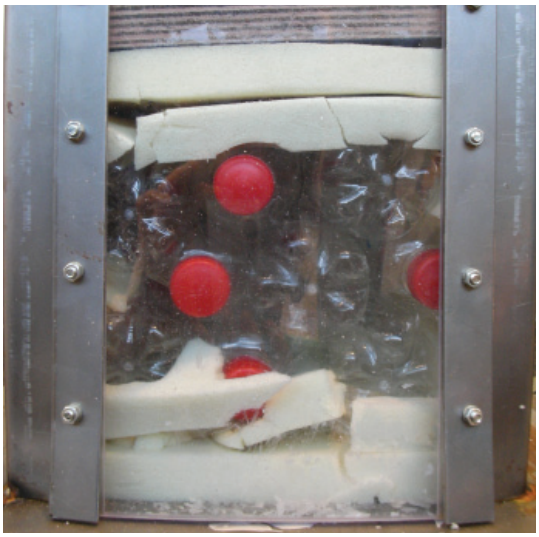

Figure 93. This PU foam has low tear resistance and thus was torn apart during the compression test



Figure 94. Damage on the PU foam (medium tear resistance) from the bottles' bases

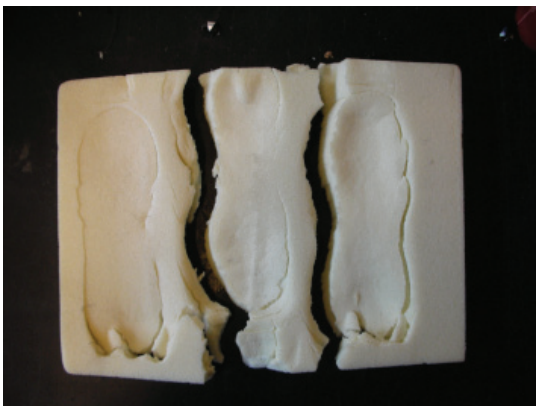

Figure 95. Damages to the PU foam (low tear resistance) after the compression test

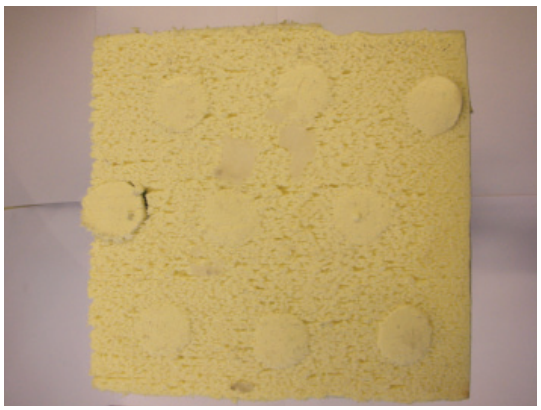

Figure 96. The caps penetrated the total thickness (50mm) of the PU foam (medium tear resistance)

To achieve a better distribution of the applied loads, or in other words, to extend the contact surface between the bottles and the wooden piece on which the force is applied, Polyurethane Spray Foam was inserted in the gaps between the bottles. Unfortunately, the concentrated forces from the bottles's caps and bases to the foam surfaces were not avoided, and thus neither the damage of the foam.

The PUR infill tends to crack under the compressive forces, yet it helps the bottles retain their shape. We notice that a bottle surrounded by hardened PUR, even when it bursts, it will not lose the roundness of its shape and flatten (as it happens it the compression tests with samples without PUR in between them).

Another advantage of using PUR, when we consider the case of a vacuum bag wrapped around the bottles to keep them together, is that the PUR infill reduces the stresses at the membrane of the bag, caused by the geometry and array of the bottles. However, since PUR is hardened before the application of the bag, it forces the bottles into a fixed position, cancelling the effect of the vacuum that will be applied in a later stage. Even worse, as the PUR foam tends to expands, it causes the bottles to move apart, minimising the contact area between them.

On the disadvantages related to the use of PUR, we can add the fact that it is not an eco-friendly material and that it is difficult to detach it from the bottles, at the end-of-life of the module.



Figure 97. Upper sample bursted at the base but did not lose its shape due to the PUR foam around it



Figure 98. PUR foam around the bottles does not prevent the damage of the PU foam from the caps



Figure 99. PUR can easily crack under compression



Figure 100. Concentrated stresses appear at the vacuum bag around the area of the caps

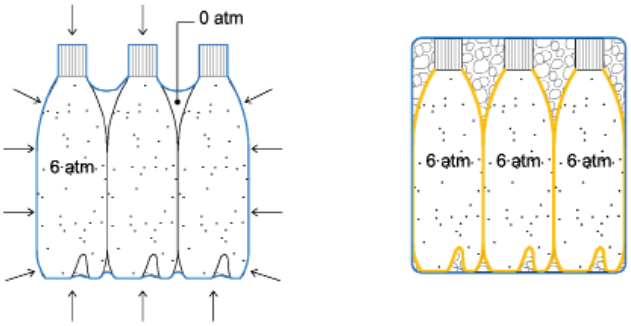

Figure 101. The application of PUR between the bottles before adding the vacuum bag protects the membrane from the caps but also cancels its effect of keeping the bottles tightly together

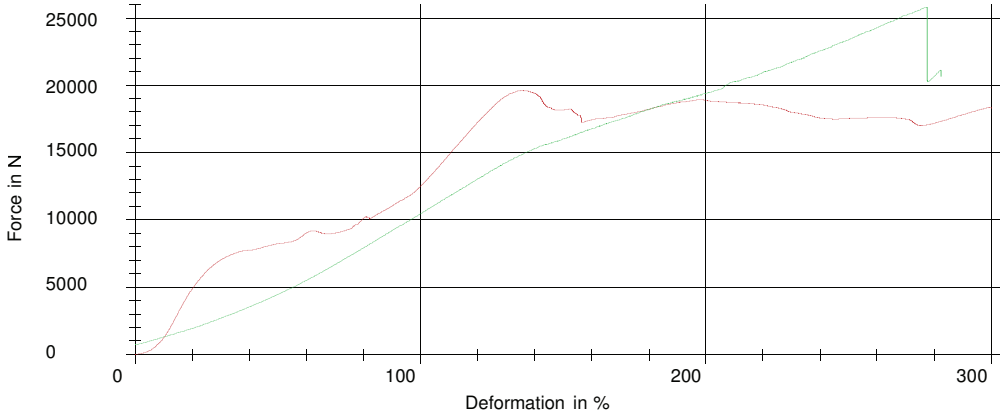

Sample	F_{max} N	dL at F_{max} mm
	19600	67,8
	25800	138,7

Sample: 9 * Type "33" (a-i) 0,5L + 6gr CO_2
Cap sealing: epoxy inside (end +top of cap) and Teflon tape
Test settings: top and bottom layer of PU 50mm thick foam (stronger than in previous tests), 20mm thick side layer of PU foam, PUR between samples, samples placed upright

Sample: 9 * Type "32" (a'"-i'") 0,5L + 6gr CO_2
Cap sealing: pilfer-proof ring, epoxy inside (end +top of cap) and Teflon tape
Test settings: top and bottom layer of PU 50mm thick foam (stronger than in previous tests), 20mm thick side layer of PU foam, PUR between samples

Figure 102. Force over displacement graph presenting the results of the compression tests (layers of PU foam of medium tear resistance added in the safety container)

In relation to the above, a different configuration of the bottles was examined, to achieve equal conditions of distribution of the forces at the top and bottom of the system. The bottles were thus placed with an interchanging configuration of base-cap-base (instead of base-base/cap-cap configuration). This configuration not only does not prevent the damaging of the foam, but is in fact performing worse for various reasons. First, when the bottles are subjected to compression (extreme loadcase), the caps transfer concentrated stresses at the bases' of the adjacent bottles and cause their deformation at that point. Another issue in favour of the base-base configuration is that it is easier and quicker to stack the bottles together.



Figure 103. Base-cap-base configuration, with PUR applied between the samples



Figure 104. Deformation at the base caused by the concentrated loads deriving from the adjacent cap

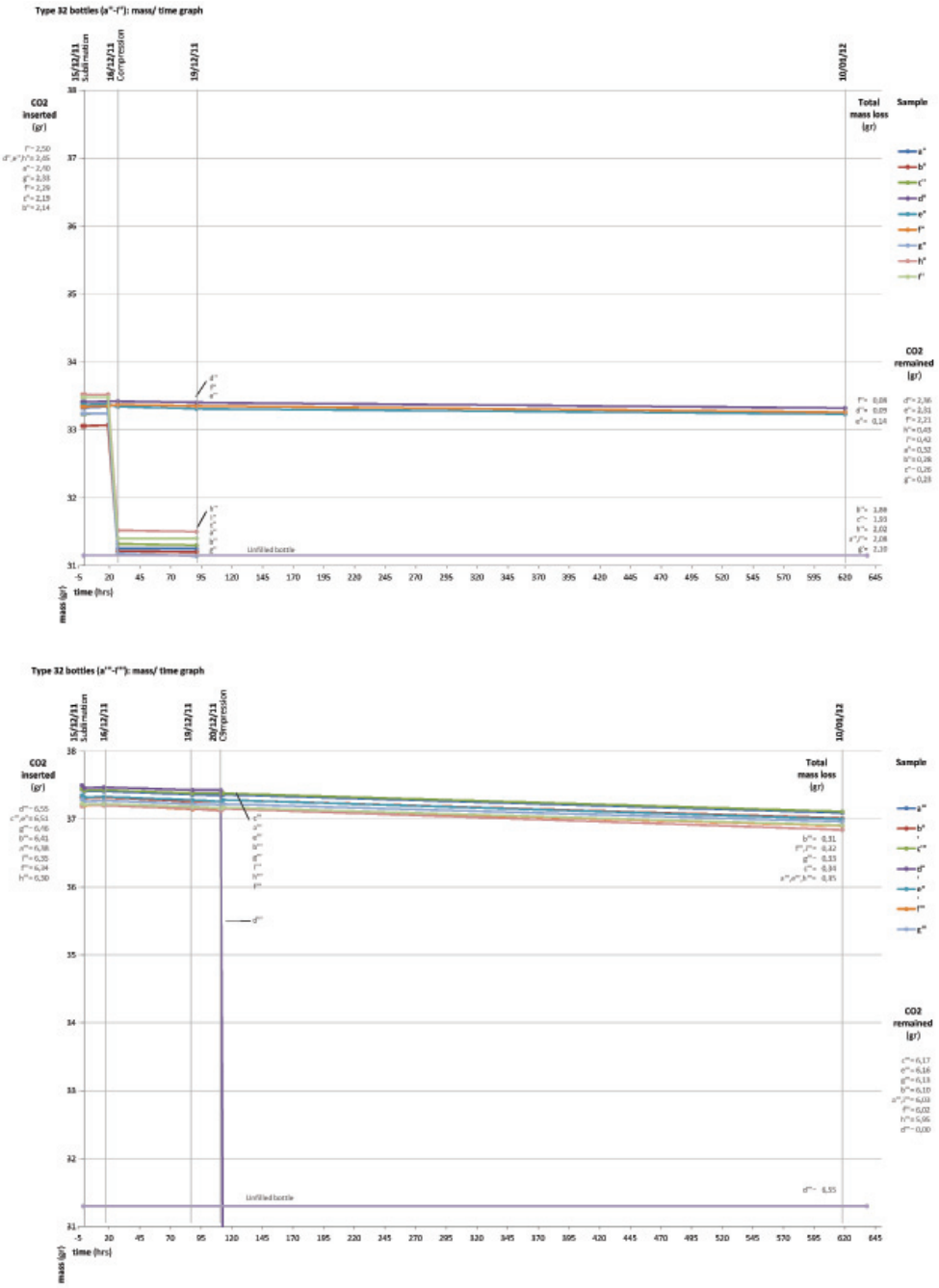

Figure 105. Mass over time graphs and chart, depicting the mass loss of Type 32 bottles before and after compression

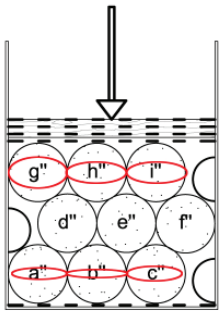

Figure 106. Type 32, 9 bottles (a''-i''), 2gr C02. Cap sealing: pilfer-proof ring, epoxy inside(end +top of cap) and Teflon tape. Test settings: top and bottom protective bubble foil, half pvc tubes between boundary samples protective bubble foil during compression. Max. force: 31000N (displ.: 125mm). Max. displacement: 145mm. The samples that leaked and deformed are noted with red

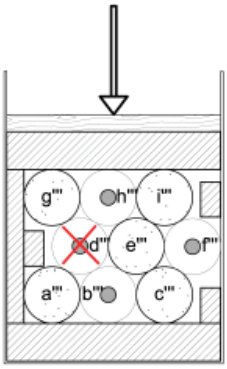

Figure 107. Type 32, 9 bottles (a'''-i'''), 6gr C02. Cap sealing: pilfer-proof ring, epoxy inside (end +top of cap) and Teflon tape. Test settings: top and bottom double layer of PU foam, foam strips between boundary samples, Interchanging configuration (base-cap-base). Max. force: 19000N. Max. displacement: 135mm. The samplethat bursted is noted with red

TYPE 32	MASS MEASUREMENT (gr)						LEAKAGE						
DATE	15/12	15/12	16/12	16/12	19/12	10/01	Leakage % during sublimation	Leakage % from 15 Dec. to 16 Dec.	Leakage % per day 15 -16 Dec.	Leakage % compression test	Leakage % from 16 Dec. to 10 Jan.	Leakage % per day 16Dec- 10Jan	Total leakage %
TIME LINE (hrs)	-2	0	19	27	91	620							
Code Description													
a'' 2gr/ p-p ring, epoxy+Teflon	33,33	33,33	33,34	31,25	31,25	-	0,00	-0,03	-0,04	6,27	-	-	6,24
b'' 2gr/ p-p ring, epoxy+Teflon	33,06	33,06	33,07	31,21	31,2	-	0,00	-0,03	-0,04	5,62	-	-	5,63
c'' 2gr/ p-p ring, epoxy+Teflon	33,23	33,23	33,24	31,32	31,3	-	0,00	-0,03	-0,04	5,78	-	-	5,81
d'' 2gr/ p-p ring, epoxy+Teflon	33,41	33,41	33,42	33,42	33,4	33,32	0,00	-0,03	-0,04	0,00	0,30	0,01	0,27
e'' 2gr/ p-p ring, epoxy+Teflon	33,37	33,37	33,38	33,34	33,31	33,23	0,00	-0,03	-0,04	0,12	0,33	0,01	0,42
f'' 2gr/ p-p ring, epoxy+Teflon	33,34	33,34	33,35	33,37	33,35	33,26	0,00	-0,03	-0,04	-0,06	0,33	0,01	0,24
g'' 2gr/ p-p ring, epoxy+Teflon	33,24	33,24	33,24	31,18	31,14	-	0,00	0,00	0,00	6,20	-	-	6,32
h'' 2gr/ p-p ring, epoxy+Teflon	33,52	33,52	33,52	31,52	31,5	-	0,00	0,00	0,00	5,97	-	-	6,03
i'' 2gr/ p-p ring, epoxy+Teflon	33,48	33,48	33,48	31,4	31,4	-	0,00	0,00	0,00	6,21	-	-	6,21
						Average	0,00	-0,02	-0,03	4,01	0,32	0,01	4,13
DATE	15/12	15/12	16/12	19/12	20/12	20/12	10/01	Leakage % during sublimation	Leakage % from 15 Dec. to 20 Dec.	Leakage % per day 15 -20 Dec.	Leakage % compression test	Leakage % from 20 Dec. to 10 Jan.	Leakage % per day 20Dec- 10Jan	Total leakage %
TIME LINE (hrs)	-2	0	16	88	111	113	618							
Code Description														
a''' 6gr/ p-p ring, epoxy+Teflon	37,44	37,41	37,41	37,36	37,35	37,36	37,09	0,08	0,16	0,03	-0,03	0,72	0,03	0,93
b''' 6gr/ p-p ring, epoxy+Teflon	37,32	37,31	37,32	37,26	37,26	37,28	37,01	0,03	0,13	0,03	-0,05	0,72	0,03	0,83
c''' 6gr/ p-p ring, epoxy+Teflon	37,45	37,42	37,43	37,38	37,38	37,38	37,11	0,08	0,11	0,02	0,00	0,72	0,03	0,91
d''' 6gr/ p-p ring, epoxy+Teflon	37,5	37,46	37,47	37,43	37,43	29,93	-	0,11	0,08	0,02	20,04	-	-	20,19
e''' 6gr/ p-p ring, epoxy+Teflon	37,35	37,32	37,33	37,28	37,26	37,28	37	0,08	0,16	0,03	-0,05	0,75	0,04	0,94
f''' 6gr/ p-p ring, epoxy+Teflon	37,22	37,2	37,21	37,14	37,16	37,16	36,9	0,05	0,11	0,02	0,00	0,70	0,03	0,86
g''' 6gr/ p-p ring, epoxy+Teflon	37,29	37,26	37,27	37,22	37,21	37,22	36,96	0,08	0,13	0,03	-0,03	0,70	0,03	0,88
h''' 6gr/ p-p ring, epoxy+Teflon	37,19	37,21	37,2	37,15	37,12	37,15	36,84	-0,05	0,24	0,05	-0,08	0,83	0,04	0,94
i''' 6gr/ p-p ring, epoxy+Teflon	37,23	37,21	37,22	37,18	37,16	37,17	36,91	0,05	0,13	0,03	-0,03	0,70	0,03	0,86
							Average	0,06	0,14	0,03	2,20	0,73	0,03	3,04

* Expected C02 loss through bottle wall is 0,04gr per week for 0,5L PET bottles
Blue line indicates that sublimation occurred between measurements
Red line indicates that a compression test took place between measurements
Significant C02 loss and noticeable deformation after compression test
Total C02 loss and major permanent deformation after compression test (flattening)
Bursting at base
Mass augmentation after compression test

2.1.2.4. Conclusions

The experimental procedures presented in this chapter may prove the outstanding structural rigidity of the internally pressurized bottles but also highlight the failure risks of the proposal. The CO_2 leakage occurring from the bottles indicates that the core's rigidity will decrease in a short period of time, and eventually the bottles will return to their prior, un-pressurised condition. Even more, fatigue loading may cause the deformation of the cap and bottle neck, facilitating the escape of CO_2 from the cap.

Measures in order to reduce the CO_2 permeation rate such as the use of new bottles and not reclaimed, the application of expensive barrier coatings that can difficultly be separated from the PET surface, and the application of adhesive on the caps, complicate and delay the production process of the module and interfere with the recyclability of the PET bottles.

On the other hand, the observed resistance of the bottles under compressive loading, impressive as it may be, is also not necessary for the efficient performance of a typical building module. The question that arises in this case is whether the bottles used in their original, un-pressurised state, can compose a core structure, that shows sufficient stiffness and strength. In this scenario, the production of the module would be significantly simplified.

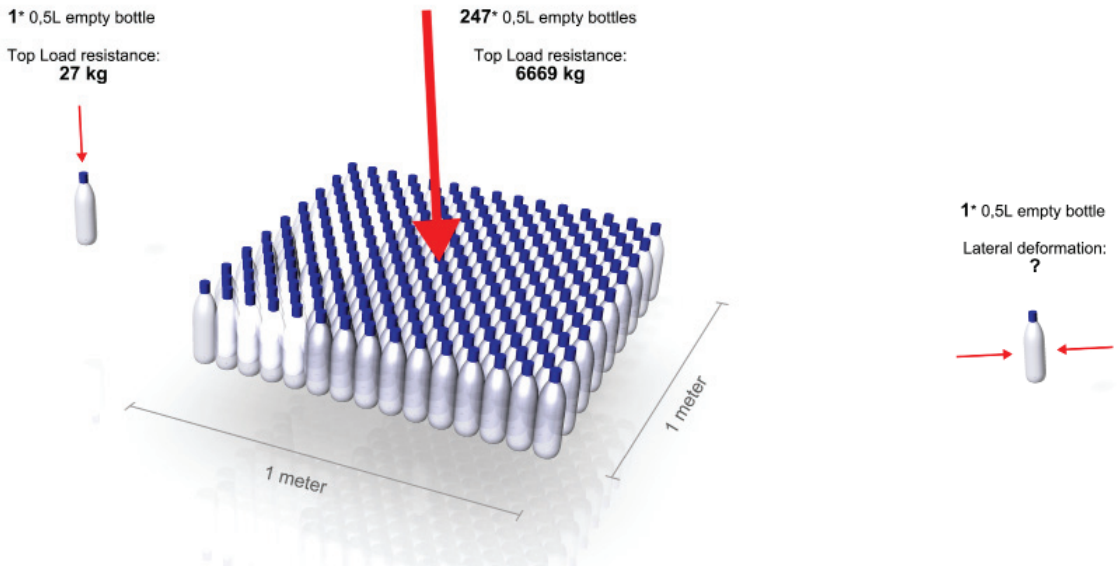

Figure 108. Hypothetical strength on top loading, of a 1sq.m area component composed out of empty bottles. The resistance of the system under lateral deformation is not known

2.1.3. Capped non-pressurized bottle

2.1.3.1 Overview

In this section the resistance of empty capped bottles under compressive loading is examined. Bottles of 3 different sizes and of different geometry are tested in order to choose the optimal configuration. The case of permanently deforming the bottle so as to fit more easily in a standard construction panel is also evaluated.

2.1.3.2. Experimental procedures

i. Compressive strength of bottles

At first, a series of Type 32 bottles were tested under top loading. In general, the samples show initial resistance to deformation under compression up to the value of 300N (approximately). After this point, the neck starts to collapse in the bottle, until the next stable and stiff configuration is reached. At this stage the cap and neck are entirely and permanently emerged in the bottle and the PET walls are in contact with the compression head of the machine (Deformation= 60mm). This configuration can withstand up to 700N before the bottles start to lose their stiffness again.

Sample 2 (Test no 2-7) showed deformation softening due to the several loading cycles to which it was subjected. At Test no.7, a hole was introduced to the wall surface. The sample withstood 170N before buckling.



Figure 109. Type 32, Sample 1 (Test no. 1)



Figure 110. Stiff configuration (Deformation: 60mm)

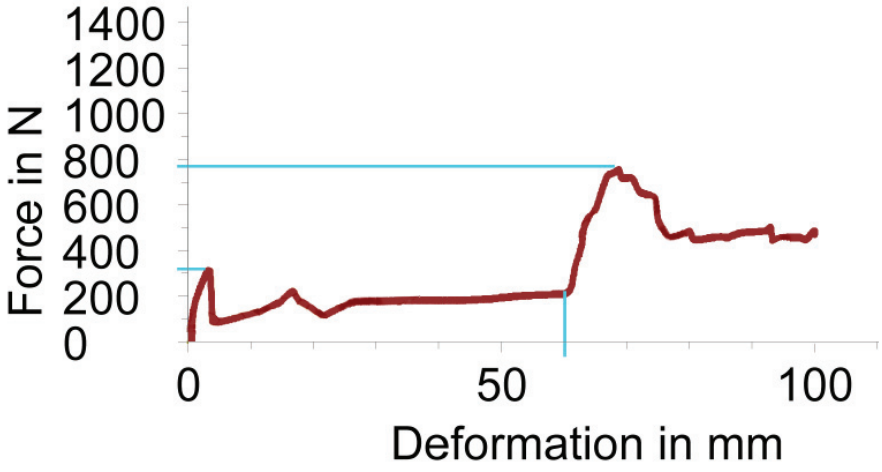

Figure 111. Force over Deformation graph depicting the observed behaviour of Type 32 bottles under compression. After 60mm of deformation the bottle starts to built up strength due to its geometry

The test concerning Type 34 bottles (1L, CSD) showed that this type is less rigid than Type 32. Usually big bottles have similar weight to that of smaller ones (therefore wall thickness is less), a fact that makes them more efficient beverage containers but less potential for structural elements. In our case, the waist at the middle of the bottle is an additional weak point, that lowers the resistance of the bottle to deformation. Thus we see that for sample 4 (deformed by 100mm at 850N load), the deformation was located around the waist and the neck did not collapse in the bottle. Sample 6 (Test no. 14) withstood 100N loading before starting to buckle at its waist.

Type 35 bottles (1,5L, non-CSD) also deform more easily than Type 32 bottles, due to their base and rib design. The ribs however act as hinge points, allowing the bottle to recover once the load is removed.

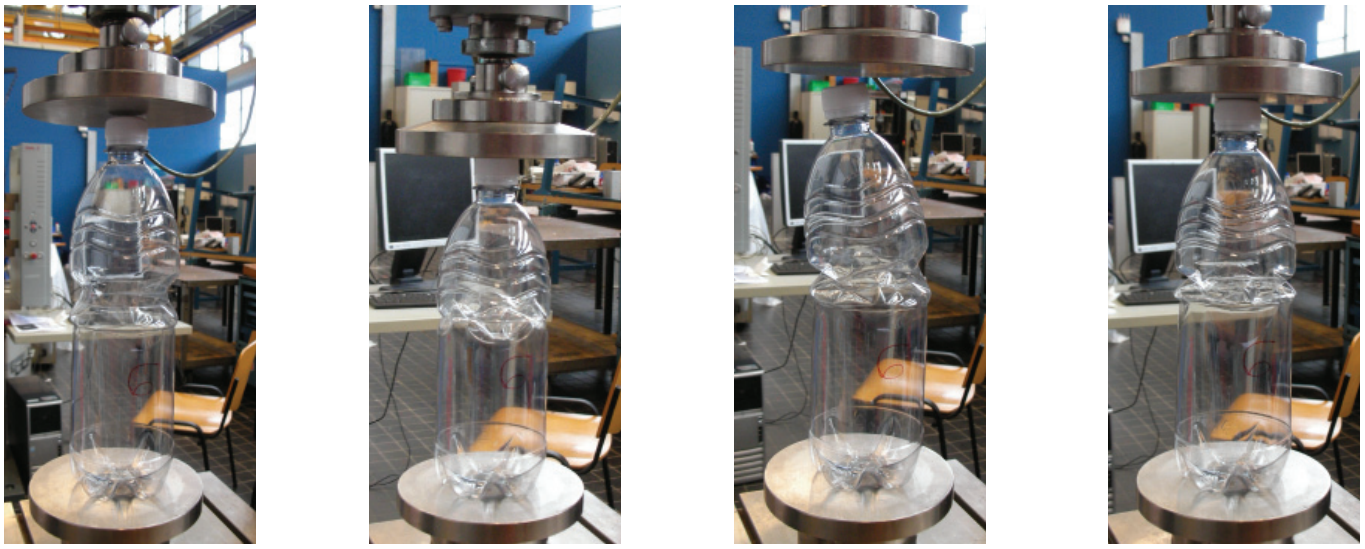

Figure 112. Type 34, Sample 6 (Test no. 14)

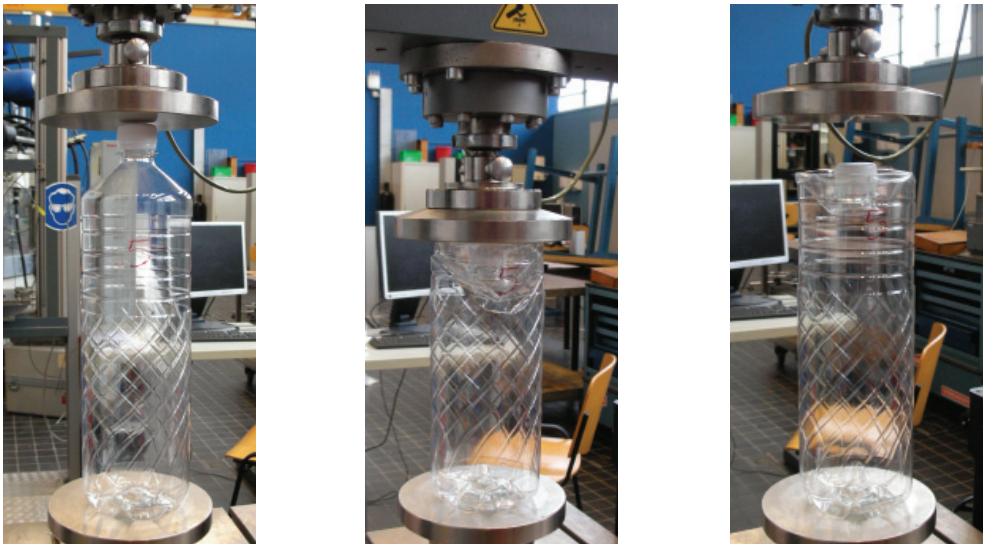

Figure 113. Type 35, Sample 5 (Test no. 11-13)

Test results:

Test no.	Specimen identifier	Sample	Type	F_{max} N	dL at F_{max} mm	Test speed mm/min
1		1	32	680	67.5	10
2		2	32	288	3.0	
3				305	3.1	
4				330	3.7	
5				158	1.7	
6				685	55.8	
7		*cut*		405	50.4	
8		3	32	758	68.7	200
9				498	77.3	
10		4	34	198	70.9	
11		5	35	873	99.7	
12				1450	149.8	
13				408	82.4	
14		6	34	253	43.5	

Series graph:

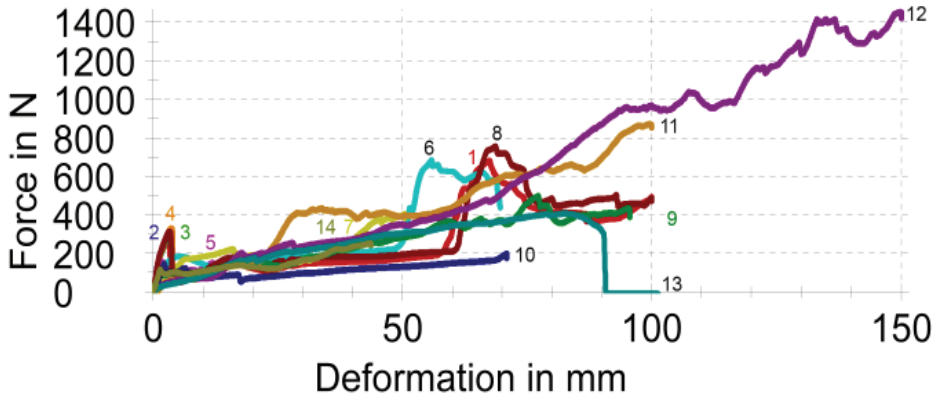

Figure 114. Data from the top-load tests performed with samples 1-6 (Types 32, 34, 35)

After determining the behaviour of one bottle under top loading, 9 Type 32 bottles (a-i), empty and sealed, were places in the safety container and tested under compression. The samples were compressed until total deformation reached 57mm and the caps were completely sank into the bottles. The caused deformation was permanent and the upper part of the bottles' walls was folded to form pentagons or hexagons in plan. Thus, due to the applied loading, a honeycomb structure was naturally formed.



Figure 115. Configuration of bottles before Test no. 1

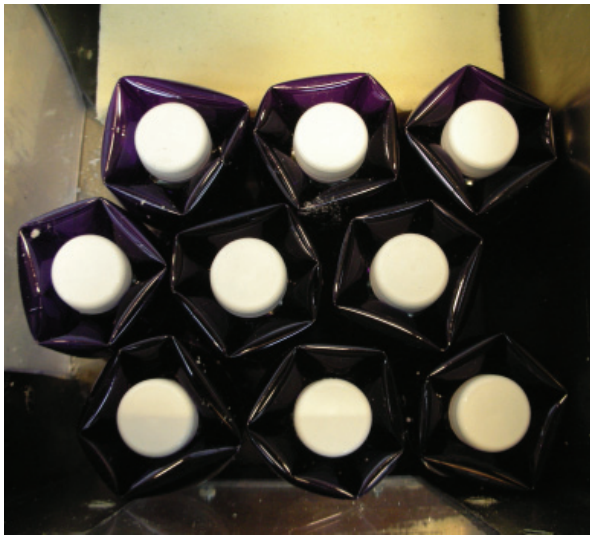

Figure 116. Configuration of bottles after Test no. 1

The already deformed samples (from Test no. 1) were subjected to 4 loading cycles. Between cycles there was loss in stiffness and strength observed. Throughout the tests however, the bottles repositioned themselves to form a much better hexagonal pattern.

The tests showed, judging from the curves in the Force/Deformation graph, that the limit of 2000N of compression load on 9 bottles can form a reliable safety margin.

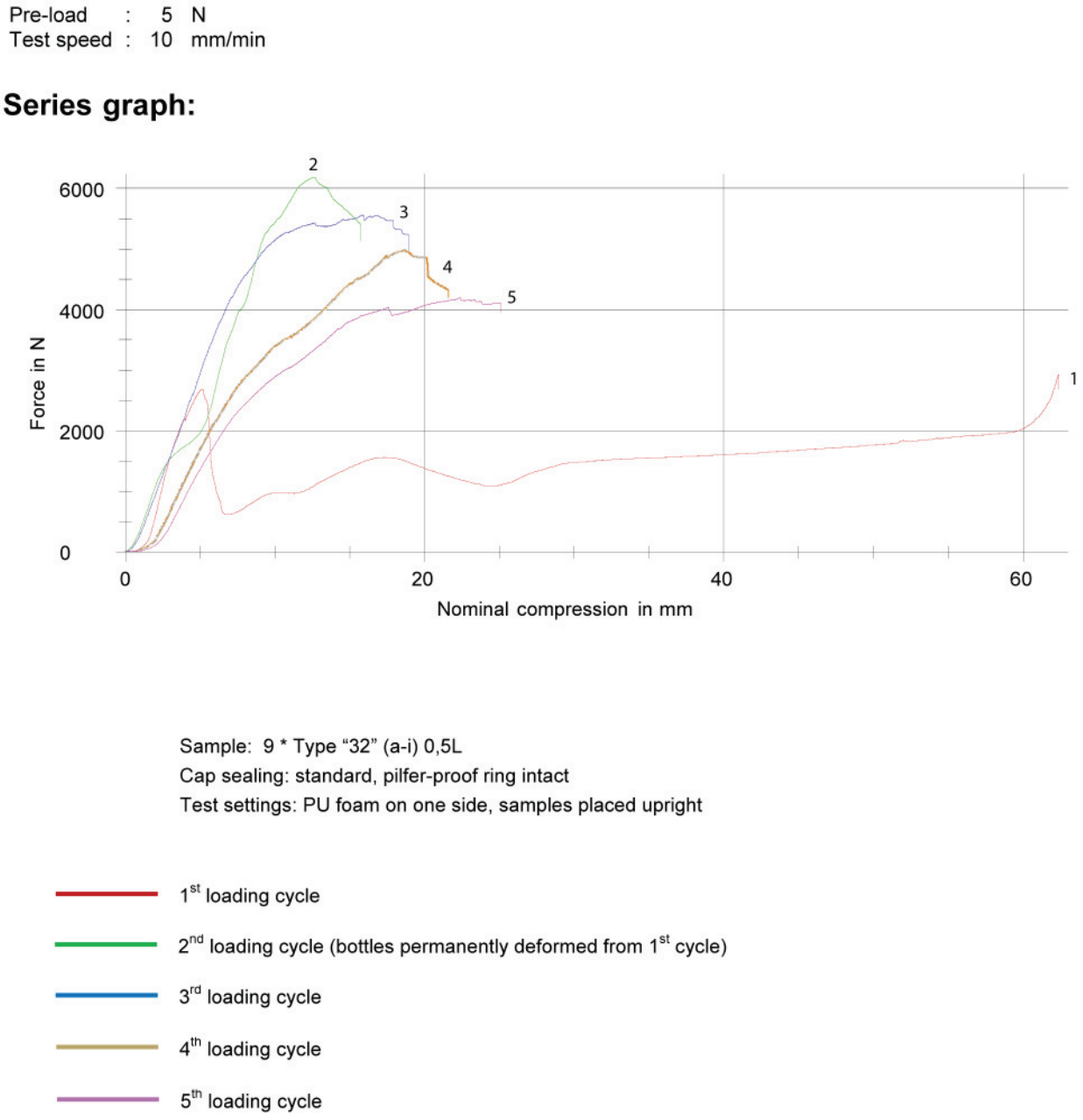

Figure 117. Data from the top-load tests performed with 9 Type 32 bottles (samples a-i)

9 Type 34 bottles (a-i) were also tested together under compression. The samples were first compressed to a max. deformation of 25mm (Test no. 1-6) to observe their stiffness and ability to recover. During Test no.1, the system resisted 950N before buckling started to occur to some of the samples. The displacement was purely elastic and the initial shape was recovered once the load was removed. Test no.2 gave similar results, with the system being displaced by 4mm and no permanent deformation occurring once unloaded. During this test, the buckling at the waist of the bottles started to become visible. During Test no.3, the bottles were displaced by 7mm, fact that resulted in 0,5mm of permanent deformation. After this cycle the bottles started to lose strength between cycles, indicating that some damage was affecting the system. The fact that by Test no. 4 already 1/3 of the strength was lost shows that the material is sensitive in cycling loading. By Test no. 5 the damage is visible and 0,8mm of permanent deformation were added to the system. Then Test no. 6 showed that the design strength of the system is around 100N. Lastly, Test no. 7 was performed at a 20 times higher speed, in order to observe the behaviour of the system when pushed to its limits. Thus the last curve on the Force/ Displacement graph is not comparable to the rest.

To conclude, this type of bottle was found unsuitable for its use as structural element because of the damage that appeared between each loading cycle. This means that people walking on the module, for example, would cause significant degradation to the system.

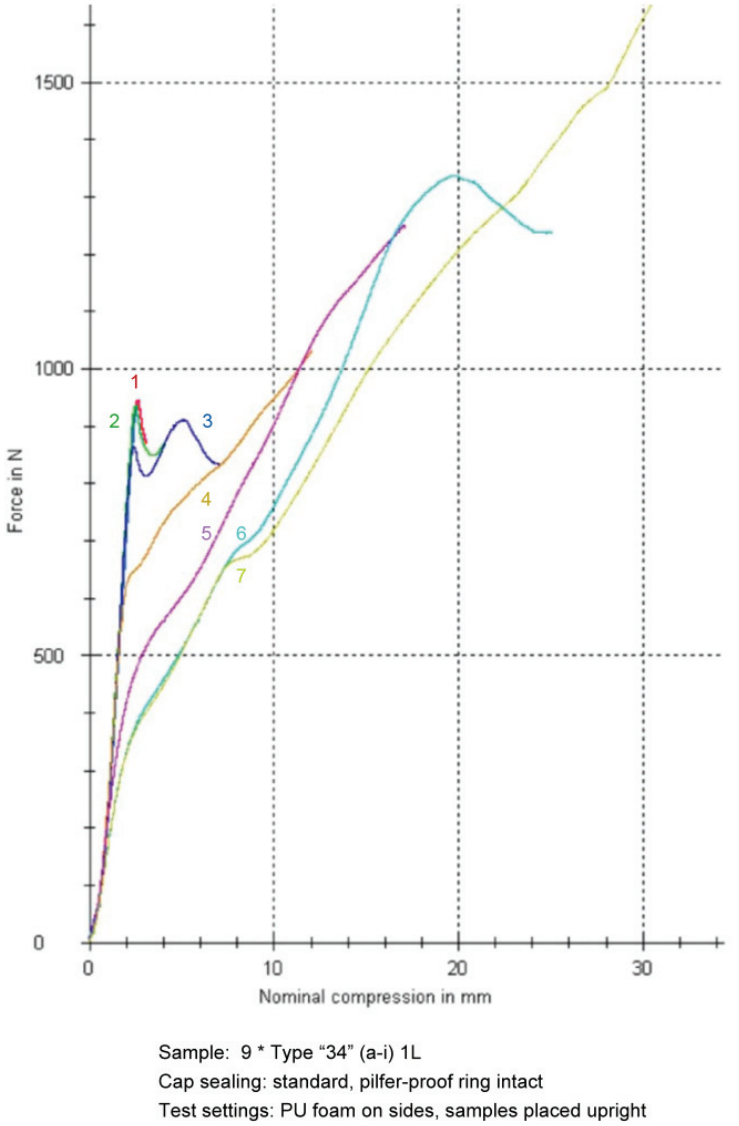

Figure 118. Data from the top-load tests performed with 9 Type 34 bottles (samples a-i)

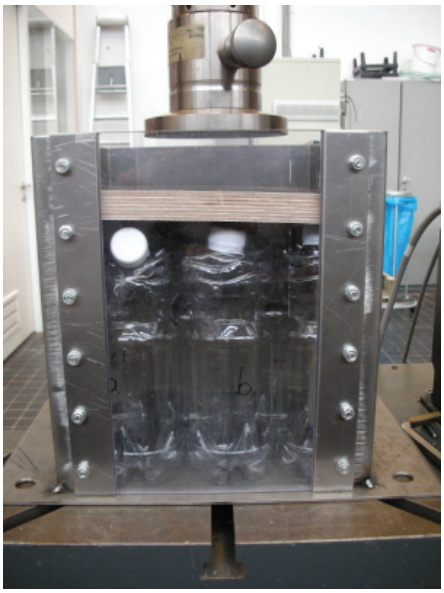

Figure 119. Permanent deformation after Test no. 7

ii. Cyclic loading and creep tests

To evaluate the performance of Type 32 bottles regarding fatigue, a cyclic loading test was performed with a constant applied force equal to 200N (speed 10mm/min, 10.000 cycles), a value that approximates the load the bottles will be subjected to in the real construction. In order to observe the loss in material strength between cycles, it was necessary to record the changes in displacement in a Strain/Time graph. From the experiment, the following observations were made:

• The system stabilizes over time adhering consistent properties (max and min deformation tend to stabilize)
• A minimum deformation is seen when force is released from the specimens. This deformation is thus related to the creep of the bottles due to the loading (and the time given to them to relax)
• In the Strain/Time graph a cycling change in the values of the -other than that- stable max and min deformation is observed, related to the day-night temperature circumstances
• Minimum displacement occurs at highest temperatures due to the air contained in the bottles. An increase in temperature increases the internal pressure and the resistance of the bottles to the applied force, and so strain is less.

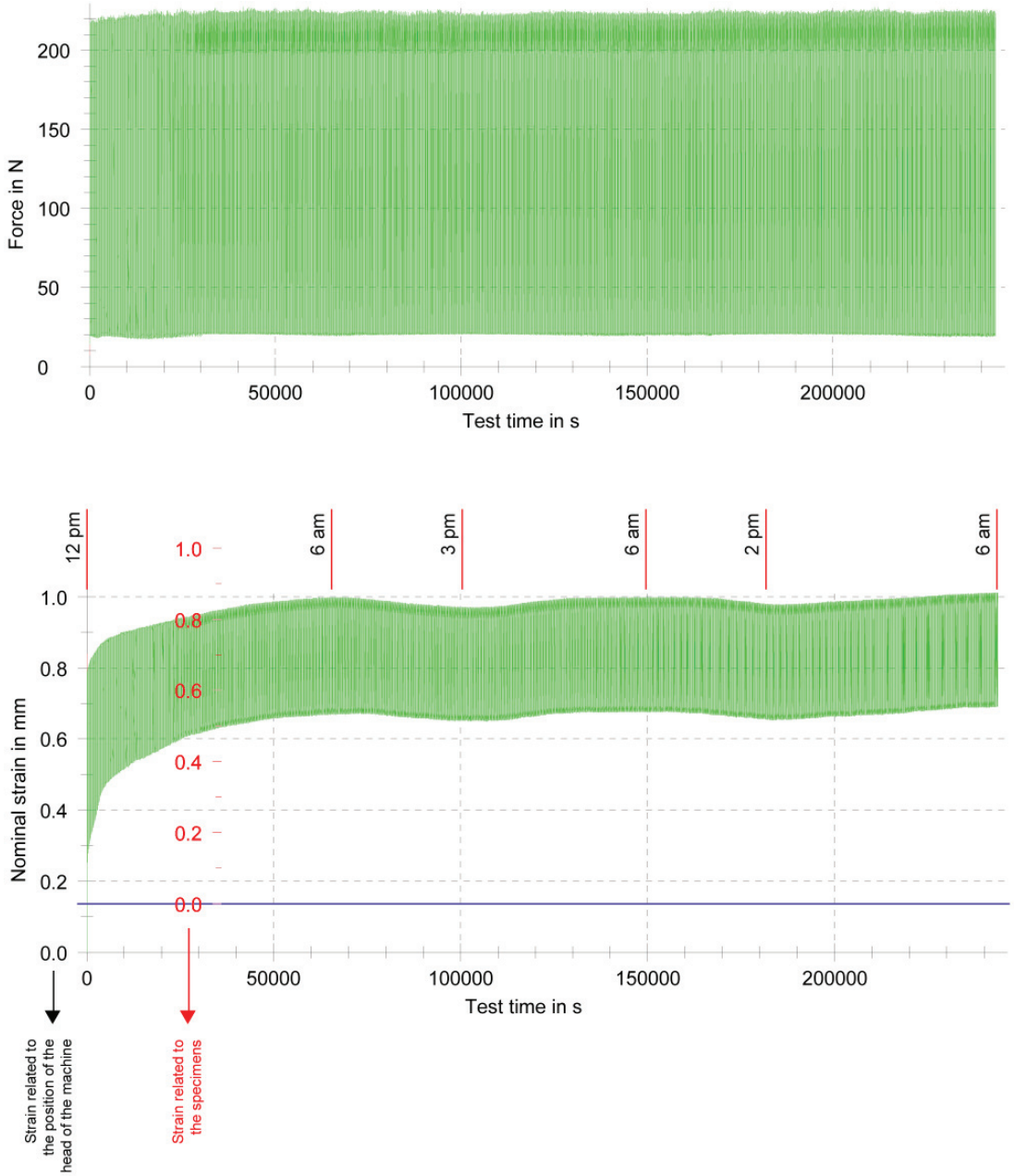

Figure 120. Graphs depicting the behaviour of 9 Type 32 bottles under fatigue loading

In order to compare the normal to the “crushed”bottles, the cyclic loading test was repeated with 9 “crushed”bottles. The same bottles, previously described cyclic loading test, were compressed (deformation: 60mm/ speed: 500 mm/min), to be tested again under cycling loading. The bottles were individually compressed in order for the settings to be controlled, and therefore for the applied deformation at each bottle to be equal.

It was noticed that the folding of the bottles’ neck differed between specimens and is probably related to the material. Usually the folding is divided in 5 parts (maybe related to the 5 points of the petaloid base and thus possible lines of weaknesses along the bottle). As the folded sides are not equal, the shape which the top of the bottles acquire may complicate their later-on packing.

Nr	F_{max} N	dL at F_{max} mm	Test speed mm/min
1.15	319	3,6	500
1.16	269	59,8	
1.17	357	3,8	
1.18	327	3,5	
1.19	327	3,3	
1.20	317	3,5	
1.21	349	3,7	
1.22	397	60,0	
1.23	336	3,8	
1.24	307	3,5	



Series graph:

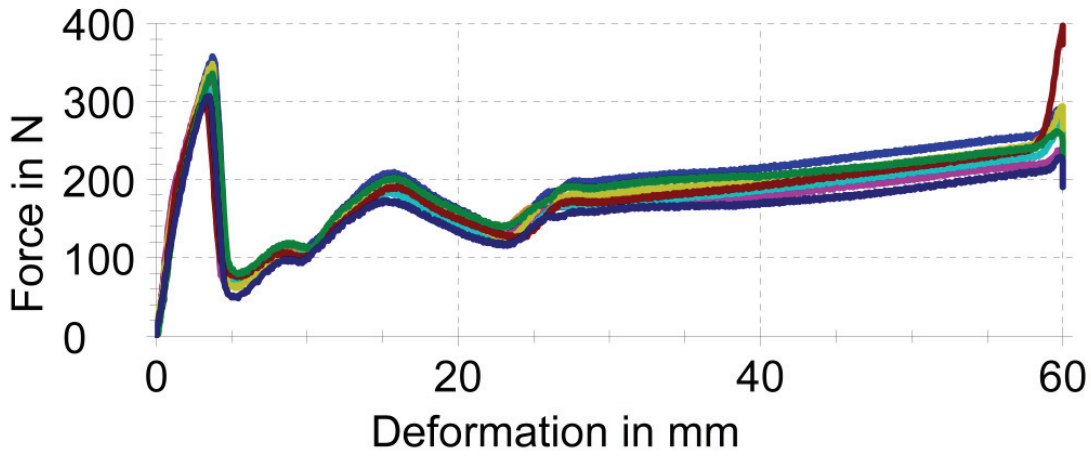

Samples:

9 Type 32 bottles (0,5L, CSD) compressed individually until deformation equals to 60mm

Figure 121. Force/ Displacement graph showing the behaviour of Type 32 bottles under compression

The 9 crushed Type 32 bottles (a'-i') were placed in hexagonal array in the safety container and subjected to a cycle loading test with same parameters as the ones in the previous test, when the bottles were un-crushed. The results showed also in this case a gradual stabilisation of the system and a cyclic behaviour dependent on the maximum and minimum room temperature. Yet an important difference between the behaviour of the regular and the crushed bottles is that the displacement of the latter is higher. Referring to the top-load tests performed, we notice that the slope (thus the young's modulus) at the stress/strain graphs is steeper when the bottles are initially compressed than the point where they start to build-up strength again, after passing 60mm of displacement. This lower value of Young's modulus for the crushed bottles can explain the seen difference in displacement, seen in the graph below.

Another observation to be made is that the crushed bottles reach the maximum deformation more abruptly and that this value is not reached again, once the system stabilises.

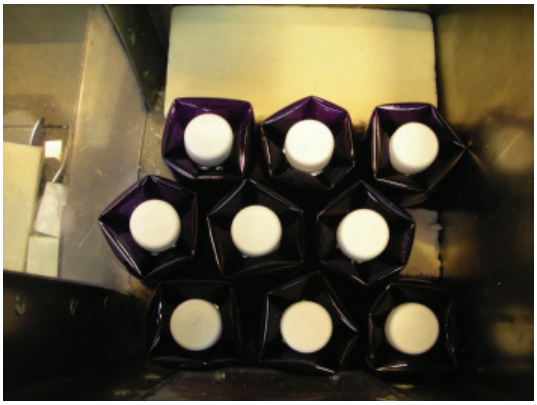



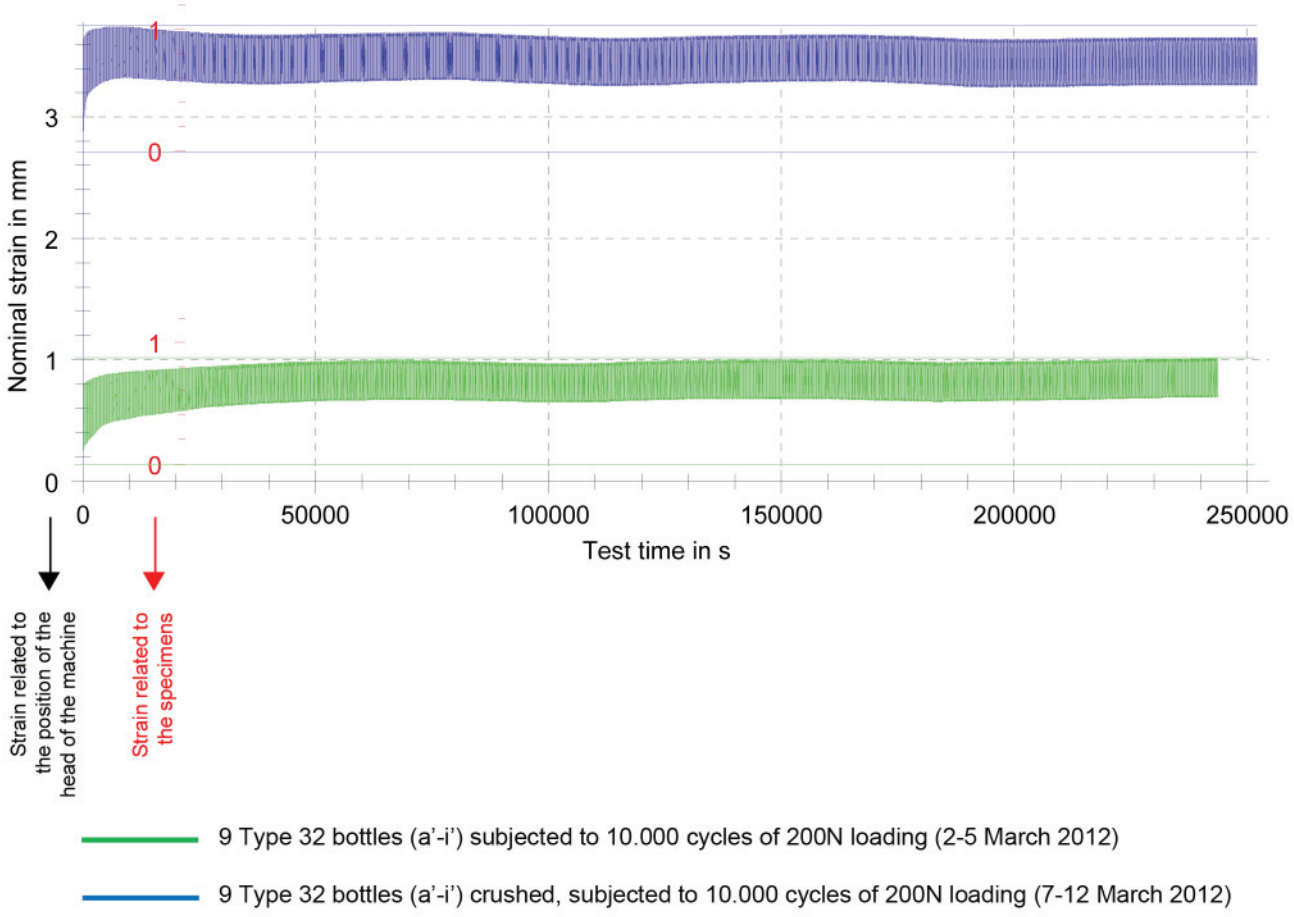

Figure 122. Results of the cyclic loading tests performed with normal and crushed Type 32 bottles

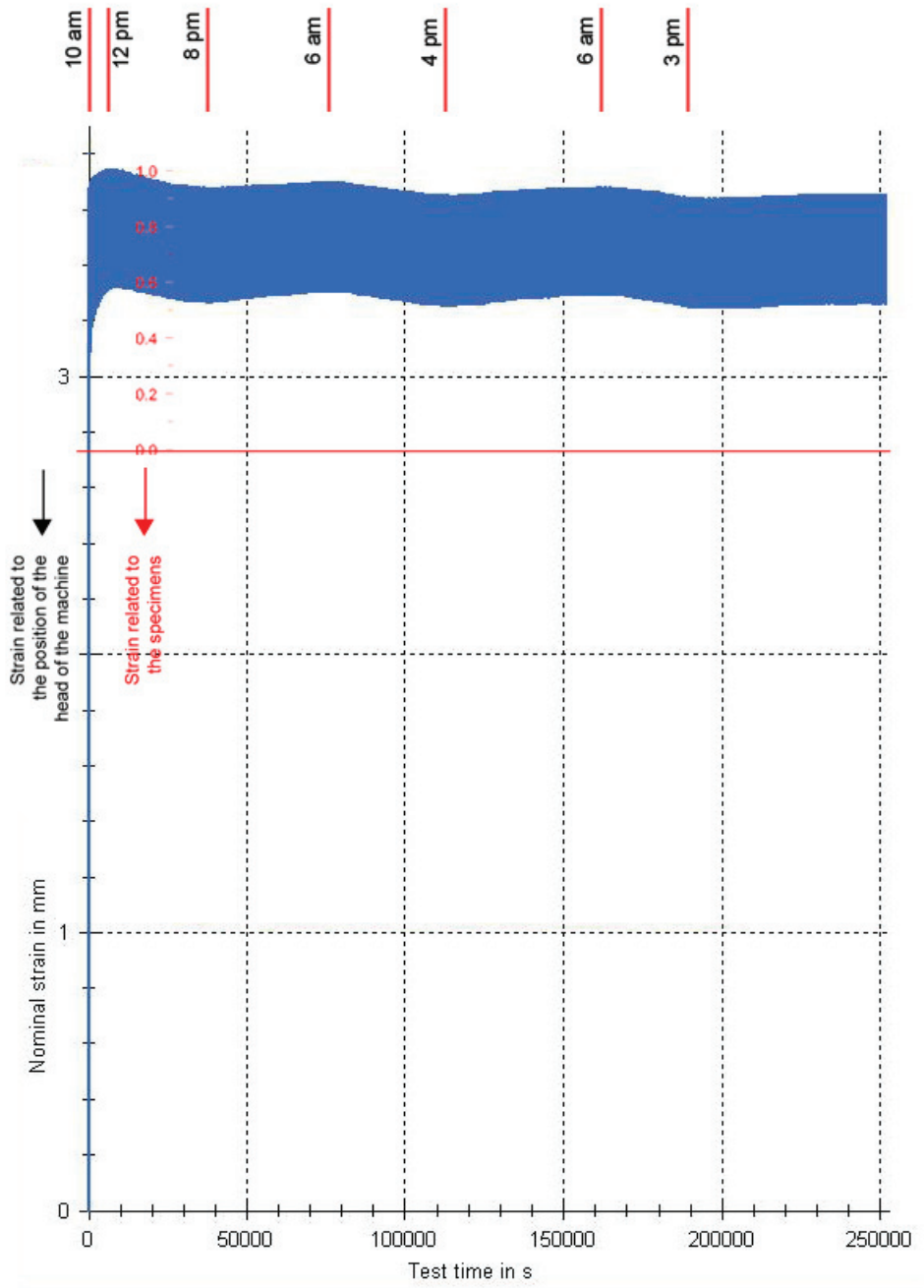

Figure 123. Results of the cyclic loading test performed with 9 crushed Type 32 bottles

Finally, the crushed bottles were tested under creep. A constant load of 200N was applied at the 9 bottles for 100.000h. The bottles showed the same sensitivity to temperature changes, yet, apart the initial instant deformation, the deflection of the bottles over time did not significantly increase.

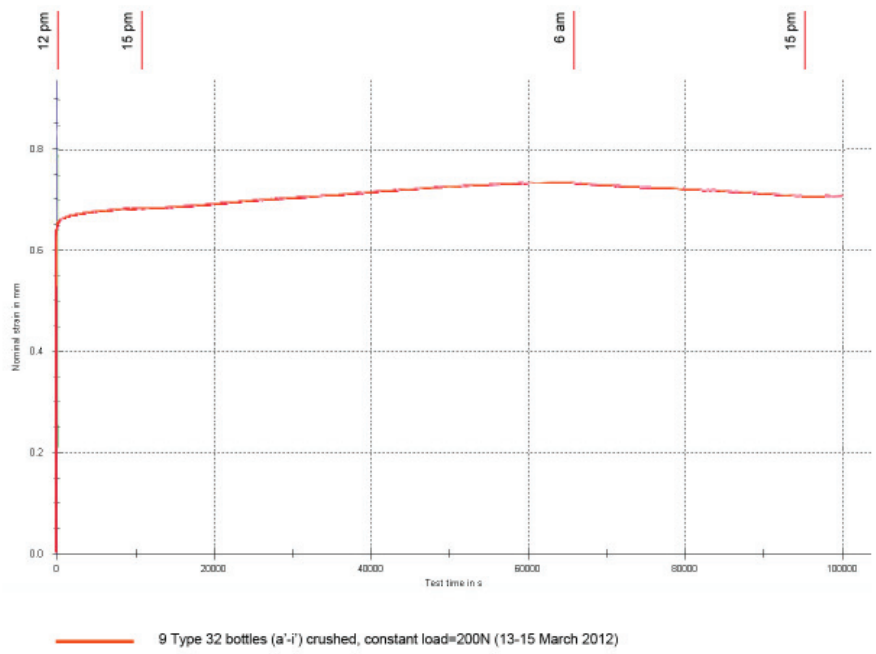

Figure 124. Defleciton/Time graph from the creep test performed with 9 crushed Type 32 bottles

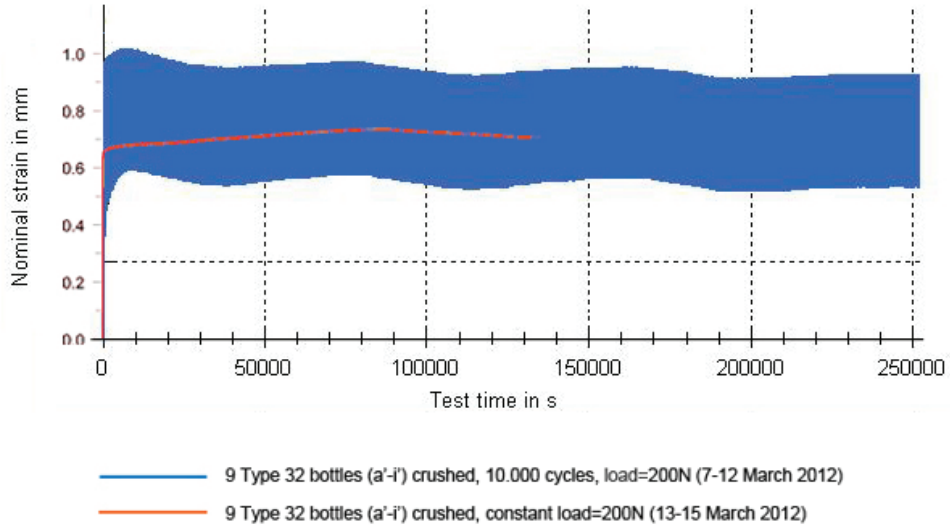

Figure 125. Deflection/Time graph comparing the data from the fatigue and creep tests performed with 9 crushed Type 32 bottles

2.1.3.3. Conclusions

What can be concluded from this series of tests is that the empty bottles (Type 32/0,5L in particular) can be used for the synthesis of the module's core. Under the load range to be expected in a normal structure their behaviour is stable and no permanent deformation occurs. Also buckling at the waist is not observed at these levels of loading.

Regarding the crushed bottles, it can be derived that, although their shape is more convenient in connecting the bottle to the facings, its performance is inferior. By damaging the bottle, in fact, its overall degradation is facilitated. Thus the simple bottles should be preferred. Nonetheless this will result in time saving during the production of the module.

2.2. PET-bottle core for a FRP composite module

2.2.1. Alternative scenarios proposal and assessment

The understanding of the empty, capped PET bottle properties and structural behaviour, gained through the physical experiments, forms the basis for the development of alternative design scenarios for a sandwich component. The relationship between the FRP outer skins of the composite module and its PET-bottle-core, investigated in these scenarios, is determined taking into consideration the design principles of the project. Therefore special consideration is given to the avoidance of adhesives and the simplicity of the components and the connection details.

In defining the synthesis of the module, two main issues are dealt with, the geometrical array and spacing of the bottles, and the connection between the bottles and the FRP skin.

i. Relationship between bottles

The method the bottles are packed in the module is affecting the density of the core, and determines the way the stresses are distributed throughout the structure as well as the transferring of shear forces.

First decision to be taken is whether the lateral contact between the bottles is intended or not. Although theoretically a closed-pack distribution of the bottles would allow the distribution of shear stresses between the bottles, in this case the geometry of the bottle- differing from that of a cylindrical tube- is permitting only a limited amount of contact areas between the bottles. In addition, given the fact that the stiffness of the bottles considering lateral deformation is very low, it is concluded that the transferring of shear forces should not rely on the PET bottles. This allows the freedom to arrange the bottles in open-pack structures, reducing the amount of used bottles and so the density and weight of the core and the connection points, and therefore resulting in a simpler and cheaper structure. In this case, shear force should be taken either by the connections or additional side elements, an issue to be discussed in proceeding chapters.



Figure 126. Alternative packing systems considered for the organisation of the bottles in the core

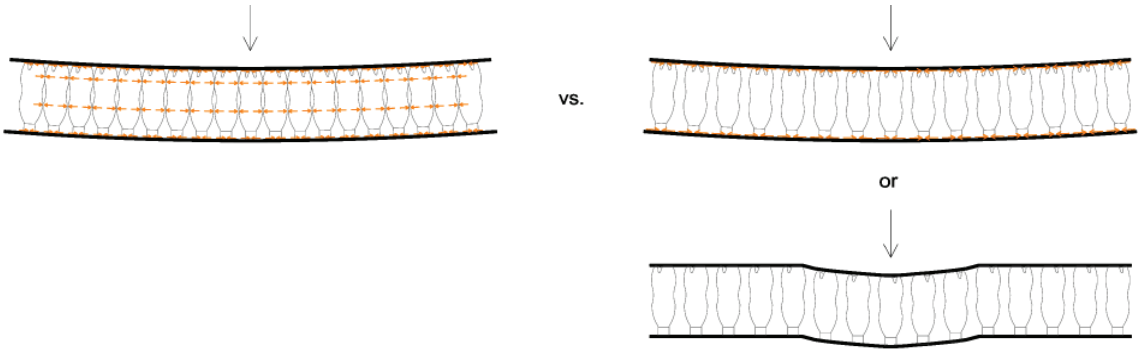

Figure 127. In an open-pack distribution, shear stresses will only be transferred at the connections of the bottles to the facings. The efficiency of this solution in transferring shear needs to be tested

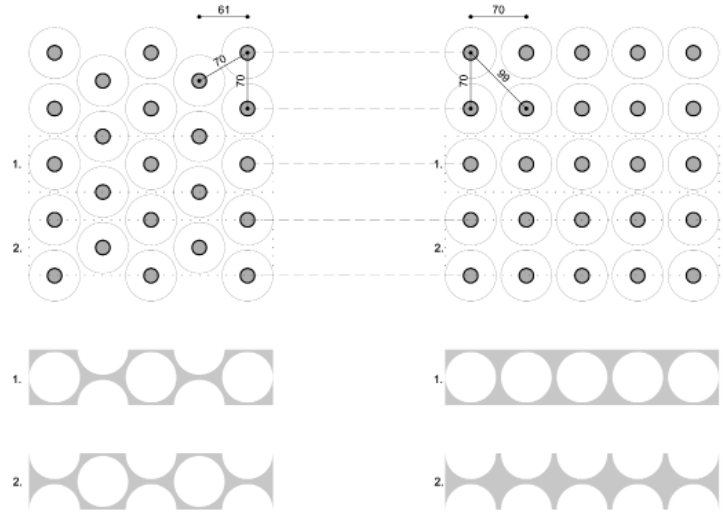

Figure 129. The advantages of the hexagonal array on the left over the square arrangement on the right, considering the equal distribution of the loads

Then, considering the pattern of the bottles' distribution, it is important to decide if a square array would result in a better performance than a hexagonal (60°) or face-centered-square (45°) array. Although the square array results in a pattern where all sides are equal- simplifying the shape of the boundaries- the advantage of an even distribution of the bottles in a given area, obtained by a hexagonal or face-centered-square array, is much more important when the distribution of the stresses is examined. Therefore this logic is preferred for the core and specifically a 45° array is chosen, which results in an equal spacing of the bottles along the x and y axis.

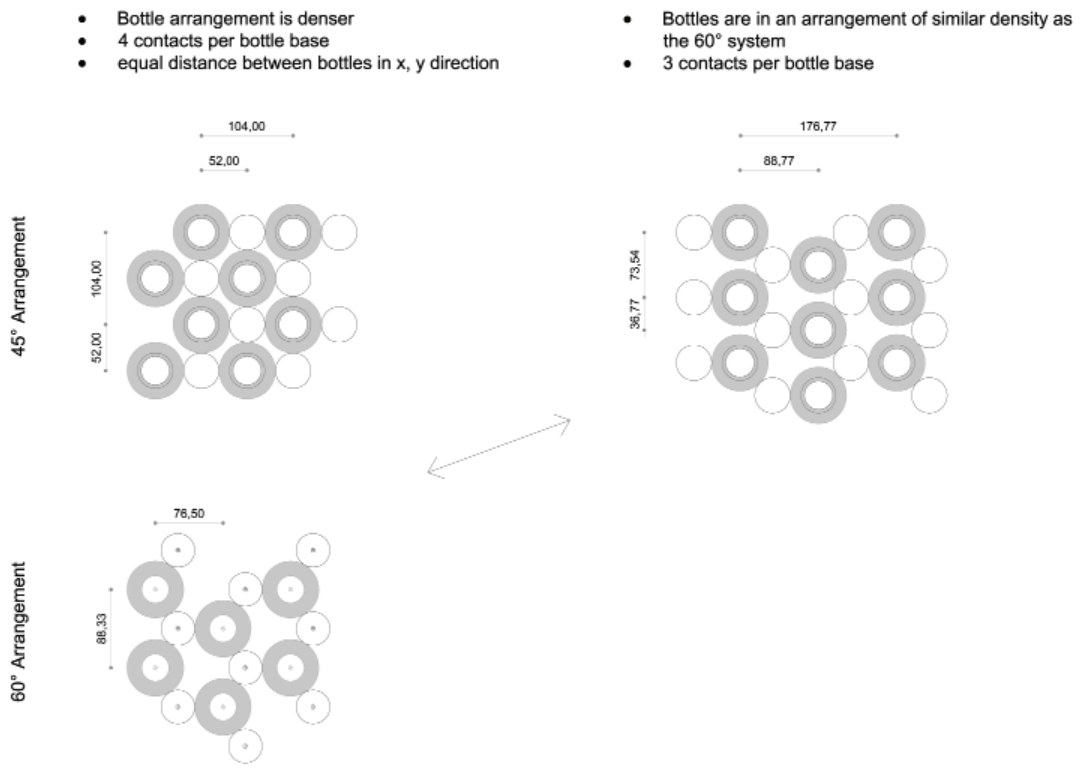

Figure 128. Comparison of the 45° and 60° arrangement patterns

ii. Relationship between bottles and FRP skin

Determining factor for the development of alternative concepts is the intention to design a composite module that can be easily disassembled and the materials can be separated for re-use or recycling. This design restriction eliminates the possibility of using adhesive to bond the skin with the core or to fill gaps between the bottles and the skin with casting materials. Taking into account that the assembly process should be also effortless and quick, solutions such as the screwing of the caps or the bottles's bases on the skin are discarded as well.

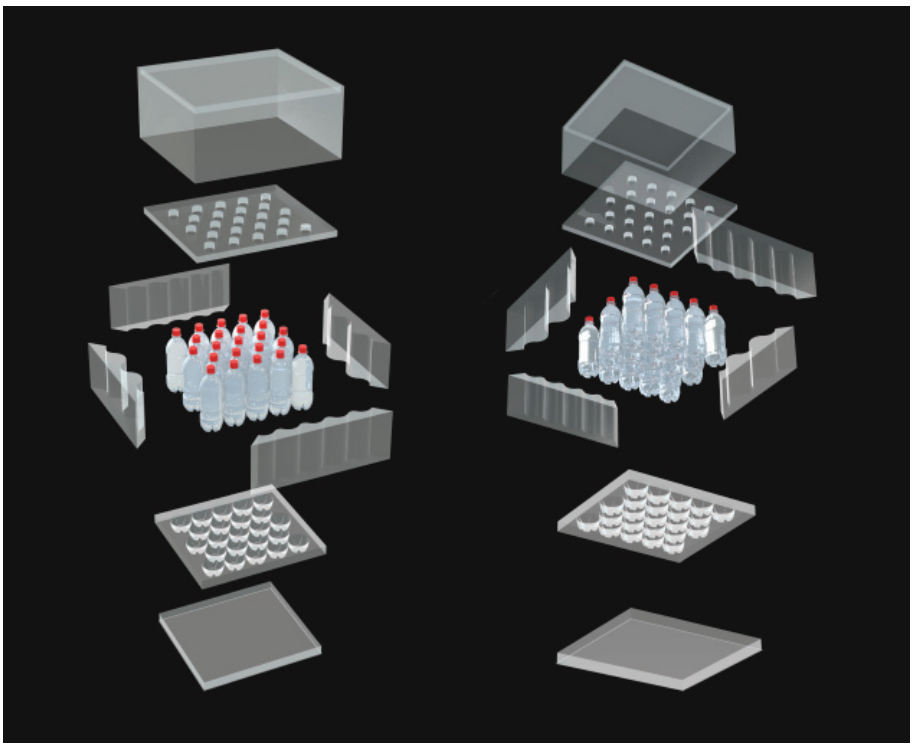

Figure 130. Concept for a modular composite block





Figure 131. Mold used at the production line, to quickly organise the bottles in a hexagonal array (photograph taken at the Ducona factory)

What is taken advantage of is, however, the potential of the chosen skin material to form complex 3D shapes that can follow the geometry of the bottles. Therefore, although it has been considered to re-shape the bottles, by crushing their caps into the main bottle body, in order to make them suitable for fitting in between planar skin surfaces, it is preferred to opt for a corrugated skin structure that surrounds the bottles, achieving a more efficient connection between the two components. In addition, the skin surface itself, acquires extra stiffness due to this 3D geometry. Nonetheless, even if a very complicated form can be achieved with the use of FRP, a more simplified geometry is sought, so as to minimise the cost and labour related to the required moulds and also in order to make the design more generic and not limit it by closely relating it to the geometry of one bottle type. Even more, the possibility to decrease the number of necessary moulds (by designing the upper and lower skin equal for example) and the number of required components (by substituting the composite side components with a truss) is investigated.

An additional parameter that defines the development and assessment of different scenarios is the objective of minimising the used material palette. Once more it is examined if it is more convenient to keep the skin surfaces planar and introduce an additional material that bridges the complicated shape of the bottles with the 2D surface of the skin, rather than designing a corrugated skin surface. Materials such as foam or more eco-friendly alternatives such as paper pulp are considered but eventually rejected as they cannot provide efficient connection between the skin and the core without the use of adhesives.

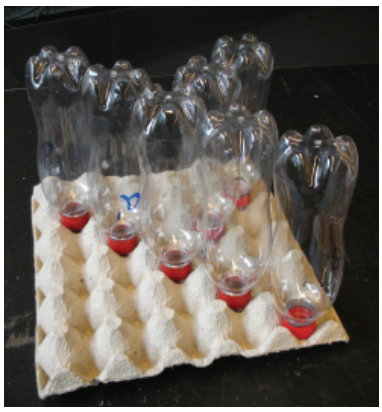

Figure 132. Paper-pulp egg-trays can be a solution to the problem of packing the bottles in the mold





Figure 133. Mock-up out of paper pulp, creating a surface that matches to the geometry of the bottles' bases, that could form the layer inbetween the core and the lower FRP skin



Figure 134. Screwing the caps on the skin and then attaching the bottles may create a stable connection, it is however a time consuming process



Figure 135. Crushing the bottles to obtain a more orthogonal shape is a time consuming process as well

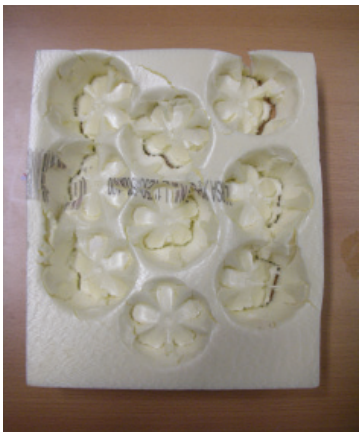

Figure 136. 3D milling the negative of the bottles' base in a foam material is a workable solution that clashes however with most of the design criteria

Proceeding, tables with information for 5 alternative scenarios will be presented. The components and assembly method of the modules in each proposal are examined and the proposals are assessed on whether they meet the design criteria.

Case no. 1: "Egg-tray"

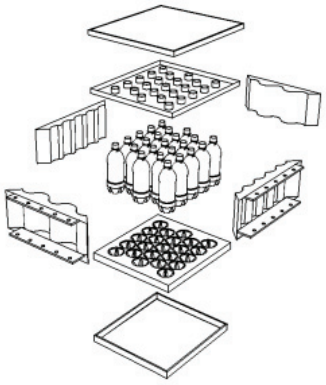

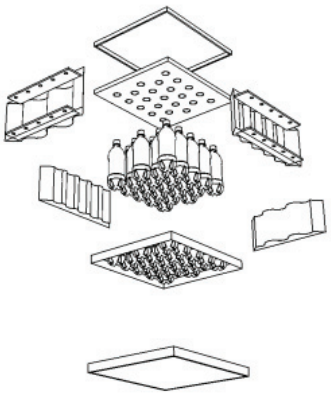





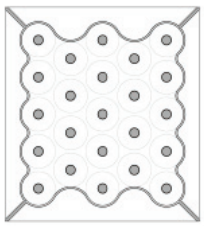

Plan

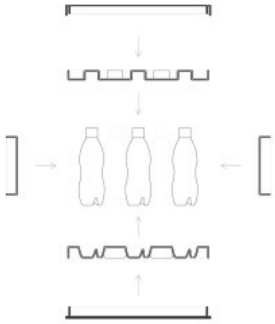

Assembly

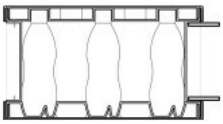

Section

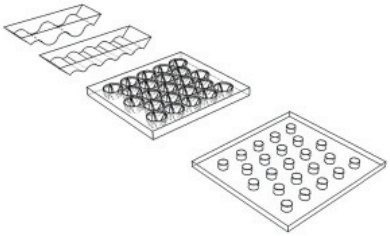

Molds

positive
neutral
negative

Case 1				
Complexity of mold	Material choice	Assembly ease	Structural performance	After life
Comments				
+				
• The GFRP skin takes advantage of the bottles' shape to fix them in place • The solution takes advantage of the possibilities of GFRP for free-form shapes	• Minimises the variety of used materials	• Clips easily due to shape (self-centring ring required for tolerance) • Process of bottle filling can be an independent procedure from the laminating of the shell and can take place even on site	• Skin is stiff due to its corrugated shape	• Easy to separate the materials
-				
• Complicated form of mold raises cost and fabrication time of the components				

Case no. 2: Foam at boundaries

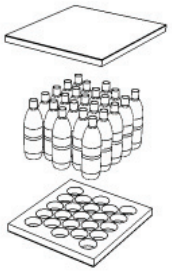

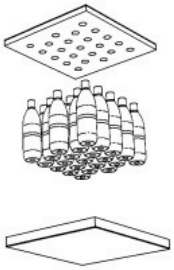

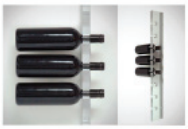



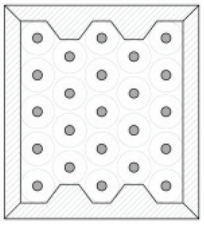

Plan

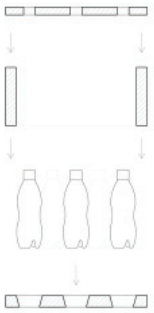

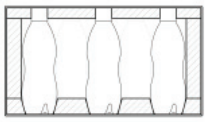

Section



Assembly

positive
neutral
negative

Case 2				
Complexity of mold	Material choice	Assembly ease	Structural performance	After life
Comments				
+				
• No mold required		• Easy to fit the bottles in the holes		
-				
• Holes on foam need to be precisely cut	• Foam is the most lightweight solution for the solid material surrounding the bottles but not eco-friendly • The use of foam weakens the PET bottle core concept • Translucency is not an option	• Lamination is the last step of the panel's production so it can not arrive as separate parts on site (and be assembled for example by the community in the natural disasters scenario)	• Foam is not be capable of handling large shear stresses • Foam is not reducing the point stresses from the bottles' caps and in fact the thin GFRP skin is not as strong as in other versions where it is corrugated • Rotation of bottles is not prevented	• Difficult to cut the panel open • Foam and GFRP skin can be very difficultly seperated

Case no. 3:
Simplified 3D faces

a.

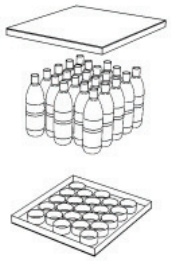

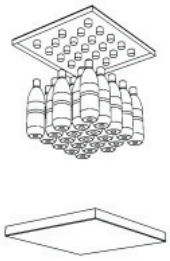



b.

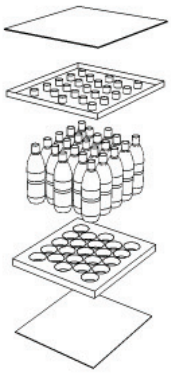

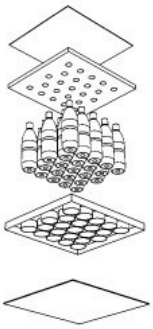



c.

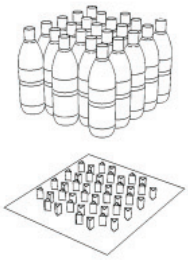

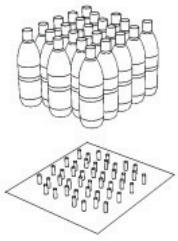

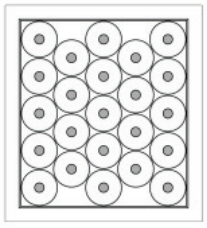

Plan

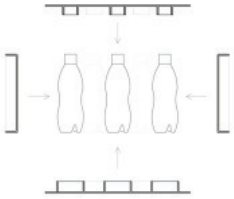

Assembly

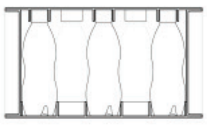

Section

positive
neutral
negative

Case 3a				
Complexity of mold	Material choice	Assembly ease	Structural performance	After life
Comments				
+				
• Ready made GFRP sheets can be used • Simple GFRP cylinders are glued on the GFRP plates, to fix the bottles	• Minimises the variety of used materials • It is not necessary for the bottles to be identical, provided that they have the same height and neck diameter	• Easy to fit the bottles in place (also there is no restriction due to the form of the base) • Process of bottle filling can be an independent procedure from the laminating of the shell and can take place even on site	•	• Easy to separate the materials
-				
			• Risk of failure of the adhesive due to shear stress? • Limited cohesion between the bottles and the GFRP skin • Rotation of bottles is not prevented	

Case 3b				
Complexity of mold	Material choice	Assembly ease	Structural performance	After life
Comments				
+				
• Ready made GFRP sheets can be used • Perforated sheets are quicker to produce than attaching cylindrical parts on the GFRP plates	• Minimises the variety of used materials	• Easy to fit the bottles in place (also there is no restriction due to the form of the base) • Process of bottle filling can be an independent procedure from the laminating of the shell and can take place even on site	•	• Easy to separate the materials
-				
			• Risk of damaging the PET wall at the point of contact with the GFRP perforated plate (over the bottle's base) • Contact between exterior and interior (perforated) plates? • Rotation of bottles is not prevented	

Case no. 4: Caps attached to upper face



screw caps

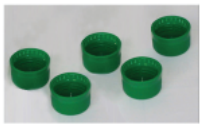

integrate caps during lamination

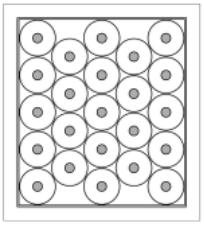

Plan

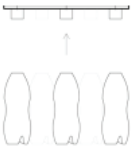

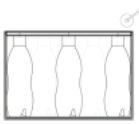

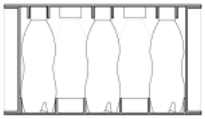

Section

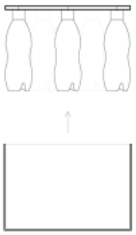

Assembly

Case no. 5: "Crushed" bottles



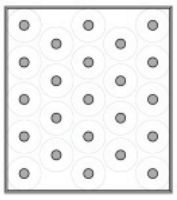

Plan

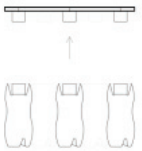

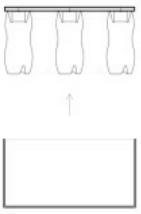



Preparation

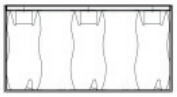

Section

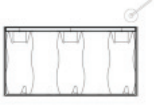

Assembly

positive neutral negative

Case 4a				
Complexity of mold	Material choice	Assembly ease	Structural performance	After life
Comments				
+				
• Simple mold	• It is not necessary for the bottles to be identical, provided that they have the same height and neck diameter			
-				
	• Extra sheet (mdf?) required between the bottles and the GFRP skin, to allow the screwing. This adds to final mass of the module and rules out the possibilities for translucency	• Screwing the caps in place is a time consuming procedure • Lamination is the last step of the panel's production so it can not arrive as separate parts on site (and be assembled for example by the community in the natural disasters scenario)	• No connection between the base of the bottles and the bottom of the GFRP box	• Difficult to cut the panel open • Difficult to separate the GFRP skin from the inbetween sheet (mdf?)

Case 4b				
Complexity of mold	Material choice	Assembly ease	Structural performance	After life
Comments				
+				
• Positioning the caps in the correct place complicates the mold	• It is not necessary for the bottles to be identical, provided that they have the same height and neck • Minimises the variety of used materials	• Bottles can be easily set in place		
-				
		• Lamination is the last step of the panel's production so it can not arrive as separate parts on site (and be assembled for example by the community in the natural disasters scenario)	• Is the integrated caps able to withstand the shear forces?	• Difficult to separate the caps from the GFRP skin • Difficult to cut the panel open

positive neutral negative

Case 5				
Complexity of mold	Material choice	Assembly ease	Structural performance	After life
Comments				
+				
• Ready made GFRP sheets can be used	• Minimises the variety of used materials • The bottles adquire a shape that is conforming better to the products available at the market		• Forces are distributed more evenly (point loads from the caps are avoided)	
-				
	• Use of adhesive	• Crushing the bottles is time-consuming • Bottles need to be glued in the correct position • Lamination is the last step of the panel's production so it can not arrive as separate parts on site (and be assembled for example by the community in the natural disasters scenario)	• Damage is intentionally induced to the material which is more susceptible to fatigue failure • The Young's Modulus of the crushed bottles is lower than that of the regular bottles • Risk of delamination • It is not guaranteed that all crushed bottles are equally rigid (that damage done is at the same level)	• Difficult to cut the panel open • Difficult to separate bottles from GFRP skin

2.2.2. Design proposal chosen for further development

From the list of developed scenarios, the solution presented below is chosen for further development, as it meets most of the criteria. This design suggests the use of one mould in order to produce the corrugated surface of both upper and lower skin. This mould produces large plates of this corrugated pattern that can be cut off along guiding grooves, providing a wide range of possible module sizes. The bottles are connected to the skins due to their geometry and no other material is included in-between. Specifically, the bottles' caps are inserted in the cylindrical protrusions of the surface, whereas the bottles' bases are surrounded by them.

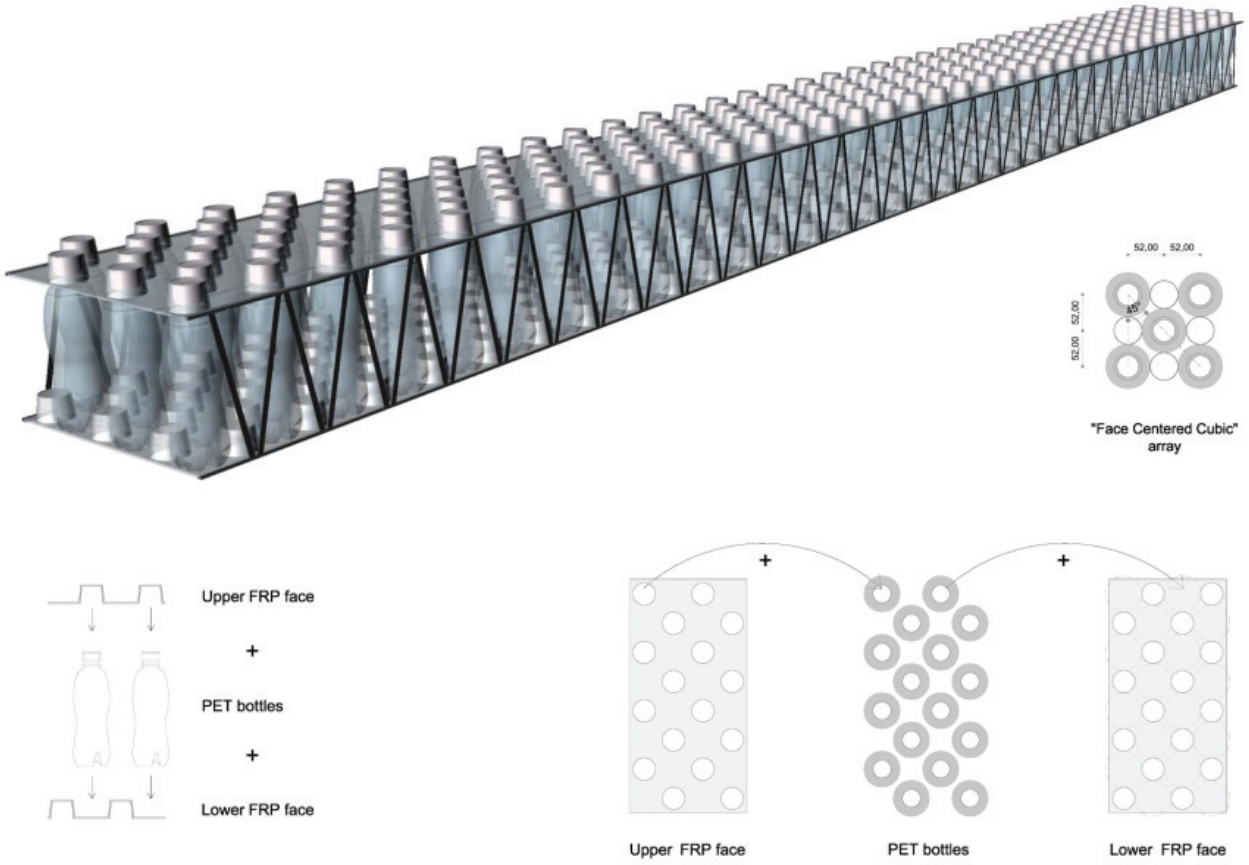

Figure 137. Proposal chosen for further development and testing

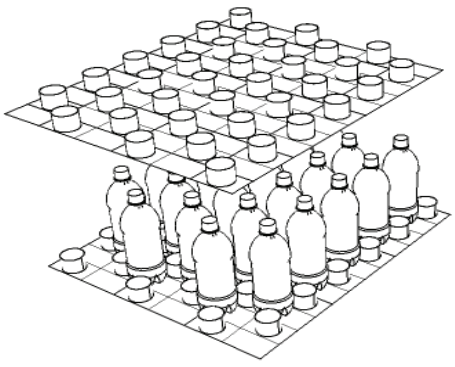

Between every 3 cylinders of the lower plate a circle can be inscribed of diameter of 1mm less than that of the bottles' maximum diameter at the base. This assures the pin connection of the bottles at the lower plate. Considering the cavity of the cylinder in the upper plate however, this is bigger than the cap in order to allow tolerances during the assembly process. To establish a pin connection at the upper cylinders as well, a self-centering component is introduced, with hinged sides that push the cap into place.

Figure 138. Upper and lower facing are the same

Considering the array of the bottles, although a hexagonal pattern was first chosen, eventually it was replaced by a 45° array that results in equal spacing of the bottles at both axis and a better holding of the bottles' bases by introducing one more cylinder (from 3 to 4) for each bottle. This geometrical array, and in combination with the fact that the lower and upper plate are the same, makes it feasible to combine the modules together, as the modules themselves start to act as "LEGO" bricks. Thus, the modules can be formed into beams, floor panels and walls, providing a solution for an integrated building system. To allow the connection between the modules, the FRP bulges are thus redesigned as conical frustums.

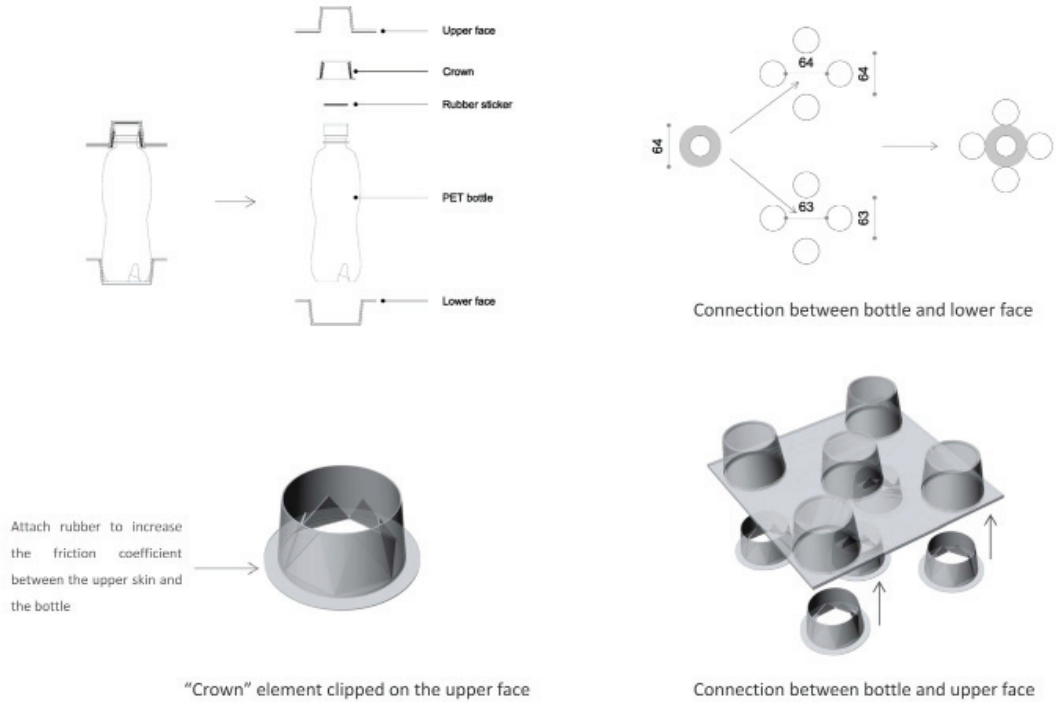

Figure 139. Connection details between the bottles and the lower and upper facing

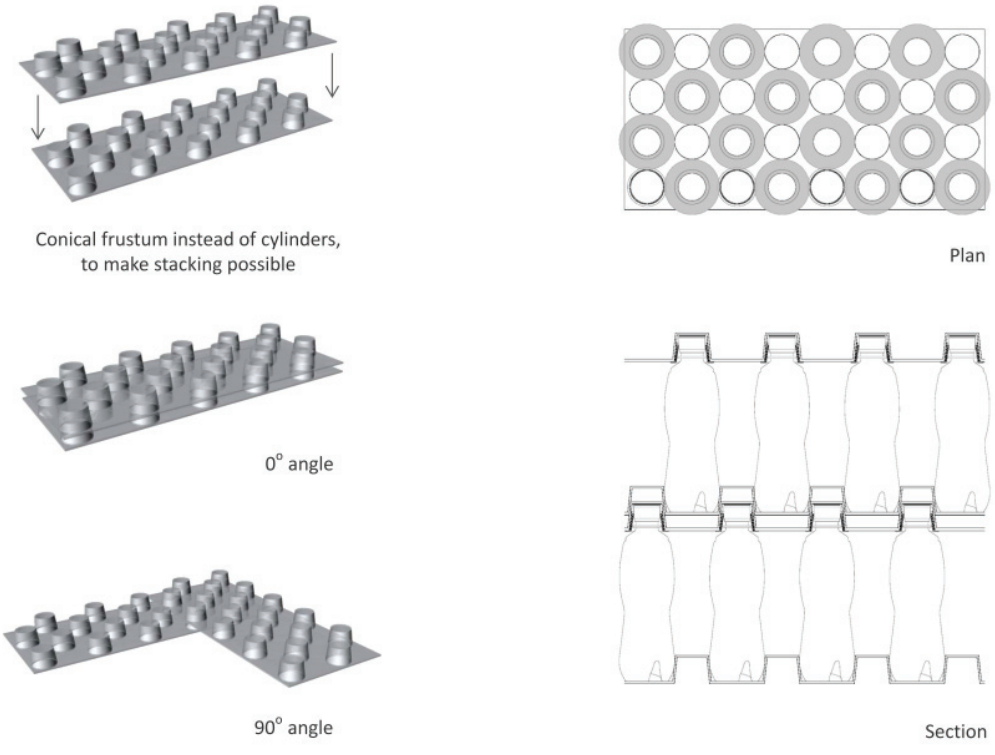

Figure 140. Possibility for stacking and connecting the modules with each other

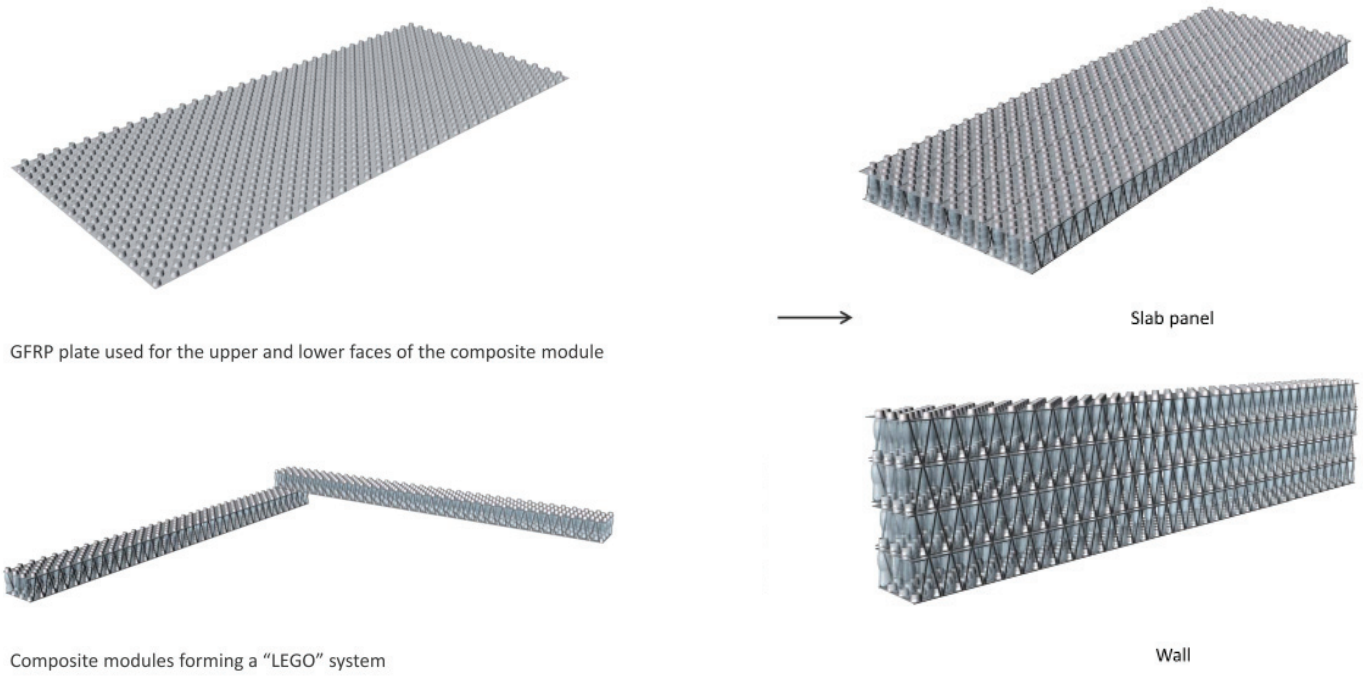

Figure 141. The modules can be formed into beams, plates and walls, creating an integral building system

To minimise the amount of FRP components, the side closing elements are substituted by a continuous steel cable truss, similarly to the way the heads of a drum are connected to each other. The steel cables are pre-tensioned in order not only to join the upper and lower plate together but also to adequately receive the shear forces that can develop due to bending of the component.



Figure 142. A truss is introduced at the sides of the module to receive the shear stresses

At this point it should be mentioned that, when designing a sandwich module, a number of possible failure modes should be taken into consideration, with governing that of deflection. In our case, and provided that the FRP skin has sufficient thickness and strength, the shear strength and compression strength of the core, are playing a determining role for the performance of the module. In addition, the efficiency of the connections between the bottles and the faces, is crucial for the avoidance of face wrinkling.

To understand and evaluate the design and especially the properties and performance of the core, hand calculations are accompanied by the building of a full scale prototype, since many aspects regarding the behaviour of the structure cannot be predicted due to its non-linear character (ex. steel cables transform the module to an adaptive structure). This prototype, thus, forms the main tool at this stage of the design for the comprehension, development and optimisation of the module.

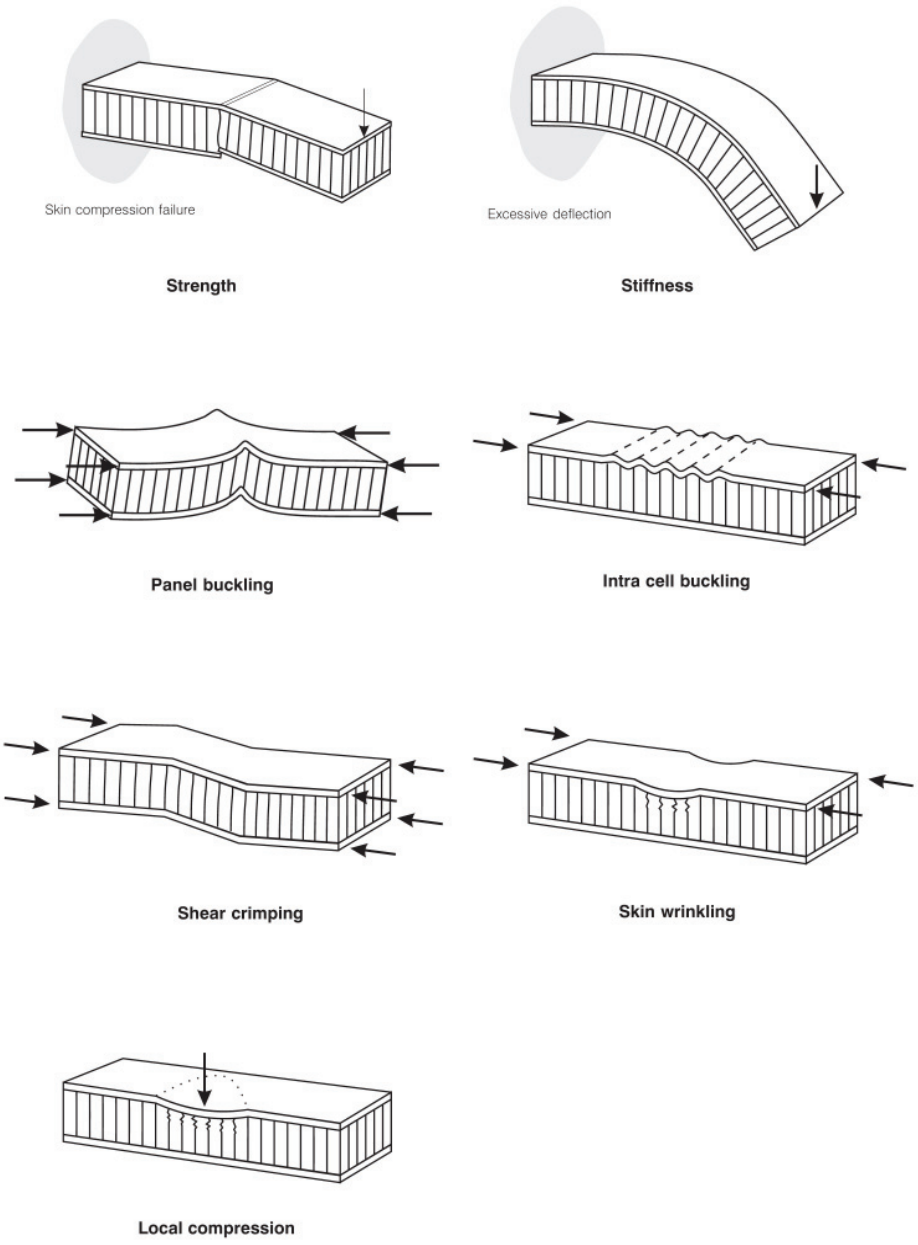

Figure 143. Standard failure modes of composite panels with a honeycomb core

Source: HexWeb Honeycomb Sandwich Design Technology

				Beam: Simple support, central load		
	Property	**Symbol**	**Imput value**	**Formula**	**Output**	**Unit**
Beam	Length	ℓ	2,392			m
	Width	b	0,312			m
	Height	h		$h= t_c + 2*t_f$	0,18	m
	Area (xy plane)	A		$A= \ell*b$	0,746	m^2
Face	Face thickness	t_f	0,003			m
	Young's modulus	E_f	14.100.000.000			Pa
	Compressive modulus	E^C_f	10.300.000.000			Pa
	Yield strength	σ_y	221.000.000			Pa
	Tensile strength	$\sigma_{tens.}$	207.000.000			Pa
	Compressive strength	$\sigma_{compr.f}$	172.000.000			Pa
	Height btw centroids of faces	d		$d= t_c + t_f$	0,177	m
	Poisson's ratio	v_f	0,33			
	Density	ρ_f	1.800			Kg/m^3
Bottle	Compressive modulus	E^C_b	230.408.709,726			Pa
	Poisson's ratio	v	0,4			
	Shear modulus	G_b		$G_b= E^C_b/ 2*(1+v)$	161.286.096,808	Pa
	Number of bottles in 1 row (width)	no_w	3			
	Number of bottles in 1 column (length)	no_l	23			
	Total number of bottles	no_b		$no_b=2*no_w*no_l$	138	
	Mass	m_b	0,03063			Kg
	Area (section in z direction)	A_b	0,00022			m^2
	Volume	V_b	0,000464			m^3
	Density	ρ_b		$\rho_b= m_b/V_b$	66,013	Kg/m^3
Core	Core thickness	t_c	0,174			m
	Mass	m_c		$m_c= no_t*m_b$	4,227	Kg
	Volume	V_c		$V_c= t_c*A$	0,130	m^3
	Density	ρ_c		$\rho_c= m_c/V_c$	32,551	Kg/m^3
	Core, Compressive modulus	E^C_c				Pa
	Core, Shear modulus (of rigidity)	G_c				Pa
	Cell opening (distance between bottles)	s	0,072			m
	Compressive strength	$\sigma_{compr.c}$				Pa
Load	Load	W	2.500			N
	Beam mass	m_{be}		$m_{be}= \ell*b*t_f*2*\rho_f + no_t*m_b$	12,287	Kg
	Beam weight	W_b		$W_b= m_{be}*g$	120,413	N
	Total load	W_{tot}		$W_{tot}= W+W_b$	2.620,413	N
				Calculations		
Stiffness	Sec. moment of inertia (xz plane)	I_{xz}		$I=2*b*t_f*(d/2)^2$	0,0000147	m^4
	Bending stiffness	D		$D= (E_F*t_F*d^2*b)/2$	206.733,805	$N*m^2$
	Shear stiffness only bottle section	S		$S= A_b*no_w*G_c$	106.448,824	N
Deflection	Bending deflection coefficient	k_b	0,0208	$k_b=1/48$		
	Shear deflection coefficient	k_s	0,250	$k_s=1/4$		
	Deflection, bending	δ_b		$\delta_b=(k_b*W_{tot}*\ell^3)/D$	0,003614	m
	Deflection, shear	δ_s		$\delta_s=(k_s*W_{tot}*\ell)/S$	0,014721	m
	Total deflection	δ		$\delta= \delta_b +\delta_s$	0,018335	m
	Allowed deflection	δ_a		$\delta_a= \ell/360$	0,006644	m
Force	Maximum Shear Force	F		$F=W_{tot}/2$	1.310,206	N
Moment	Maximum Bending Moment	M		$M= (W_{tot}*\ell)/4$	1.567,007	N*m
Stresses	Core stress (due to F) only bottle section	τ_c		$\tau_c= F/(no_w*A_b)$	1.985.161,233	Pa
	Facing stress (due to M)	σ_f		$\sigma_f= M/(d*t_f*b)$	163.077,405	Pa
Dimpling	Critical dimpling stress	σ^D_{cr}		$\sigma^D_{cr}= (2*E_f*t_f^2)/((s^2)*(1-v_f^2))$	54.941.458,123	Pa
Wrinkling	Critical wrinkling stress	σ^W_{cr}		$\sigma^W_{cr}= 0.82*E_f*((E_c*t_f)/(E_f*t_c))^0.5$	0,000	Pa

Figure 144. Hand calculations approximating the behaviour of the module. The properties noted with red colour cannot be estimated with simple hand calculations due to the complexity of the system

Comments
Minimum value from CES (14.1 - 31 Gpa)
Minimum value from CES (10.3 - 31 Gpa)
Average value from CES
Minimum value from CES (207 - 345) MPa
Minimum value from CES (172 - 345) MPa
Simplified approximation considering the faces planar
Average value from CES (0.307 - 0.353)
Average value from CES (1.6e3 - 2e3 kg/m^3)
Sum from compression tests (on 14-02-2012, 07-03-2012), case 1
Assumption for bottle closed (air inside). Crystalline PET v= 0.381- 0.396 (CES)
Case 1: only the thickness of the bottle is calculated for the section area
Approximation using the simplified core thickness
Area of section (in z direction) is calculated using only the thickness of the bottles
As area of section is calculated the area of of the bottles (in z direction)
It should be lower than the face's compressive and yield strength
Critical dimpling stress should be less tha the face's compressive strength
E_c- core's compressive modulus

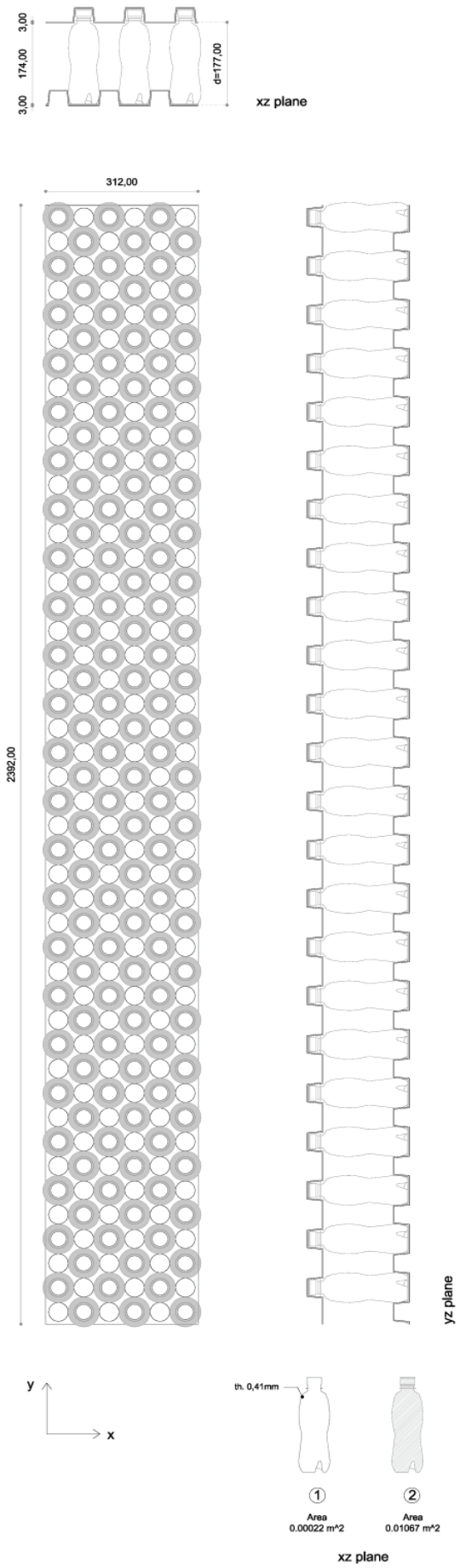

2.2.3. Prototype building and testing

2.2.3.1 Process

i. Adopted approximations

Main objective of the full scale prototype is to understand the behaviour of the PET bottle core and its relationship with the exterior faces. First it is necessary to investigate if the bottles and the skin can work together as a coherent composite element, and then to determine the compressive and shear strength of the core and define the steps to be taken for its improvement.

To prove the concept it is therefore not important to built the prototype identically to the proposed design, but rather some approximations can be allowed. Such are the replacement of the FRP faces (3mm thickness in the design) by mdf plates (18mm thickness in the prototype- therefore resulting stiffness is equal for the two plates) or some simplifications in the geometry of the upper and lower plates' protruding elements.

ii. Building process

The full scale prototype consists of a composite beam of dimensions 2,4*0,3*0,2m. The upper and lower skin of the sandwich is realised by mdf plates of 18mm thickness, drilled either until the middle or at full thickness, to receive the bottles. For the core, 104 Type 32 PET bottles (CSD, 0,5L -sponsored by DUCONA) are used (empty and capped).

Regarding the truss at the long sides of the beam, first rubber bands are used, to identify if the concept is working and then they are replaced, in quest for the optimal material and configuration that can bind the upper and lower plate together and handle the shear stresses.

Along the experiments, the connection details between the bottles and the plates also gradually change, so as to minimise deflection at the middle of the span.

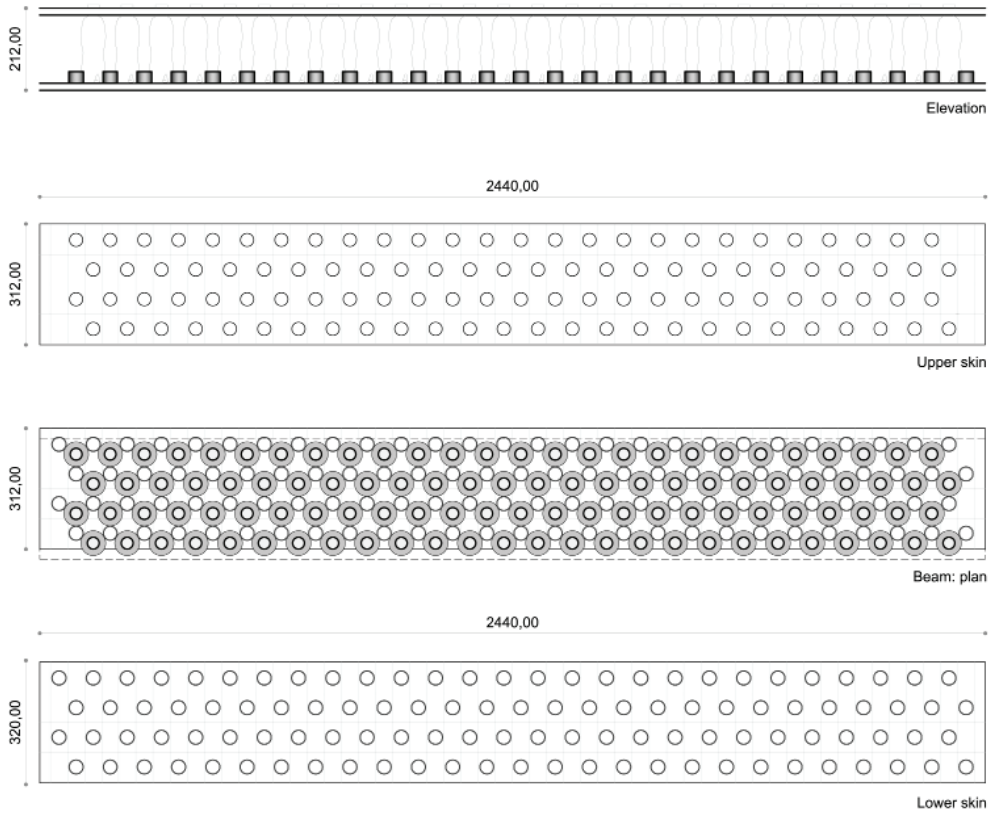

Figure 145. Drawings of the full scale prototype

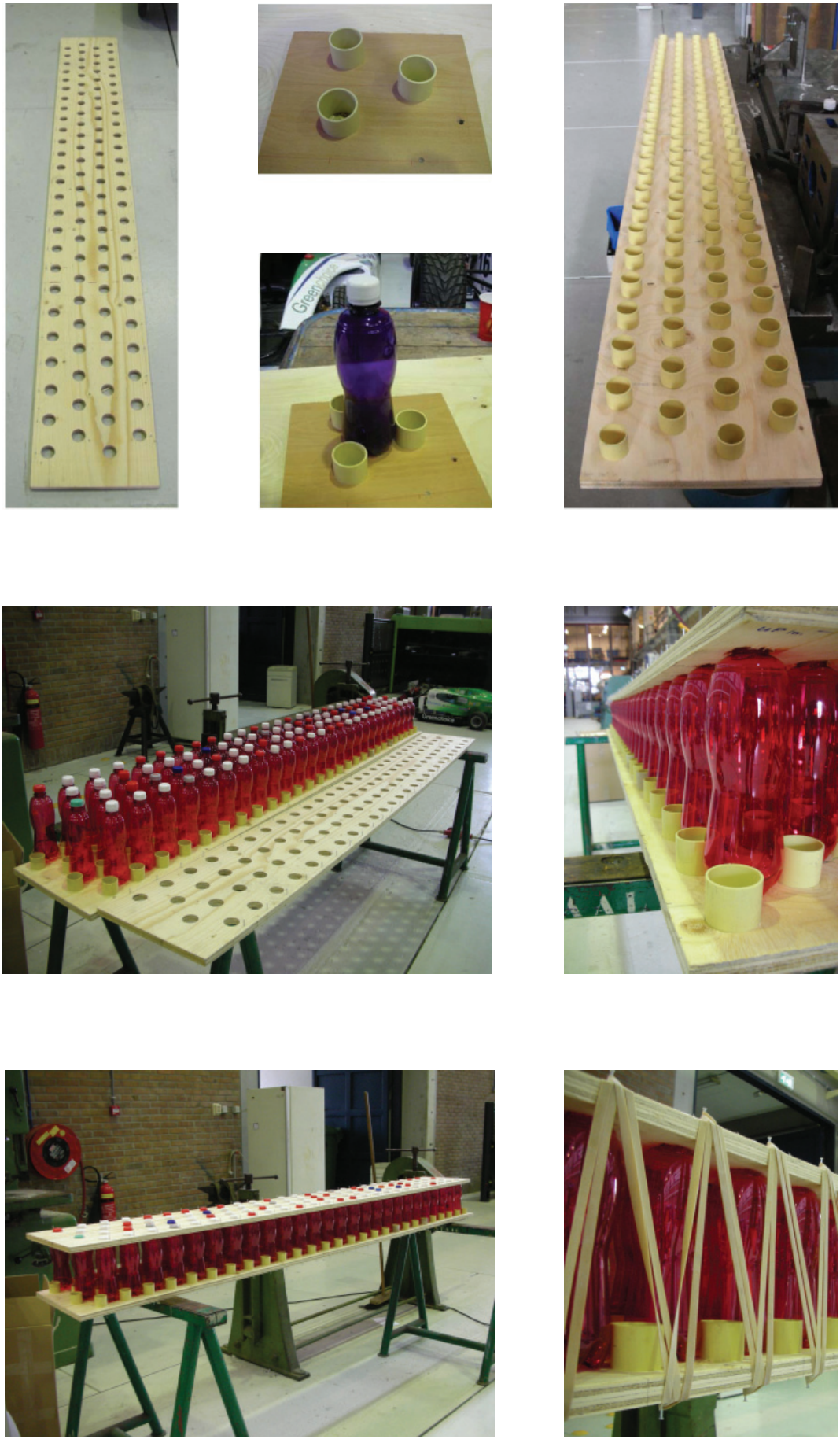

Figure 146. In the above pictures the building process of the full scale prototype can be seen

iii. Testing procedure

The first series of experiments is focused on the deflection of the beam at the middle of the span due to bending under its own load (appr. 240N) or the application of point load at the middle, that does not exceed the value of 400N. During the experiments, the deflection of the lower and upper plate are noted, as well as the distance between the plates at the middle and at the sides. By keeping the value of the applied point load constant, changes to the prototype between tests can be easily evaluated for their effectiveness. Creep relaxation is also recorded during the experiments.

As it will be analysed below, four main aspects are investigated through this series of tests, concerning the connection between the caps and the upper plate, the connection of the bases to the lower plate, the buckling of the bottles at their waist, and the connection between the upper and lower plate and the distribution of shear stress. Improvements at the above sectors are reflected to the total deformation of the beam at the middle and at the way the bottles are moving when bending occurs.

Regarding the displacement of the bottles when the beam is subjected to bending, the desired behaviour is the bottles to follow the curvature of the upper and lower plate, always staying perpendicular to them. This indicates that shear stresses are successfully transferred and that the upper and lower plate work together as a composite beam.

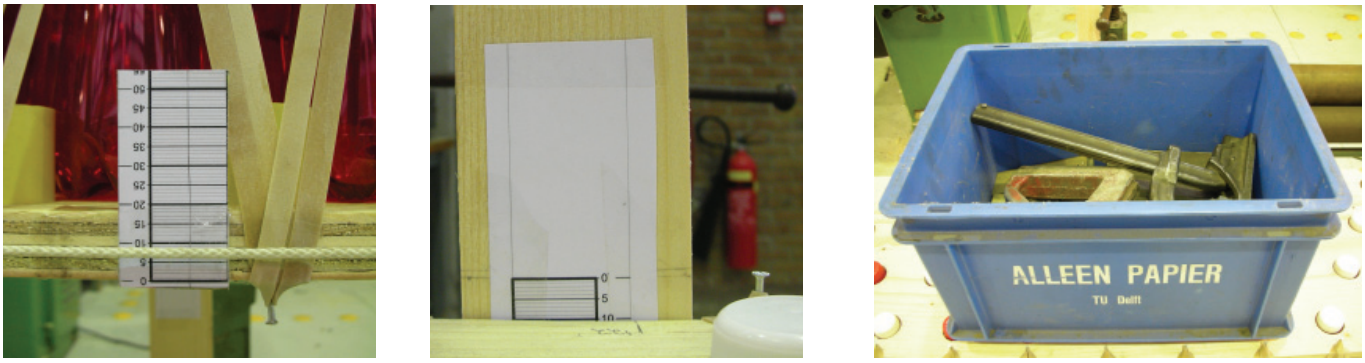

Figure 147. Measuring and loading methods followed during the experiments

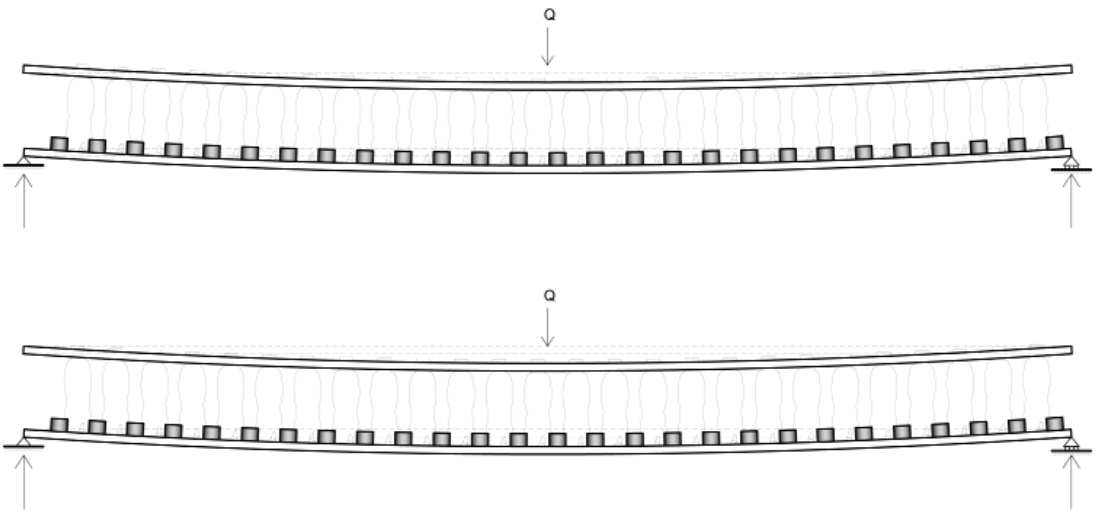

Figure 148. Different deformation pattern under bending, related to the ability of the core to transfer shear stresses. In the first drawing the ideal situation is depicted, whereas in the second, the behaviour of a core with a low shear modulus is approximated

2.2.3.2 Experimental procedures and results

i. Bottle's cap to upper face connection

At the first physical experiments it is clearly observed that the bottles move down parallel to the z axis . As a result, and especially at the first tests (no. 1-4), where the bottles' caps can move freely in the mdf holes of the upper plate, the total deflection of the beam when subjected to a 400N point load at the middle of its span, is 5,5 times higher than the maximum allowed deflection.

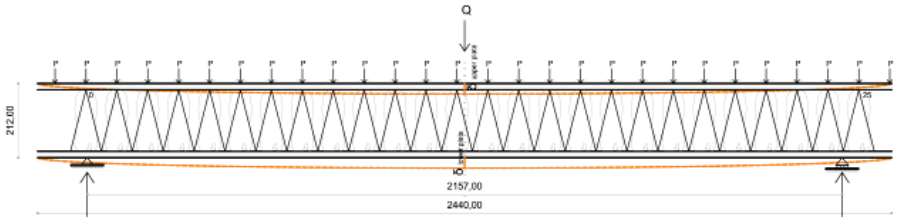

Date:	25/04/2012
Test no. :	3
Uniform load P :	Own weight (total ≈ 240N)
Point load Q :	400N, middle of span (applied on the upper mdf plate)
Truss configuration :	Two diagonals between bottles (Warren truss approximation)
Truss material :	Natural rubber bands, connecting 1 nail up to 1 nail down
Bottles-plates connection:	Bottles' caps can move freely (diameter of mdf holes larger than the caps)



	Time	Before loading	Immediately after loading	Immediately after un-loading
Displacement (middle of the span)	δ lower plate (mm)*	7	47	12
	δ upper plate (mm)**	10	52	
Distance between mdf plates	D left (mm)	212	213	
	D middle (mm)	210	210	
	D right (mm)	211	213	

* The depicted value is affected by the method of measurement, in this case, the deflection of the rope. Thus the value should be used only as point of reference between the tests and not an accurate indication of the deflection of the beam

** The depicted value is affected by the method of measurement, in this case, from irregularities of the floor surface. Thus the value should be used only as point of reference between the tests and not an accurate indication of the deflection of the beam

Figure 149. Data related with experiment no. 3

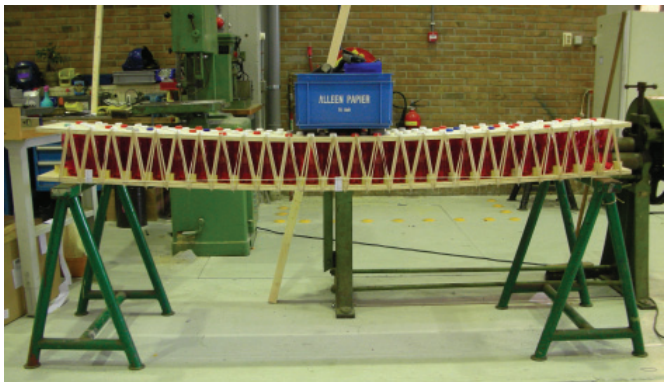

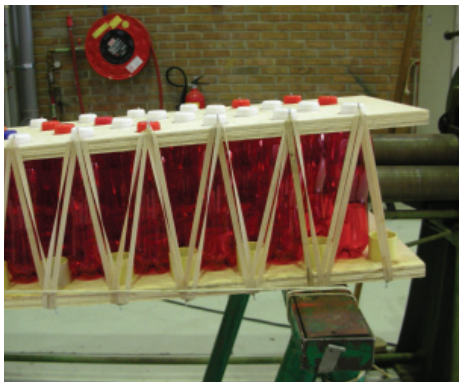

Figure 150. The deflection of the beam during Test no. 3 is depicted above. The bottles move downwards without following the curvature of the upper and lower mdf plate and the distance between the plates increases at the sides of the beam

First step to decrease the observed deformation is to restrict the movement of the caps by inserting pieces of 3mm thick PVC soft in the mdf holes, either at the left side of the cap- for the bottles located from the middle of the span ant to the left, or at the right side, for the bottles on the right side. By repeating the loading test after the modification, the beam immediately works better, deflecting even 11mm less than before.

Then metal strips of 1,5mm thickness are added in the holes opposite to the pvs soft, completely blocking the movement of the caps along the x axis (length of the beam) and enabling the caps to better follow the movement of the upper plate, when bent.

The cylindrical bulge of the upper plate should completely constrain the movement of the cap in the xy plane, and concerns are expressed whether the hinged self-centering element can perform this task. Alternatively it is proposed that the cylinders of the upper plate are open from above -and still bigger than the cap diameter to allow tolerances- so that an extra cap element can be placed after the positioning of the plate, fixing the bottles and the plate together.

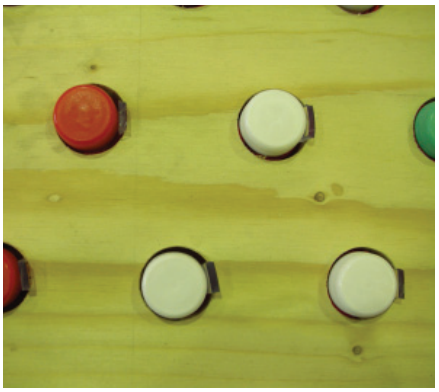

Figure 151. Modifications made to the prototype in order to restrict the movement of the bottles along the x axis (length of the beam)

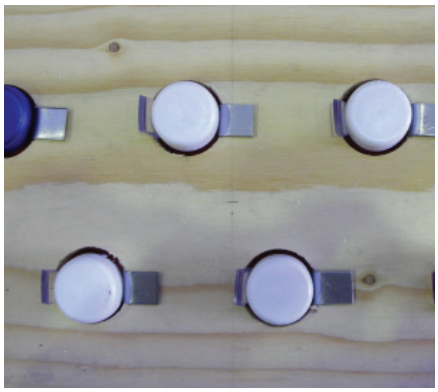

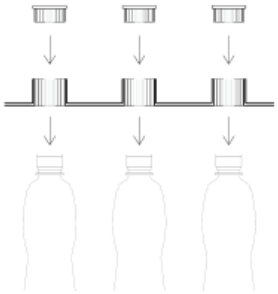

Figure 152. Proposed capping system for fixing the bottles in place

ii. Bottle's base to lower face connection

In order to achieve better cooperation of the lower plate and the bottles, pieces of PVC soft are applied at the connections between the bottles' bases and the PVC cylinders of the lower plate (only at the bottles at the exterior rows), in an attempt to tighten the connection. Yet, deformation is only slightly diminished (by 1mm) and as it will be later discovered (when the bottles will be removed from the lower plate) local deformation occurs at the contact point between the PET wall and the PVC soft piece.

Focusing on the hexagonal array of the bottles and the PVC cylinders, it can be seen that the 2 cylinders confining each bottle's movement along the x axis (length of the beam) are not aligned with the axis of symmetry of the bottles. Therefore, the cylinders, in loose contact with the bottles, cannot efficiently transfer shear stresses to the petaloid bases. Even more, as the bottles' resistance to lateral deformation is very low, the bottles easily deform and escape the pressure applied by the cylinders. Also, due to the geometry of the base (the diameter decreases at the lower part of the bottle) rotation along the z axis can easily occur.

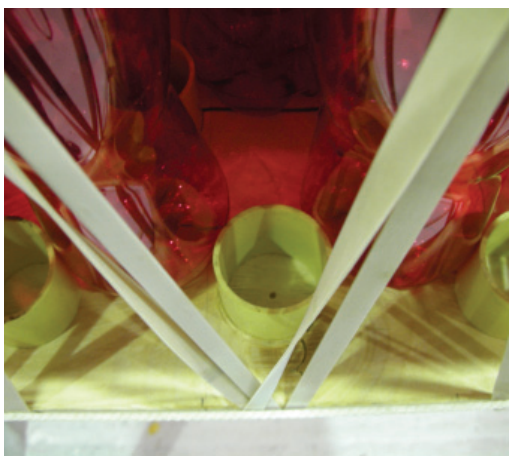

Figure 153. Connection between the bottles and the lower mdf plate

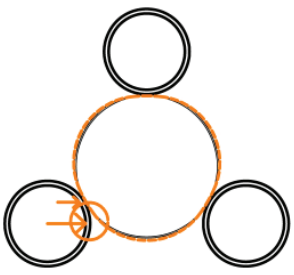

Figure 154. Transferring of shear only occurs in two points

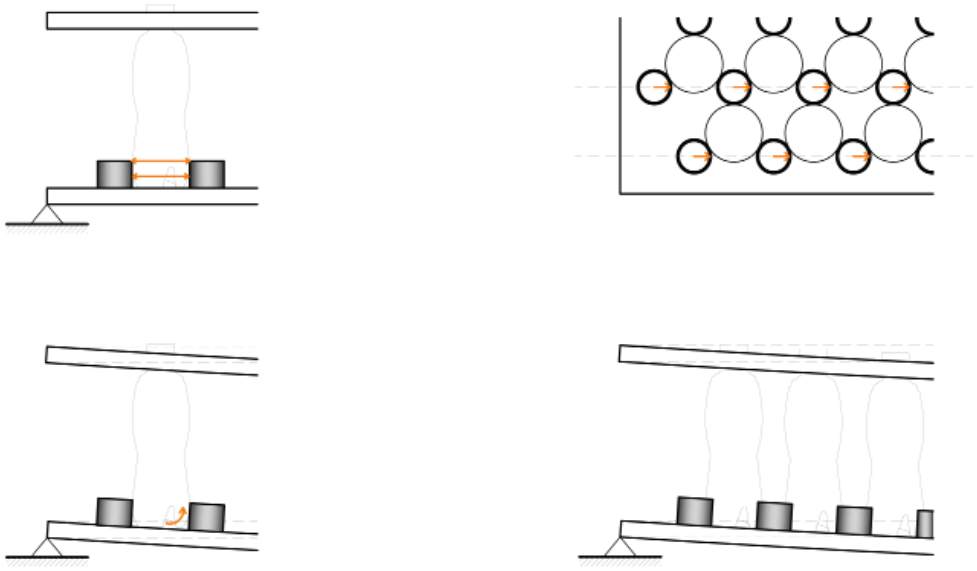

Figure 155. Because of the loose contact between the cylinders of the lower facing and the bottles, due to the array of the bottles and the geometry of the bottle's base, the bottles do not follow the curvature of the facings when these are bent under loading

Changing the array of the bottles from hexagonal to 45 degrees can improve the transfer of shear forces from the bottles to the cylinders of the lower face, but probably not significantly. The issue of localising stress in 3 or 4 contact point still remains, as well as the possibility of the bottle to deform freely. The bottle in fact is behaving as a "joystick"and because of the reduced stiffness at the contact point with the cylinders, it is unable to follow the movement of the lower plate when this is bent.

Examining the base of the bottle, it is observed that the strongest point of it is in fact located at the centre of the bottom of the base, where the thickness of the PET wall is maximum due to the effect of gravity during the blow molding manufacturing process. An effective connection able to transfer shear would be to insert a nail from the lower FRP plate up to the centre of the bottle's base. However, this involves the risk of damaging the bottle from the puncture. In addition, it increases the assembly and disassembly time to a non acceptable level.

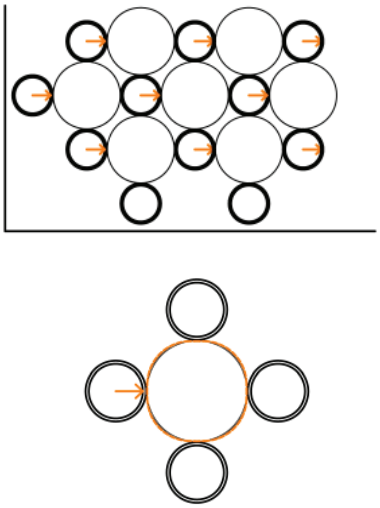

Figure 156. A 45° pattern cannot significantly alter the base-lower plate connection, since the bottle can still deform freely

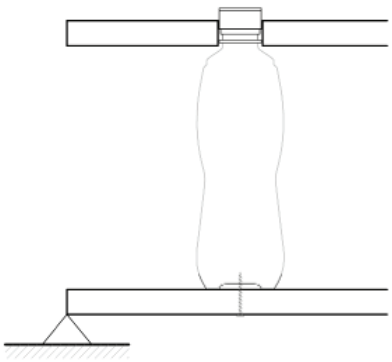

Figure 157. Introducing a nail to connect the bottle to the facing may create a stable connection, it damages however the bottle and the FRP skin

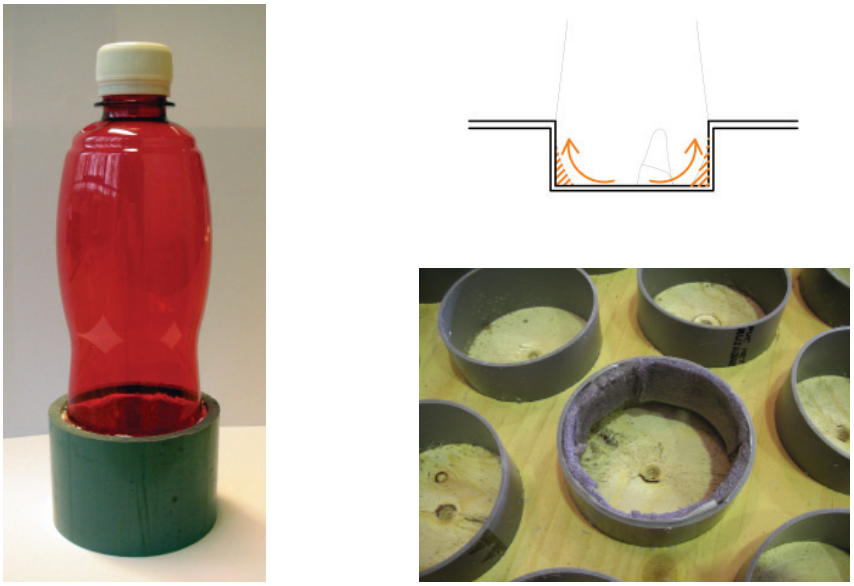

Figure 158. Squeezing the bottle into a cylindrical holding that has foam material attached in its interior wall results in a connection that considerably minimises the movement of the bottle and the x and y axis and its rotation over the z axis

Altering the design of the lower base so that the cylinders contain the bottles rather than surrounding them may be an in-between solution. Yet, even though the stiffness appears to be slightly higher at the first 20mm of the height of the base, the petaloid shape is still reducing the contact area, in fact limiting it to only a thin ring along the height of the base. To overcome this problem the cylinder's diameter can be designed 1-2 mm smaller than the maximum diameter of the bottle. As the bottle deforms to fit in, a bigger surface is found in contact with the cylinder. To avoid damaging the PET surface due to the contact with the cylinder and the applied pressure, the possibility to integrate a foam material during the lamination around the interior of the cylinder should be examined.

Looking into this proposal with draft mock-ups and eventually by changing the base of the prototype, it is realised that when the bottles are pushed into the tighter cylinder that contains a layer of spongy foam around its interior surface, not only the cooperation of the bottle and the lower plate is significantly improved, but also the bottle is slightly internally pressurised, becoming more rigid. In addition to that, since the cylinder is reducing the actual height of the bottle, bucking at the waist seems to be reduced.

Elaborating on the above solution, two alternatives exist. In order to avoid the existence of two different moulds, the initial design concept can be used, only this time switching between the upper and lower plate, so that the bottles' bases fit in the cylinders and the bottles' caps are hold by the cylinders surrounding them. A closer look at this solution nevertheless reveals the weak connection between the bottle's strongest part (the cap) and the upper plate and such an alternative should be avoided. It is much more preferable to accept the fabrication of two different moulds- of the same logic but with cylinders of different diameter- if the performance is significantly enhanced. Moreover, this facilitates the stacking of the "LEGO" components and allows to simplify the shape of the protrusions, from a conic frustum to a cylinder.

In any case, when considering the cooperation of the lower plate and the bottles' bases, it should not be disregarded the positive effect of the side elements, compressing the plates together, and therefore increasing the friction between the bases and the lower plate.

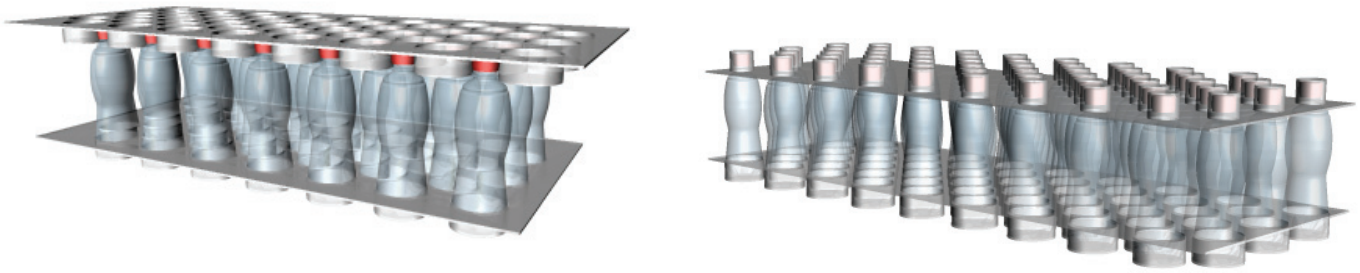

Figure 159. Two different alternatives. In the first, the same mold is used to produce both the upper and lower plate, yet the effectiveness of the caps-upper plate connection is reduced (compared to previous solutions). The second solution, although demanding two different molds, promises better connections between the bottles and the facings, and is thus preferred

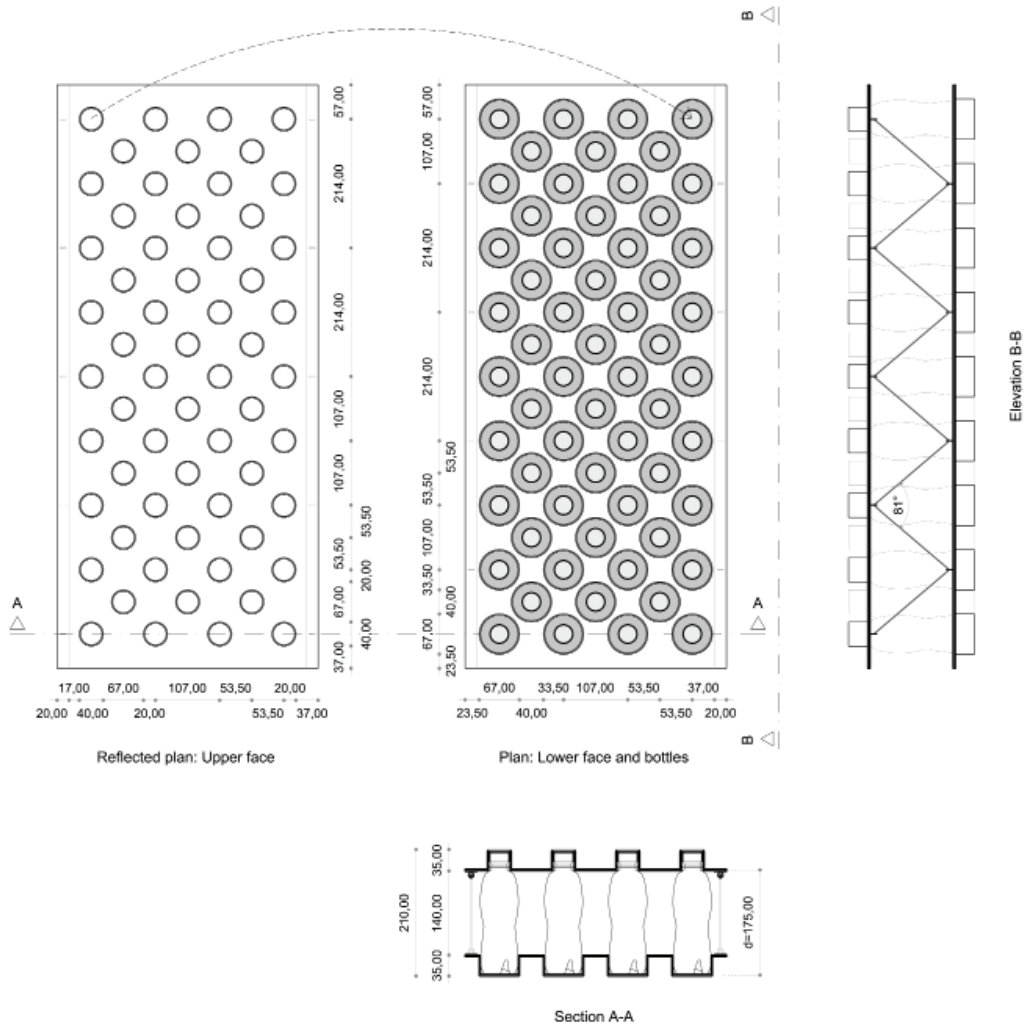

Figure 160. Drawings of the revised module

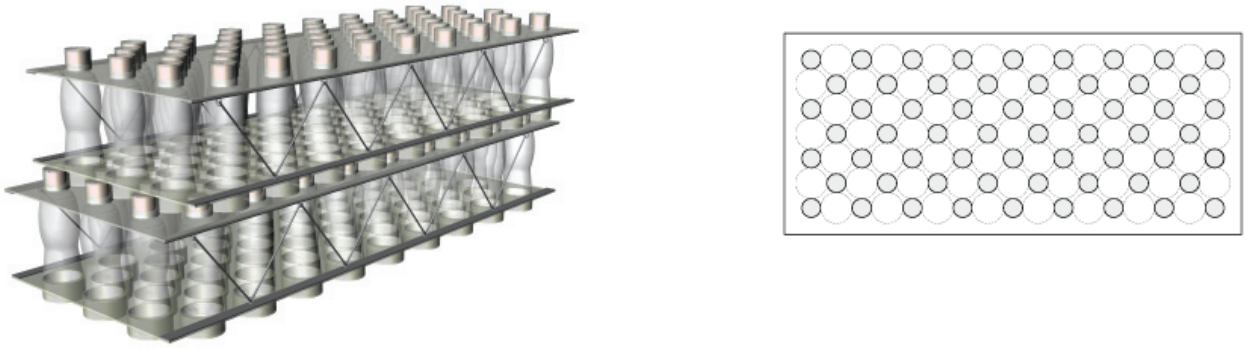

Figure 161. Stacking method applicable in the revised proposal

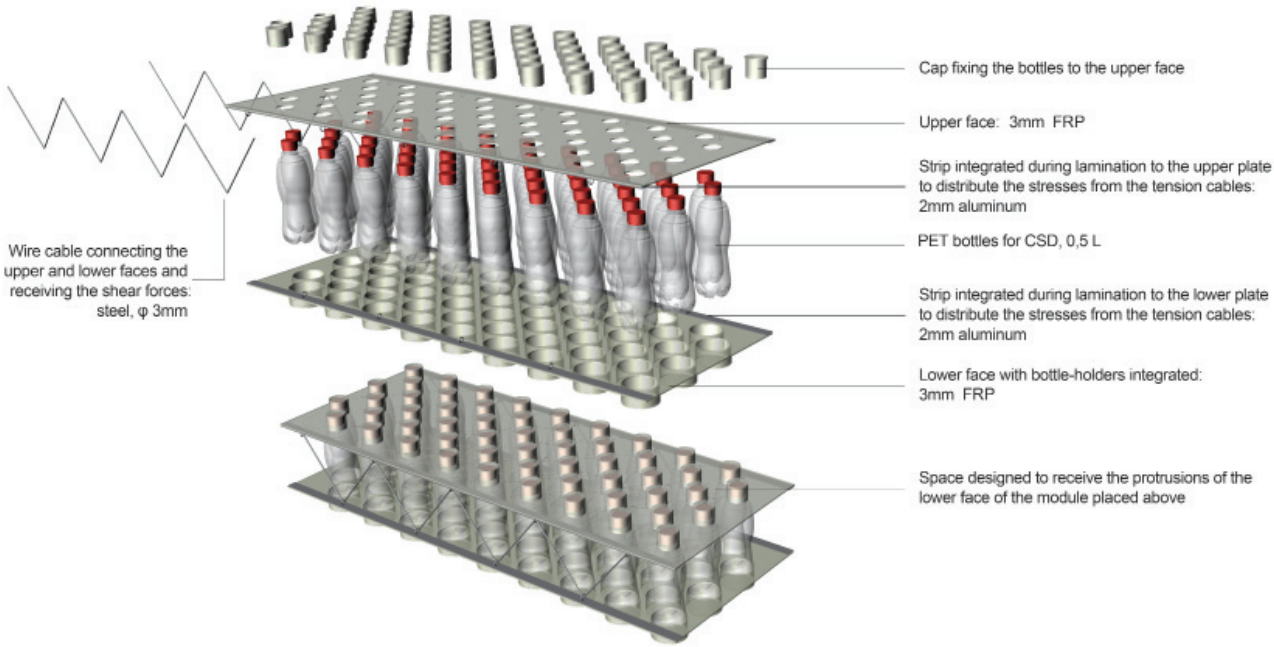

Figure 162. Components of the revised design proposal

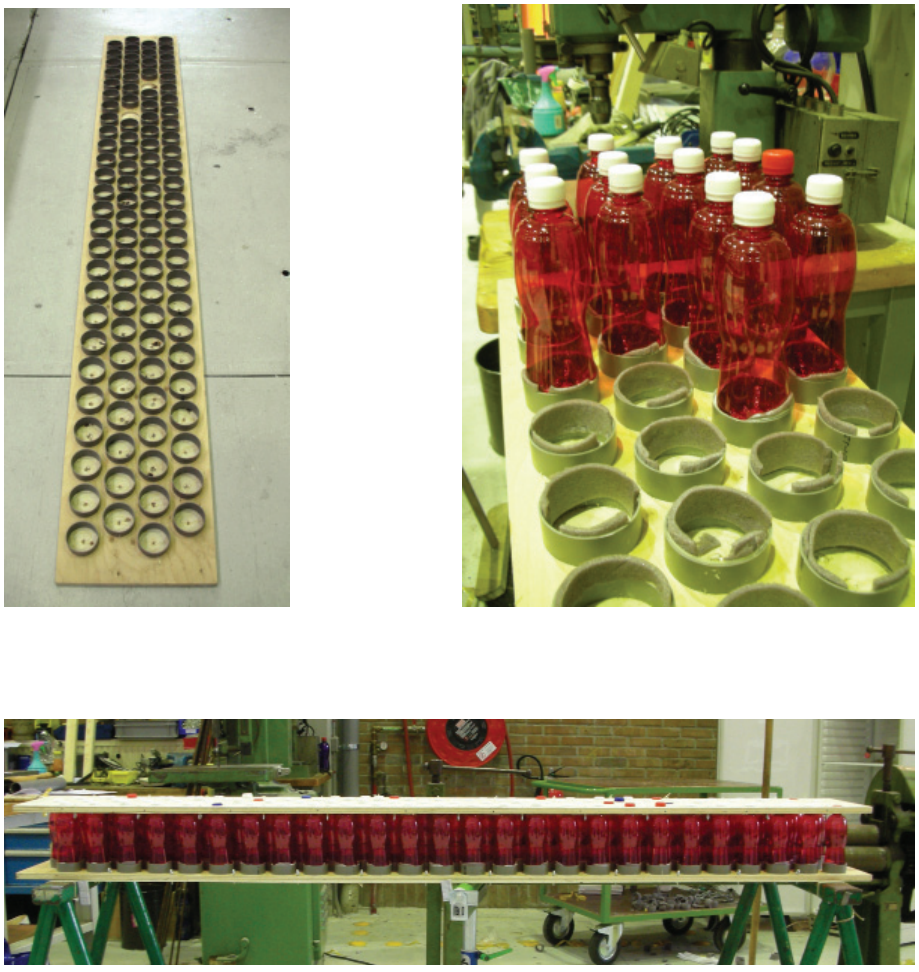

Figure 163. Modifications made at the prototype to improve the bottles-lower facing connection

iii. Buckling of the bottle's waist

An issue first noticed when clamps where applied at the short sides of the beam, and later on becoming a concerning matter when the prestressed steel cables were installed at the long sides of the prototype, is the buckling of the bottles' waist, when local compressive force is applied.

By experimenting with different alternatives, it is concluded that by inserting a tight steel belt around the bottle's waist, the buckling effect at the middle is prevented. Moreover it is observed, that the belt works as a limiting border that does not allow the deformation caused by a lateral force in one part of the bottle to surpass the belt and extend to the other. The belt- similarly to the tight cylinder containing the bottle's base whose behaviour was explained in the above section, increases the pressure caused by the air contained in the bottle, making the bottle more rigid.

Yet, adding a belt over each bottle is a complicated and time consuming procedure that can be avoided, since the cylinders a the base are improving the bottle's performance, and if point loads due to prestressing of cables or the existence of clamps, are more carefully designed and located along the structure. Characteristically, once the prestressed steel cables are replaced by steel strips screwed at the mdf sides, the buckling effect at the bottles at the front lines decreases.





Figure 164. Buckling at the waist of the bottle was observed to some specimens when additional compressive load was locally introduced





Figure 165. By attaching a steel strip around the waist, buckling can be avoided



Figure 166. Buckling at the waist can also be reduced in the case where the bottles are squeezed in the cylindrical holders of the lower facing



iv. Upper and lower face cooperation and transfer of shear forces

One of the most crucial matters that needs to be solved is the transfer of the developed horizontal shear stresses, developed at the contact surfaces between the faces and the PET bottle core due to bending, and the vertical shear stresses developed in respect to the occurring vertical shear forces. Given the fact that the connections between the bottles and the faces can be characterised as pinned connections (and thus the bottles in combination with the faces do not act as a Vierendeel truss beam that supposes fixed connections between its elements) and that the bottles are arranged vertically to the faces, the design without the appearance of a rigid side element or a truss component, lacks the ability to handle shear stresses. Without this elements, the bottles are simply transferring half of the load to the lower plate, which acts individually from the upper one (also dealing with half of the load). To give a solution to this problem, and achieve a structure where the upper and lower plate are acting together, benefiting from the high stiffness resulting from the height difference between them, it is impediment to introduce diagonal elements able to handle the shear stresses.

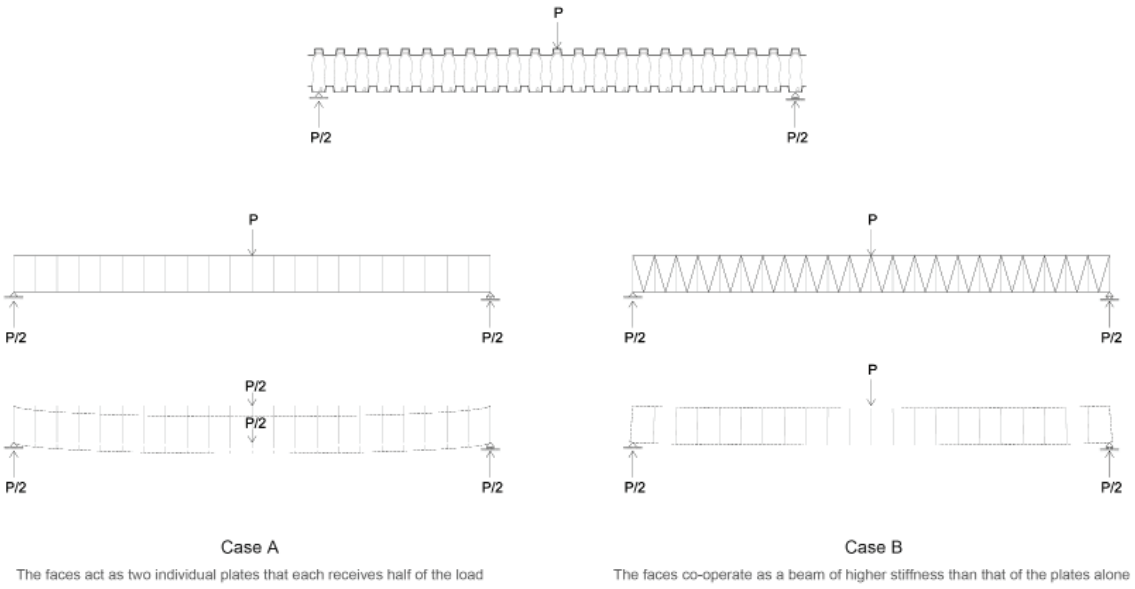

Figure 167. The existence of diagonal elements at the sides of the beam is crucial for the handling of shear stresses and the decreasing of the deformation

Before starting with the physical experiments, a brief study to the behaviour of different truss configurations is intended, to get an insight of the elements to be expected to receive the maximum or minimum forces, and to determine which are going to work in tension and which in compression. In continuation, different alternatives are considered including the possibility of placing the bottles diagonally instead of vertically. The alternatives are assessed according to their performance and feasibility and then the first proof of concept is intended by using rubber bands to connect the upper and lower plate of the full scale prototype.

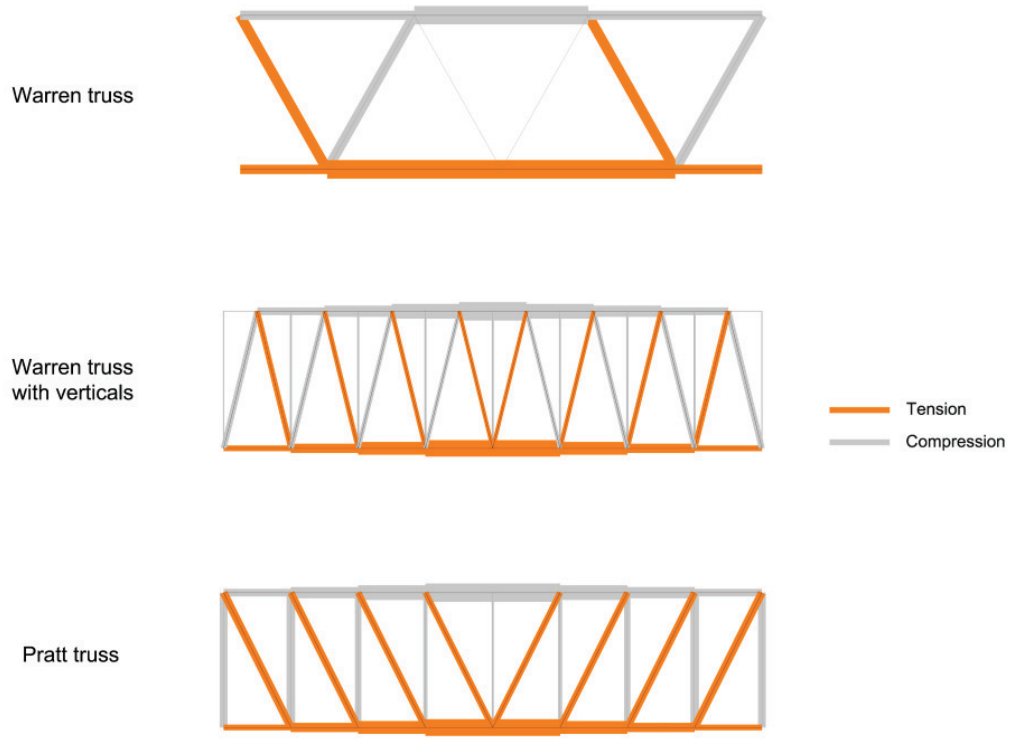

+

- All vertical elements are in compression and take the same force, equal to the force applied at the joint (except verticals at the supports where they take half the standard joint load)
- The diagonal members can be formed by one continuous steel wire that can be pre-stressed at its ends

-

- Pre-stress in required

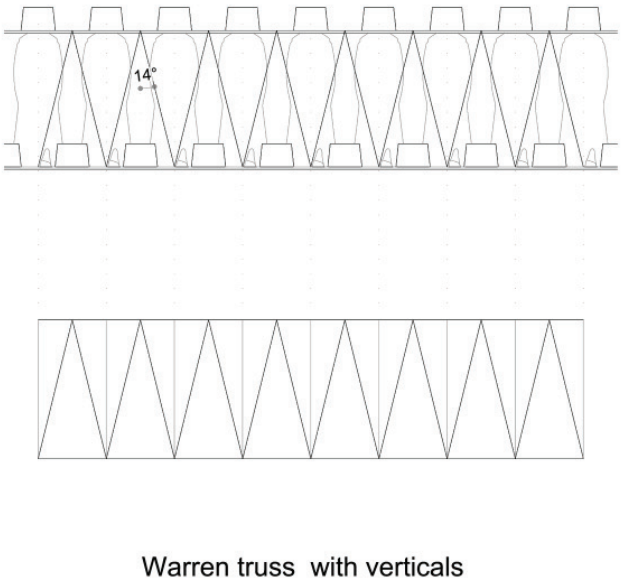

Warren truss with verticals

Figure 168. Advantages and disadvantages between different truss configurations

+

- Force of all elements is equal apart middle elements, where it is 0
- No extra elements are required to take the shear

-

- Half of the bottles are in tension
- It is difficult to keep a bottle that is under tension in contact with the face (also for the same reason it is difficult to perform a physical experiment to test the bottle in tension)
- Bottles are receiving the load at an angle that is not corresponding to their position of optimal performance. Deformation at the waist is thus more
- The panels require a complicated design
- Assembly is very difficult due to different angles

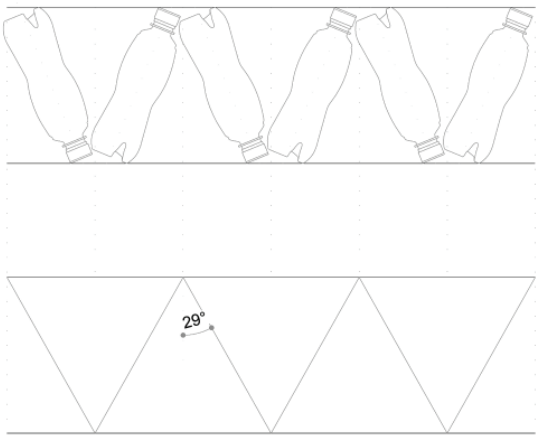

Warren truss

+

- Vertical elements in compression/ diagonal in tension
- The tensile members can be separate elements
- Pre-stress of the diagonal elements is not necessary

-

- Loads vary along the length in all the members
- Only the vertical element in the middle of the span takes force equal to the load applied at each joint. The rest vertical elements take more
- One steel wire instead of separate members cannot be applied

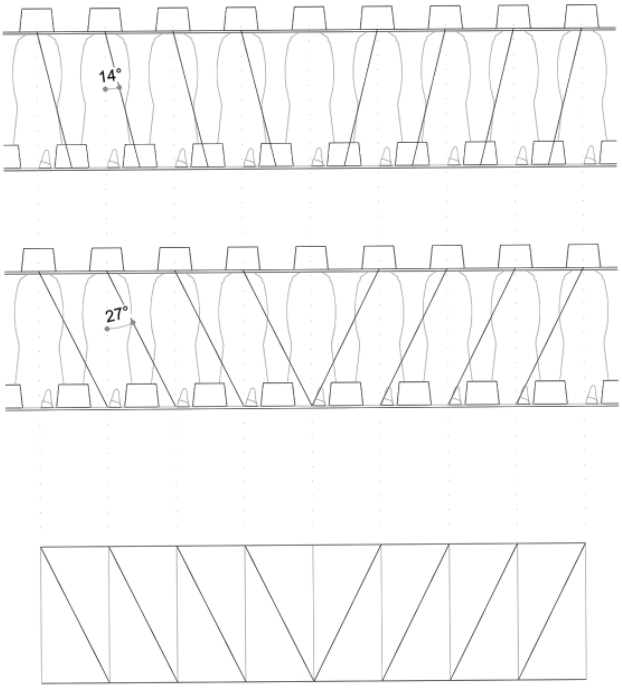

Pratt truss

Figure 169. Advantages and disadvantages between different truss configurations

	Property	Symbol	no. panels	x (no.panels*λ)	Formula	Output	Unit
	Maximum Shear Force	V_t	0	0,000	$V_t=Q_t/2$	219,402	N
Shear	Shear at x distance from supports	V_x	1	0,088	$V_x=(Q_j/\lambda)*(n_h*\lambda/2-x)$	201,849	N
			2	0,176		184,297	N
			3	0,264		166,745	N
			4	0,352		149,193	N
			5	0,440		131,641	N
			6	0,528		114,089	N
			7	0,616		96,537	N
			12	1,056		8,776	N
Moment	Maximum Bending Moment	M_t	$n_h/2$		$M_t=(Q_t*\frac{1}{4}_t)/8$	121,110	N*m
	Bending moment at x distance from supports	M_x	1	0,088	$M_x=(Q_j/\lambda)*(x/2)*(n_h*\lambda-x)$	18,535	N*m
			2	0,176		35,526	N*m
			3	0,264		50,971	N*m
			4	0,352		64,873	N*m
			11	0,968		118,933	N*m
			12	1,056		120,478	N*m
Axial Force	Up, horizontal elem. at middle, (Max,compression)	FU_{max}	$n_h/2$		$FU_t=M_t/d$	634,082	N
	Up, horizontal elem. at x, (compression)	$FU_{(x-1.x)}$	1	0,088	$FU_{(x-1.x)}=M_x/d$	97,042	N
			2	0,176		185,997	N
			3	0,264		266,866	N
			4	0,352		339,647	N
			11	0,968		622,687	N
			12	1,056		630,774	N
	Diagonal, at x (tension)	$FG_{(x-1.x)}$	1	0,088	$FG_{(x-1.x)}=(V_{(x-1)}+V_x)/2*\lambda/d$	97,042	N
			2	0,176		88,955	N
			3	0,264		80,868	N
			4	0,352		72,782	N
			11	0,968		64,695	N
			12	1,056		56,608	N
	Diagonal, at x (tension), Horiz. Component	$FG_{(x-1.x)}x$	1	0,088	$FG_{(x-1.x)}x=sina*FG_{(x-1.x)}$	40,608	N
			2	0,176		37,224	N
			3	0,264		33,840	N
			4	0,352		30,456	N
			11	0,968		27,072	N
			12	1,056		23,688	N
	Diagonal, at x (tension), Vertical Component	$FG_{(x-1.x)}y$	1	0,088	$FG_{(x-1.x)}y=cosa*FG_{(x-1.x)}$	88,137	N
			2	0,176		80,793	N
			3	0,264		73,448	N
			4	0,352		66,103	N
			11	0,968		58,758	N
			12	1,056		51,413	N
	Down, horizontal elem. at x, (tension)	$FD_{x-1.x}$	1	0,088	$FD_{(x-1.x)}=FU_{(x-1.x)}-FG_{(x-1.x)}x$	56,434	N
			2	0,176		148,774	N
			3	0,264		233,026	N
			4	0,352		309,192	N
			11	0,968		595,615	N
			12	1,056		607,086	N
	Vertical elem. at supports (compression)	FV_R	0		$FV_R=FD_{(x,x+1)}y+Q_e$	96,913	N
	Intermediate vertical elem. at x (compression)	FV_x	1	0,088	$FV_R=FD_{(x,x+1)}y+Q_j$	98,345	N
			2	0,176		91,000	N
			3	0,264		83,655	N
			4	0,352		76,310	N
			11	0,968		68,966	N
			12	1,056		17,552	N

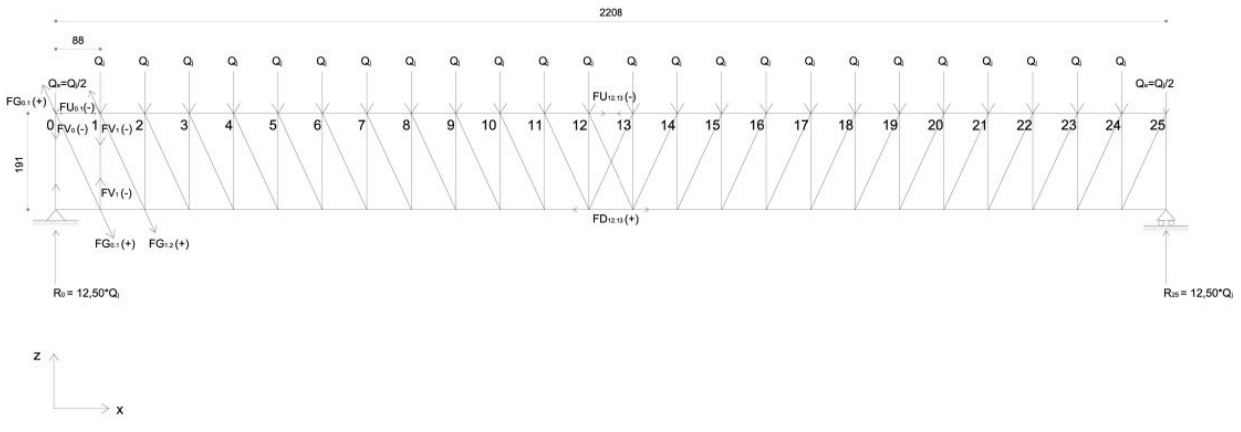

Figure 170. Pratt truss configuration. Approximation depicting the elements that will receive the maximum and minimum amount of internal stresses

	Property	Symbol	no. panels	x (no.panels*λ)	Formula	Output	Unit
Shear	Maximum Shear Force	V_t	0	0,000	$V_t=Q_t/2$	219,402	N
	Shear at x distance from supports	V_x	1	0,044	$V_x= (Q_t/\lambda)*(n_h*\lambda/2-x)$	210,626	N
			2	0,088		201,849	N
			3	0,132		193,073	N
			4	0,176		184,297	N
			5	0,220		175,521	N
			6	0,264		166,745	N
			7	0,308		157,969	N
			23	1,012		17,552	N
			24	1,056		8,776	N
			25	1,100		0,000	N
Moment	Maximum Bending Moment	M_t	$n_h/2$		$M_t= (Q_t*i_t)/8$	121,110	N*m
	Bending moment at x distance from supports	M_x	0	0,000	$M_x= (Q_t/\lambda)*(x/2)*(n_h*\lambda-x)$	0,000	N*m
			1	0,044		9,461	N*m
			2	0,088		18,535	N*m
			3	0,132		27,223	N*m
			4	0,176		35,526	N*m
			23	1,012		119,899	N*m
			24	1,056		120,478	N*m
			25	1,100		120,671	N*m
Axial Force	Up, horizontal elem. at middle, (Max,compression)	FU_{max}	$n_h/2$		$FU_t= M_t/d$	634,082	N
	Up, horizontal elem. at x, (compression)	$FU_{(x-1.x)}$	0-1		$FU_{(x-1.x)}= M_x/d$ *	0,000	N
			1-2			97,042	N
			2-3				
			3-4			185,997	N
			4-5				
			23-24			630,774	N
			24-25				
	Down, horizontal elem. at x, (tension)	$FD_{x-1.x}$	0-2		$FD_{(x-1.x+1)}= M_x/d$ *	49,532	N
			2-4			142,531	N
			22-24			627,741	N
			24-26			631,785	N
	Diagonal, at x	$FG_{(x-1.x)}$	0-1	Compression	$FG_{(x-1.x)}=((V_{(x-1)}+V_x)/2)*\lambda/(d*\sin a)$	220,645	N
			1-2	Tension		211,639	N
			2-3	Compression		202,633	N
			3-4	Tension		193,627	N
			4-5	Compression		184,621	N
			23-24	Tension		13,509	N
			24-25	Compression		4,503	N
	Vertical elem. at supports (compression)	FV_R	0		$FV_R=R-FG_{0.1}*\cos a$	4,388	N
	Intermediate vertical elem. at x (compression)	FV_x	1		$FV_x=Q_i$	8,776	N
			2			8,776	N
			24			8,776	N

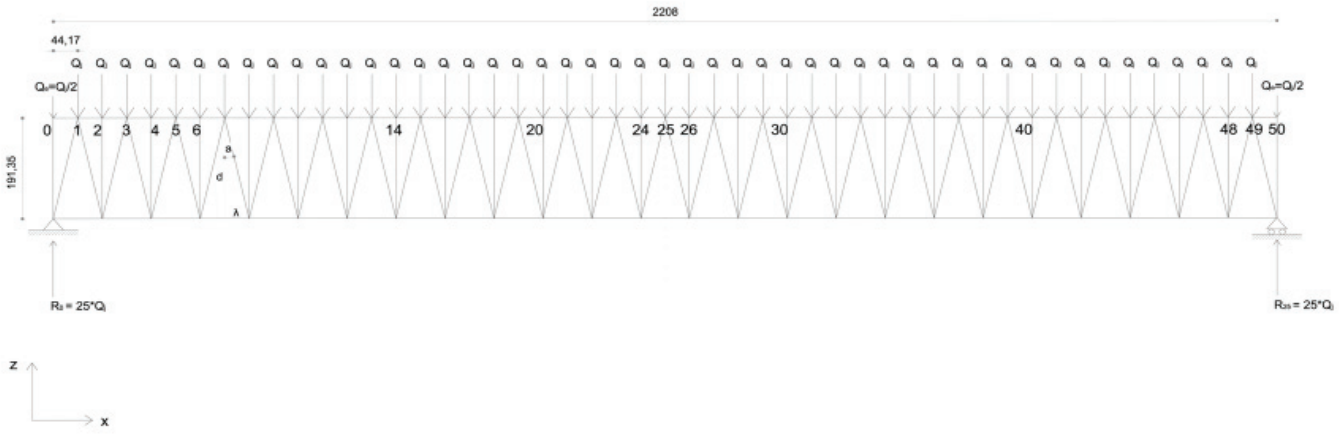

Figure 171. Warren truss configuration. Approximation depicting the elements that will receive the maximum and minimum amount of internal stresses

Also before proceeding into testing of the rubber bands as part of the prototype, tension tests are performed with 2 types of rubber bands to acquire an indication of the load to be expected from the rubber bands due to a given elongation (the one found in the case of the prototype). Also it is examined the damage of the material to be obtained after cyclic loading and its recovery rate after unloading occurs. Result of this test is also the choice of the most suitable rubber band between the two types, to be used at the prototype.

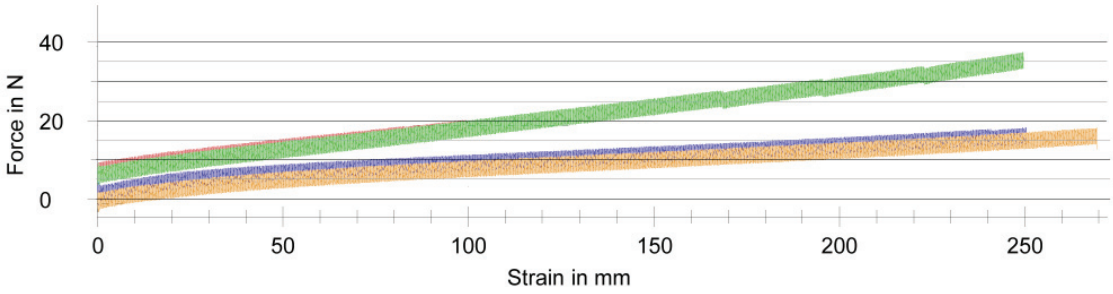

Type 1, Caoutchouc rubber band from "Hevea Brasiliensis", (120*10*1mm)

Sample a, test no. 1, speed test 25mm/min

Sample a, test no. 2, speed test 100mm/min

Type 2, Caoutchouc rubber band from "Hevea Brasiliensis", (165*8*1mm)

Sample a, test no. 1, speed test 100mm/min

Sample a, test no. 2, speed test 100mm/min



Figure 172. Force/strain graph considering two different rubber band types

Type 1, Caoutchouc rubber band from "Hevea Brasiliensis", 120*10*1mm						
Property	**Symbol**	**Imput value**	**Formula**	**Output**	**Unit**	**Comments**
Length	l	0,24			m	Properties from manufacturer
Working length	l_w		$l_w=l/2$	0,12	m	From the band only half length will be calculated (as it is round)
Width	w	0,01			m	"
Thickness	t	0,001			m	"
Strain, maximum	ε_{max}	600-650			%	"
Breaking strength minimum	$\sigma_{b,min}$	323,6			N	"5kgf per 1,5mm width", for 10mm=33kgf=323,6N
Strain, normal usage	ε_{norm}	100-200			%	Properties from manufacturer
Tear strength	σ_t	34.400			N/m	Average property from CES (24,8-44 N/mm)
E modulus min	E_{min}	1.200.000			Pa	Minimum value from CES (0,0012-0,0021GPa)
E modulus max	E_{max}	2.100.000			Pa	Maximum value from CES (0,0012-0,0021GPa)
Assumed elongation	**Δl**	**0,11**			m	
Pairs in each row	ppr	26				From each pair, only 1 band will be taken into account
Number of rows	r	2				
Calculations (using data from CES and properties from manufacturer)						
Section area	A		A= w*t	0,00001	m^2	
Force min at Δl	F_{min}		$F_{min}=E_{min}*(\Delta l/l_w)*A$	11,00	N	
Force max at Δl	F_{max}		$F_{max}=E_{max}*(\Delta l/l_w)*A$	19,25	N	
Tensile test, 19-04-2012						
Sample	**Test no.**	**Δl (mm)**	**Force at Δl (N)**	**Elastic constant k (N/mm)**		**Comments**
a	1	50	9,1	0,18		Speed: 25mm/min
		90	15	0,17		
		150	19,3	0,13		
	2	150	20	0,13		Speed: 100mm/min
		250	30	0,12		
		300	35	0,12		
Calculations (using data from physical experiment)						
Range where assumed deformation lies (mm):		min	90	max	150	
Force at these limits (N):		min	15,0	min	19,3	
Force at estimated deformation (N):		**16,43**				
Type 2, Caoutchouc rubber band from "Hevea Brasiliensis", 165*8*1mm						
Property	**Symbol**	**Imput value**	**Formula**	**Output**	**Unit**	**Comments**
Length	l	0,33			m	
Working length	l_w		$l_w=l/2$	0,165	m	
Width	w	0,008			m	
Thickness	t	0,001			m	
Tensile test, 19-04-2012						
Sample	**Test no.**	**Δl (mm)**	**Force at Δl (N)**	**Elastic constant k (N/mm)**		**Comments**
a	1	70	10	0,14		Speed: 100mm/min
		200	15	0,08		
		250	17,0	0,07		
	2	200	14	0,07		Speed: 100mm/min
		270	17	0,06		

Figure 173. Calculations predicting the force each rubber band will contribute to the prototype

Then, by starting the experiments with the prototype, the first indication that tensioned elements at the sides of the beam improve its performance occurs when a second layer of rubber bands- more tensed than the first layer- is applied at both long sides. Then the deformation at the middle of the span is decreased by 7mm. Simultaneously, the rubber bands denote all the disadvantages related to the use of an adaptive system (such as elastic bands, or tensioned steel cables) for the connection and cohesion of the sandwich beam. When the point load is applied at the middle of the span, half of the bands, due to the truss configuration (Warren Truss), are being compressed, losing part of their effectiveness. Deformation is increasing when the load is kept constant for a period of time, due to the creep effect occurring at the rubber bands and also deformation decreases when the relaxation time after unloading increases. The position of the applied point load affects the deflection of the bands and the beam and it can be noticed that the distance between the upper and lower mdf plate is not kept constant.

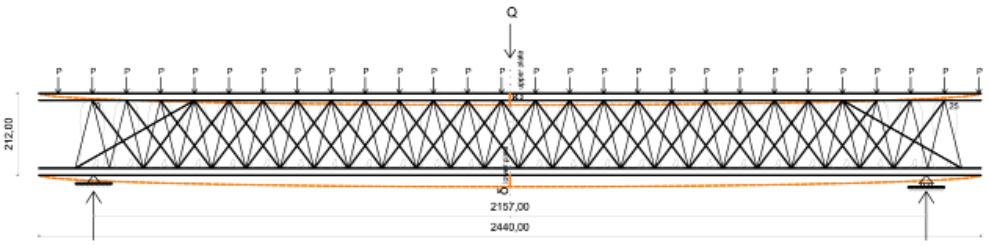

Date:	27/04/2012
Test no. :	11
Uniform load P :	Own weight (total = 240N)
Point load Q :	400N, middle of span (applied on the upper mdf plate)
Truss configuration :	Two diagonals between bottles (Warren truss approximation) and a 2nd layer of diagonals (Warren truss approximation)
Truss material :	Natural rubber bands, connecting 1 nail up to 1 down (half in tension) and 4 nails up to 1 down (same band tensed and compressed)
Bottles-plates connection:	Pieces of PVC soft are inserted between the bottles' caps and the mdf upper plate and between the bottles' bases (only those placed in the exterior rows) and the pvc tubes attached at the lower plate



	Time	Before loading	Immediately after loading	After 30 min under loading	After 1 hour under loading	Immediately after un-loading
Displacement (middle of the span)	δ lower plate (mm)*	8,5	33	35	35	13
	δ upper plate (mm)**				37	
Distance between mdf plates	D left (mm)	212	212			
	D middle (mm)	211	210			
	D right (mm)	211	212			

* The depicted value is affected by the method of measurement, in this case, the deflection of the rope. Thus the value should be used only as point of reference between the tests and not an accurate indication of the deflection of the beam

** The depicted value is affected by the method of measurement, in this case, from irregularities of the floor surface. Thus the value should be used only as point of reference between the tests and not an accurate indication of the deflection of the beam

Figure 174. Data related to the deformation observed during test no. 11

Figure 175. Deformation observed during test no. 11



Replacing the rubber bands with steel cable, φ 3mm, at first did not result in considerable changes. The reason behind this behaviour is related to the fact that only one cable and turnbuckle were used at each long side of the beam. In consequence, the cable close to the turnbuckle was fully tensed but the tension hardly reached the other end of the cable. Once 2 cables where introduced at each side, tensioned at both ends, deformation dropped by 5mm By decreasing the tension, the deformation at the middle increased again.

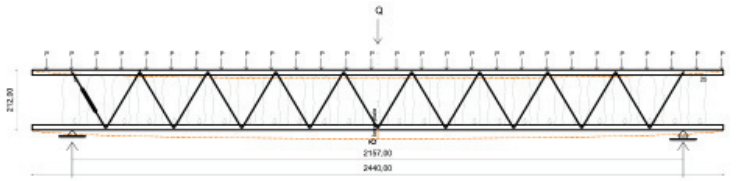

Date:	01/05/2012
Test no. :	14
Uniform load P :	Own weight (total = 240N)
Point load Q :	400N, middle of span (applied on the upper mdf plate)
Truss configuration :	Continuous truss, 60° angle between diagonal elements (Warren truss approximation)
Truss material :	One 3mm steel cable at each side tensed at the left end (threads until the middle of the turnbuckle)
Bottles-plates connection:	Pieces of PVC soft are inserted between the bottles' caps and the mdf upper plate and between the bottles' bases (only those placed in the exterior rows) and the pvc tubes attached at the lower plate

	Time	Before loading	Immediately after loading	After 30 min under loading	Immediately after un-loading	5 min after un-loading
Displacement (middle of the span)	δ lower plate (mm)*	6	26	27,5	11,5	10,5
Distance between mdf plates	D left (mm)		210			
	D middle (mm)		210			
	D right (mm)		212			

* The depicted value is affected by the method of measurement. In this case, the deflection of the rope. Thus the value should be used only as point of reference between the tests and not an accurate indication of the deflection of the beam

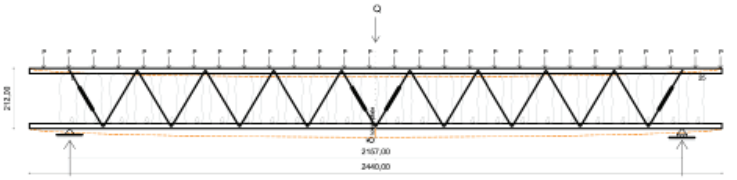

Date:	02/05/2012
Test no. :	17
Uniform load P :	Own weight (total = 240N)
Point load Q :	400N, middle of span (applied on the upper mdf plate)
Truss configuration :	Continuous truss, 60° angle between diagonal elements (Warren truss approximation)
Truss material :	Two 3mm steel cables at each side tensed at the corners and at the middle of the span (6 turnbuckles in total)
Bottles-plates connection:	Pieces of PVC soft are inserted between the bottles' caps and the mdf upper plate and between the bottles' bases (only those placed in the exterior rows) and the pvc tubes attached at the lower plate. Steel strips are inserted opposite the PVC soft pieces to fix the caps to the upper plate

	Time	Before loading	Immediately after loading	After 15 min under loading	Immediately after un-loading	18 hours after un-loading
Displacement (middle of the span)	δ lower plate (mm)*	4	21	23	11	9**
Distance between mdf plates	D left (mm)	210	210			
	D middle (mm)	209	209			
	D right (mm)	210,5	210,5			

* The depicted value is affected by the method of measurement. In this case, the deflection of the rope. Thus the value should be used only as point of reference between the tests and not an accurate indication of the deflection of the beam

** One cable slipped the clamp and got detached from the turnbuckle

Figure 176. Changes in the deflection of the beam, by introducing 3 more turnbuckles at each side

Figure 177. Deflection of the beam during test no. 17



Another problem affecting the efficiency of the steel cables is their holding by circular hooks, which- by being screwed at the sides of the beam, damage locally the mdf and gradually tend to be pulled out. This behaviour points out a problem to be expected at the actual design where the mdf is replaced by a 3mm FRP skin, and the proper connection of the hooks is necessary in order to avoid stress concentration. Maybe the incorporation of aluminum strips with the hooks welded on, to the composite surface during lamination can be considered.

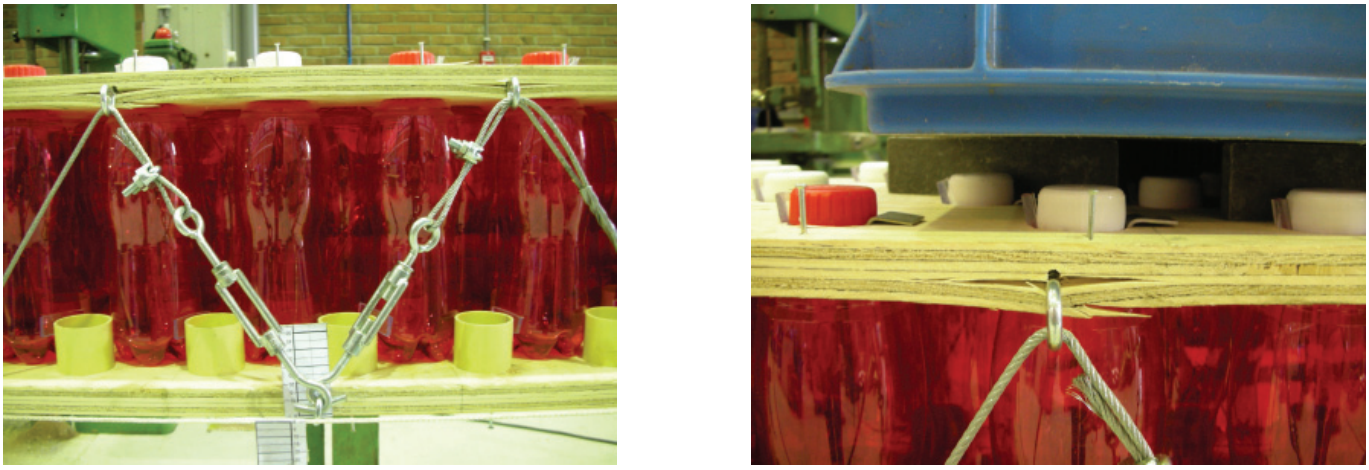

Figure 178. Failure of the mdf plated due to local stress

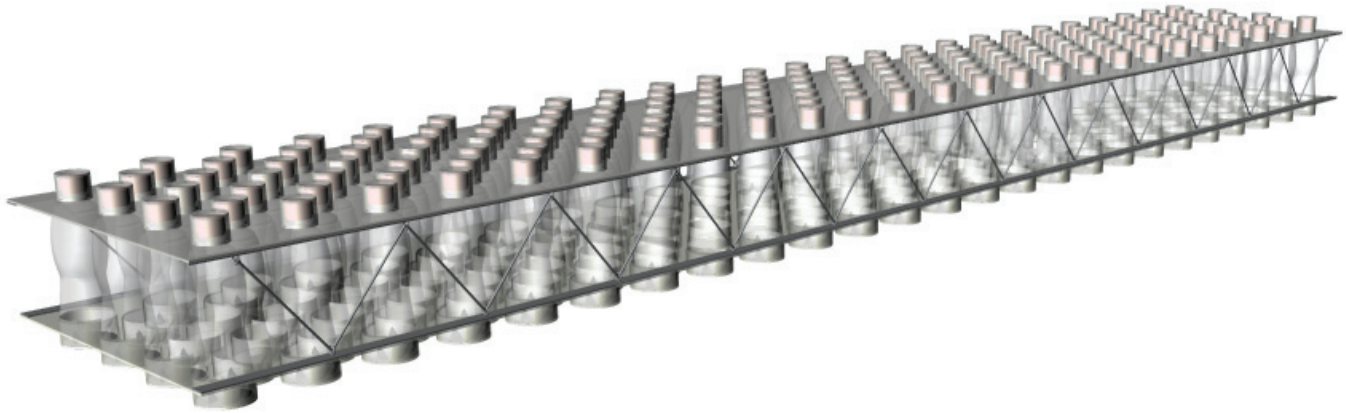

Figure 179. Steel stripes need to be incorporated at the ends of the FRP plates during lamination, to avoid failing due to point loads form the truss elements

When the lower mdf plate was changed in the prototype, so the bottom cylinders can include the bottles instead of surrounding them, a more dense truss was tested. The circular hooks in this version are placed in the interior surface of the mdf plates (such would be the case in the actual design, as suggested in the paragraph above) in order to avoid the tearing caused at the mdf sides from the tensioning of the cables. The height of the truss is therefore reduced. In addition, to avoid the buckling caused at the bottles next to the position of the turnbuckles, the hooks are placed with a spacing aligned to the array of the bottles and always resulting in the grid-line between the bottles. It is intended this way to divide the applied stress into two bottles and thus reduce the waist buckling that was observed before. Yet, as the new truss is denser, tensioning the cables is a much more demanding process, and despite the effort, the tension at the steel cables dramatically drops as we move away from the turnbuckles. As it can be expected, not sufficient pre-tensioning results in parts of the cable to be experiencing compression, when the point load is applied at the middle of the beam. In relation to that, when the beam was loaded after the change of the lower mdf plate (where the connection between the lower plate and the bottles' bases was evidently improved), the deformation at the middle of the span was only decreased by 1mm. By increasing the tension at the cables and repeating the test, deflection was decreased by 2mm more, but even so the result was still 2,5 times larger than the allowed deflection.

This two experiments (no. 23-24) are proving the disadvantages of the proposed solution. In addition, through the building of the prototype, insight was gained at the difficulties and implications related with the installation of the steel cables and the achievement of an equally distributed tension along their length. Doubts are expressed if the proposed solution can guarantee a quick and easy assembly or the efficient bonding between the upper and lower plate (due to its adaptive character).

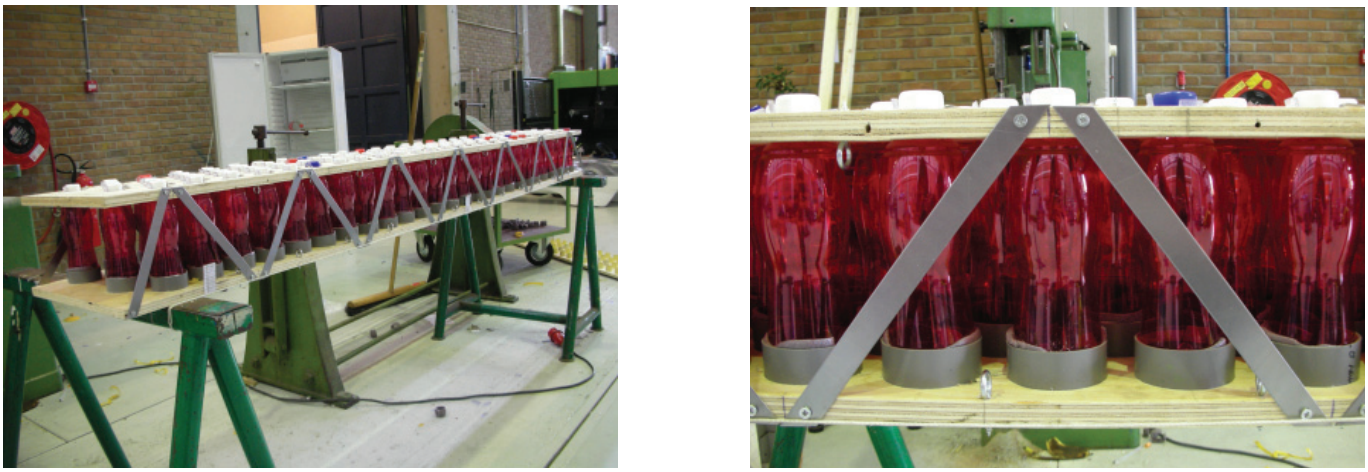

Figure 180. Steel stripes screwed at the mdf sides replace the steel tensioned cable

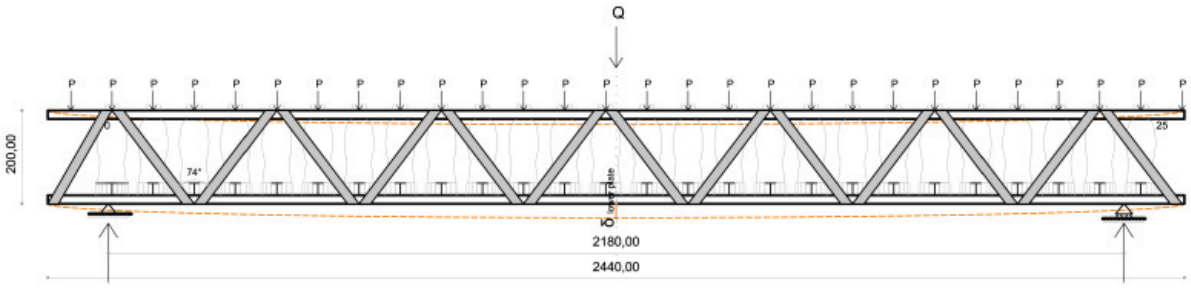

Figure 181. Drawing showing the spacing of the truss, as this was constructed in the prototype

As a consequence, the steel cables are replaced in the prototype by steel stripes of 270*20*1,5mm dimensions, screwed on the sides of the mdf plates. Their configuration is creating a Warren type truss at the sides of the beam, with a spacing bridging every two bottles (from cap to base). The first tests show that this modification significantly alters the behaviour of the structure and reduces its deflection at the middle. Although some permanent deformation is noticed at the prototype due to the previous testing, the deflection at the middle of the span, caused only by the point load (400N) ranges from 2-5mm, according to the different test settings. An indication of the contribution of the beam's own weight to the deflection observed at the start of each experiment can be vaguely obtained when the beam is turned upside down. By comparing the deflection at the middle between the two positions we can assume a 3mm of displacement to be attributed to the structure's own weight (appr. 240N), yet no safe conclusions can be derived, since a combination of different settings related to the two different positions is expected to be influencing the result.

Date:	09/05/2012
Test no. :	25
Uniform load P :	Own weight (total ≈ 240N)
Point load Q :	400N, middle of span (applied on the caps)
Truss configuration :	Continuous truss, 74° angle between diagonal elements (Warren truss approximation), aligned with bottles' array
Truss material :	Individual steel stripes (27*20*1,5mm) screwed at the sides of the upper and lower plate
Bottles-plates connection:	Pieces of PVC soft and steel strips are inserted between the bottles' caps and the mdf upper plate. New mdf used for the lower plate, with φ 70mm holes (φ holes at previous plate= 38mm) drilled until the middle of its thickness and pvc tubes inserted in them to receive the bottles



	Time	Before loading	Immediately after loading	5 min under loading	Immediately after un-loading
Displacement (middle of the span)	δ lower plate (mm)*	6**	9	9	8
Distance between mdf plates	D left (mm)	200	200		
	D middle (mm)	200	200		
	D right (mm)	200	200		

* The depicted value is affected by the method of measurement, in this case, the deflection of the rope. Thus the value should be used only as point of reference between the tests and not an accurate indication of the deflection of the beam

** The depicted value is not purely reflecting the deflection of the beam under its own weight, as the beam presents permanent deformation due to the previous experiments

Figure 182. After installing the steel stripes, deflection is significantly minimised

What is important to mention, however, is that due to the permanent deformation of the beam, when this is turned upside down, it presents an upward curvature, that is not cancelled out neither by the effect of the structure's own weight nor by the impact of the applied point load. Considering more carefully the process of installing the steel stripes at the structure, it can be said that since these stiff elements were applied while the beam was already deformed (the cables were not removed but only after the stripes were applied), they contributed to the "crystallization"of this shape.

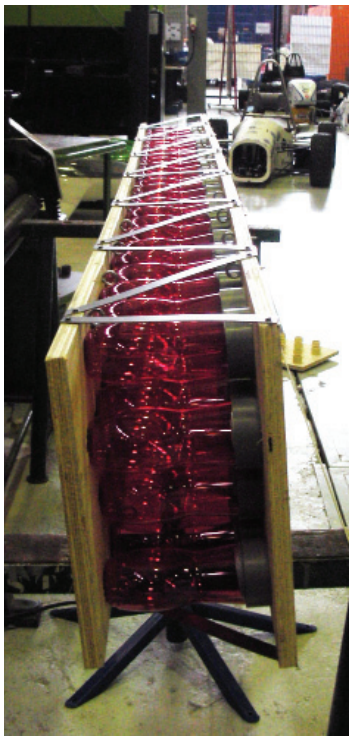

Figure 183. Beam was permanently curved when the stripes were attached



Figure 184. Deflection of the beam under point load applied in the middle (Test no 25)



Figure 185. By turning the beam upsidedown, its permanent deformation can work in cancelling the deflection due to the beam's own weight

Taking into account the above observation and also the fact that the actual module is mainly composed by polymers, it can be suggested that the beam is slightly deformed when the steel truss is applied. Objective of this precamber effect caused by the geometry of the beam, is to nullify the deformation caused by the beam's own weight and thus minimise the total deflection of the structure, when loaded.

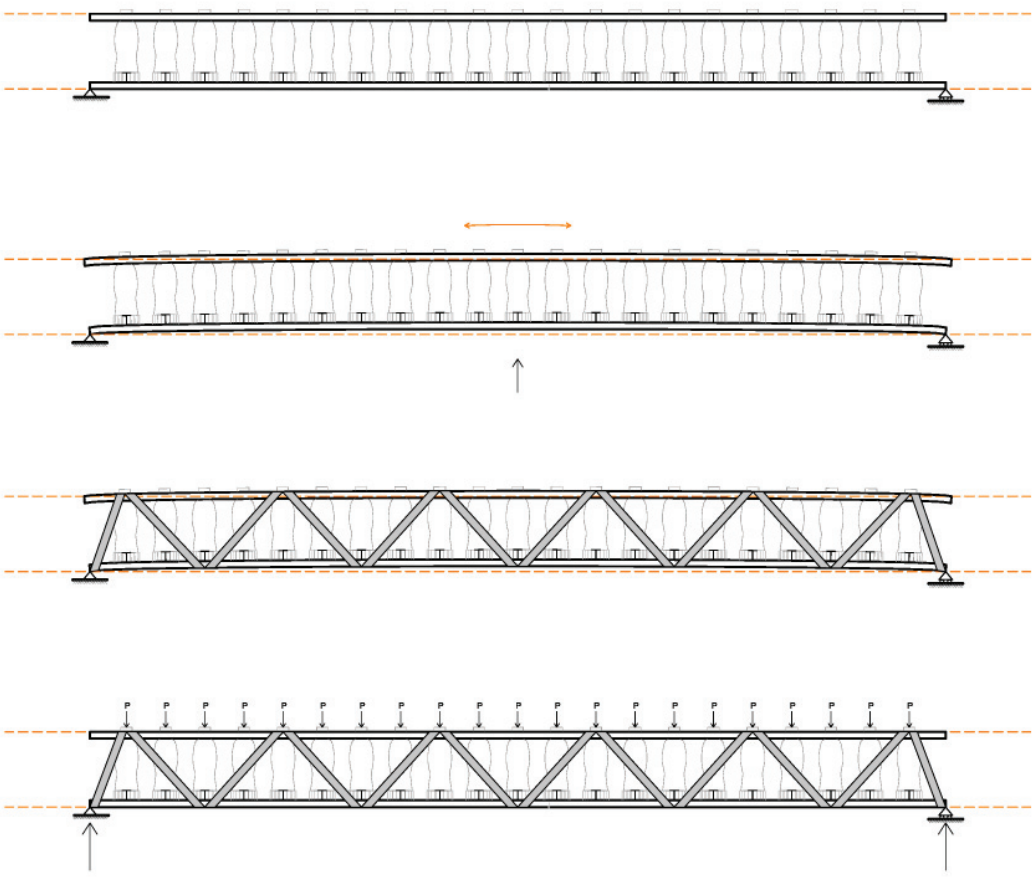

Figure 186. Method of precambering the structure during the production process of the module

Taking into account the above observation and also the fact that the actual module is mainly composed by polymers, it can be suggested that the beam is slightly deformed when the steel truss is applied. Objective of this precamber effect caused by the geometry of the beam, is to nullify the deformation caused by the beam's own weight and thus minimise the total deflection of the structure, when loaded.

Another advantage of the steel truss is that is causing the structure to behave better under creep conditions and also to recover instantly when it is unloaded. Further testing should take place, however, to determine the behaviour of the structure under constant and fatigue loads.

Nonetheless, this solution, apart from being more effective, it is also simpler to assemble. Regarding the actual module, the steel stripes can be welded together in continuous truss elements that can be then adjusted at the sides of the modules and screwed on steel inserts, incorporated in the FRP faces during lamination.

The performance of the structure with this modification can also be more easily understood and predicted, with the help of course of hand calculations, since the system is much less adaptive than before.

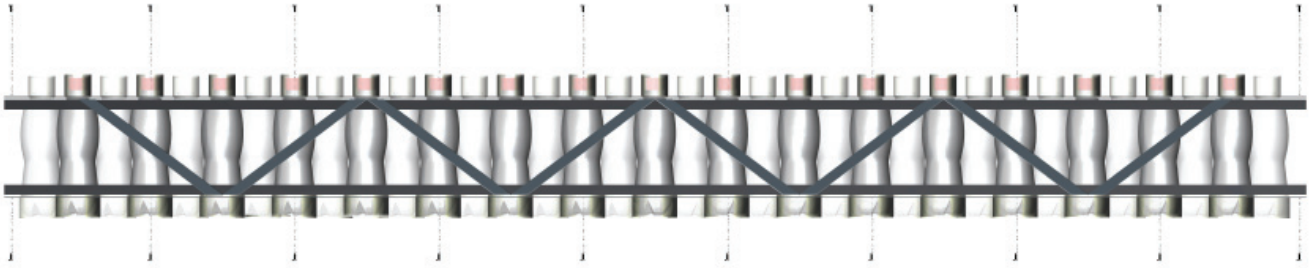

Figure 187. Elevation showing the geometry and application method of the steel truss

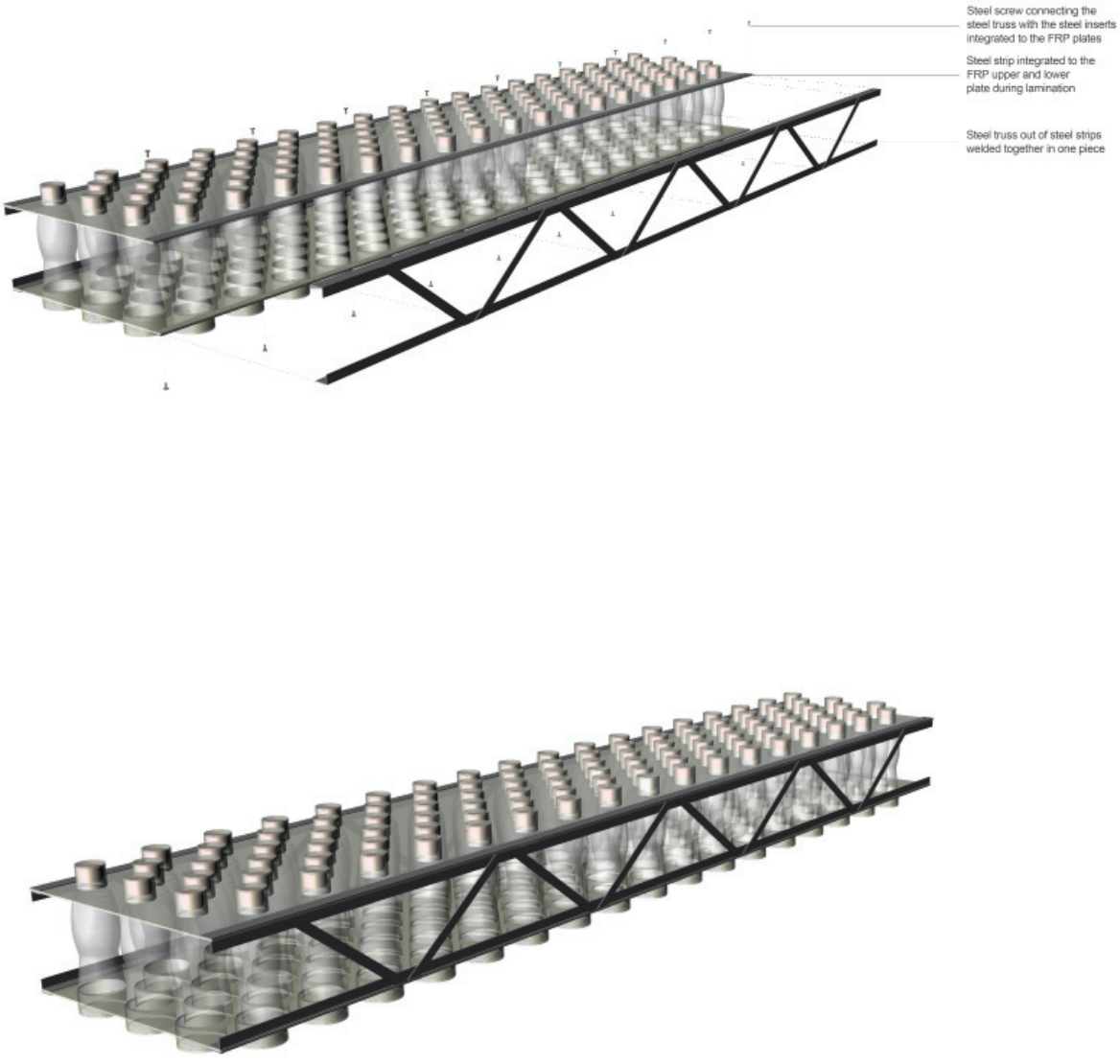

Figure 188. 3D aspects of the module

v. Deflection of module

For a composite panel, the issue of deflection can be of a much more governing design factor than the strength of the structure. Similarly in our case, before starting to concern about the strength limits of the module, its deflection under different loadcases should be measured, analysed and understood, and then steps towards its minimization should be taken. This focus on the matter of deformation can be easily explained as at the first experiments, when the beam receives a total load of 640N (240N own weight, 400N point load at middle), the deflection appears to be exceeding the acceptable service limits by 5,5 times, while the strength limitations of the structure are not nearly reached under this loadcase.

In antithesis to standard beams, where the shear deflection can be neglected, in a composite beam the resulting deflection is a combination of shear and bending deflection. The deflection due to bending is related to the faces and is influenced by the bending stiffness D of the upper and lower face combined (E modulus of the material, section and distance between centroids of plates are determining factors). Shear deflection is attributed to the core and thus related to its height and shear stiffness S.

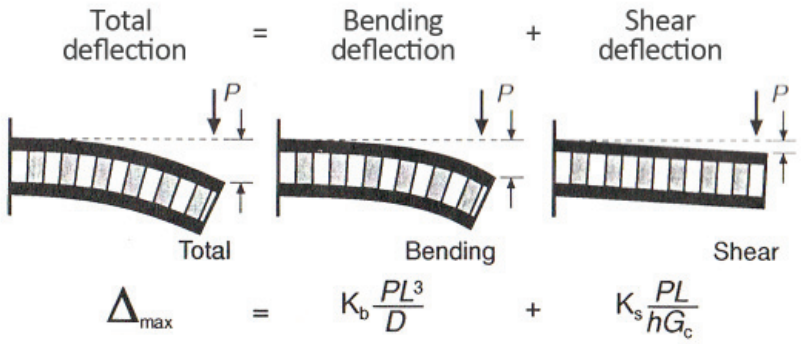

Figure 189. Deflection observed in sandwich panels and beams

Source: BITZER, T. Honeycomb Technology
Materials, design, manufacturing, applications and testing

From the above it can be derived the importance of achieving the faces and the PET bottle core work as a coherent unit, in order to minimise deflection. The cooperation relies therefore to the effectiveness of the connections between the bottles and the faces and the introduction of diagonal elements at the core that can take the shear stresses.

Modifications to the prototype done throughout the experiments are focused at the above points of interest and their effectiveness is assessed according to their effectiveness in decreasing deflection. The comparative tables presented below can give an overview of the alterations that took place and the gradual improvement of the module's behaviour.

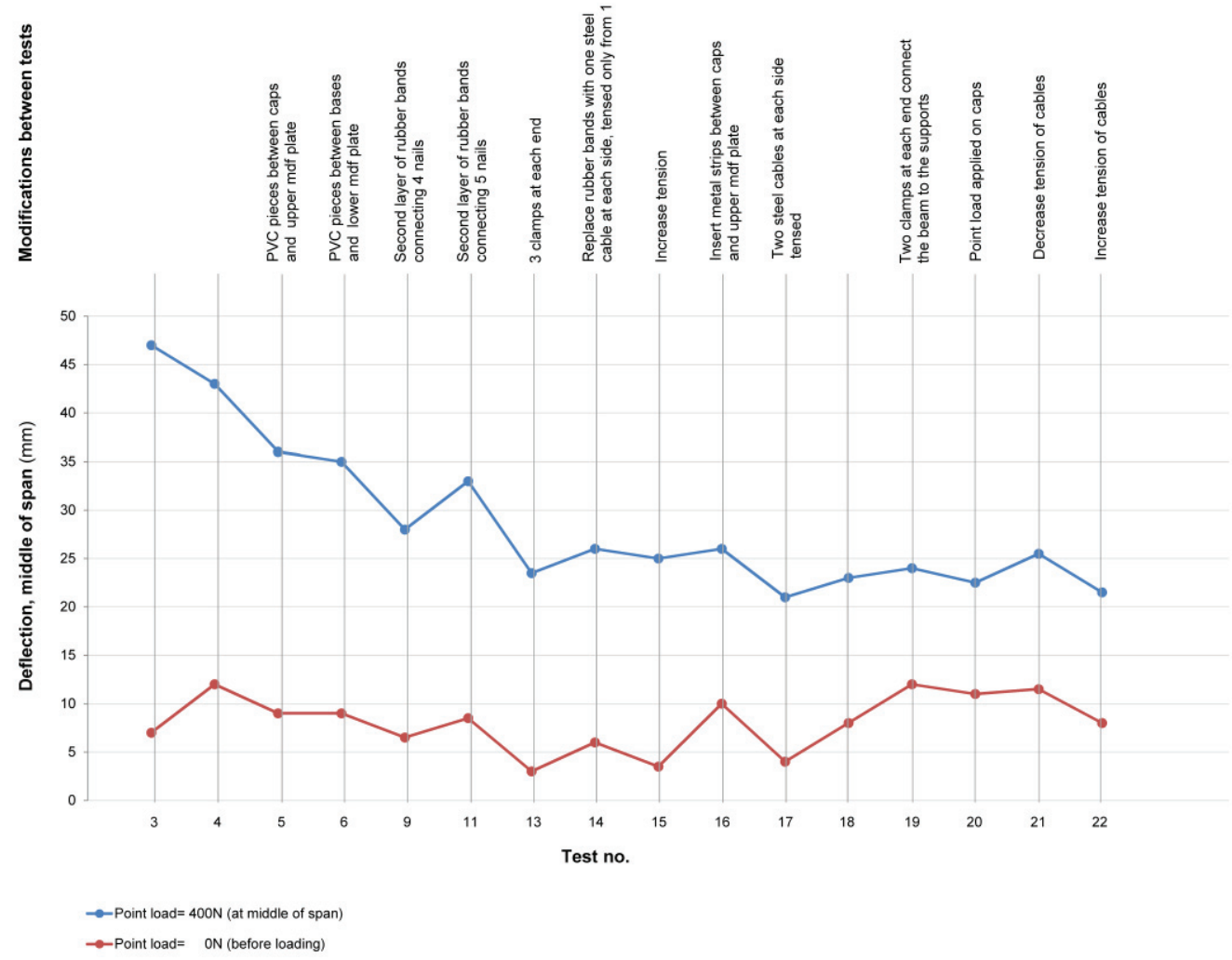

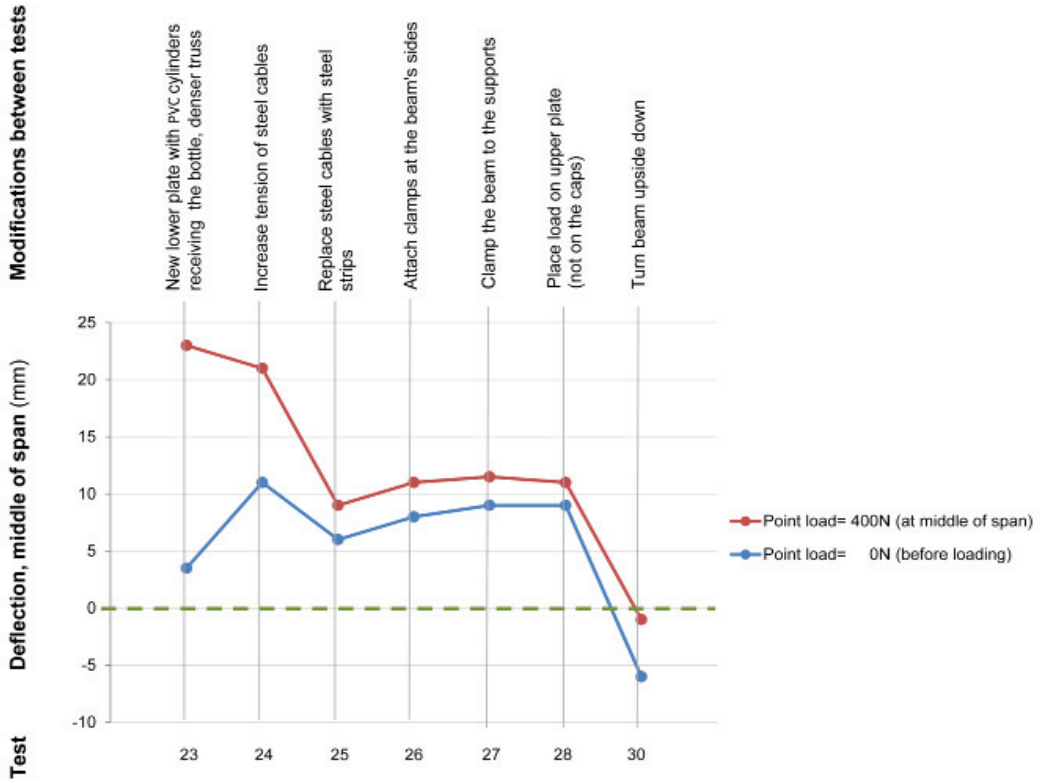

Figure 190. Graphs showing the effect of the modifications done at the prototype on the deflection of the beam due to its own weight and a point load applied at the middle of the span

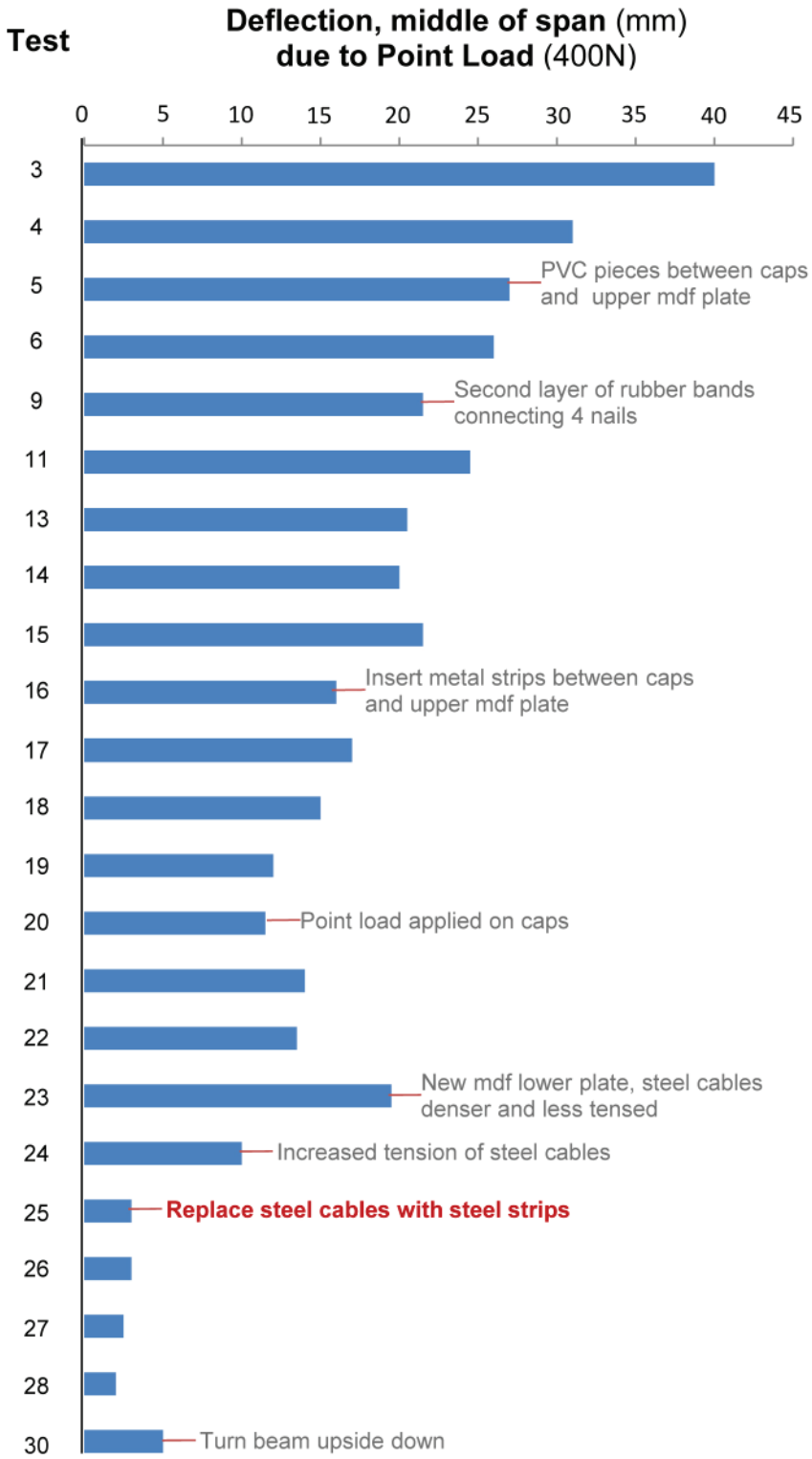

Figure 191. Chart showing the effect of the modifications done at the prototype on the deflection of the beam due to a point load applied at the middle of the span

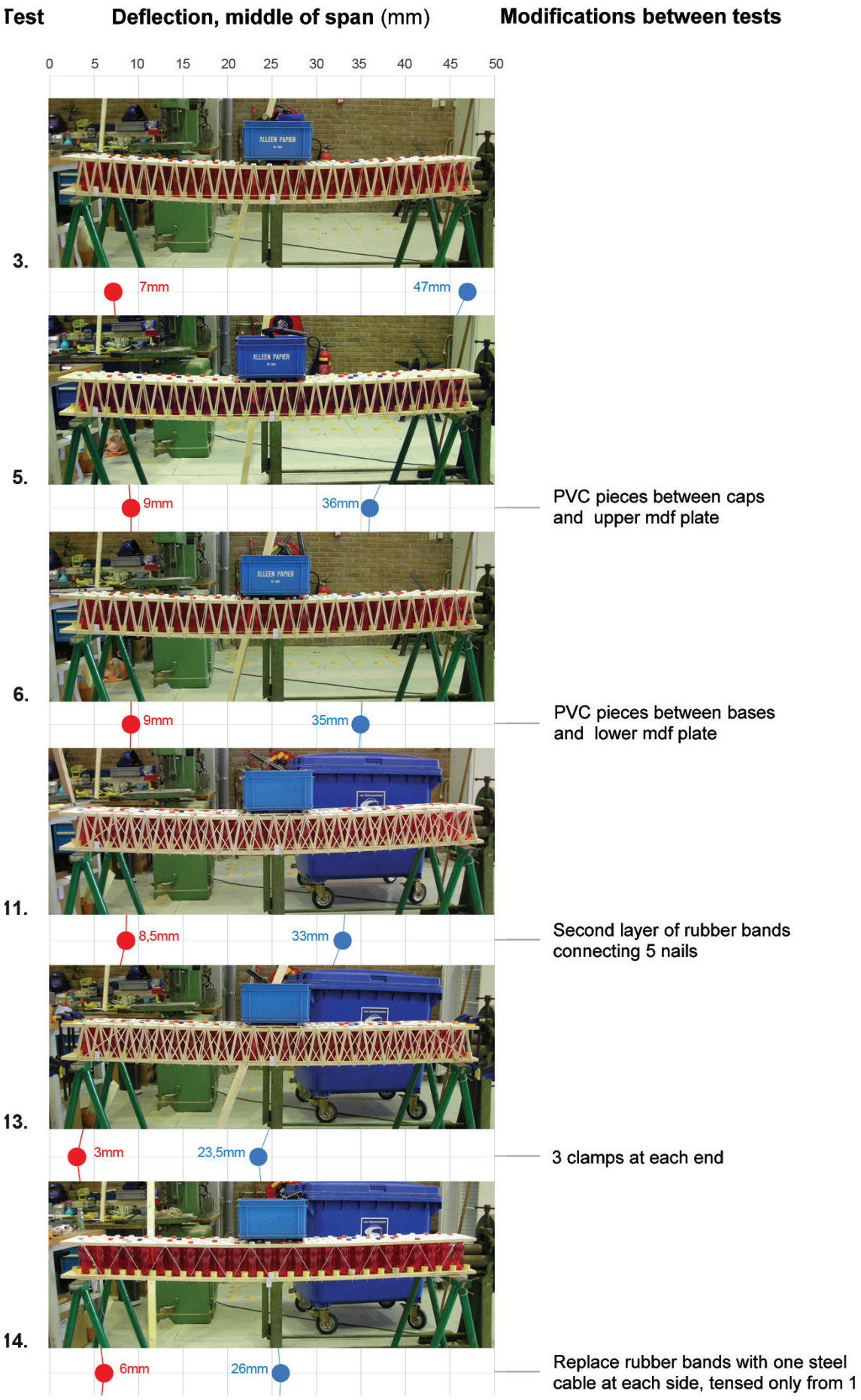

Figure 192. Graphs and pictures showing the effect of the modifications done at the prototype on the deflection of the beam due to a point load applied at the middle of the span

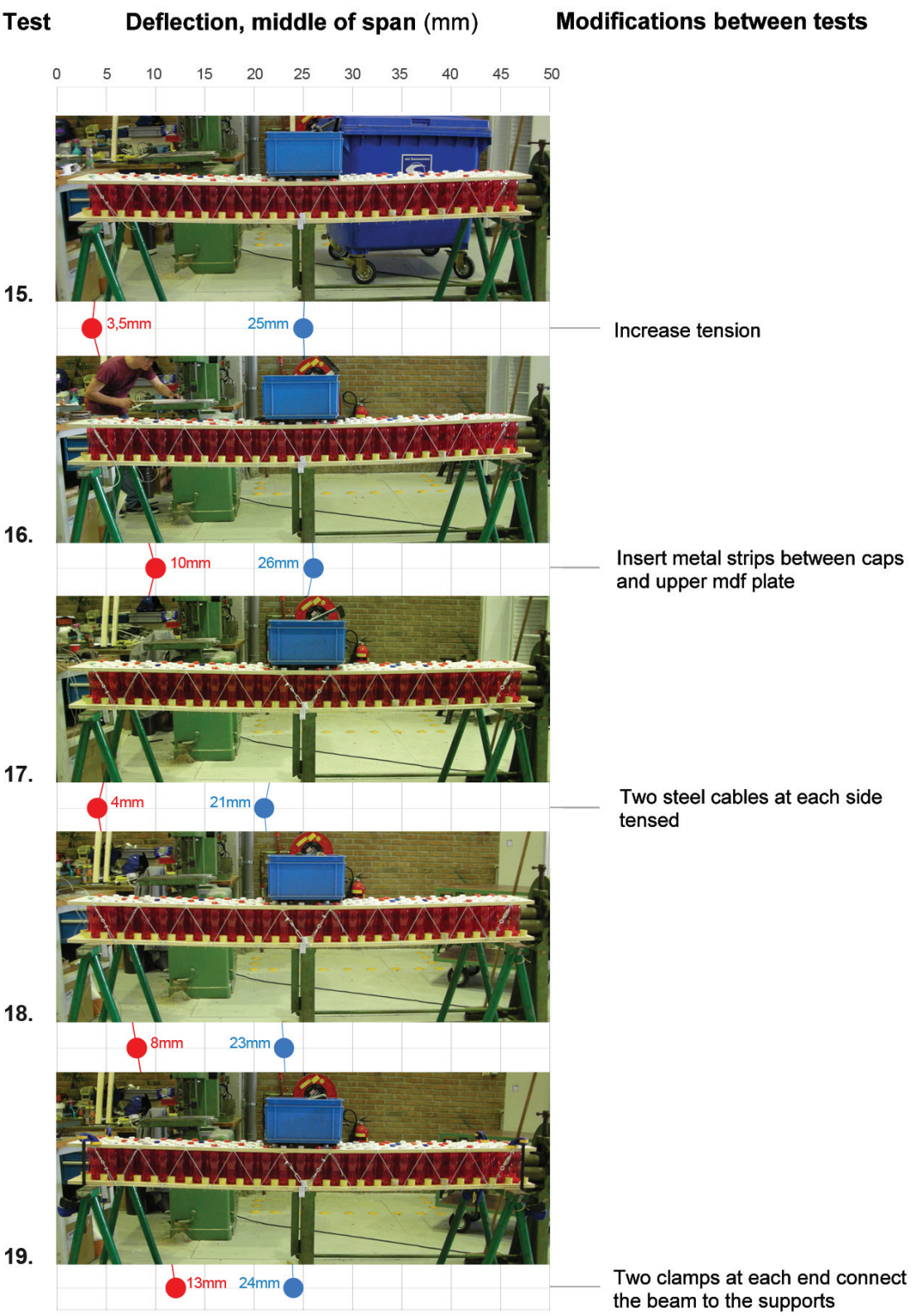

Figure 193. Graphs and pictures showing the effect of the modifications done at the prototype on the deflection of the beam due to a point load applied at the middle of the span

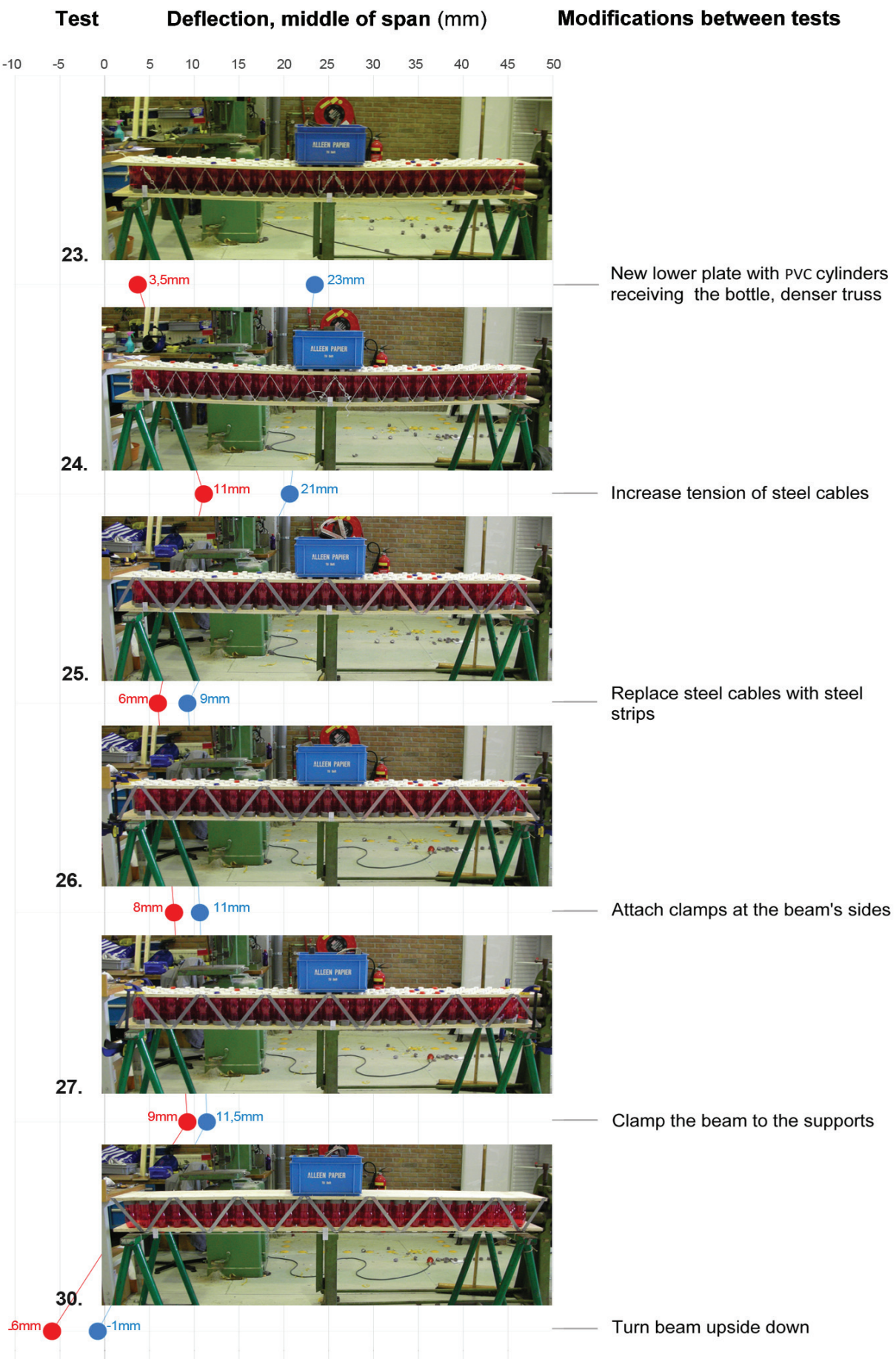

Figure 194. Graphs and pictures showing the effect of the modifications done at the prototype on the deflection of the beam due to a point load applied at the middle of the span

2.2.3.3 Comparison of experimental results and hand calculations

In order to interpret the results from the prototype testing, a series of hand calculations is performed to form the basis of comparison between the physical experiments and the theoretical approach. As the role of these calculations at this phase is to simply give a point of reference, a series of simplifications are adapted. More elaborate calculations will follow once the prototype testing is completed and the design is updated according to the observations. Also, these elaborate calculations will concern the performance of the proposed design and not that of the prototype (that is the properties of the actual materials will be taken into account and not of those used for the prototype).

Returning to the simplified calculations, using the properties of the material used in the prototype, these evolve around the study of 3 extreme cases. In all cases the corrugated faces are assumed to be planar (the 3D structure will in fact improve the stiffness of the structure, thus the worse case scenario is studied) and the holed drilled in the faces of the prototype are not taken into account (as in the actual design they do not exist as such). The calculations focus on the developed moments and bending stresses due to the structure's own weight and the applied point load at the middle of the span and predict the deflection due to bending only. Calculating shear deflection would not be of any value before testing the prototype, as many unknown aspects about the behaviour of the core do not yet allow its proper approximation to be used for the calculations.

The deflection of the prototype is thus compared to the three extreme situations listed below:
Case A: One mdf plate
In this case the deflection of one mdf plate is examined

Case B: Two mdf plates working individually
In this scenario the distance between the two mdf plates in the z axis is similar to that seen in the prototype. In between the plates the PET core is situated. The role of the bottles is only to divide the applied load to the two plates and no shear stress is transferred through them

Case C: Two mdf plates working as a composite beam
This ideal situation assumes that the core and faces compose a uniform beam that presents a much higher bending stiffness than the plates individually, because of the distance between the plates in the z axis (same as in Case 2 and in the prototype)

For all three cases the applied uniform load is 240N and the point load at the middle of the span is 400N. The mdf plates are 18mm thick.

The maximum allowed deflection, determined as the value equal the 1/250 of the span is another important value used for the comparison of the results.

The performed calculations and experiments locate the performance of the beam between case 2 and 3, indicating that the structure, even in the case of the rubber bands, can transfer some shear stresses and work as a composite beam. At the last series of experiments, where the steel stripes are installed, the performance tends to be much closer to that of case 3, showing that the gap between the 2 individual plates and the ideal composite beam is gradually closing.

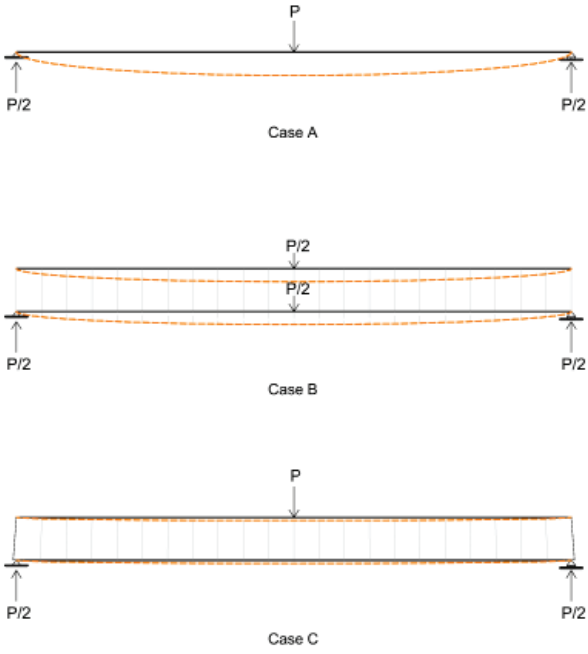

Figure 195. The three study cases

Beam: Simple support, central load							
	Property	Symbol	Imput value	Formula	Output	Unit	Comments
Beam	Length	ℓ	2,440			m	
	Width	b	0,312			m	
	Area (xy plane)	A		A= ℓ*b	0,761	m^2	
	Length (bottle edge to bottle edge)	ℓ_b	2,317			m	
	Width (bottle edge to bottle edge)	b_b	0,294			m	
	Distance between centroid of supports	ℓ_c	2,157			m	
Face (MDF)	Face thickness	t_f	0,018			m	
	Young's modulus	E_f	1.800.000.000			Pa	Minimum value from CES (1,8 - 3,2 Gpa)/ Perpendicular to board
	Yield strength	σ_y	5.000.000			Pa	Average value from CES (4,5 - 5,5) MPa
	Tensile strength	σ_{ten}	8.500.000			Pa	Minimum value from CES (8,5 - 21) MPa
	Compressive strength	σ_{compr}	3.000.000			Pa	Minimum value from CES (3 - 7) MPa
	Height btw mdf faces (including mdf thickness)	d	0,212		0,000	m	Simplified approximation considering the faces planar
	Height btw centroids of faces	d_c		d_c= d - t_f	0,194	m	Simplified approximation considering the faces planar
	Poisson's ratio	ν_f	0,25				Average value from CES (0.2 - 0.3)
	Density	ρ_f	750			Kg/m^3	Average value from CES (0,6e3 - 0,9e3 kg/m^3)
	Upper/lower plate mass	m_{pl}		m_{pl}=ρ_f*t_f*A	10,277	kg	
	Upper/lower plate weight	W_{pl}		W_{pl}=m_{pl}*g	100,820	N	
Bottle	Compressive modulus	E^c_b	230.408.709,700			Pa	Sum from compression tests (on 14-02-2012, 07-03-2012), case 1
	Poisson's ratio	v	0,4				Assumption for bottle closed (air inside). Crystalline PET v= 0.381- 0.396 (CES)
	Shear modulus	G_b		G_b= E^c_b/ 2*(1+v)	161.286.096,790	Pa	
	Number of bottles in 1 row (width)	no_w	4				
	Number of bottles in 1 column (length)	no_l	26				
	Total number of bottles	no_b		no_b=no_w*no_l	104		
	Mass	m_b	0,03063			Kg	
	Thickness of PET surface	t_{PET}	0,00041			m	
	Minimum radius	r	0,026			m	
	Height of bottle	h_b	0,203			m	
	Area (section in z direction)	A_b	0,00022			m^2	Case 1: only the thickness of the bottle is calculated for the section area
	Volume	V_b	0,000464			m^3	
	Density	ρ_b		ρ_b= m_b/V_b	66,013	Kg/m^3	
Core	Core thickness	t_c	0,173			m	
	Mass	m_c		m_c= no_b*m_b	3,186	Kg	
	Core weight	W_c		W_c=m_c*g	31,250	N	
	Volume	V_c		V_c= t_c*A	0,132	m^3	Approximation using the simplified core thickness
	Density	ρ_c		ρ_c= m_b/V_c	24,187	Kg/m^3	
	Cell opening (distance between bottles)	s	0,088			m	Length

Figure 196. Properties related to the prototype

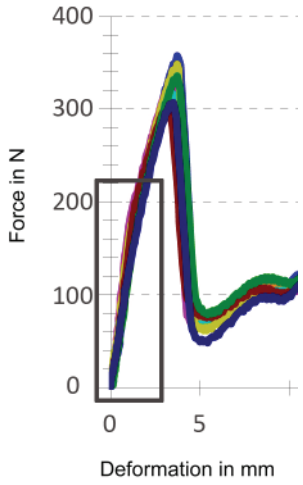



Figure 197. Calculations defining the Compressive modulus of the bottles (Case 1 is chosen, as worse case scenario)

Case	Property	Symbol	Imput / formula	Comments
	Bottle height (mm)	L	203	
Case 1	Area (m_2)	A_1	0.000082	Max. diameter, only thickness calculated
Case 2		A_2	0.000706	Cap diameter, solid
Case 3		A_3	0.003216	Max. diameter, solid
	Compressive modulus	E^C_b	$E^C_b = (F*L) / (A*\Delta l)$	

Test No.	Maximum force F_{max} (N)	Deformation Δl at F_{max} (mm)	E^C_b (Pa or N/m^2)		
			Case 1	Case 2	Case 3
Compression Test 14-02-2012					
2	288	3	237,658,536.59	27,603,399.43	6,059,701.49
3	305	3.1	243,568,056.65	28,289,774.28	6,210,379.55
4	330	3.7	220,797,626.90	25,645,050.15	5,629,790.24
5	158	1.7	230,086,083.21	26,723,879.35	5,866,622.77
SUM	270.25	2.875	233,027,575.84	27,065,525.81	5,941,623.51
MIN	158	1.7	220,797,626.90	25,645,050.15	5,629,790.24
MAX	330	3.7	243,568,056.65	28,289,774.28	6,210,379.55
Compression Test 7-03-2012 (max. test speed)					
15	319	3.6	219,366,531.17	25,478,832.23	5,593,300.86
17	357	3.8	232,577,021.82	27,013,195.17	5,930,135.51
18	327	3.5	231,292,682.93	26,864,022.66	5,897,388.06
19	327	3.3	245,310,421.29	28,492,145.25	6,254,805.52
20	317	3.5	224,219,512.20	26,042,492.92	5,717,039.80
21	349	3.7	233,510,217.53	27,121,583.34	5,953,929.68
23	336	3.8	218,896,020.54	25,424,183.69	5,581,304.01
24	307	3.5	217,146,341.46	25,220,963.17	5,536,691.54
SUM	329.88	3.59	227,789,843.62	26,457,177.30	5,808,074.37
MIN	307	3.3	217146341.5	25220963.17	5536691.542
MAX	357	3.8	245310421.3	28492145.25	6254805.518

SUM	300.06	3.23	230,408,709.73	26,761,351.55	5,874,848.94

Load	Uniformly distributed load	q	0			N/m^2	From regulations: Category A (domestic and residential), floors
	Uniform load on beam area	Q		$Q= q*A$	0,000	N	
	Beam mass	m_{be}		$m_{be}= i*b*t_f*2*\rho_f + no_c*m_b$	23,740	Kg	
	Beam weight	W_{be}		$W_{be}= m_{be}*g$	232,890	N	
	Total uniform load	Q_{tot}		$Q_{tot}= Q+W_{be}$	232,890	N	
	Point Load	P	0			N	Applied in the middle
Calculations, Case A: 1 plate							
Stiffness	Sec. moment of inertia (xz plane) of 1 plate	I_{pl}		$I_{pl}=(b*(t_f\wedge3))/12$	0,0000001516	m^4	
	Bending stiffness	D		$D=E_f*I_{pl}$	272,938	$N*m^2$	
Simple supported beam, uniform load							
Moment	Support coefficient	M_{coef}	0,125	$M_{coef}=1/8$			
	Maximum Bending Moment, Upper plate	M		$M= (Q_{tot}*l_x)*M_{coef}$	62,793	N*m	
Bending Stress	Bending stress (due to M), upper plate	σ_f		$\sigma_f= M*(t_f/2)/I_{pl}$	3.727.030,87	Pa	It should be lower than the face's compressive and yield strength
Deflection	Bending deflection coefficient	k_b	0,0130	$k_b=5/384$			
	Deflection, bending, upper plate	δ_b		$\delta_b=(k_b*Q_{tot}*l_x\wedge3)/D$	0,111501	m	
	Allowed deflection	δ_a		$\delta_a= l_x/250$	0,008628	m	
Simple supported beam, point load, middle of span							
Moment	Support coefficient	M_{coef}	0,250	$M_{coef}=1/4$			
	Maximum Bending Moment, Upper, Lower plat	M		$M= (P*l_x)*M_{coef}$	0,000	N*m	
Bending Stress	Bending stress (due to M), Upper, Lower plate	σ_f		$\sigma_f= M*(t_f/2)/I_{pl}$	0,000	Pa	It should be lower than the face's compressive and yield strength
Deflection	Bending deflection coefficient	k_b	0,0208	$k_b=1/48$			
	Deflection, bending, Upper, Lower plate	δ_b		$\delta_b=(k_b*P*l_x\wedge3)/D$	0,000000	m	
	Allowed deflection	δ_a		$\delta_a= l_x/250$	0,008628	m	
				Total deflection	**0,112**	**m**	
Calculations, Case B: 2 individual plates							
Stiffness	Sec. moment of inertia (xz plane) of 1 plate	I_{pl}		$I_{pl}=(b*(t_f\wedge3))/12$	0,0000001516	m^4	
	Bending stiffness	D		$D=E_f*I_{pl}$	272,938	$N*m^2$	
Load	Load, upper plate	Q_{up}		$Q_{up}= Q/2+W_{pl}$	100,820	N	
	Load, lower plate	Q_{down}		$Q_{down}= Q/2+W_{pl}+W_c$	132,070	N	
Simple supported beam, uniform load							
Moment	Support coefficient	M_{coef}	0,125	$M_{coef}=1/8$			
	Maximum Bending Moment, Upper plate	M_{up}		$M_{up}= (Q_{up}*l_x)*M_{coef}$	27,184	N*m	
	Maximum Bending Moment, Lower plate	M_{down}		$M_{down}= (Q_{down}*l_x)*M_{coef}$	35,609	N*m	
Bending Stress	Bending stress (due to M), upper plate	$\sigma_{f.up}$		$\sigma_{f.up}= M_{up}*(t_f/2)/I_{pl}$	1.613.462,963	Pa	It should be lower than the face's compressive and yield strength
	Bending stress (due to M), lower plate	$\sigma_{f.down}$		$\sigma_{f.down}= M_{down}*(t_f/2)/I_{pl}$	2.113.567,906	Pa	It should be lower than the face's compressive and yield strength
Deflection	Bending deflection coefficient	k_b	0,0130	$k_b=5/384$			
	Deflection, bending, upper plate	$\delta_{b.up}$		$\delta_{b.up}=(k_b*Q_{up}*l_x\wedge3)/D$	0,048270	m	
	Deflection, bending, lower plate	$\delta_{b.down}$		$\delta_{b.down}=(k_b*Q_{down}*l_x\wedge3)/D$	0,063231	m	
	Allowed deflection	δ_a		$\delta_a= l_x/250$	0,008628	m	
Simple supported beam, point load, middle of span							
Moment	Support coefficient	M_{coef}	0,250	$M_{coef}=1/4$			
	Maximum Bending Moment, Upper, Lower plat	M		$M= ((P/2)*l_x)*M_{coef}$	0,000	N*m	
Bending Stress	Bending stress (due to M), Upper, Lower plate	σ_f		$\sigma_f= M*(t_f/2)/I_{pl}$	0,000	Pa	It should be lower than the face's compressive and yield strength
Deflection	Bending deflection coefficient	k_b	0,0208	$k_b=1/48$			
	Deflection, bending, Upper, Lower plate	δ_b		$\delta_b=(k_b*(P/2)*l_x\wedge3)/D$	0,000000	m	
	Allowed deflection	δ_a		$\delta_a= l_x/250$	0,008628	m	
				Total deflection (down)	**0,063**	**m**	
Calculations, Case C: composite beam							
Stiffness	Sec. moment of inertia (xz plane)	I_b		$I_b=2*b*t_f*(d/2)\wedge2$	0,0001057	m^4	
	Bending stiffness	D		$D= (E_f*t_f*d\wedge2*b)/2$	190.227,398	$N*m^2$	
Load	Load, beam	Q_{tot}			232,890	N	
Simple supported beam, uniform load							
Moment	Support coefficient	M_{coef}	0,125	$M_{coef}=1/8$			
	Maximum Bending Moment	M_{max}		$M_{max}= (Q_{tot}*l_x)*M_{coef}$	62,793	N*m	
Bending Stress	Bending stress (due to M)	σ_f		$\sigma_f= M_{max}/(d*t_f*b)$	0,068	Pa	It should be lower than the face's compressive and yield strength
Deflection	Bending deflection coefficient	k_b	0,0130	$k_b=5/384$			
	Deflection, bending, upper plate	δ_b		$\delta_b=(k_b*Q_{tot}*l_x\wedge3)/D$	0,000160	m	
	Allowed deflection	δ_a		$\delta_a= l_x/250$	0,008628	m	
Simple supported beam, point load, middle of span							
Moment	Support coefficient	M_{coef}	0,250	$M_{coef}=1/4$			
	Maximum Bending Moment	M_{max}		$M_{max}= (P*l_x)*M_{coef}$	0,000	N*m	
Bending Stress	Bending stress (due to M)	σ_f		$\sigma_f= M_{max}/(d*t_f*b)$	0,000	Pa	It should be lower than the face's compressive and yield strength
Deflection	Bending deflection coefficient	k_b	0,0208	$k_b=1/48$			
	Deflection, bending, upper plate	δ_b		$\delta_b=(k_b*P*l_x\wedge3)/D$	0,000000	m	
	Allowed deflection	δ_a		$\delta_a= l_x/250$	0,008628	m	
				Total deflection	**0,000160**	**m**	

Point load = 0 N

Figure 198. Hand calculations concerning the behaviour of the three study cases under uniformly distributed load equal to the weight of the structure

Load	Uniformly distributed load	q	0			N/m^2	From regulations: Category A (domestic and residential), floors
	Uniform load on beam area	Q		Q= q*A	0,000	N	
	Beam mass	m_{be}		m_{be}= i*b*t_f*2*ρ_f + no_c*m_b	23,740	Kg	
	Beam weight	W_{be}		W_{be}= m_{be}*g	232,890	N	
	Total uniform load	Q_{tot}		Q_{tot}= Q+W_{be}	232,890	N	
	Point Load	P	400			N	Applied in the middle
Calculations, Case A: 1 plate							
Stiffness	Sec. moment of inertia (xz plane) of 1 plate	I_{pl}		I_{pl}=(b*(t_f^3))/12	0,0000001516	m^4	
	Bending stiffness	D		D=E_f*I_{pl}	272,938	$N*m^2$	
Simple supported beam, uniform load							
Moment	Support coefficient	M_{coef}	0,125	M_{coef}=1/8			
	Maximum Bending Moment, Upper plate	M		M= (Q_{tot}*i_s)*M_{coef}	62,793	N*m	
Bending Stress	Bending stress (due to M), upper plate	σ_f		σ_f= M*(t_f/2)/I_{pl}	3.727.030,87	Pa	It should be lower than the face's compressive and yield strength
Deflection	Bending deflection coefficient	k_b	0,0130	k_b=5/384			
	Deflection, bending, upper plate	δ_b		δ_b=(k_b*Q_{tot}*i_s^3)/D	0,111501	m	
	Allowed deflection	δ_a		δ_a= i_s/250	0,008628	m	
Simple supported beam, point load, middle of span							
Moment	Support coefficient	M_{coef}	0,250	M_{coef}=1/4			
	Maximum Bending Moment, Upper, Lower plat	M		M= (P*i_s)*M_{coef}	215,700	N*m	
Bending Stress	Bending stress (due to M), Upper, Lower plate	σ_f		σ_f= M*(t_f/2)/I_{pl}	12.802.706,553	Pa	It should be lower than the face's compressive and yield strength
Deflection	Bending deflection coefficient	k_b	0,0208	k_b=1/48			
	Deflection, bending, Upper, Lower plate	δ_b		δ_b=(k_b*P*i_s^3)/D	0,306412	m	
	Allowed deflection	δ_a		δ_a= i_s/250	0,008628	m	
				Total deflection	**0,418**	**m**	
Calculations, Case B: 2 individual plates							
Stiffness	Sec. moment of inertia (xz plane) of 1 plate	I_{pl}		I_{pl}=(b*(t_f^3))/12	0,0000001516	m^4	
	Bending stiffness	D		D=E_f*I_{pl}	272,938	$N*m^2$	
Load	Load, upper plate	Q_{up}		Q_{up}= Q/2+W_{pl}	100,820	N	
	Load, lower plate	Q_{down}		Q_{down}= Q/2+W_{pl}+W_c	132,070	N	
Simple supported beam, uniform load							
Moment	Support coefficient	M_{coef}	0,125	M_{coef}=1/8			
	Maximum Bending Moment, Upper plate	M_{up}		M_{up}= (Q_{up}*i_s)*M_{coef}	27,184	N*m	
	Maximum Bending Moment, Lower plate	M_{down}		M_{down}= (Q_{down}*i_s)*M_{coef}	35,609	N*m	
Bending Stress	Bending stress (due to M), upper plate	$\sigma_{f,up}$		$\sigma_{f,up}$= M_{up}*(t_f/2)/I_{pl}	1.613.462,963	Pa	It should be lower than the face's compressive and yield strength
	Bending stress (due to M), lower plate	$\sigma_{f,down}$		$\sigma_{f,down}$= M_{down}*(t_f/2)/I_{pl}	2.113.567,906	Pa	It should be lower than the face's compressive and yield strength
Deflection	Bending deflection coefficient	k_b	0,0130	k_b=5/384			
	Deflection, bending, upper plate	$\delta_{b,up}$		$\delta_{b,up}$=(k_b*Q_{up}*i_s^3)/D	0,048270	m	
	Deflection, bending, lower plate	$\delta_{b,down}$		$\delta_{b,down}$=(k_b*Q_{down}*i_s^3)/D	0,063231	m	
	Allowed deflection	δ_a		δ_a= i_s/250	0,008628	m	
Simple supported beam, point load, middle of span							
Moment	Support coefficient	M_{coef}	0,250	M_{coef}=1/4			
	Maximum Bending Moment, Upper, Lower plat	M		M= ((P/2)*i_s)*M_{coef}	107,850	N*m	
Bending Stress	Bending stress (due to M), Upper, Lower plate	σ_f		σ_f= M*(t_f/2)/I_{pl}	6.401.353,276	Pa	It should be lower than the face's compressive and yield strength
Deflection	Bending deflection coefficient	k_b	0,0208	k_b=1/48			
	Deflection, bending, Upper, Lower plate	δ_b		δ_b=(k_b*(P/2)*i_s^3)/D	0,153206	m	
	Allowed deflection	δ_a		δ_a= i_s/250	0,008628	m	
				Total deflection (down)	**0,216**	**m**	
Calculations, Case C: composite beam							
Stiffness	Sec. moment of inertia (xz plane)	I_b		I_b=2*b*t_f*(d/2)^2	0,0001057	m^4	
	Bending stiffness	D		D= (E_f*t_f*d^2*b)/2	190.227,398	$N*m^2$	
Load	Load, beam	Q_{tot}			232,890	N	
Simple supported beam, uniform load							
Moment	Support coefficient	M_{coef}	0,125	M_{coef}=1/8			
	Maximum Bending Moment	M_{max}		M_{max}= (Q_{tot}*i_s)*M_{coef}	62,793	N*m	
Bending Stress	Bending stress (due to M)	σ_f		σ_f= M_{max}/(d*t_f*b)	0,068	Pa	It should be lower than the face's compressive and yield strength
Deflection	Bending deflection coefficient	k_b	0,0130	k_b=5/384			
	Deflection, bending, upper plate	δ_b		δ_b=(k_b*Q_{tot}*i_s^3)/D	0,000160	m	
	Allowed deflection	δ_a		δ_a= i_s/250	0,008628	m	
Simple supported beam, point load, middle of span							
Moment	Support coefficient	M_{coef}	0,250	M_{coef}=1/4			
	Maximum Bending Moment	M_{max}		M_{max}= (P*i_s)*M_{coef}	215,700	N*m	
Bending Stress	Bending stress (due to M)	σ_f		σ_f= M_{max}/(d*t_f*b)	0,235	Pa	It should be lower than the face's compressive and yield strength
Deflection	Bending deflection coefficient	k_b	0,0208	k_b=1/48			
	Deflection, bending, upper plate	δ_b		δ_b=(k_b*P*i_s^3)/D	0,000440	m	
	Allowed deflection	δ_a		δ_a= i_s/250	0,008628	m	
				Total deflection	**0,000600**	**m**	

Point load = 400 N

Figure 199. Hand calculations concerning the behaviour of the three study cases under uniformly distributed load equal to the weight of the structure, and a point load applied at the middle of the span

Loadcase: Own weight ≈ 240N, Point load at middle: 0N			
	Test no./Case	Description	Deflection, middle of span (mm)
Prototype	1	1 layer of rubber band connections	7*
Hand calculations	8	2 layers of rubber band connections	6,5*
	A	1 mdf plate**	112
	B	2 mdf plates working individually	63
	C	2 mdf plates working as beam	0,43
Allowed deformation		δ_{max}= l/250	8,6

Loadcase: Own weight ≈ 240N, Point load at middle: 400N				Deflection, middle of span (mm)	
	Test no./Case	Description	Deflection, middle of span (mm)*	Before loading*	Due to point load only*
Prototype	3	1 layer of rubber band connections	47	7	40
	4	1 layer of rubber band connections	43	12	31
	5	1 layer of rubber band connections, pvc soft on holes of upper plate	36	9	27
	6	1 layer of rubber band connections, pvc soft on upper and lower plate	35	9	26
	9	2 layers of rubber band connections, pvc soft on upper and lower plate	28	6,5	21,5
	11	2 layers of rubber band connections (2nd layer more streched than in test 9), pvc soft on upper and lower plate	33	8,5	24,5
	12***	2 layers of rubber band connections (2nd layer more streched than in test 9), pvc soft on upper and lower plate, bottles' caps located at the lower plate	32	0	32
	13	2 layers of rubber band connections (2nd layer more streched than in test 9), pvc soft on upper and lower plate, bottles' caps located at the lower plate, 3 clamps at each side	23,5	3	20,5
	14	steel truss, 60°, moderate tension, pvc soft on upper and lower plate, bottles' caps located at the lower plate	26	6	20
	15	steel truss, 60°, moderate tension (more than in Test 14), pvc soft on upper and lower plate, bottles' caps located at the lower plate	25	3,5	21,5
	16	steel truss, 60°, moderate tension (same as in Test 15), pvc soft on upper and lower plate, bottles' caps located at the lower plate, steel strips between caps and upper plate	26	10	16
	17	steel truss, 60°, increased and uniformly distributed tension (8 turnbuckles), pvc soft on upper and lower plate, bottles' caps located at the lower plate, steel strips between caps and upper plate	21	4	17
	18	steel truss, 60°, increased and uniformly distributed tension (8 turnbuckles), pvc soft on upper and lower plate, bottles' caps located at the lower plate, steel strips between caps and upper plate	23	8	15
	19	steel truss, 60°, increased and uniformly distributed tension (8 turnbuckles), pvc soft on upper and lower plate, bottles' caps located at the lower plate, steel strips between caps and upper plate, clamps connecting beam to the supports	24	12	12
	20	steel truss, 60°, increased and uniformly distributed tension (8 turnbuckles), pvc soft on upper and lower plate, bottles' caps located at the lower plate, steel strips between caps and upper plate, load applied on caps	22,5	11	11,5
	21	steel truss, 60°, increased and uniformly distributed tension (8 turnbuckles), pvc soft on upper and lower plate, bottles' caps located at the lower plate, steel strips between caps and upper plate, load applied on caps, stress lower than Test 20	25,5	11,5	14
	22	steel truss, 60°, increased and uniformly distributed tension (8 turnbuckles), pvc soft on upper and lower plate, bottles' caps located at the lower plate, steel strips between caps and upper plate, load applied on caps, stress higher than Test 21	21,5	8	13,5
Hand calculations	A	1 mdf plate**	418		
	B	2 mdf plates working individually	216		
	C	2 mdf plates working as beam	0,6		
Allowed deformation		δ_{max}= l/250	8,6		

* The depicted value may be affected by the method of measurement, in this case by the delfection of the rope used as a point of reference

** The force applied in this approximation is that of the weight of the composite beam (bottles+2plates) and not the own weight of 1 plate

*** Different measuring system used during this test. The values should not be directly compared to the output of the other tests

Figure 200. Comparison of the data obtained from the experiments and the hand calculations of the three extreme case studies

2.2.3.4. Estimation of PET-bottle core properties

The performance of the composite module is supposed to exceed that of the prototype for the following reasons:

- The upper and lower facings are corrugated 3D surfaces and not perforated flat sheets, as they are approximated in the prototype
- The mass of the FRP facings can be the 1/2 to 1/3 of that of the mdf plates, a fact that reduces the self-weight of the beam and the deflection due to it
- The quality of the connections between the facings and the bottles is enhanced (firmer holding of the bottles is expected)
- The array of the bottles is redesigned to be denser

In addition it should be taken into account that the permanent deformation of the beam due to continuous testing when experimenting with different truss approaches is affecting the deflection values observed. This means that by using the output values per se we cannot draw safe conclusions about the performance of the module.

Nevertheless, processing the data, an indication of the shear modulus of the core can be given, which can be used as a worse-case scenario value, since the modulus expected in the actual design is much greater. These properties can be then combined with the already determined properties of the FRP facings, to roughly predict the performance of the beam under different loadcases.

The calculation of the shear modulus of the core is based on the last version of the prototype (steel truss) and only to the deflection values observed due to the applied point load, since the permanent deformation of the beam due to previous testing does not allow to draw safe conclusions about the deformation due to the beam's own weight. The average value of the beam deflection (2-5mm) under 400N point load applied at the middle of the span, observed during tests no. 25-30, is used for the calculations. From this value, the deformation due to bending- which is 1/5 to 1/8 of the total deflection- is subtracted, and the remaining deflection is attributed to shear. Therefore an indication of the shear stiffness and modulus of the core can be made, which is then used to predict if the deflection of the beam under the standard loadcase applied for Category A buildings (domestic and residential buildings) is within the service limit. For this calculation, the material assumed for the facings is Glass Fiber Reinforced Polyester, the properties of which are well determined. As the shear modulus calculated is expected to be lower than the actual value, the above calculation can show if it is possible to use the module for category A building or not.

The calculations confirm the possibility to use the composite beam structure in Category A buildings and thus the project can proceed in the design of the facings and then of an integral building system based on this composite principle.

GFRP (hexagonal array): deflection at middle of span (hypothetical)							
	Property	**Symbol**	**Imput value**	**Formula**	**Output**	**Unit**	**Comments**
Beam	Length	ℓ	2,440			m	
	Width	b	0,312			m	
	Area (xy plane)	A		$A = \ell * b$	0,761	m^2	
Face (MDF)	Face thickness	t_f	0,003			m	
	Young's modulus	E_f	14.100.000.000			Pa	Minimum value from CES (14.1 - 31 Gpa)
	Yield strength	σ_y	221.000.000			Pa	Average value from CES
	Tensile strength	$\sigma_{tens.}$	207.000.000			Pa	Minimum value from CES (207 - 345) MPa
	Compressive strength	$\sigma_{compr.f}$	172.000.000			Pa	Minimum value from CES (172 - 345) MPa
	Height btw mdf faces (including mdf thickness)	d	0,156			m	Simplified approximation considering the faces planar
	Height btw centroids of faces	d_c		$d_c = d - t_f$	0,153	m	Simplified approximation considering the faces planar
	Poisson's ratio	v_f	0,33				Average value from CES (0.307 - 0.353)
	Density	ρ_f	1.800			Kg/m^3	Average value from CES (1.6e3 - 2e3 kg/m^3)
	Upper/lower plate mass	m_{pl}		$m_{pl} = \rho_f * t_f * A$	4,111	kg	
	Upper/lower plate weight	W_{pl}		$W_{pl} = m_{pl} * g$	40,328	N	
Bottle	Compressive modulus	E^c_b	230.408.709,700			Pa	Sum from compression tests (on 14-02-2012, 07-03-2012), case 1
	Poisson's ratio	v	0,4				Assumption for bottle closed (air inside). Crystalline PET v= 0.381- 0.396 (CES)
	Shear modulus	G_b		$G_b = E^c_b / 2*(1+v)$	161.286.096,790	Pa	
	Number of bottles in 1 row (width)	no_w	4				
	Number of bottles in 1 column (length)	no_l	26				
	Total number of bottles	no_b		$no_b = no_w * no_l$	104		
	Mass	m_b	0,03063			Kg	
	Thickness of PET surface	t_{PET}	0,00041			m	
	Minimum radius	r	0,026			m	
	Height of bottle	h_b	0,203			m	
	Area (section in z direction)	A_b	0,00022			m^2	Case 1: only the thickness of the bottle is calculated for the section area
	Volume	V_b	0,000464			m^3	
	Density	ρ_b		$\rho_b = m_b / V_b$	66,013	Kg/m^3	
Core	Core thickness	t_c		$t_c = d - 2*t_f$	0,150	m	
	Mass	m_c		$m_c = no_b * m_b$	3,186	Kg	
	Core weight	W_c		$W_c = m_c * g$	31,250	N	
	Volume	V_c		$V_c = t_c * A$	0,114	m^3	Approximation using the simplified core thickness
	Density	ρ_c		$\rho_c = m_c / V_c$	27,896	Kg/m^3	
	Cell opening (distance between bottles)	s	0,088			m	Length
Load	Uniformly distributed load	q	0			N/m^2	From regulations: Category A (domestic and residential), floors
	Uniform load on beam area	Q		$Q = q * A$	0,000	N	
	Beam mass	m_{be}		$m_{be} = \ell * b * t_f * 2 * \rho_f + no_b * m_b$	11,407	Kg	
	Beam weight	W_{be}		$W_{be} = m_{be} * g$	111,906	N	
	Total uniform load	Q_{tot}		$Q_{tot} = Q + W_{be}$	111,906	N	
	Point Load	P	400			N	Applied in the middle

Figure 201. Properties and applied loadcase for the calcilation of the core's shear modulus and the prediction of the composite beam's structural behaviour

Hand calculations_ Deflection due to bending_ Composite beam (Case C)							
Stiffness	Sec. moment of inertia (xz plane)	I_b		$I_b=2*b*t_f*(d_c/2)^2$	0,0000930	m^4	
	Bending stiffness	D		$D= (E_F*t_F*d_c^2*b)/2$	167.421,946	$N*m^2$	
Simple supported beam, uniform load							
Moment	Support coefficient	M_{coef}	0,125	$M_{coef}=1/8$			
	Maximum Bending Moment	M_{max}		$M_{max}= (Q_{tot}*l_s)*M_{coef}$	63,463	N*m	
Bending Stress	Bending stress (due to M)	σ_f		$\sigma_f= M_{max}/(d*t_f*b)$	0,065	Pa	It should be lower than the face's compressive and yield strength
Deflection	Bending deflection coefficient	k_b	0,0130	$k_b=5/384$			
	Deflection, bending	$\delta_{b.o.w.}$		$\delta_{b.o.w.}=(k_b*Q_{tot}*l_s^3)/D$	0,000188	m	
Simple supported beam, point load, middle of span							
Moment	Support coefficient	M_{coef}	0,250	$M_{coef}=1/4$			
	Maximum Bending Moment	M_{max}		$M_{max}= (P*l_s)*M_{coef}$	218,000	N*m	
Bending Stress	Bending stress (due to M)	σ_f		$\sigma_f= M_{max}/(d*t_f*b)$	0,223	Pa	It should be lower than the face's compressive and yield strength
Deflection, Bending	Bending deflection coefficient	k_b	0,0208	$k_b=1/48$			
	Deflection, bending	$\delta_{b.p.l.}$		$\delta_{b.p.l.}=(k_b*P*l_s^3)/D$	0,000516	m	
Total deflection at middle of span due to bending							
	Total deflection due to bending	$\delta_{tot.b}$		$\delta_{tot.b}= \delta_{b.o.w.}+ \delta_{b.p.l.}$	**0,000703**	m	
Hand calculations_ Deflection due to shear							
Imput values from prototype testing							
	Deflection, own weight, middle of span	$\delta_{o.w.}$	?			m	Cannot be specified due to permanent deformation of the beam
	Deflection, point load, middle of span	$\delta_{p.l.}$	0,003			m	Values vary from 2-5mm (Test no. 25-30)
Calculation of core's Shear modulus							
	Deflection due to shear, point load, middle	$\delta_{s.p.l.theoretical}$		$\delta_{s.p.l.theoretical}= \delta_{p.l.}-\delta_b$	0,0025	m	
Stiffness	Shear deflection coefficient	k_s	0,250	$k_s=1/4$			
	Shear stiffness	**S**		$S=(k_s*P*l_s)/\delta_{s.p.l.theoretical}$	87.750,184193	N	
	Core, Shear modulus	G_c		$G_c= S /(b*t_c)$	1.714.942,624	Pa	
	Core, Shear modulus, only bottle section	$G_{c.b}$		$G_c=S_b /(A_b*no_w)$	99.716.118,401	Pa	

Figure 202. Calculation of the core's shear modulus based on the results of the prototype testing (no. 25-30) and the properties found in Figure 201

Load	Uniformly distributed load	q	800			N/m^2	From regulations: Category A (domestic and residential), floors
	Uniform load on beam area	Q		Q= q*A	609,024	N	
	Beam mass	m_{be}		m_{be}= l*b*t_f*2*ρ_f + no_b*m_b	11,407	Kg	
	Beam weight	W_{be}		W_{be}= m_{be}*g	111,906	N	
	Total uniform load	Q_{tot}		Q_{tot}= Q+W_{be}	720,930	N	
	Point Load	P	600			N	Applied in the middle
Hand calculations_ Deflection due to bending_ Composite beam (Case C)							
Stiffness	Sec. moment of inertia (xz plane)	I_b		I_b=2*b*t_f*(d_c/2)^2	0,0000197	m^4	
	Bending stiffness	D		D= (E_F*t_F*d_c^2*b)/2	277.314,570	$N*m^2$	
Simple supported beam, uniform load							
Moment	Support coefficient	M_{coef}	0,125	M_{coef}=1/8			
	Maximum Bending Moment	M_{max}		M_{max}= (Q_{tot}*l)*M_{coef}	219,884	N*m	
Bending Stress	Bending stress (due to M)	σ_f		σ_f= M_{max}/(d_c*t_f*b)	0,042	Pa	It should be lower than the face's compressive and yield strength
Deflection	Bending deflection coefficient	k_b	0,0130	k_b=5/384			
	Deflection, bending	$\delta_{b.o.w.}$		$\delta_{b.o.w.}$=(k_b*Q_{tot}*l^3)/D	0,000492	m	
Simple supported beam, point load, middle of span							
Moment	Support coefficient	M_{coef}	0,250	M_{coef}=1/4			
	Maximum Bending Moment	M_{max}		M_{max}= (P*l)*M_{coef}	327,000	N*m	
Bending Stress	Bending stress (due to M)	σ_f		σ_f= M_{max}/(d*t_f*b)	0,334	Pa	It should be lower than the face's compressive and yield strength
Deflection, Bending	Bending deflection coefficient	k_b	0,0208	k_b=1/48			
	Deflection, bending	$\delta_{b.p.l.}$		$\delta_{b.p.l.}$=(k_b*P*l^3)/D	0,000655	m	
Total deflection at middle of span due to bending							
	Total deflection due to bending	$\delta_{tot.b}$		$\delta_{tot.b}$= $\delta_{b.o.w.}$+ $\delta_{b.p.l.}$	**0,001147**	m	
Hand calculations_ Deflection due to shear							
Stiffness	Shear deflection coefficient	k_s	0,250	k_s=1/4			
	Shear stiffness	S	87.750,184			N	Value calculated using data from the prototype testing
Simple supported beam, uniform load							
Force	Maximum Shear Force	F		F=Q_{tot}/2	360,465	N	
Shear Stress	Core stress (due to F) only bottle section	τ_c		τ_c= F/(no_w*A_b)	409.619,344	Pa	As area of section is calculated the area of of the bottles (in z direction)
Deflection, Shear	Shear deflection coefficient	k_s	0,125	k_s=1/8			
	Deflection, shear	$\delta_{s.o.w.}$		$\delta_{s.o.w.}$=(k_s*Q_{tot}*l)/S	0,002506	m	
Simple supported beam, point load, middle of span							
Force	Maximum Shear Force	F		F=P/2	300,000	N	
Shear Stress	Core stress (due to F) only bottle section	τ_c		τ_c= F/(no_w*A_b)	340.909,091	Pa	As area of section is calculated the area of of the bottles (in z direction)
Deflection, Shear	Shear deflection coefficient	k_s	0,250	k_s=1/4			
	Deflection, shear	$\delta_{s.p.l.}$		$\delta_{s.p.l.}$=(k_s*P*l)/S	0,004171	m	
Total deflection at middle of span due to shear							
	Total deflection due to shear	$\delta_{tot.s}$		$\delta_{tot.s}$= $\delta_{s.o.w.}$+ $\delta_{s.p.l.}$	**0,006677**	m	
Total deflection at middle of span due to bending and shear							
	Total deflection (bending+shear)	δ_{tot}		δ_{tot}= $\delta_{tot.b}$+ $\delta_{tot.s}$	**0,007823**	m	
	Allowed deflection	δ_a		δ_a= l_b/250	0,008720	m	
	Total deflection within service limit			$\delta_{tot} \leq \delta_a$	**TRUE**		

Figure 203. Prediction of the structural behaviour of a composite beam with properties as found in Figure 201, under a central point load of 800N and a uniform load of 600N

2.3. FRP facings
2.3.1. Design proposal to be further developed

2.3.1.1. Criteria

A design proposal for the outer skin of the composite module is formulated, based on the results of the full-scale prototype testing and guided by the following criteria and demands:

• Avoid the use of steel for the side elements working on shear (ex. trusses). Instead, use the same FRP material as used for the upper/lower facings, to reduce weight, simplify the production and allow for large series of modules to be quickly produced
• Design simple connections in order for the module to be easily assembled by unskilled workers
• Integrate the fastening elements between the facings and between the modules to the facings to reduce assembly complexity, time and cost
• Avoid metal inserts in the FRP facings that will dramatically increase the weight of the overall structure and complicate the recycling procedure of the module
• Opt for a module design that can be compacted and efficiently stacked with other modules, to maximise the amount of building blocks that can be shipped in one container
• Develop a design concept that can be transformed into different building components, that can be produced from the same molds or combinations of them
• Reduce the number of components to the minimum

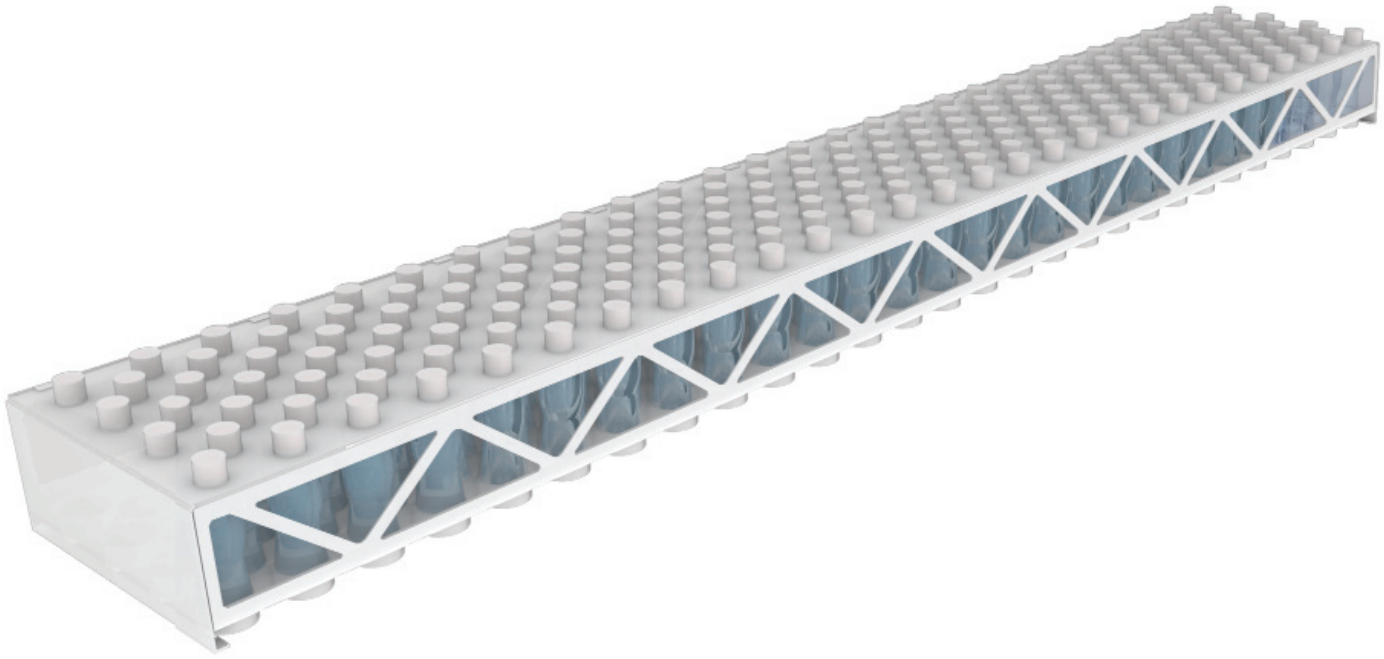

Figure 204. Design proposal for a composite beam out of FRP facings and a PET-bottle core

2.3.1.2. Proposal description

Basic element of the integral system to be developed is a wall module of 420*210*210 mm dimensions, consisted of 2 foldable FRP facings and 8 PET bottles. Since the wall module is not experiencing bending as the beam tested in the prototype, and thus the structural demands are reduced, the bottles are organised not in a 45° array but in a rectangular arrangement that requires less bottles. The spacing between the bottles is similar to the one found in the prototype and results to a grid that defines the overall dimensions of the module. The length of the module is then decided regarding the module's possible use for emergency shelters, in such a way to allow the easy handling of the module by unskilled workers with no lifting equipment available, people in physical exhaustion and children.

Each foldable facing can be re-configured into a less space-consuming flat surface suitable for shipping, due to the living hinge incorporated between the upper/lower plate and the side wall (working on shear). This molded-in hinge is in fact a strip of thinner section in between the two plates that bridges them together and allows the opening and closing of the surfaces without the need of mechanical hinges. This way, the cohesion between the upper/lower plate and the side wall is achieved and additional connections between the two surfaces are avoided. The facings, when unfolded, can be packed together in such way that 5 facing pairs can fit the height of one finished module.

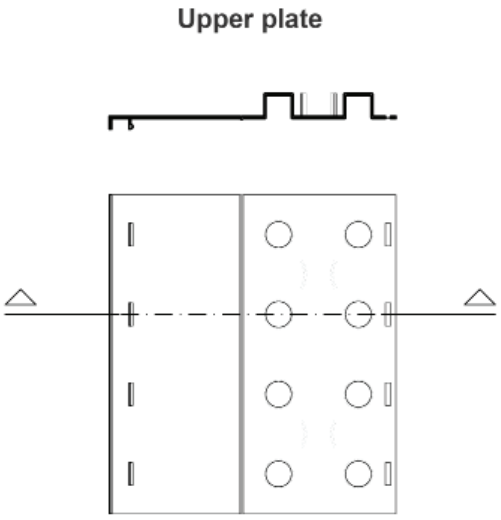

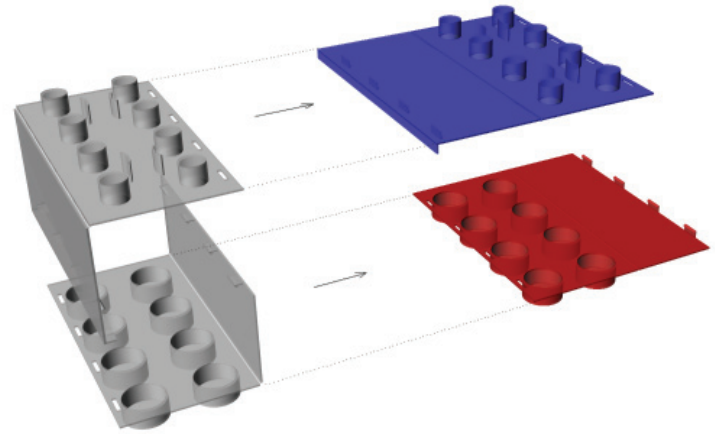

Figure 205. Unfolding of upper and lower facings of the basic wall module

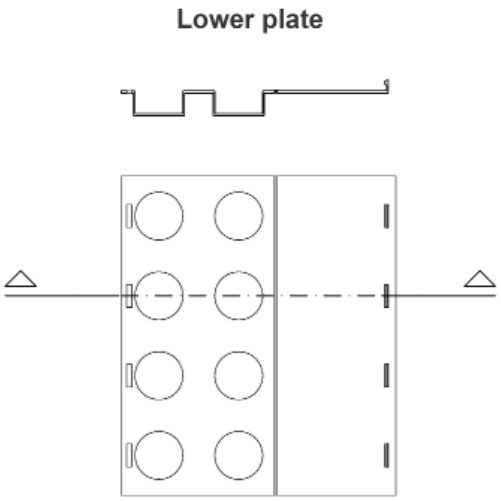

Figure 206. Plans and sections of the facings of a basic wall module

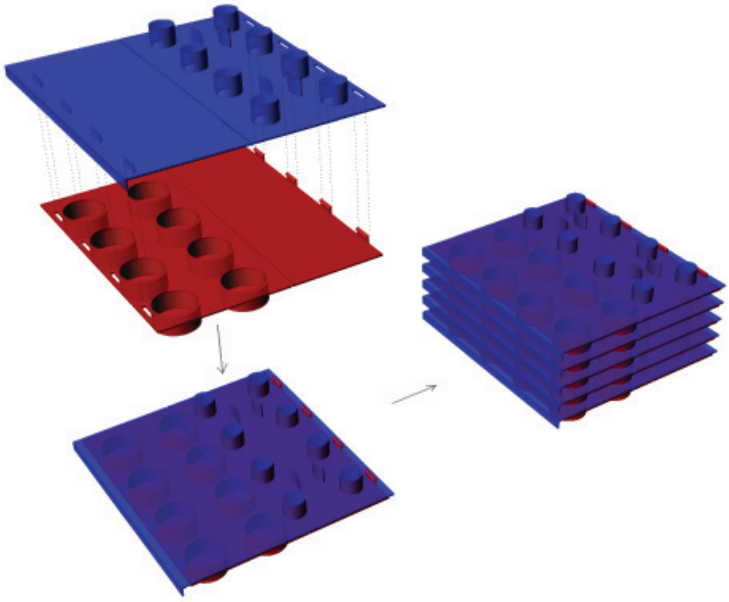

Figure 207. Stacking method for the upper and lower facings

Regarding the connection between the two folding facings, snap fit connections are integrated in the two facings to allow their simple and easy connection without the involvement of extra fastening systems. The snap fit system consists of hooks, out of the same polymeric material used for the facings, placed on the one folding surface, that deflect to fit into grooves located on the surface of the other folding facing. When the hooks are inside the grooves, they return to their original position and connection is achieved. The angled cuts on the snap fits intent to the multiple assembly and disassembly of the structure. The choice of this type of connection not only saves time during assembly and disassembly of the module, but also reduces the number of components needed for the module. This leads to savings on warehousing, labour, shipping, handling costs and it reduces the number of suppliers [30].

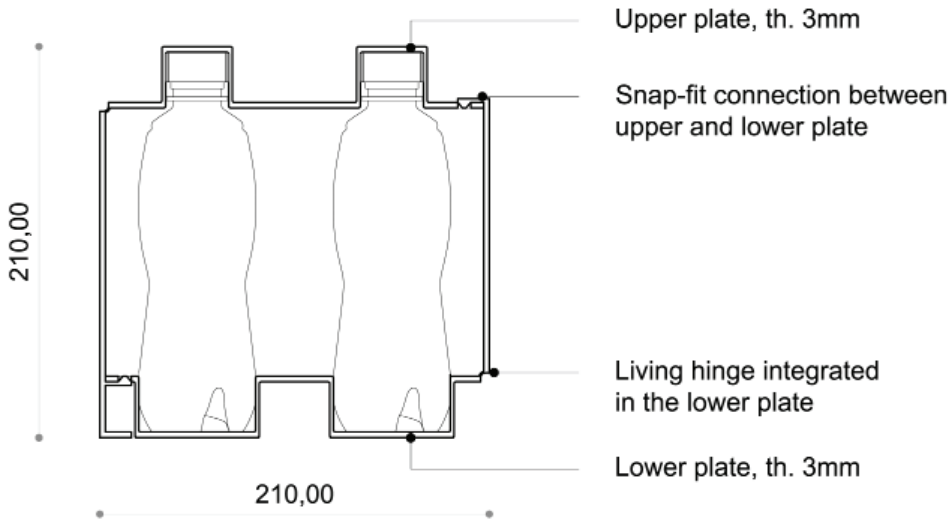

Figure 208. Basic wall module, section



Figure 209. Snap-fit connections and living hinges are popular assembly methods to be found in everyday plastic products

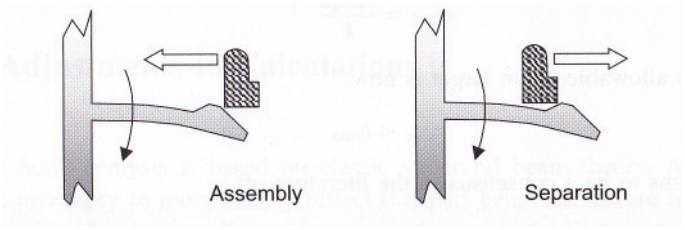

Figure 210. Principle of the Snap-fit connection
Source: BONENBERGER, P.R. The First Snap-Fit Handbook

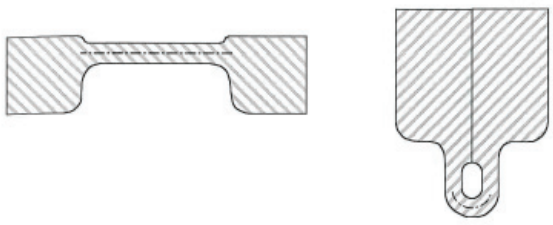

Figure 211. Principle of the living hinge. The recess at the upper part of the bridge (see figure on the left) is important in order to avoid stress concentration when the two surfaces are closed together

Source: TRES, P.A. Designing Plastic Parts for Assembly

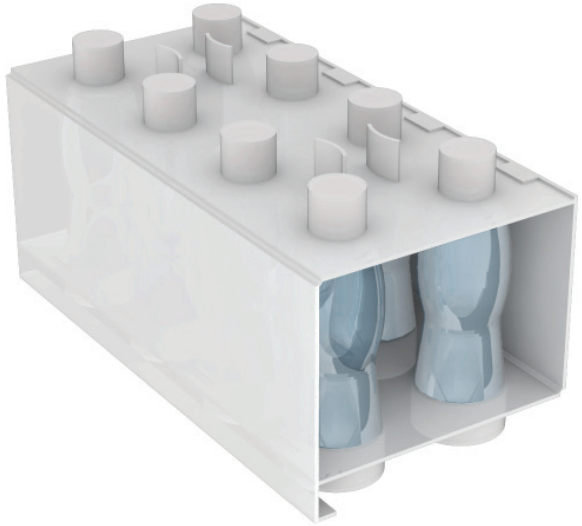

Figure 212. Aspect of the basic wall module, depicting the living hinges and snap-fit connections between the facings, and the protrusions on the upper and lower plates used for the connection of the module with other similar modules

Both upper and lower plate contain protrusions that fit around the caps and base of the bottles respectively, to obtain the optimum connection between the PET-bottle core and the FRP skin. These protrusions contribute to the stiffness of the upper and lower surface while at the same time facilitate the connection between the modules. More specifically, the cap protrusions of the upper plate fit in-between the base protrusions of the lower plate of the module to be placed above, using a “LEGO” connection logic that avoids extra fastening elements.

With this module as a basis, a system of wall and slab pieces can be developed, as well as a series of additional components to be connected to it, such as doors or roof coverings. The connection between the different components is achieved through the protrusions of their upper and lower plates.

The slab modules are based on the same grid as the wall modules, but the array of bottles in their core is denser due to the 45° distribution pattern used. The length of the module is determined by the size of a standard 20 foot container and in relation to the results from the prototype testing. As a 5,9 meter span (interior length of container) would cause the module’s deflection to surpass the allowed service limit, it is intended to cover the length of the container with two slab modules of 2,94m length each. Considering the long sides of the slab modules, when these are not in contact with the exterior can be replaced by a FRP truss structure, to reduce the weight of the module. These side trusses are in addition inclined from the perpendicular axis of the module to lock the slab pieces into place and assure their collaboration as one coherent slab. The distance between the trusses is again related to the dimensions of the prototype and additionally coincides to the length of the basic wall module,to facilitate the combination of the components. The suggestion of precambering- as this resulted from the prototype testing- is not followed, as it would further complicate the shape of the modules and their connection to the rest if the structure.

The floor and roof coverings are folded surfaces as well, to avoid seams, especially at the roof. The door and its frame, which contains protrusions for its connection to the wall pieces, can arrive as one element on site. Regarding the lighting of the interior space, variations in the translucency of the wall and slab modules can provide diffused light.

To achieve wall and slab pieces of different sizes, a system of adjustable metallic molds is proposed, based on smaller molds that can be screwed together to produce larger components. In addition the molds producing the sides of the modules can be switched, to form modules with closed sides or trusses, according to the needs. It should be mentioned that although the opposite procedure of creating bigger elements, which can be cut into smaller pieces afterwards, may seem simpler, it contains the risk of damaging the fibres at the edges of the facings and also is more time consuming, when a large series of pieces needs to be produced.

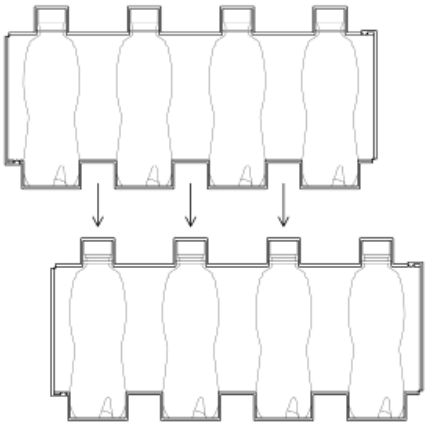

Figure 213. “LEGO” connection between wall modules

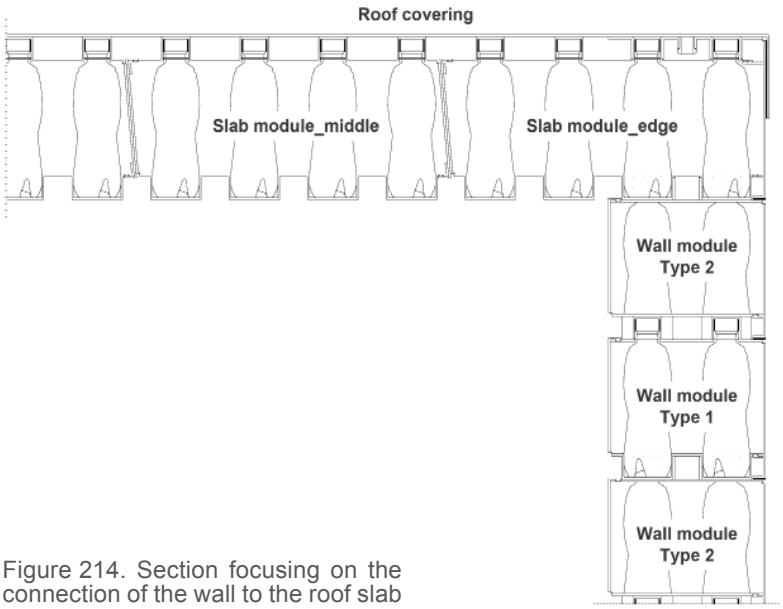

Figure 214. Section focusing on the connection of the wall to the roof slab

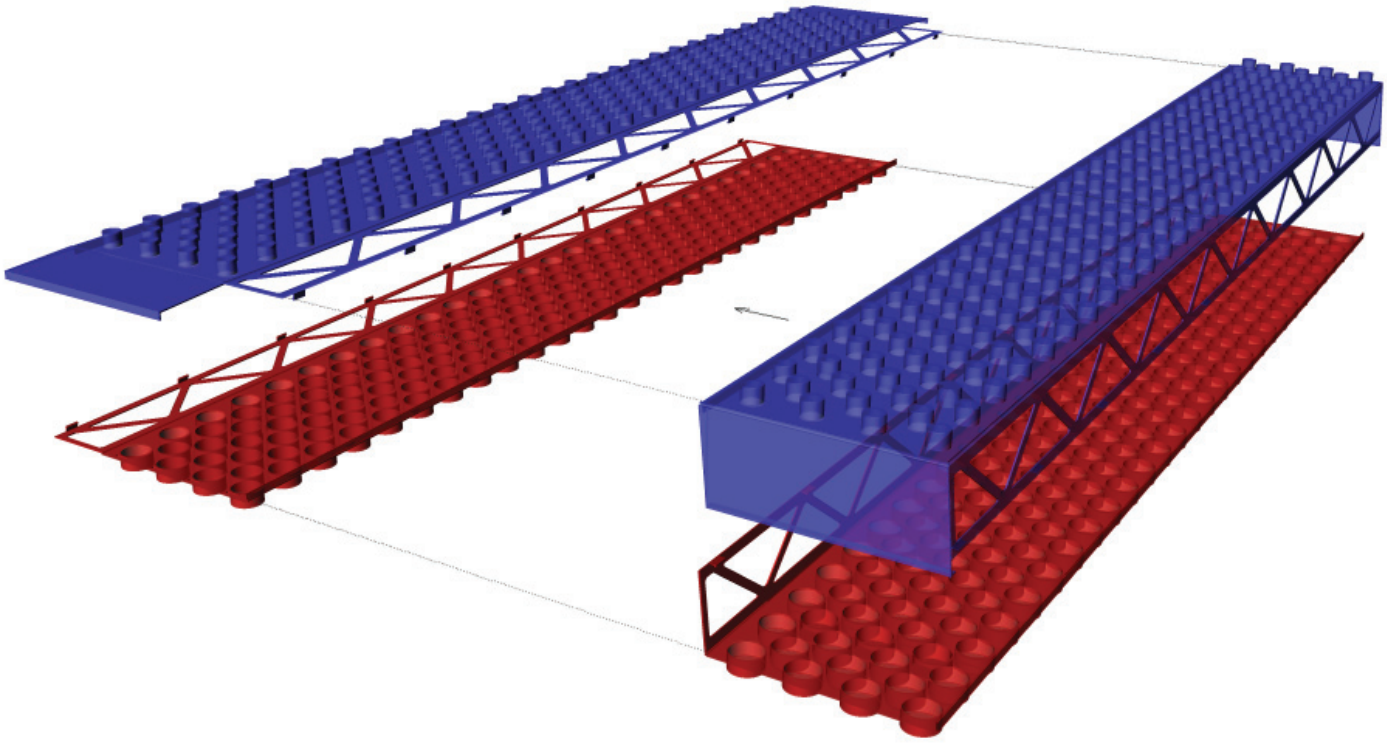

Figure 215. Slab module: components and unfolding pattern

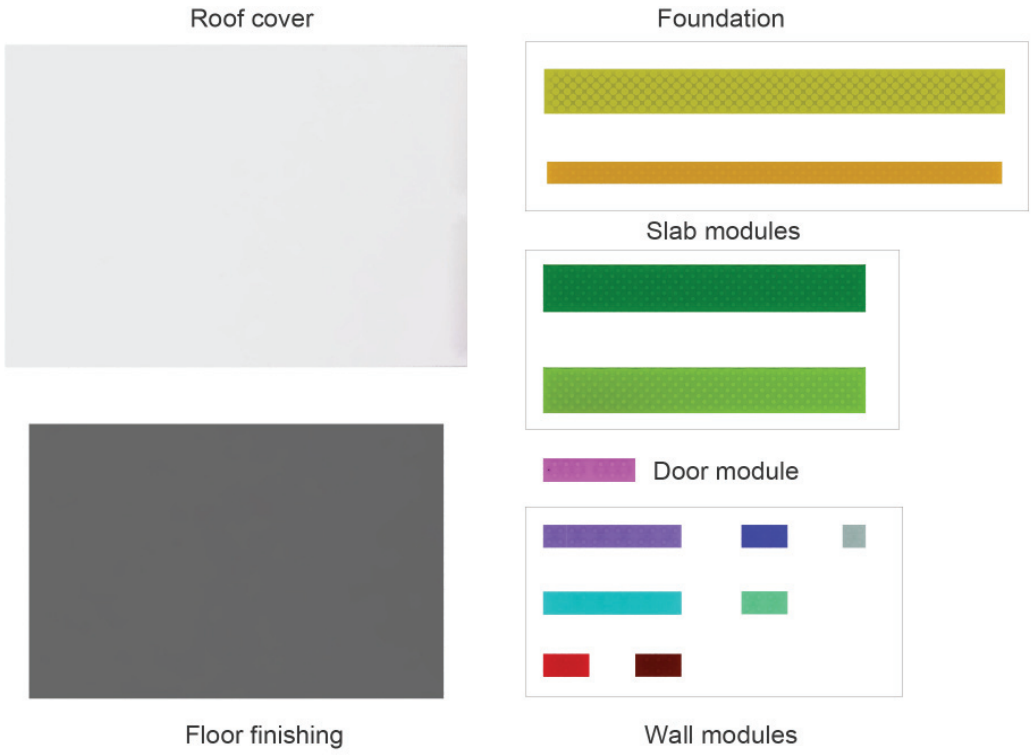

Figure 216. List of pieces for an integral building system, based on the logic of the wall module

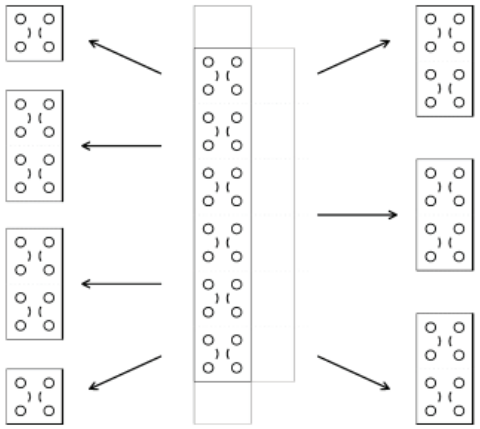

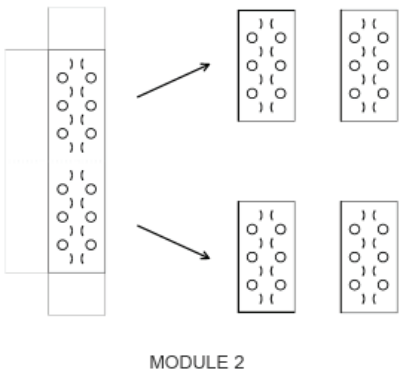

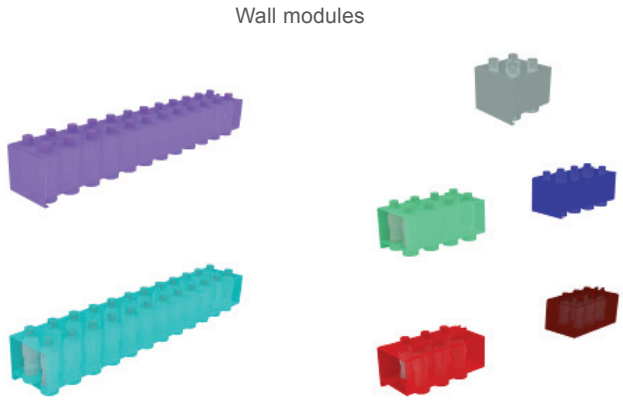

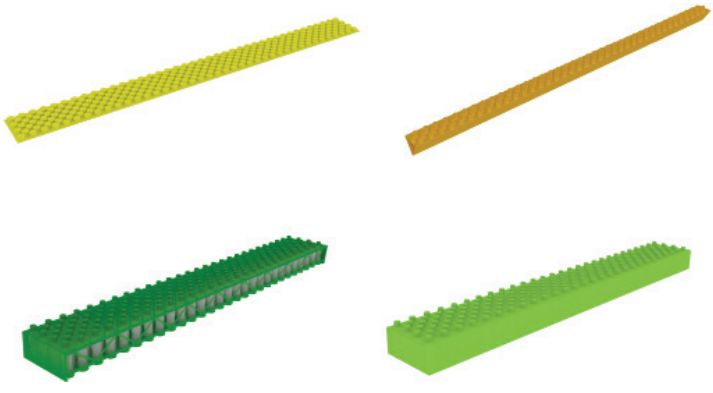

Figure 217. Steps of assembly on-site

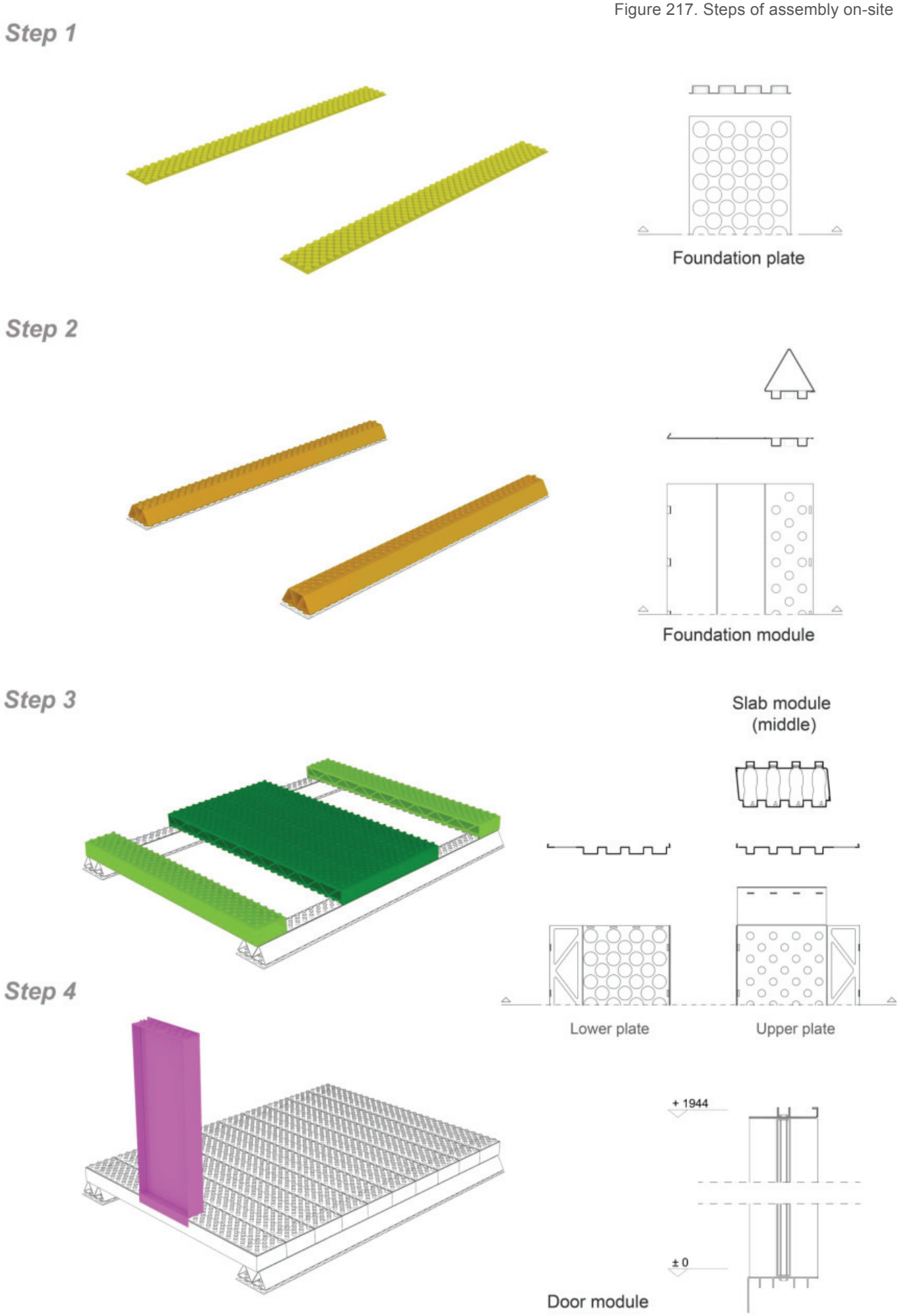

Step 5

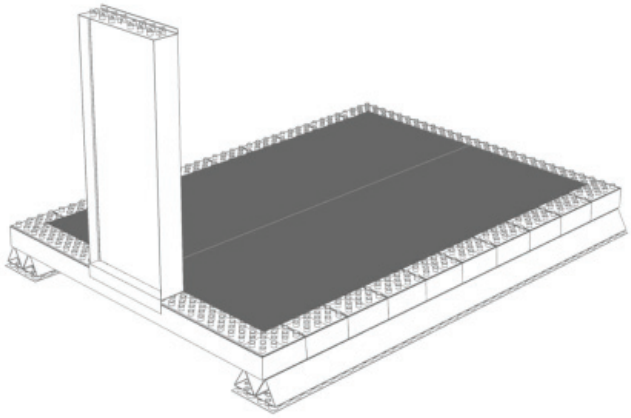

Floor finishing

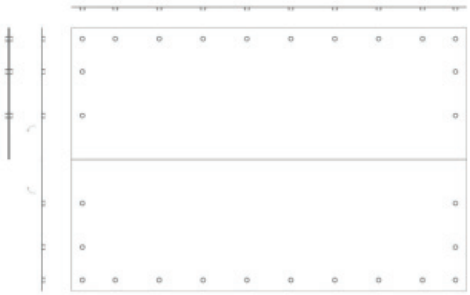

Step 6

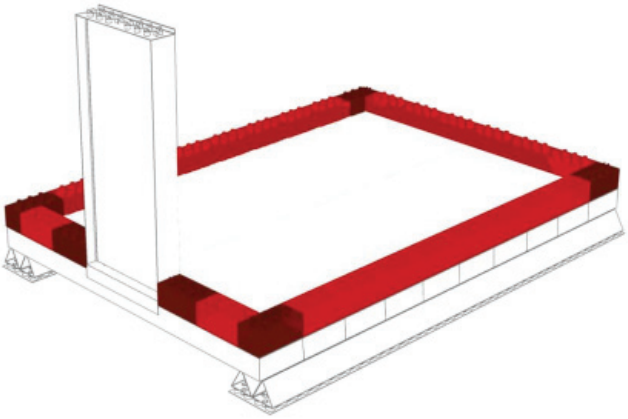

Wall module, type 1

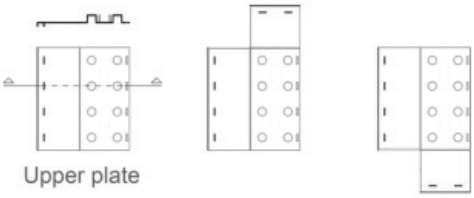

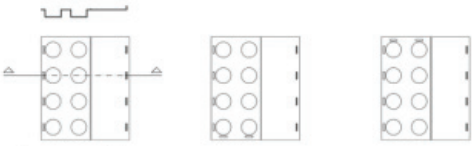

Step 7

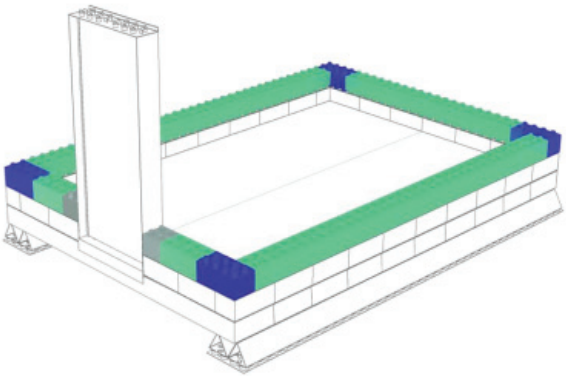

Wall module, type 2

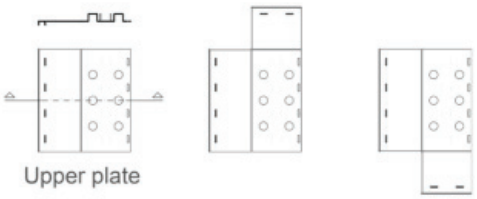

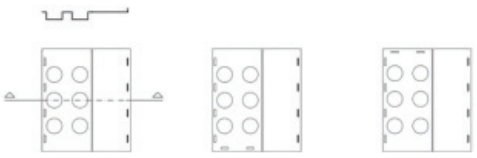

Step 8

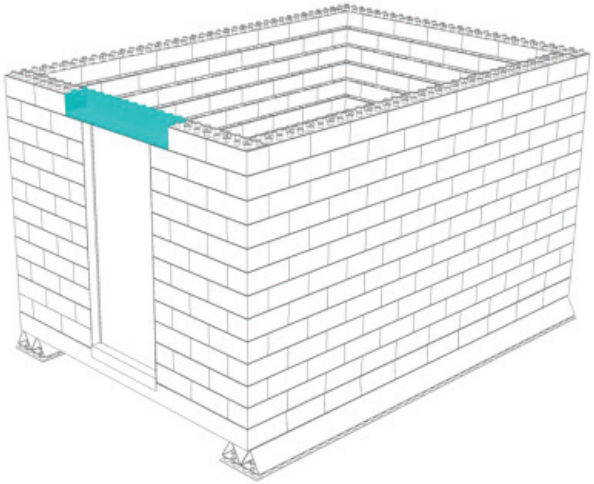

Lintel

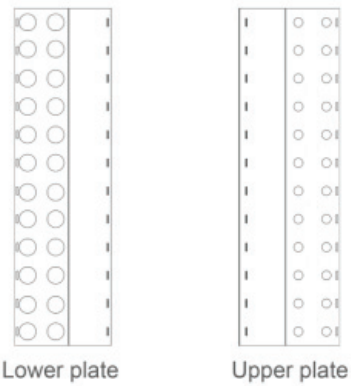

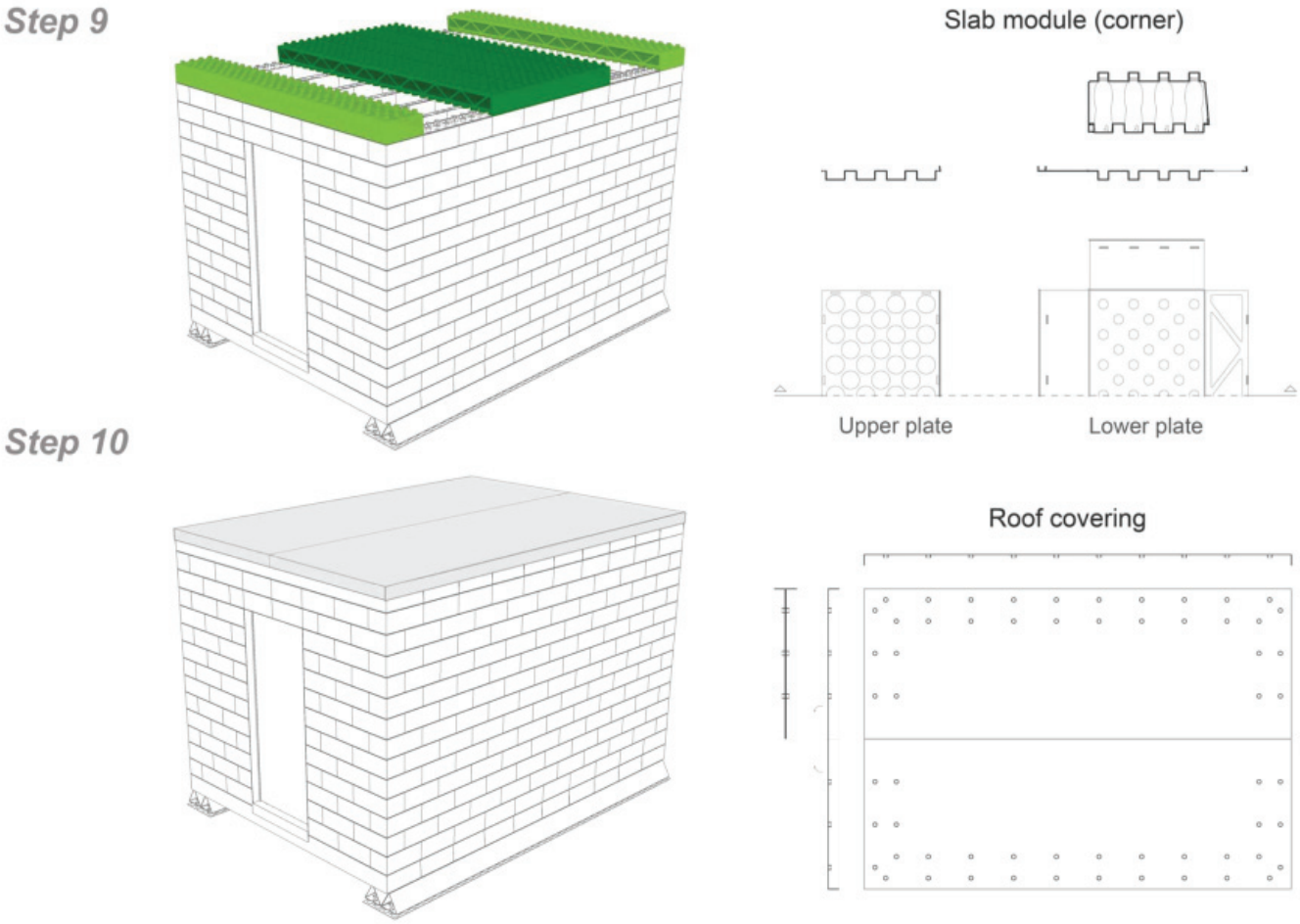

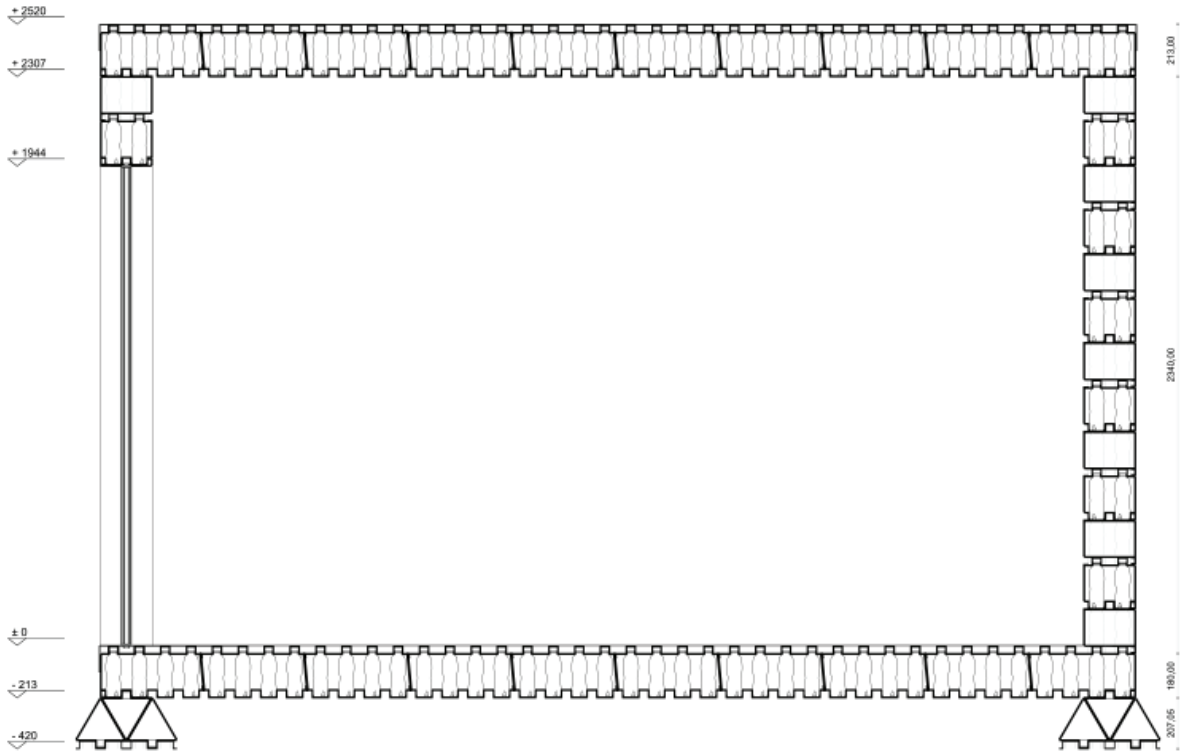

Figure 218. Typical section

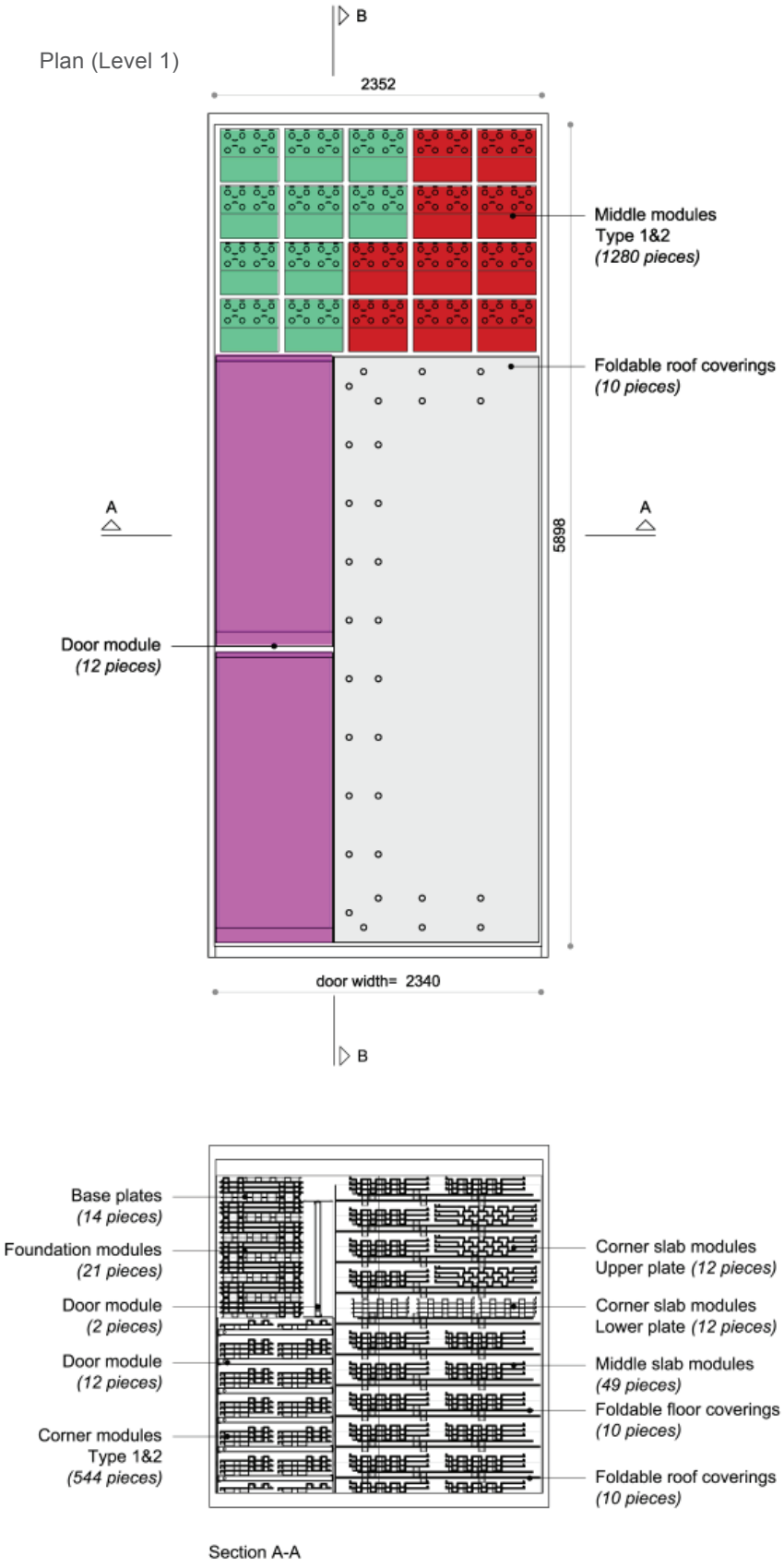

Figure 219. Organisation of the components in a standard 20 foot shipping container

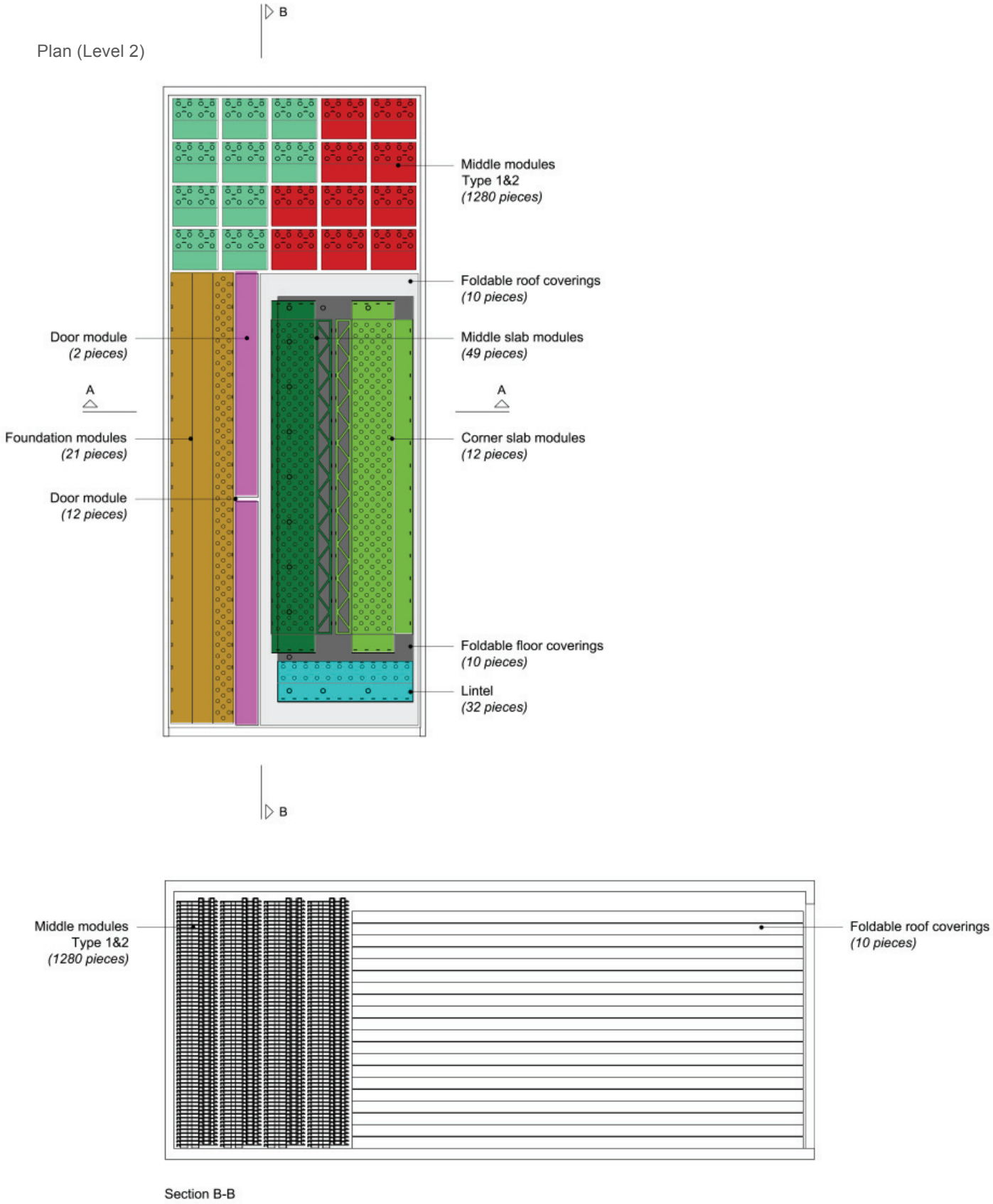

Figure 220. Organisation of the components in a standard 20 foot shipping container

2.3.2. Material selection
2.3.2.1. Criteria and material choice

The fibre reinforced composite (FRP) material chosen for the realisation of the module's facings needs to have the criteria listed below:

- Low density combined with good mechanical properties
- High impact strength
- Good performance under severe environmental conditions
- Low thermal expansion coefficient
- Durability and low maintenance requirements
- Applicability to high speed manufacturing processes that result into high-volume production of modules

while additionally it should be:

- Easily recyclable
- Able to sustain up to a million flexing cycles without the living hinges breaking
- Low-cost

Most of the FRP composite alternatives available, naming Glass Fibre Reinforced Polyester or Carbon Fibre Reinforced Epoxy as some of the most commonly used composite solutions, comply to the first list of criteria, becoming thus a favourable choice over other lightweight building materials such as aluminium or wood. However, standard thermoset composite materials fail to meet the criteria of the second list, indicating that a solution should be sought in the area of thermoplastic composites.

In fact, the issue of recyclability not only leads to the choice of a thermoplastic composite but even more, to the use of a Self-Reinforced Polymer (SRP) composite. The characteristic of this type of composites is that they are mono-materials, meaning that the fibres and the polymer matrix are made of the same material. When this attribute is combined with the reformability of thermoplastic materials, the result is a composite material that can be easily and fully recycled. The composite can be simply re-melted and re-granulated to be further reprocessed, and no separation of the fibres from the polymer matrix is required. This is a significant advantage given the fact that thermoplastics reinforced with glass or carbon fibres cannot be melted down and thus must be shredded, only to be used as lower performance short fibre reinforced composites [31].

From the different SRP composites currently being developed, based on polymers such as polyamide, polyethylene, terephthalate or polypropylene, the most advanced and commercially available material is the self-reinforced Polypropylene (Pure®, Curv™, Armordon®) [32], while also some applications of srPET exist (Aptiform).

Between the two alternatives commercially available- srPP and srPET- the first is more suitable mainly because the use of polypropylene allows the incorporation of living hinges to the module design that can sustain up to a million flex cycles without breaking [33]. Other advantages is that srPP has lower density, higher tensile modulus and strength [34]and that PP resin is cheaper than PET resin [35].

Elaborating more on the aspect of cost, the use of srPP results to a much cheaper module than the one we would obtain if using a glass or carbon fibre reinforced thermoplastic or thermoset composite, due to the lower cost of the raw material. Although thermoplastic composites need higher processing pressures than thermosets and therefore demand more expensive product tooling [36], the fact that a large quantity of modules is to be produced, turns the cost of the raw material to a much more significant factor, determining the final price of the product.

Yet, srPP as well as the other developed SRP composites, has some disadvantages that need to be taken into account. These are mostly related to the temperature sensitivity of the material, demanding accurate temperature control during manufacture and the avoidance of use of the material for high temperature applications [37]. Others have to do with the 500-1000 times higher melt viscosities of the thermoplastic than that of the thermosets, which raise the amount of required pressure for their processing and therefore increase the processing expenses [38].

Taking into account the above mentioned advantages and disadvantages, the srPP composite material is chosen for the materialisation of the facings. In order to develop the design of the module according to this technology, the Netherlands-based company Lankhorst Pure Composites b.v. (division of the Royal Lankhorst Euronete Group), that manufactures PURE®, is contacted.

	SRPET	Tegris SRPP	PURE SRPP	Curv SRPP	Armordon SRPP
Density (km/m³)	1300	780	780	920	830
Tensile Modulus (GPa)	5.0	5-6	5.5	4.2	3.3-4.5
Tensile Yield Strength (MPa)	51				
Ultimate Tensile Strength (MPa)	144	200	200	120	180
Elongation to Failure (%)	30%	7%	9%	20%	10%

Figure 221. Comparisson between srPET and srPP
Source: http://www.aptiform.com

*2.3.2.2. PURE® self-reinforced Polypropylene composite material**

i. General information

PURE® is a 100% polypropylene composite material patented by Lankhorst Pure Composites b.v. The company produces PURE® tapes that can be woven into PURE® fabric. This fabric can then be consolidated to produce flat sheets or sandwich panels and can also be formed into 3D shell structures.

The development of the material initiated in 1998 from the regulation formed by the End of Life Vehicles (ELV) Directive of the European Union, to produce motor vehicles that are 85% recyclable by 2008 and 95% by 2015. The material developed aim to overcome the recycling problems faced with glass fibre reinforced polypropylene composites used in vehicles and thus contribute to their recyclability.

Currently the prevailing market applying the material is the suitcase industry, followed by the defense industry using it to produce anti-ballistic products. Helmets, climbing sport equipment, automotive parts, and facade panels are other applications of this material.

**The presented information are gathered from the visit at the Lankhorst Pure Composites bv facilities and discussion with the Business Development Manager Fokke Bloemhof, from information material provided by the company and from the company's website http://www.pure-composites.com , unless stated otherwise*

ii. Material description

Starting with the PURE® tape, this consists of three flat co-extruded polypropylene layers: a highly oriented core (tension and heat orient the polymer chains along the tape's 0° axis [39]) of high strength and modulus and melting point at 180° C, within two thin outer layers that melt at 130° C. The lower melt skin thus serves in welding the tapes together in a compaction process using a hot-press or continuous belt. Reinforcement and impregnation occur therefore in a one step process.

Then, the tape yarn can be woven into fabric which in turn can be stacked in multiple fabric layers and consolidated with heat and pressure to produce flat rigid sheets of 3D structures. Throughout this process, a small portion of the fabric's outer lower melt layer melts and then recrystallises while cooled, binding the fibres together. The final surface has an approximately 90% fibre content and its thickness is depended on the number of fabric layers used, each of which is approximately 0,15 mm thick. No extra additives or resins are needed.

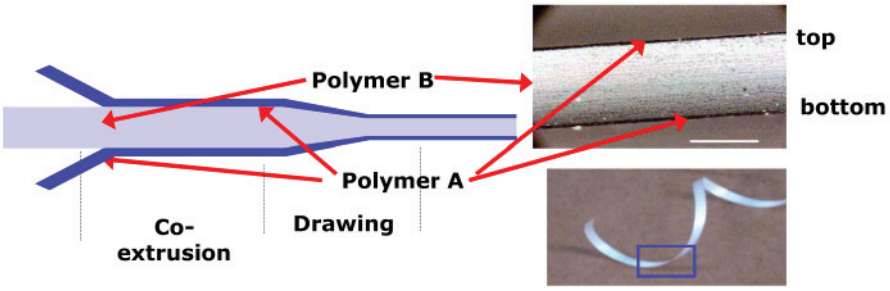

Figure 222. Production of PURE® tape

iii. Material properties

The PURE® composite material is characterised by the following properties:

• Low density

The density of the material is 780 kg/m^3 which is lower than equivalent glass fibre reinforced PP composites (Glass mat thermoplastic composite with 30% fibre content has a density of 1100 kg/m^3), resulting in important weight savings.

• High impact resistance, also at very low temperatures

The impact resistance of the material is higher than that found in PP composites reinforced with carbon or glass fibres, while the material can absorb very high impact energies even at -50° C, when amorphous PP usually enbrittles at -5 to -10° C. The improved mechanical properties are caused by the drawing and orientation of the homopolymer molecules. In the material, transferring of loads occurs from the lower property matrix to the high strength core, delaying failure mechanisms and increasing its impact strength [40]. In addition, the interfacial bonds between matrix and fibres significantly affect the impact performance of the material [41].

• High stiffness

The tensile modulus of srPP sheets (0-90° biaxial lamina) ranges between 5,5GPa-6 GPa. Although the tensile modulus of glass fibre reinforced PP (homopolymer, 30% glass fibre) ranges at the same levels (5.67 - 6.78 GPa [42]) the density of srPP is lower, resulting thus in a much favourable stiffness to weight ratio. Even more, it is believed that srPP can reach higher stiffness than bicomponent PP composites because during the compaction process of srPP molecular continuity occurs between the oriented core and the matrix [43]. Proper compaction of the fabric layers, with the suitable application of pressure (10 bar or higher preferred) and under the appropriate temperature range (140-150° C), raises the stiffness of the material, since the micro voids in the material are closed.

However, srPP is much less stiffer than thermoset composites reinforced with glass fibres (Epoxy/E-glass 60%, 0-90° biaxial lamina has 26,4 GPa tensile modulus [44]). Therefore, an increase in the thickness of the surfaces needs to be considered, for this material to be comparable to thermoset composite alternatives.

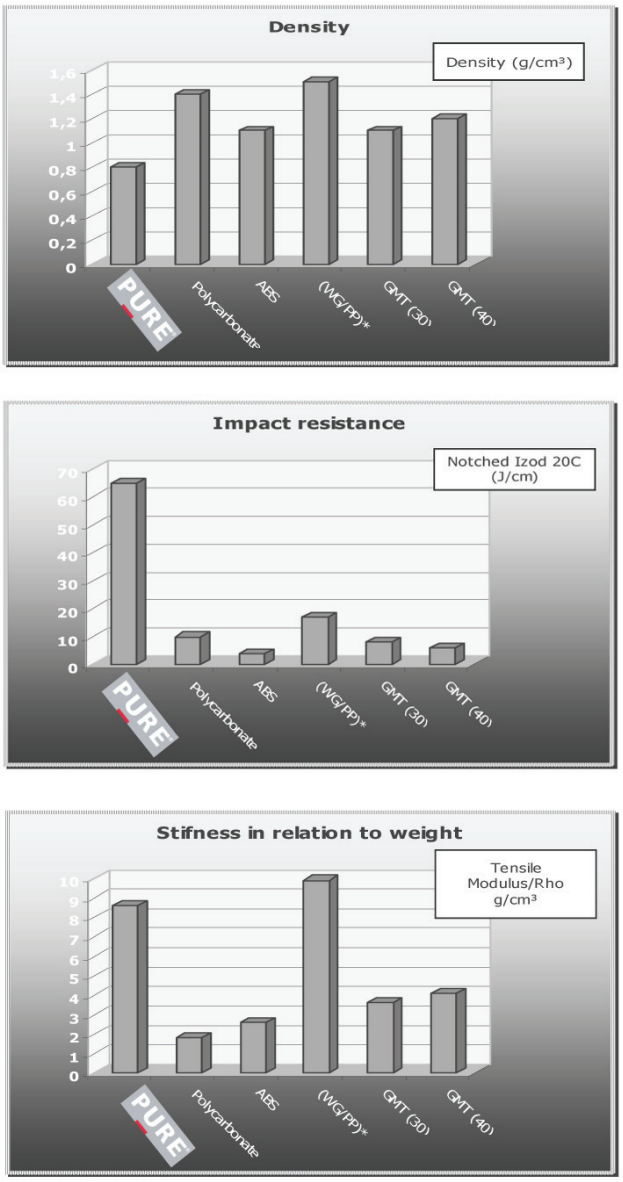

Figure 223. Properties of PURE® and comparison with non-homopolymer composites

• Low thermal expansion coefficient

PURE® sheets have a low thermal linear expansion coefficient equal to $23*10^{-6}$ m/m*K, and similar to aluminium ($22,2*10^{-6}$ m/m*K [45]). To give a scale of comparison, the thermal coefficient of linear expansion of the polymers below can be mentioned [46]:

Polyester - glass fiber-reinforced: $25*10^{-6}$ m/m*K

Polypropylene (PP), unfilled:100 - $200*10^{-6}$ m/m*K

Polypropylene - glass fiber-reinforced: $32*10^{-6}$ m/m*K

• Glass fibre free

Since PURE® composite contains no glass fibres it is easy to handle in the workplace and skin irritations related to the use of these fibres are avoided, as well as tool wear. The final surfaces can be smooth (when the mold is smooth as well) and no additional coating is required.

• Recyclable

This thermoplastic mono-material composite can be fully recycled by simply being re-melted and granulated. The granules can be re-used to produce srPP composite structures and so the material does not experience downgrading.

Yet, it should be mentioned that PURE® products result from the use of virgin PP, since using recycled PP contains risks regarding the quality of the raw material, whose consistency may vary according to different sources. Nevertheless, when this quality can be guaranteed, recycled PP is used. Therefore, according to the company's policy, waste resulting from the processing of PP tape, also when this takes place outside the company's facilities, is gathered back to the company and reused.

• Thermoformable into 3D shapes

PURE® fabric and sheets can be thermoformed to produce 3D shell structures. The transformation of the fabric layers or sheet occur due to the shearing of the fabric layers and not due to elongation of the material. The final surface does not have the same thickness as the corners tend to be thicker. Careful consideration should be given therefore to the design, as steep protrusions can cause excess stress concentration and eventual fibre breakage.



Figure 225. Helmets is a common application of this technology



Figure 226. Movement and folding of fibres due to the press forming manufacturing technique

Source: Photographs taken during the visit at Lankhorst Pure Composites bv facilities

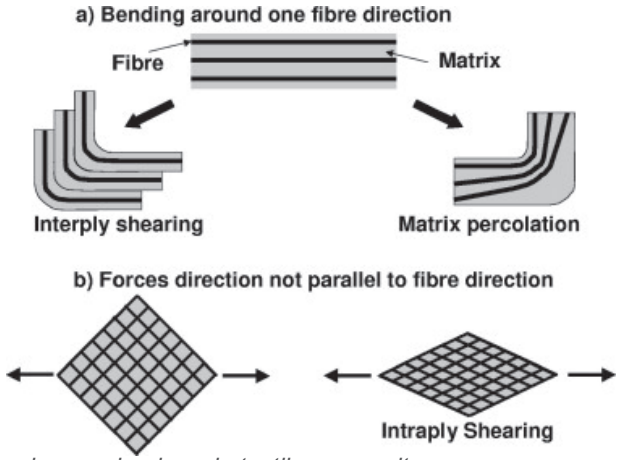

Figure 224. *Forming mechanisms in textile composites*

Source: CABRERA, N.O. et al. Non-isothermal stamp forming of continuous tape reinforced all-polypropylene composite sheet

PURE® - Technical Data Sheet

PURE® - sheets	Version: 30-03-07
Product description	Sheets based on consolidated Pure®-fabric produced of co-extruded sealable tape
Colours	grey and white
width	1200 mm
length	Standard stock 2400 mm Other lengths on request
thickness	Standard 0.3 – 2 mm (0.13 mm /layer) On request every thickness available PURE® is easy to be converted into thick panels (up to 5 cm) Optionally thin material on roll

Technical Properties		Test method	Value	Unit
Bulk density		ASTM D792	0.78	g/cm^3
Tensile modulus		ISO 527-4	5.5	GPa
Tensile strength		ISO 527-4	200	MPa
Tensile strain to failure		ISO 527-4	9	%
Flexural modulus		ISO 178	4.5-5.5	GPa
Charpy Impact (FN)		ISO 179	(N, no break)!	kJ/m^2
Charpy Impact (EP notched type A)		ISO 179	(P) 140	kJ/m^2
Izod Impact (FN)		ISO 180	(N, no break)!	kJ/m^2
Izod Impact (EP notched type A)		ISO 180	(P) 126	kJ/m^2
Instrumented Falling Dart Impact (23 ºC) (2.2 mm, clamped, 20 mm striker)		ISO 6603-2	9.51 51.46	kN (peak) J (at failure)
Instrumented Falling Dart Impact (23 ºC) (2.2 mm, clamped, 10 mm striker)		ISO 6603-2	4.96 16.40	kN (peak) J (at failure)
Instrumented Falling Dart Impact (-40 ºC) (2.2 mm, clamped, 10 mm striker)		ISO 6603-2	6.53 22.38	kN (peak) J (at failure)
Heat Deflection Temperature	1820 kPa	ASTM D648	95	ºC
	455 kPa		130	ºC
Coefficient of Thermal Expansion (-20 ºC to 100 ºC)		ASTM E228	23	10^{-6} K^{-1}
Coefficient of Thermal Conductivity (2.25 mm)		EN-ISO 12567-1	0.044*	W/m.K
Fire Behavior – burning rate (1.6 mm)		ISO 3795	29	mm/min

* Depends strongly on the sheet thickness

• Low level of translucency

Even though dense compaction that closes the micro voids in the material can lead to translucency, the levels achieved are very low.

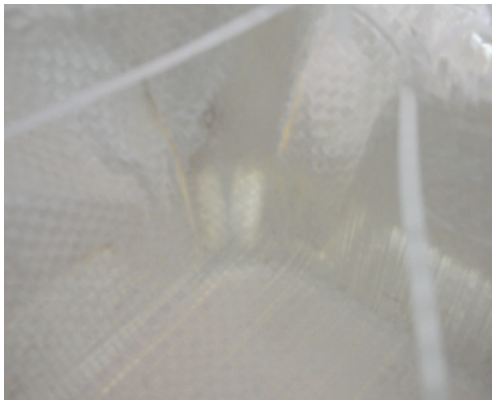

Figure 227. Translucency, although possible, has a very low level

Source: Photograph taken during the visit at Lankhorst Pure Composites bv facilities

iv. Manufacture techniques

Both PURE® fabric and sheets can be processed by using pressure thermoforming techniques. First the material needs to be heated up to its softening point(140-150° C), then pressure between 10-20 bar is applied, forcing the material against the mold and finally cooling takes place. Important in order to avoid shrinkage due to the relaxation of the material (normally occurring at temperatures over 130° C), is the proper clamping of the material before it is heated.

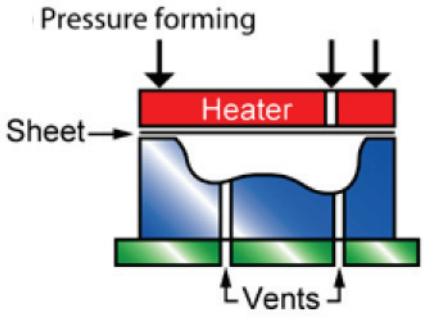

Source: CES Database

Figure 228. Press forming technique

Two different molding approaches are followed by the company: the non-isothermal and the isothermal molding. The non-isothermal is a popular approach used for the shaping of thermoplastics that involves the heating of the material outside the press and then the molding against a cold mold. The clamps on the surface, applied during the pre-heat period, need to be released at proper moment, after pressure is applied, otherwise fibre breakage can occur. Given the fact that heating time can range from 1 to 60 minutes, according to the number of fabric layers, but a molding cycle lasts 1 to 2 minutes, more pre--heating stations can be arranged to work with one moulding station. This can result to important time savings. The isothermal approach results in longer time cycles since it involves the heating of both the material and the steel or aluminium mold. It is an easy process that does not require clamping and is also possible using autoclaves. Nonetheless, both processes have a significantly faster cycling time than thermoset composites present (from few hours to days) as no chemical reaction is involved in the curing process.

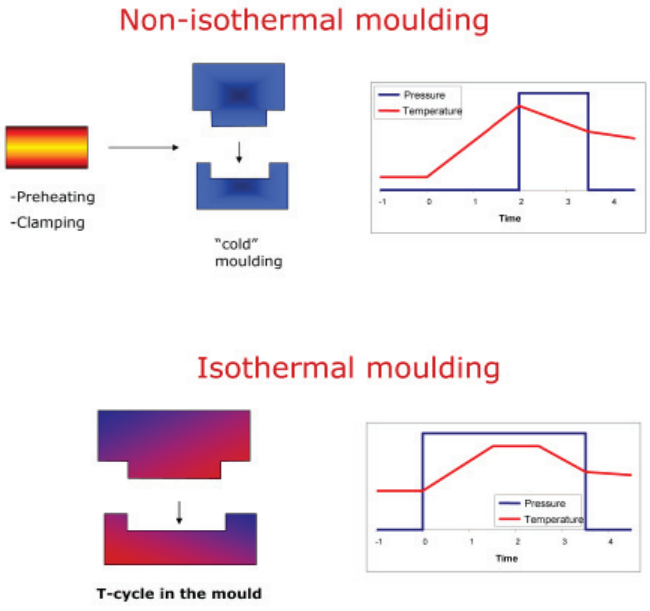

Figure 229. The two moulding approaches

Source: Photograph taken during the visit at Lankhorst Pure Composites bv facilities



Figure 230. Aluminium mold used in the isothermal moulding process

After the formation of the sheet, post molding operations such as trimming of the edge fibres are usually required. Because the material is glass-fibre free, these processes require lower cutting tool costs and improved tool life is guaranteed. Holes can be also introduced at this stage. Among the available methods- water-jet cutting, laser cutting and CNC machining with both abrasive and shear cutters- laser cutting can have the fastest results, because no mechanical movement is involved, but melts the material along the trim line. Overall, CNC machining results in a higher quality product [47].

The PURE® surfaces, if required, can be joined together by ultra-sonic welding. Welding of thermoplastic polymers, in contradiction to bonding methods, does not include adhesives or bonding agents. Ultrasonic welding in particular is based on the vibration of one part against a stationary one. Due to this vibration, heat is generated that melts the materials along the joint surface, causing their weld together [48].

Regarding the colouring of the final surfaces, two options exist, that of in-mold painting and of post-mold painting [49].

Source: Photographs taken during the visit at Lankhorst Pure Composites bv facilities

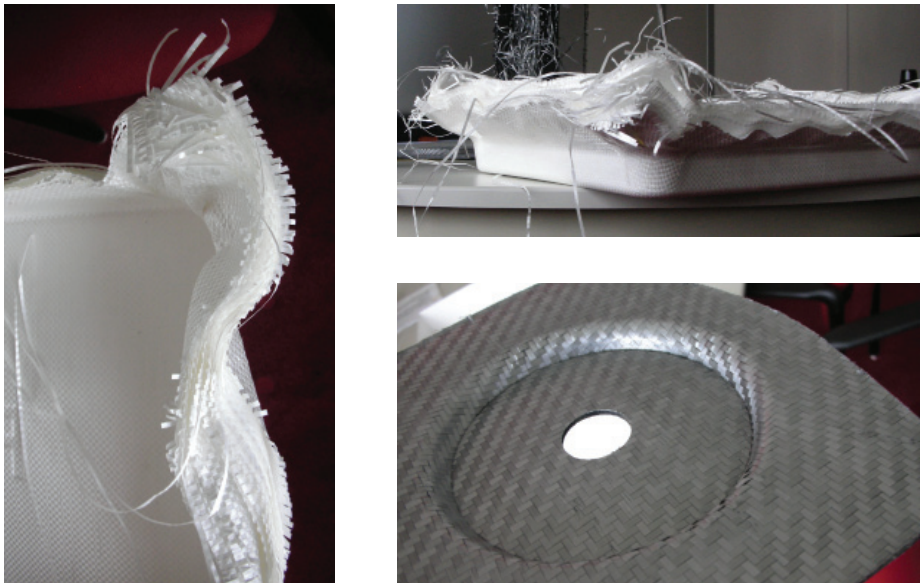

Figure 231. After the thermoforming of the fabric, trimming at the edges needs to take place. Opening of holes also occurs after the molding stage

2.3.3. Aspects susceptible to redesign

The research on the chosen material and the visit at the manufacturing company gave valuable insight on the possibilities of this technology but also the limitations and disadvantages that need to be taken into account.

Since the initial design proposal for a composite module is developed according to the philosophy of a thermoset composite material and its related manufacturing processes, modifications need to take place when shifting to the technology of self-reinforced thermoplastics. Thus, two main aspects of the design need to be reconsidered:

- The “egg-box” geometry of the upper and lower facing

The protrusions of the upper and lower facings of the modules cannot be manufactured, as the stress concentration around them would cause fibre breakage. The repeated 3D shapes need therefore to be separated from the facings and produced via another processing technique.

- Translucency of modules

The levels of translucency that can be achieved are very low and thus different methods of introducing light to the interior of the structure need to be considered.

2.4. Composite module out of srPP facings and a PET-bottle core
2.4.1. Scenarios for a foldable composite module and design to be further developed

Taking into account the aspects subjected to redesign, 3 scenarios for a foldable composite modules are formed. All concepts consist of a multi-hinged surface that can be folded into a box structure. As the walls of the module result from one continuous surface, a better cohesion between them is achieved and further connections between the sides are avoided.

The protrusions for the base and caps of the bottles are extra elements out of unreinforced polypropylene, in order for large numbers of components to be easily and quickly produced through injection molding. By separating the protrusions from the facings, the modules can be folded into thin flat structures, further minimising the occupied space in the shipping container. The upper and lower facing of the modules contain holes, either to receive the cap holders or to connect the module to each other. Variations between the concepts mainly locate in the geometry of the box and the its closure method and the assessment is based on the total area of the box and the complexity of the open surface to be molded. Another issue to be examined is the existence of the cap holders as individual elements or as a single PP corrugated surface.

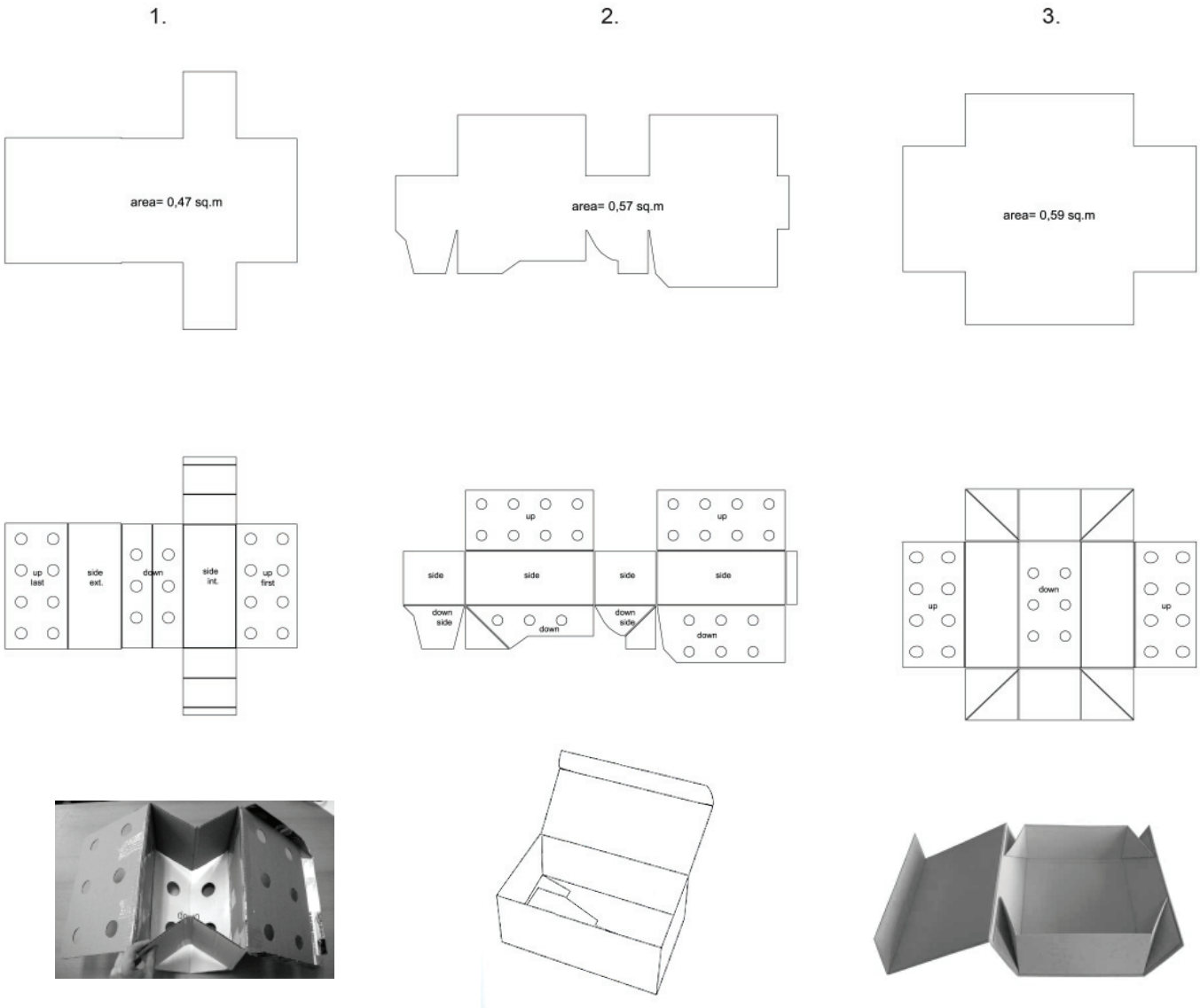

Figure 232. Three concepts for a foldable box

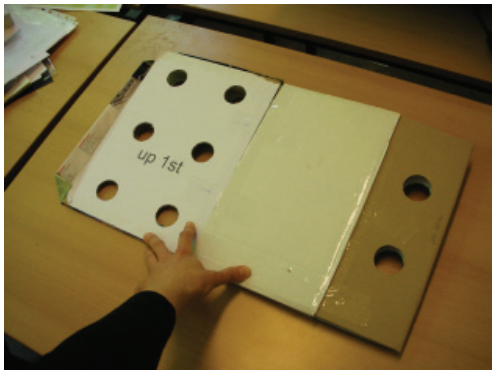

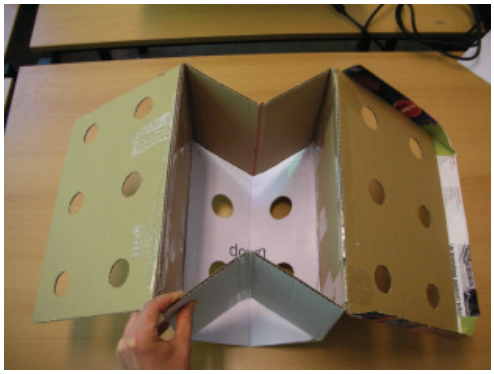

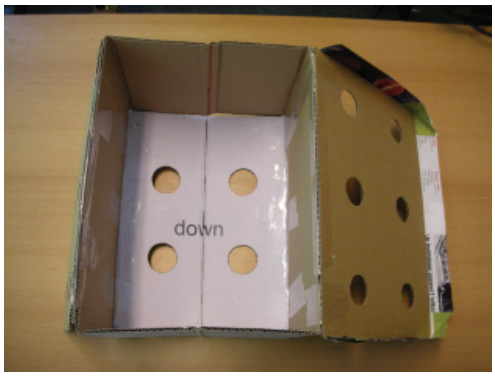

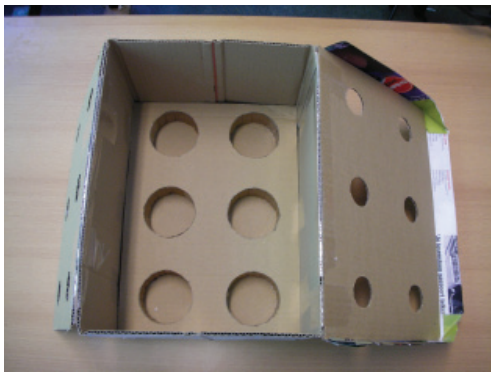

By introducing the bottle-base-holder in the box, the rectangular shape of the box is fixed



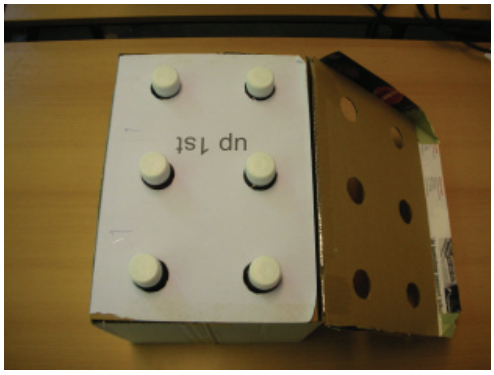





By introducing the cap fittings in the holes of the two facings, the structure is joined together

Figure 233. Concept no. 1. Steps for the assembly of the box

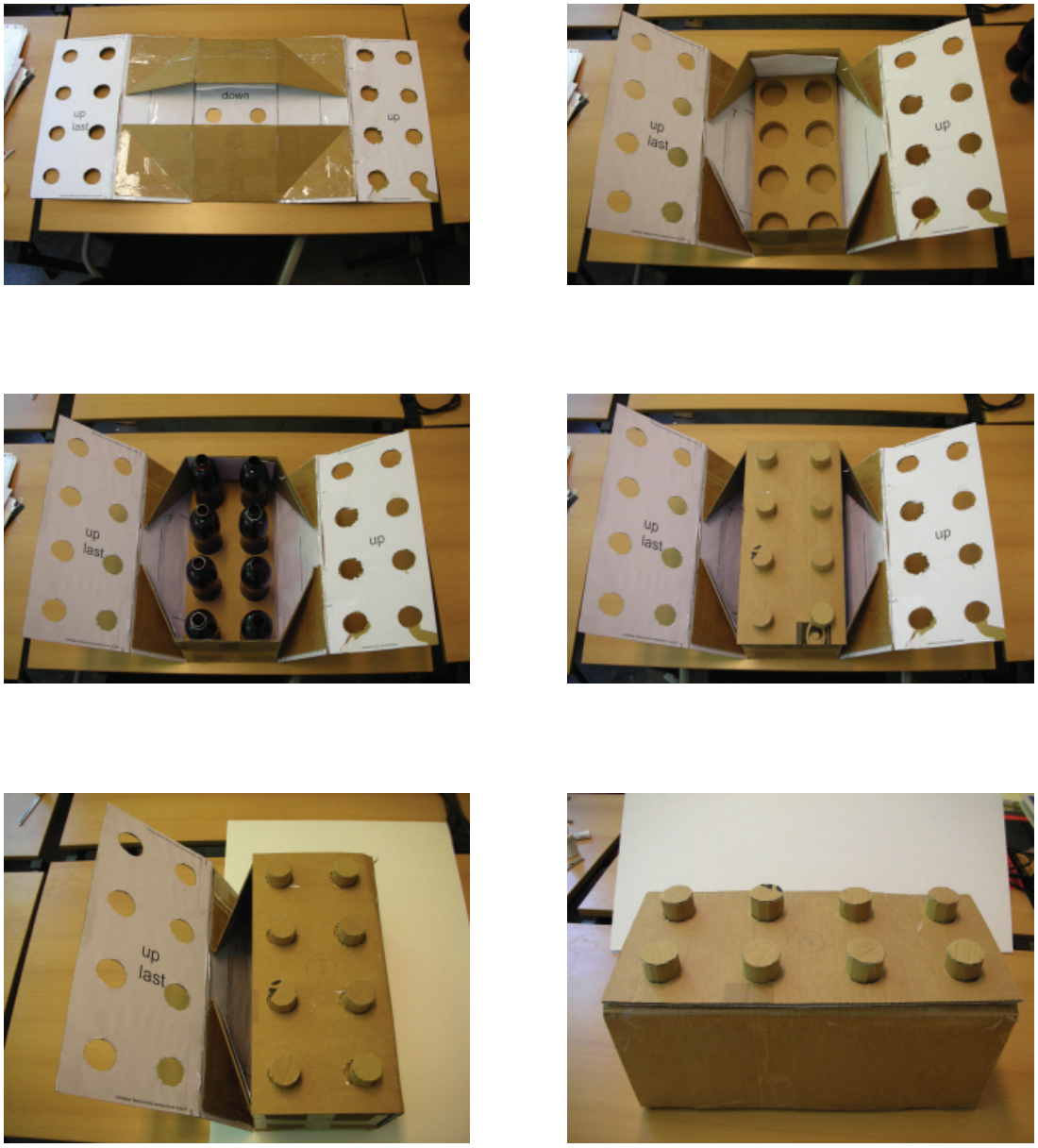

Figure 234. Concept no. 3. Steps for the assembly of the box

The concept with the less surface area and simpler closure method (no.1) is selected for further development. This proposes a foldable surface formed into a box, a PP continuous base-holder surface and individual PP cap holders. Circular holes can be introduced to the long sides of the module, where injection molded components out of PET can be press-fitted in them, to form openings.

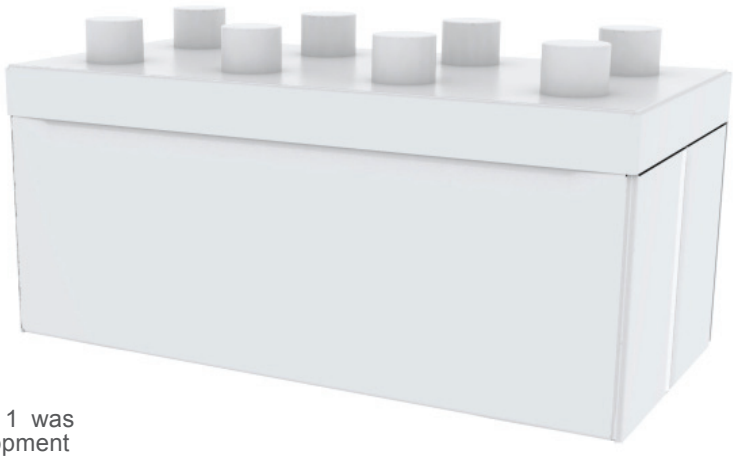

Figure 235. Concept no. 1 was selected for further development



Figure 236. Components constituting the wall module. The module weighs less than a 1,5L PET bottle filled with water

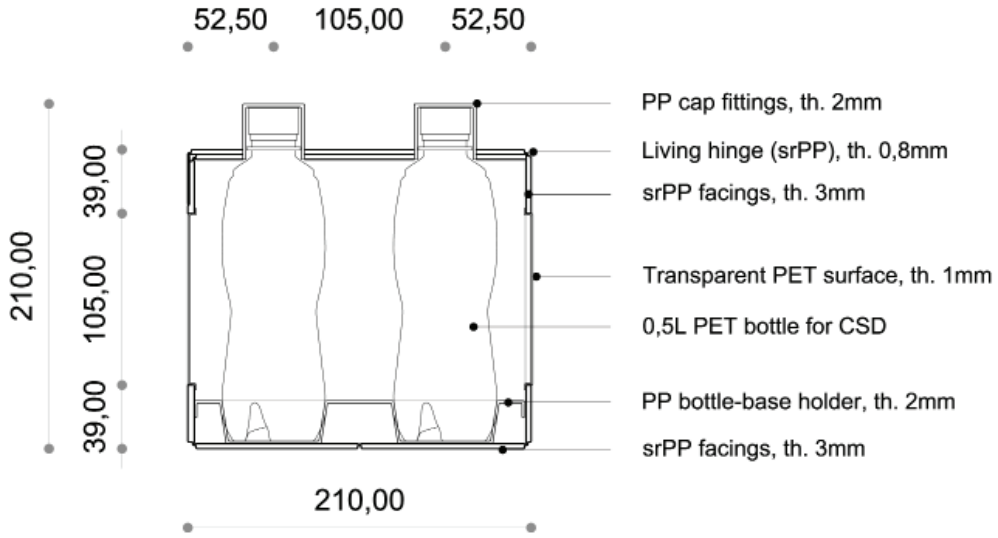

Figure 237. Section of basic wall module

Figure 238. Alternative of wall module for introducing light to the structure

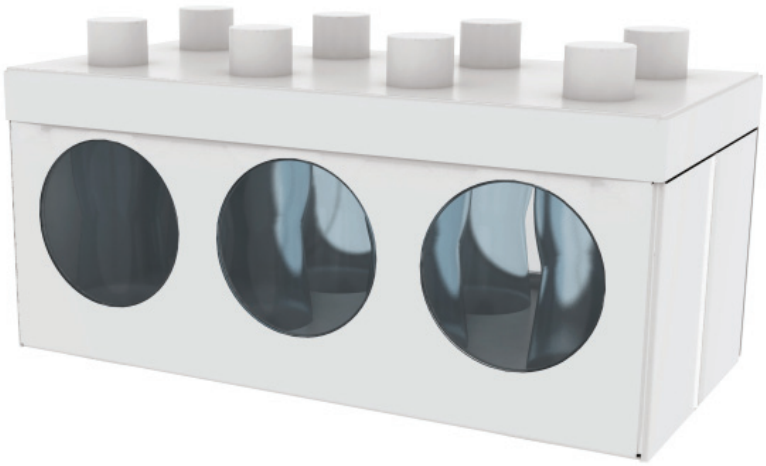



Figure 239. Exploded view showing the components required for a typical wall module

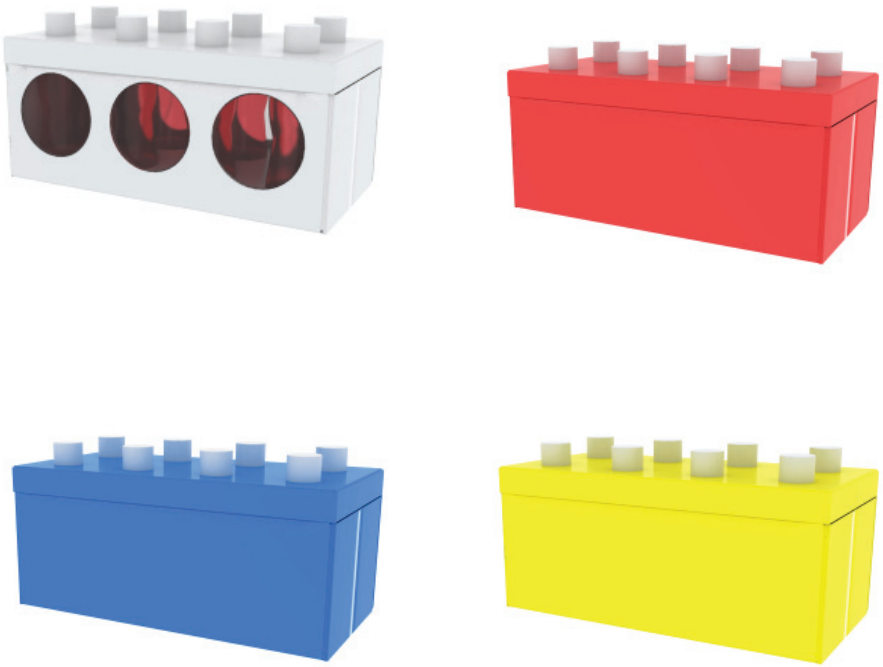

Figure 240. Variations in the colour of the bottles or the skin surfaces are possible

2.4.2. Assembly method and connection between modules

The following figures explain the assembly process for the module and the way it can be connected to similar modules.

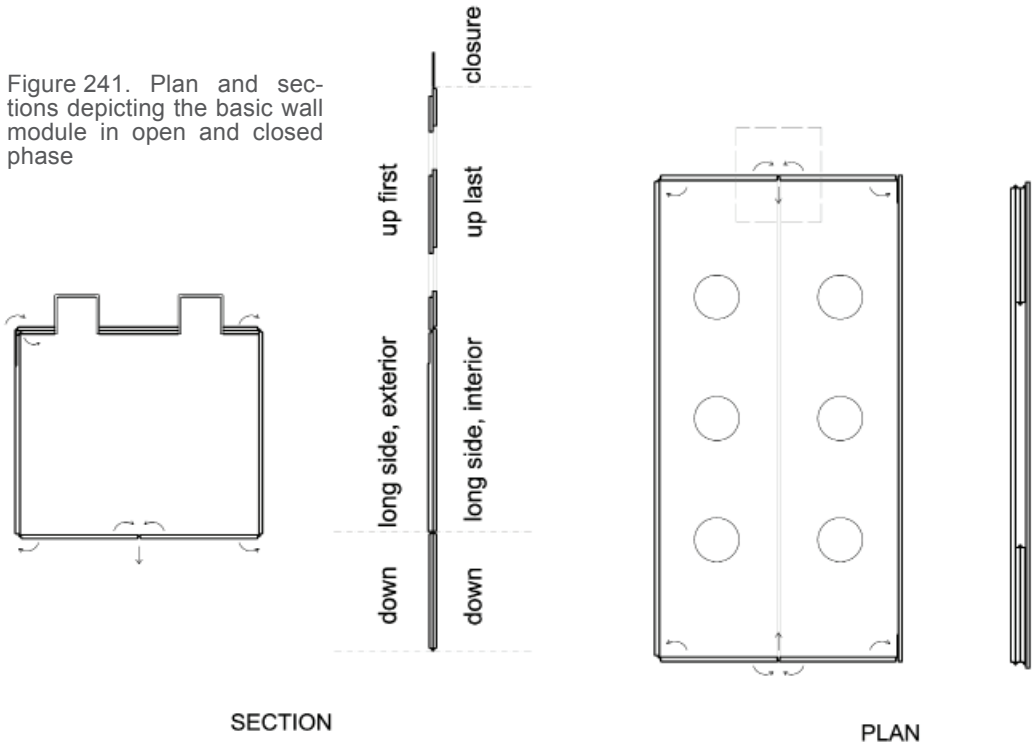

Figure 241. Plan and sections depicting the basic wall module in open and closed phase

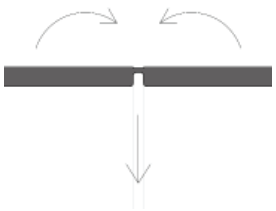

Figure 242. The living hinge is created by decreasing the thickness of the surface at that point

Figure 243. Folding procedure of the wall module

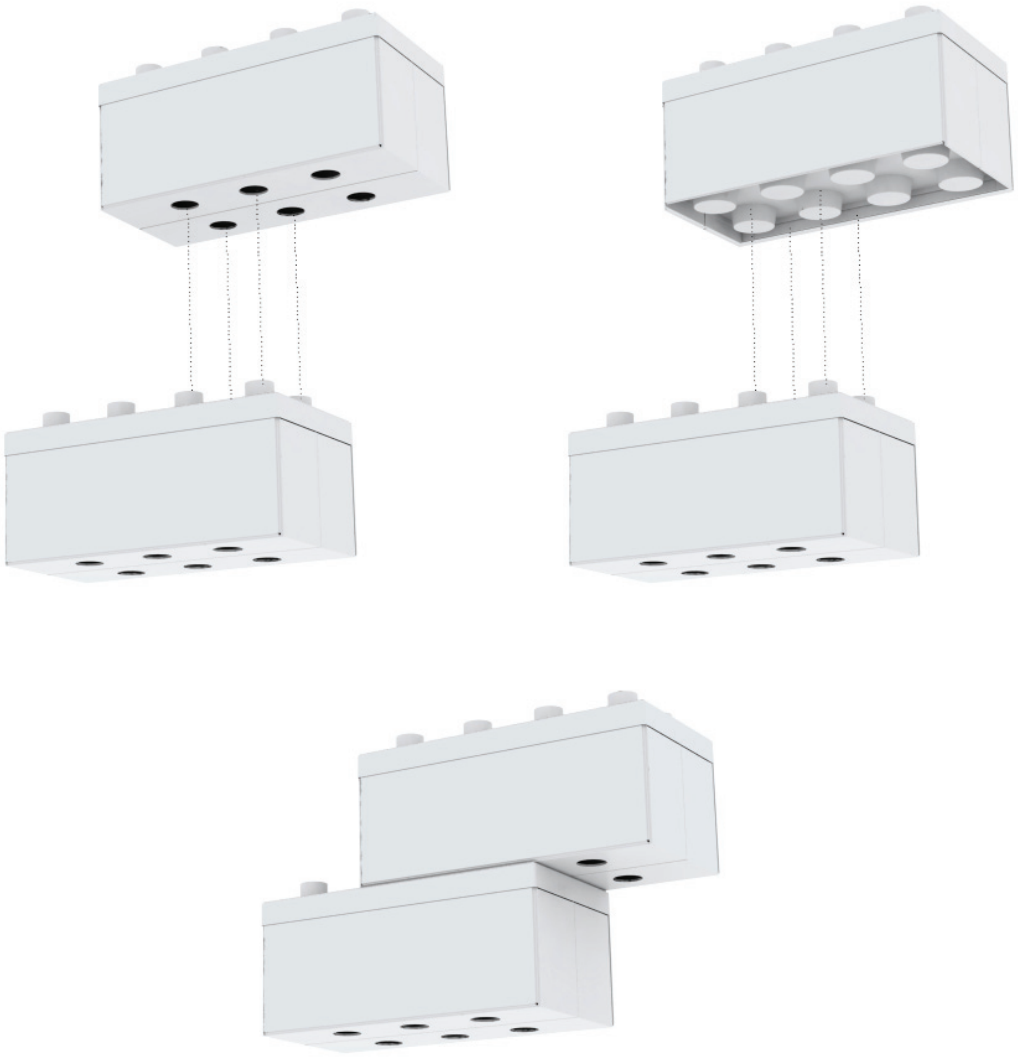

Figure 244. The protrusions of the upper facing fit in the holes situated in the lower facing of the module above, and are further stabilised by the protrusions of the bottle-base-holders

2.4.3. Manufacture process

Starting with the production of the multi-hinged foldable surface, the use of PURE® fabric is preferred instead of PURE® sheets, not only because of their easier processability but also because the thickness of the surface can be controlled. In other words, when the fabric is placed over the mold, a number of layers can be omitted when a living hinge needs to be introduced. Furthermore, due to the shape of the unfolded surface, it is possible to adjust the fabric layers accordingly, resulting in material savings. The above procedure indicates however that the non-isothermal molding technique should be avoided and the isothermal molding approach should be followed despite the lower time cycles. The fabric can be placed over the lower part of the mold according to the needs and then the upper and lower mold and the fabric can be heated until the desired temperature and then cooled down. This procedure is still allowing for large quantities of modules to be quickly produced, lowering the price of the modules.

Once the final surface is obtained, it can be trimmed using the laser-cut technique, which may not result in an equally excellent quality surface cut by CNC machining, but is much faster and very accurate.

Then the box can be welded at the sides using the method of ultrasonic welding, and painted if necessary.

Finally, the base holders, the cap holdings and the press-fitted windows can be injection molded.

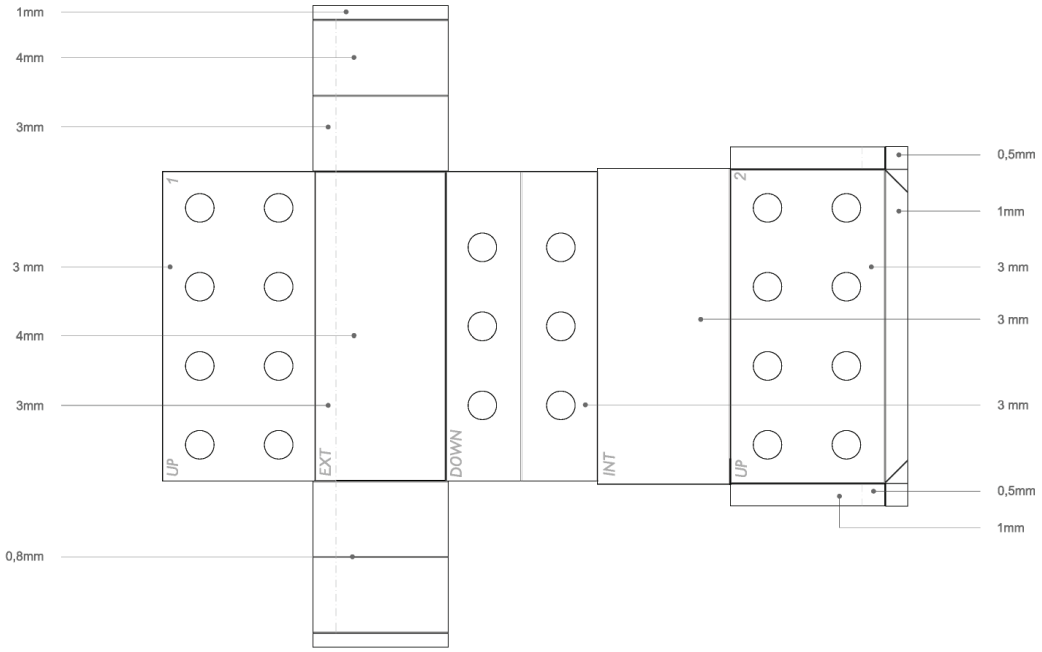

Figure 245. The surface to be molded for constructing the wall module varies in thickness

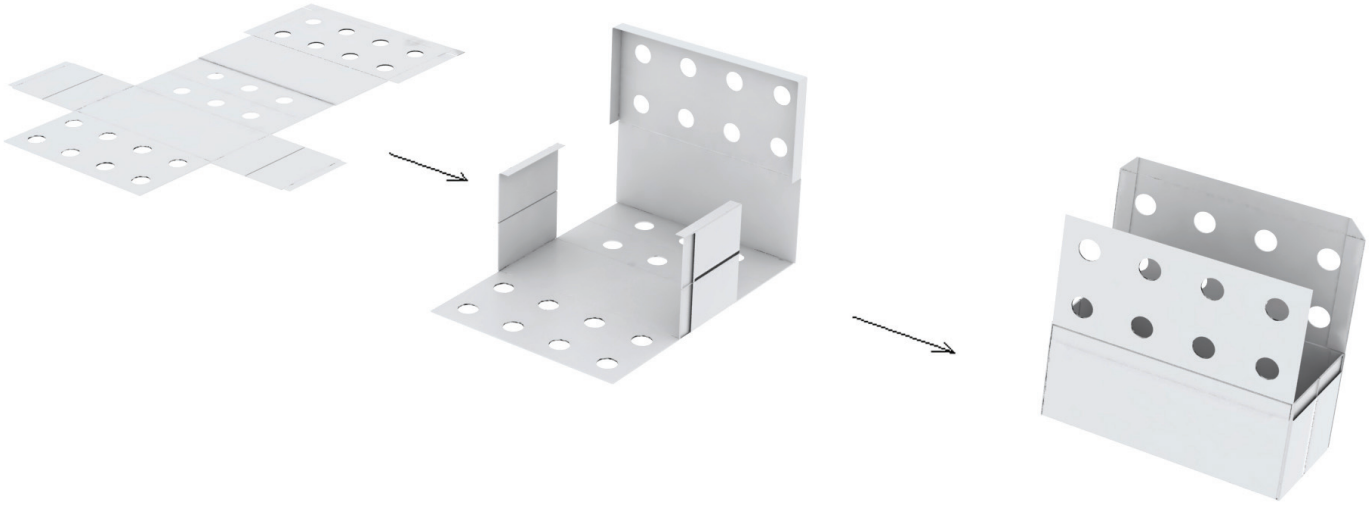

Figure 246. Once the surface is trimmed at the edges and the holes are opened, ultrasonic welding takes place to connect the small sides to the long side of the box

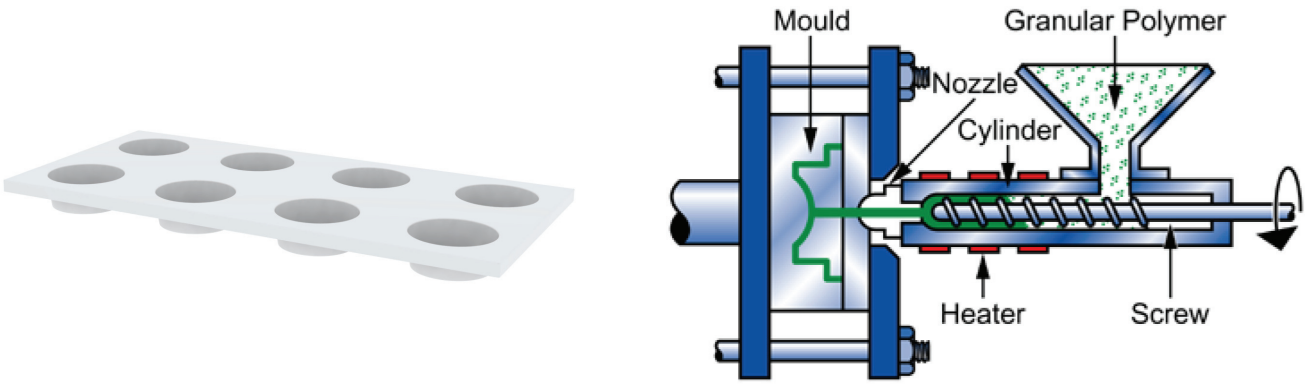

Figure 247. Components out of pure polypropylene, such as the bottle-base-holders, can be easily and quickly manufactured at large quantities, through injection molding

2.4.3. After-Life

At the end of its service life, the composite module can be disassembled, for the PET bottles to be separated from the srPP facings. The bottles can be reused at other applications or shredded to be recycled. The facings, being out of 100% polypropylene can also be easily recycled. The fact that no metal inserts are incorporated in these surfaces makes this procedure more simple. By returning the modules back to the manufacturing company, the downcycling of the material can be avoided. In other words, the srPP facings can be melted and granulated, and since there are no doubts about the quality and consistency of the material, the granules can be used again for co-extruding srPP tape.

2.5. Integral building system
2.5.1. Components and assembly on-site

The number of different components and the building logic are simplified, compared to the system developed at the beginning (before visiting *Lankhorst Pure Composites bv).* It consists of wall modules of two types that can be connected over each other and one type of slab module. A door unit, and foldable roof and floor coverings complete the system.

Figure 248. List of components for the integral building system

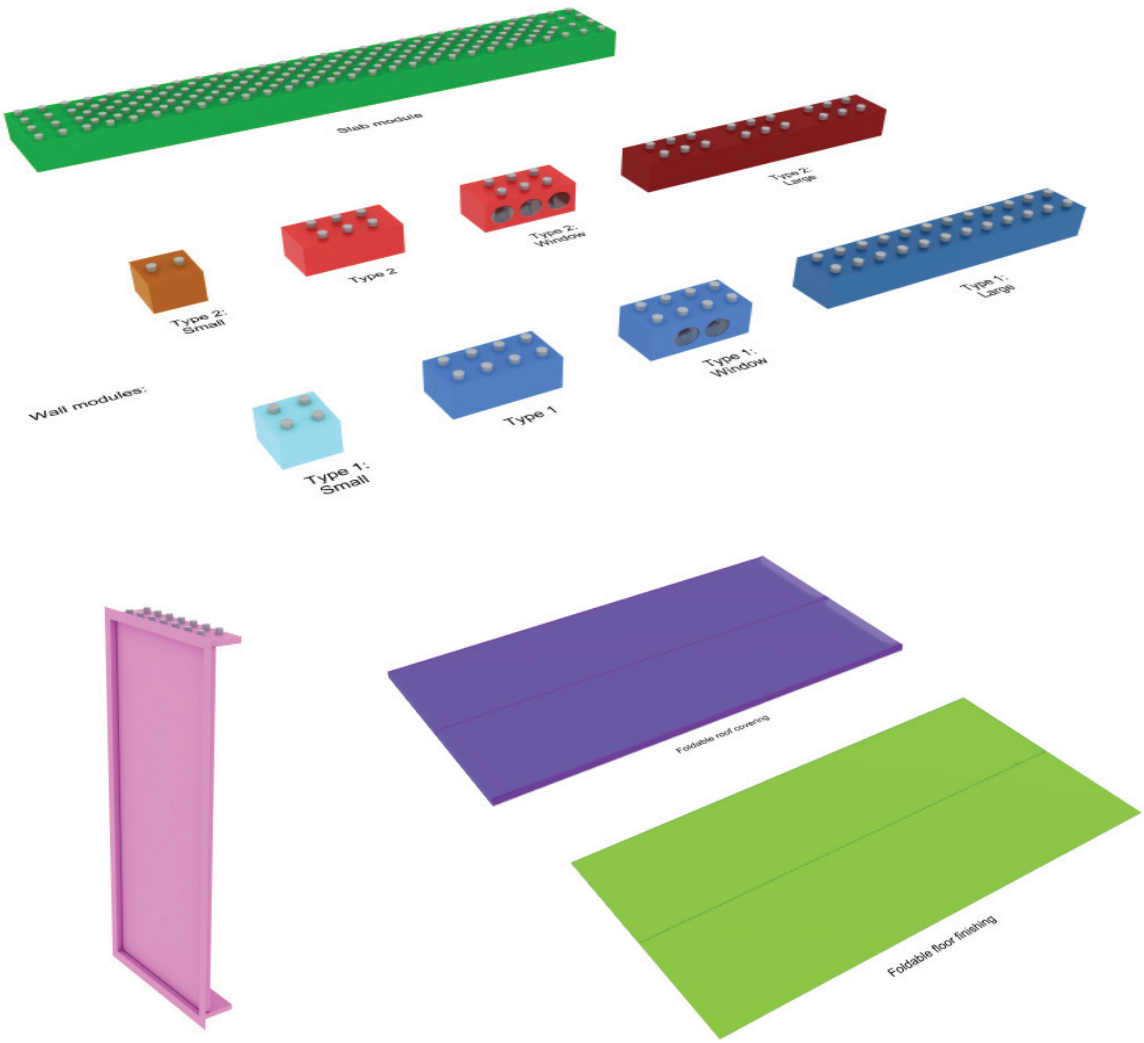

Figure 249. Steps of assembly on site

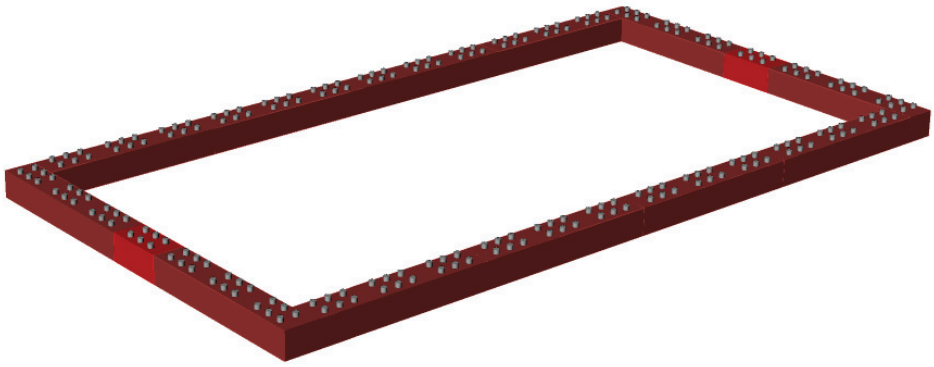

Step 1: One layer of type 2 wall modules to form the foundation

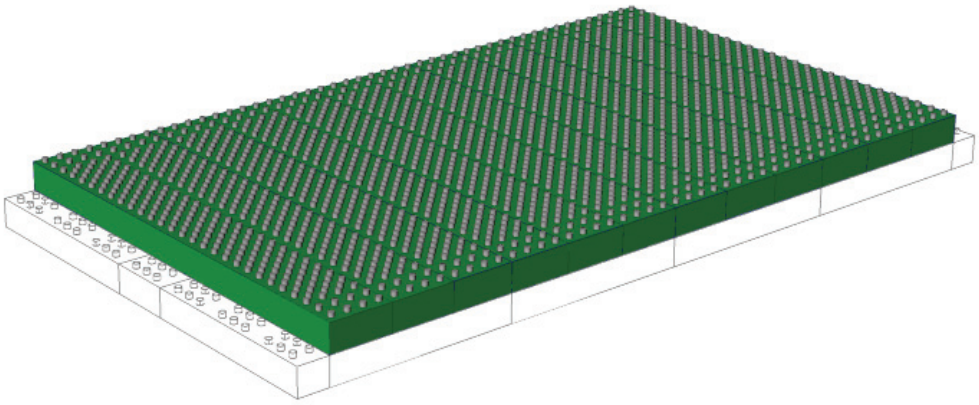

Step 2: Slab modules are placed over the foundation

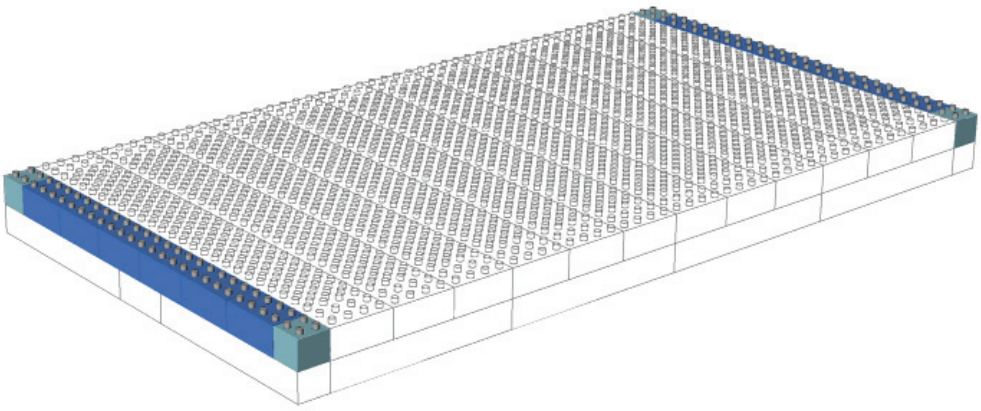

Step 3: Type 1 wall modules close the edges

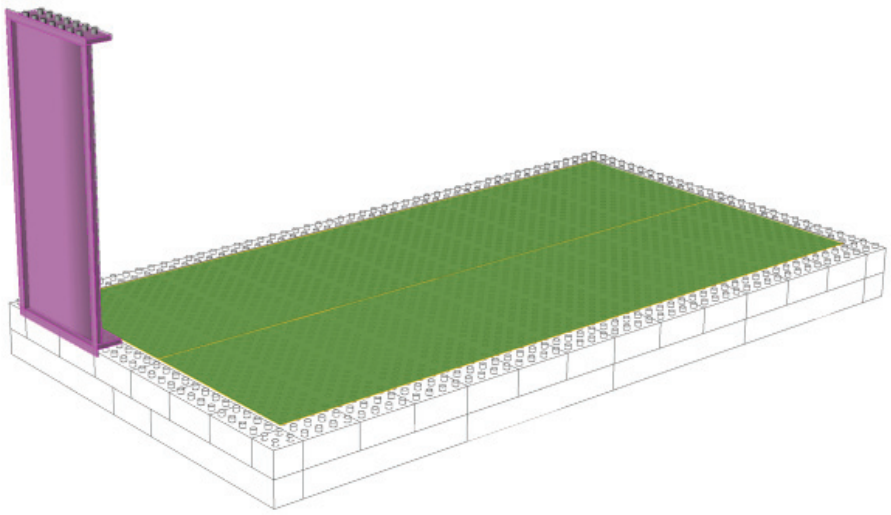

Step 4: The door component and the foldable floor covering are put into position

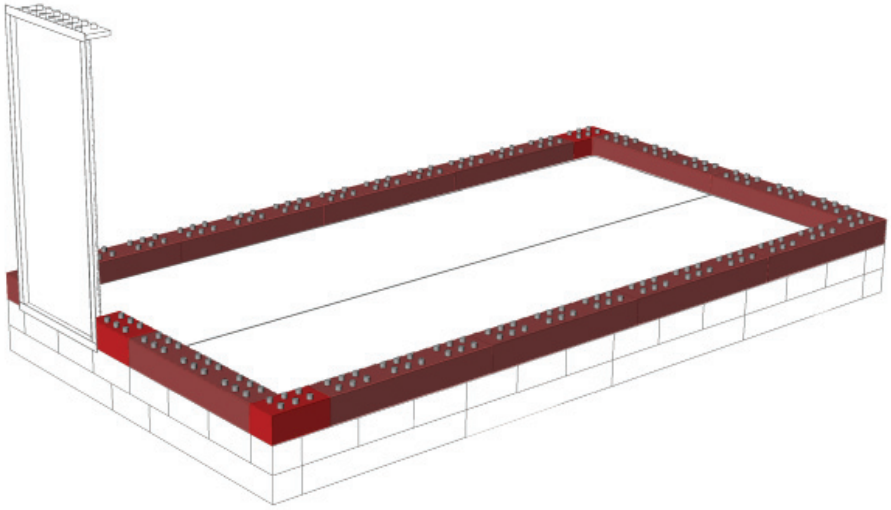

Step 5: One layer of Type 2 wall modules is placed over

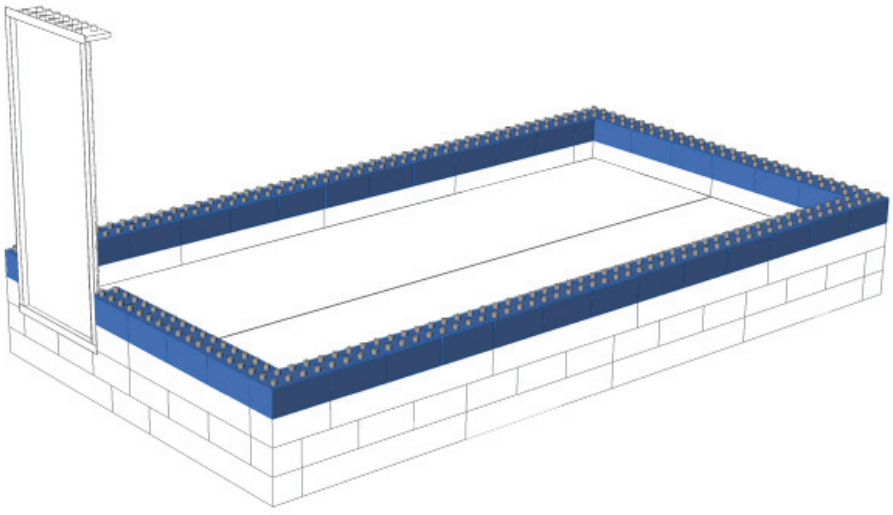

Step 6: The structure continues with Type 1 and 2 wall modules being successively interchanged. To simplify the assembly, it is suggested that the two types of wall modules are differently coloured

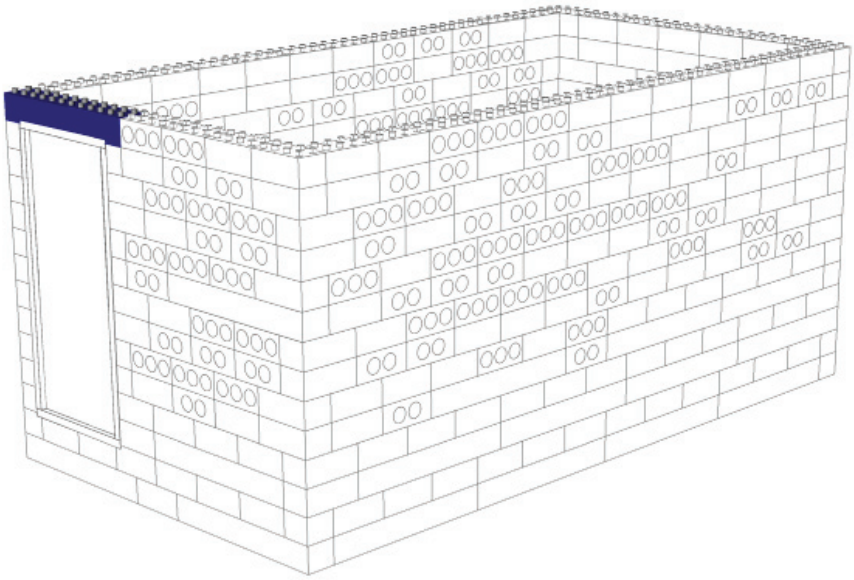

Step 7: Lintel piece (Type 1 module) is positioned over the door component

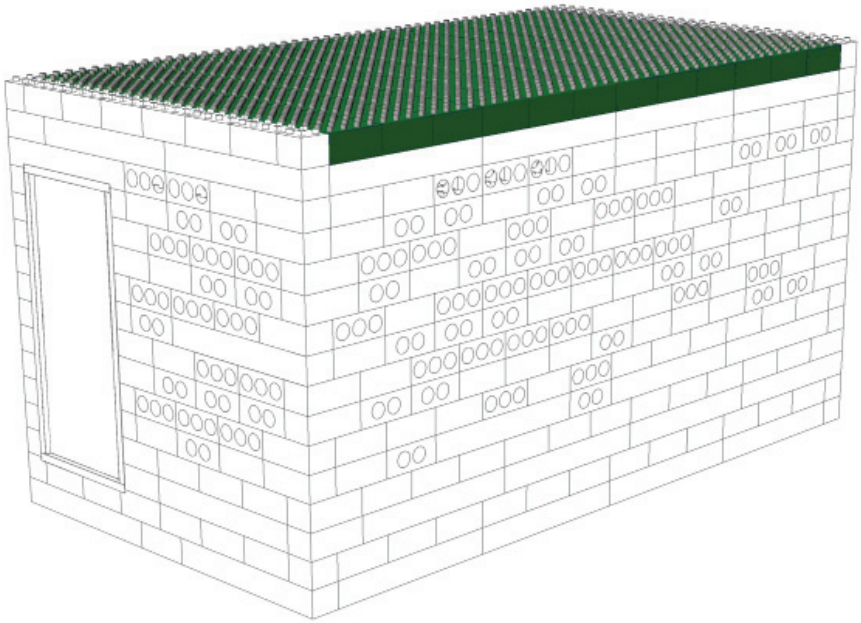

Step 8: Slab modules complete the roof and Type 1 wall modules close the edges

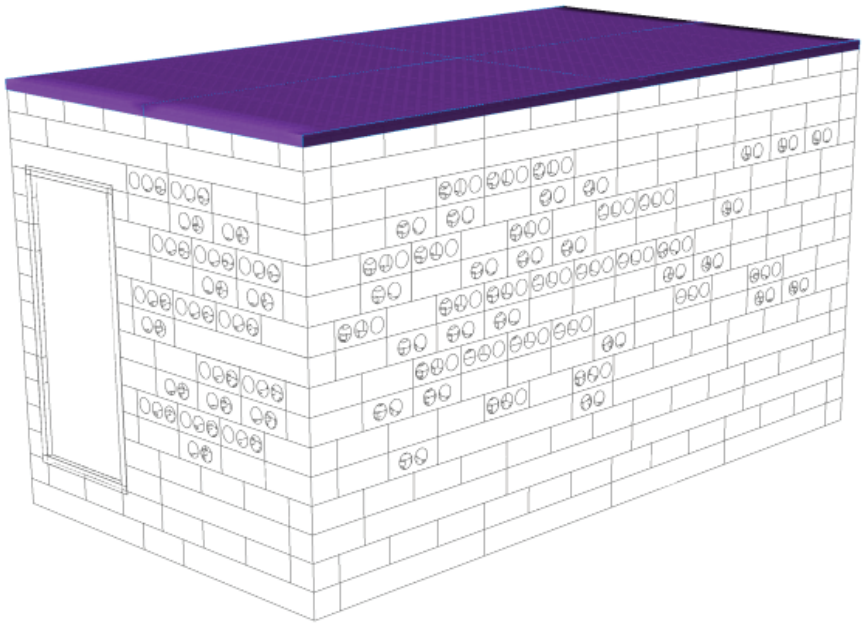

Step 9: The foldable roof covering is placed over the slab

2.5.2. Shipping

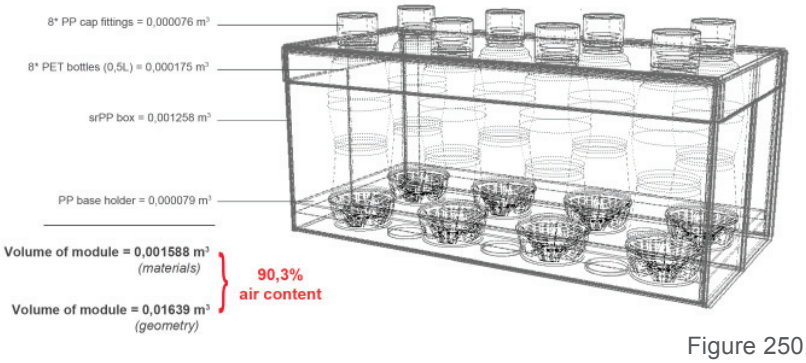

Figure 250. Volume of the wall module

By the use of lightweight materials and their efficient geometrical arrangement, the design accomplishes a low-dense structural building module. To give an example, one typical wall module weighs 1,36kg and has a 90,3% of air content. When considering the transportation of such modules, a non-reconfigurable module means that important space is occupied in the shipping container that is in fact air. To avoid transporting air and achieve large quantities of modules to be shipped overseas, the unfolding of the modules into flat surfaces is imperative. Even more, transporting empty PET bottles is not desired. Ideal scenario would be for the bottles to be collected from the surrounding area, but if this cannot be realised, an alternative is to send a small PET bottle blowing machine that will consume significantly less space than the bottles.

Another issue to be taken into account is the dimensions of the modules in regard to the dimensions of standard 20 foot shipping containers. Modules not only need to fit in the container but also to be packed together without significant empty space being left. Especially the dimension of the larger modules, such as the slab component, is thus determined by the dimension of the shipping container (2 slab modules cover the length of the container, for example).

It should be stressed again that savings in the space the modules consume when transported, in combination with their low density, can lead to enormous energy and cost savings, reduce the CO_2 emissions related to transportation and the traffic load.

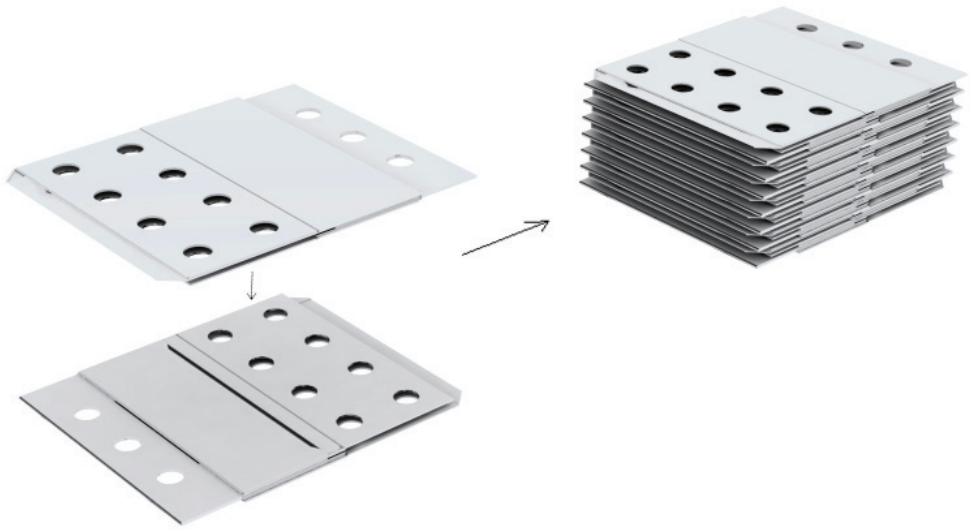

Figure 251. Stacking pattern for basic wall modules. 14 unfolded wall modules fit in the height of one folded wall module



Figure 252. Standard 20 foot shipping container
Source: http://www.thecontainerman.co.uk/



Figure 253. Small PET bottle blowing machine
Source: http://www.jmangel.com

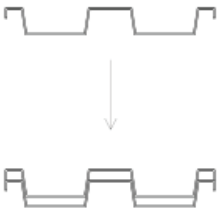

Figure 254. The design of the bottle-base-holders takes into account their stacking

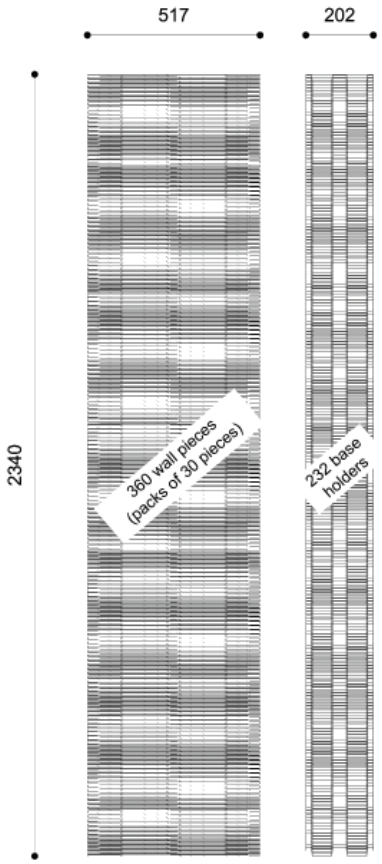

Figure 255. Number of components fitting within the height of a standard 20 foot shipping container (360 pieces is the amount of standard wall modules needed for a 16m^2 construction)

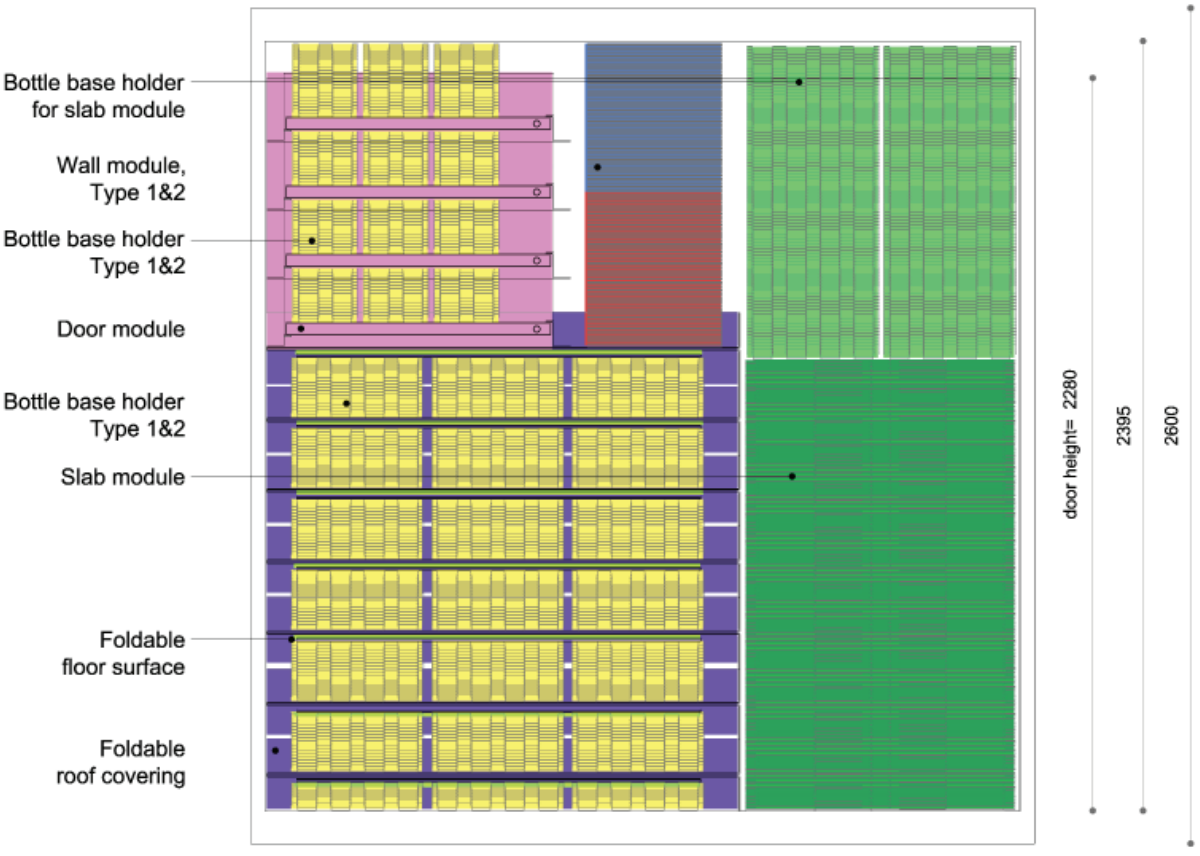

Figure 256. Section. Suggestion for the organisation of the components in the shipping container

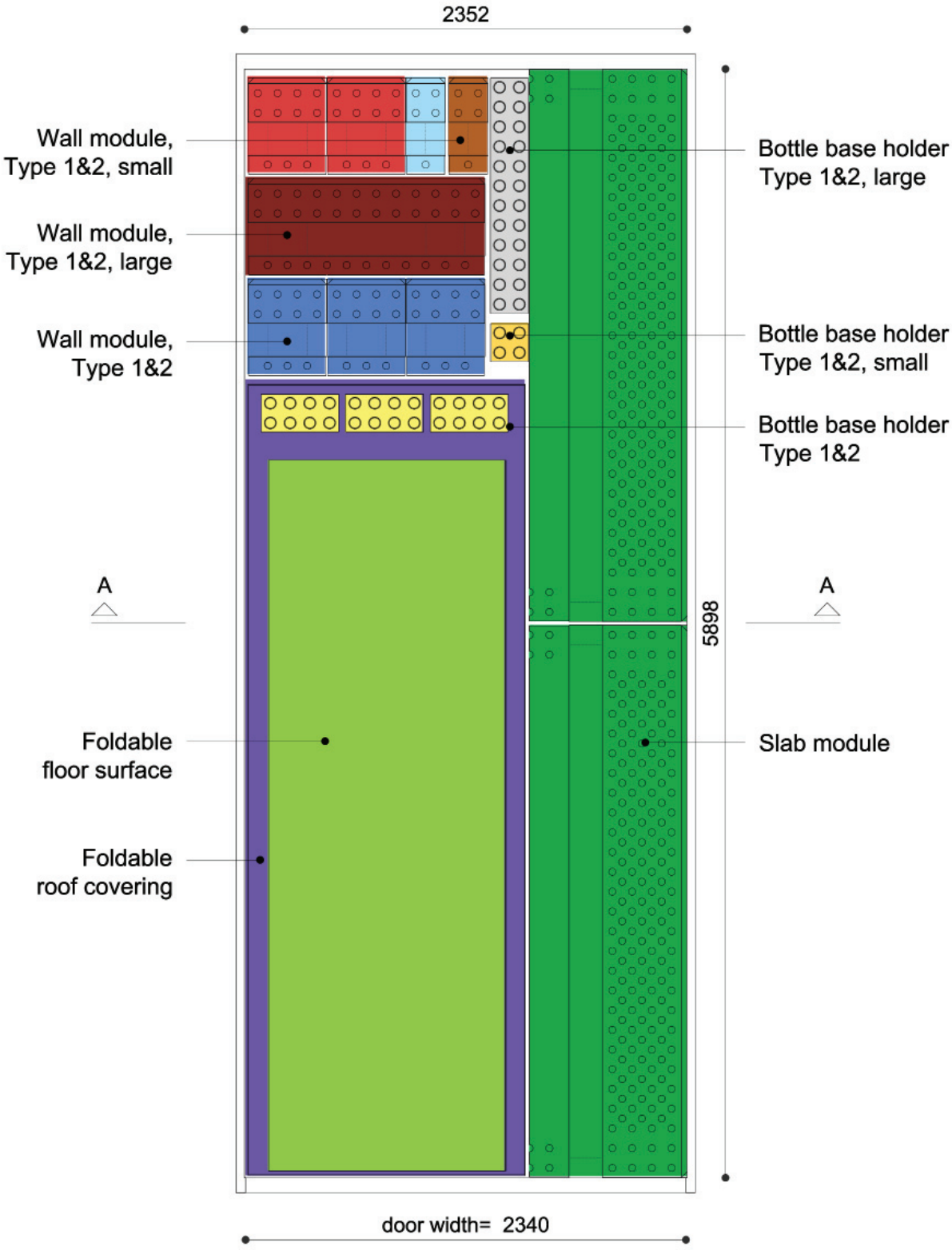

Figure 258.Plan (Level 1). Suggestion for the organisation of the components in the shipping container

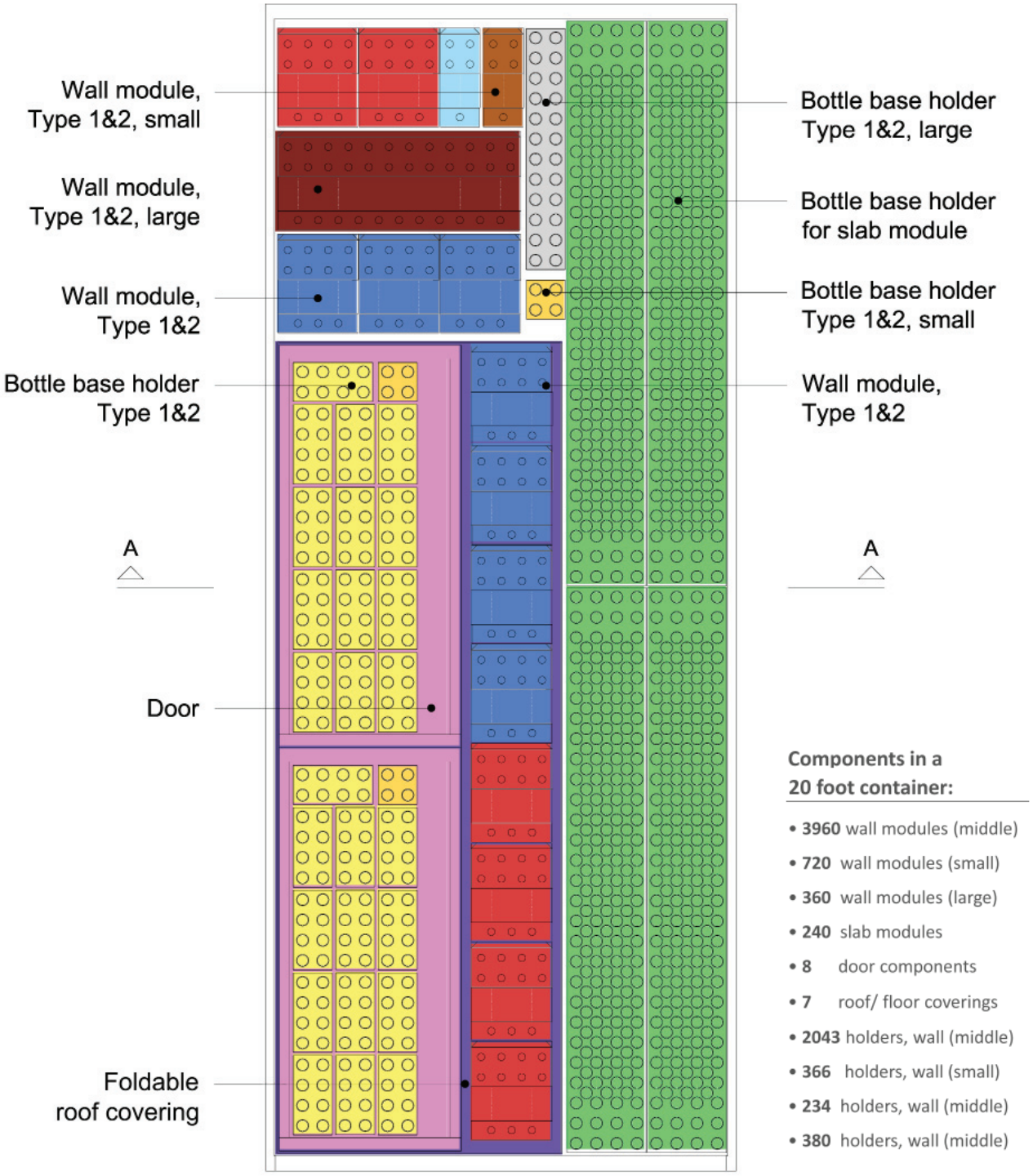

Figure 259.Plan (Level 2). Suggestion for the organisation of the components in the shipping container

2.6. Application possibilities

The integral system developed consists of modules that are cheap, lightweight and re-configurable into flat, stackable surfaces, to be shipped in large quantities. The assembly of the system is easily comprehensible and manageable by unskilled workers, and even children can handle the smaller components. Despite the intense labour required to assemble the components- that is, to place the PET bottles and close the box- temporary structures can be erected quickly and easily. This makes the system ideal in cases of natural disasters, where emergency shelters need to be built rapidly, from the victims themselves. In addition, as these modules are not standard building elements, nor are produced out of a valuable resource, there is minimum risk of these modules to be stolen on site. The shipping containers can be sent to the affected areas and when the structures are not needed anymore, the modules can be stacked back in the containers and shipped to another disaster area. In the meantime the containers can be used as community spaces.

If this system is combined with composite facility boxes (containing a small kitchen and wet room) that arrive as finished units on site, then intermediate shelters can be created. This finds application not only in cases of natural disasters, but more broadly in areas of extreme poverty. With minor modifications to the system (ex. installing insulation panels), the life of thousands of people leaving on shantytowns or being homeless can be upgraded.

With similar modifications the system can be applied in the developed world as well, for temporary student housing, holiday cabins or car shelters. Finally it can be used for exhibition pavilions or internal partition walls.

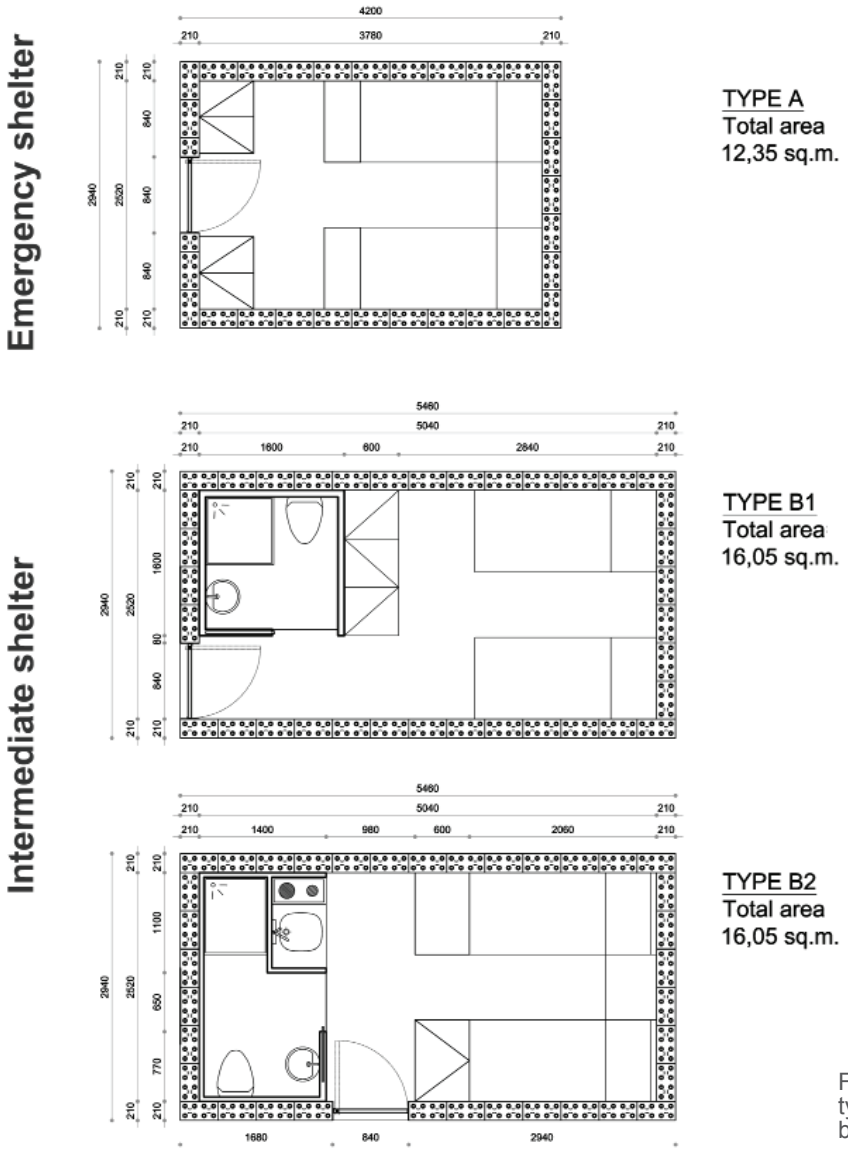

Figure 260.Plan. Shelter typology using the integral building system

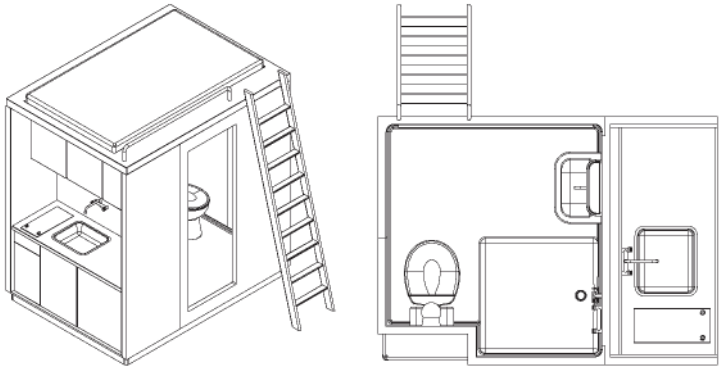

Figure 261. The Smartcube is a composite interior unit developed by Holland Composites Industrials B.V. with a kitchen and wet room integrated

Source: http://www.hollandcomposites.nl/

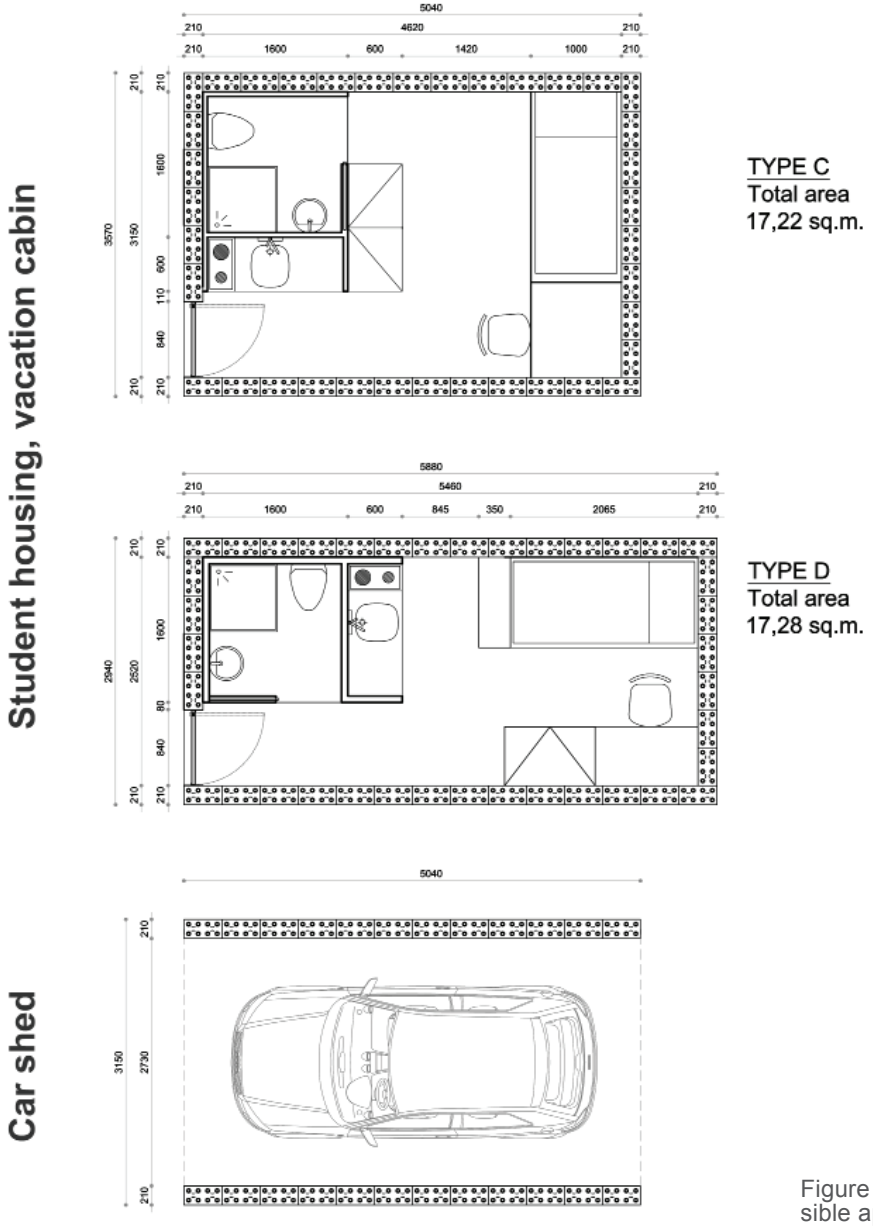

Figure 262.Plan. Other possible applications



Figure 263. Possible application of the integral building system to erect intermediate shelters after a disaster strike

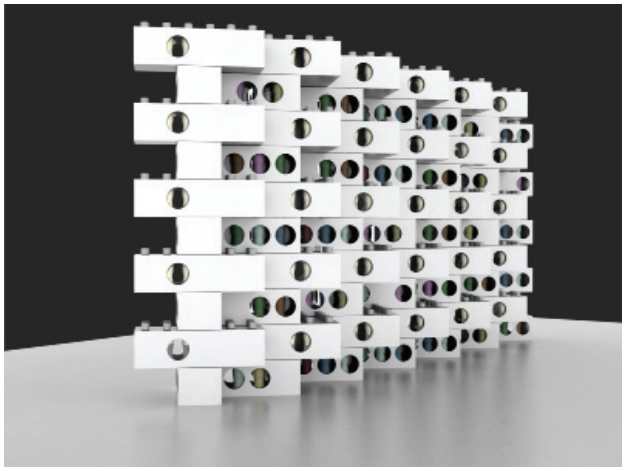

Figure 264. The wall-modules can be used in partition walls for exhibition spaces

C. Conclusion and reflection

The research presented confirmed the initial hypothesis, that it is possible to use a so considered waste product- the PET bottle- and achieve a reliable lightweight and cheap structure. It was also proven that completely separatable and recyclable thermoplastic sandwich composites can be designed to be used as structural elements.

The decisions taken during the design phase regarding the materials to be used (recovered PET bottles, srPP) and their combination (without adhesives), and the geometry (sandwich structure, rigid box) and reconfiguration of the module (foldable due to living hinges), were fundamental for achieving the initial goal of this thesis project.

What was realised through the conduction of this research was that by carefully examining materials and products, new potentials can be brought to attention that are not always related to their original use. The engineer and designer, by looking at common everyday objects differently than it is supposed to, can discover new possibilities that lead to money, material and energy savings, to interesting aesthetical results and to eco-friendly solutions. In combination with reconsidering what is to be perceived as waste and what is still functional, a broad pallet of materials begins to become available.

A closer look at everyday objects was found additionally beneficiary, as behind these ordinary products a great deal of engineering and innovation is hidden. This thesis constantly sought for inspiration in the packaging goods and other consumer products, learning from the way the materials are used and connected.

Changing the mindset and adding value to ordinary objects or waste, makes the designer question the standard used materials and look for alternatives that can have a significant impact, rather than just reproducing the “good old” techniques. Shifting from concrete to lightweight composite structures, if the project demands it, is one step, for example. Questioning the prevalence of thermoset polymeric composites is a step further.

Yet, the promising properties of these materials or objects per se mean nothing if their proper combination with other materials is not achieved. Creating efficient structures is closely related, thus, with the effort of making the most out of the resources we have in hand and by discovering their most optimum combination. It is interesting then to see the design evolve according to the way the materials guide it and not influenced by personal intuitions. As so, this project started with a vague notion of the end design result, which was only reached after a methodical study of the materials and their relationship with each other. This approach allowed the development of a much more efficient structure than the one that would have been obtained if the initial design was elaborated excluding the role of engineering and postponing it for a later stage.

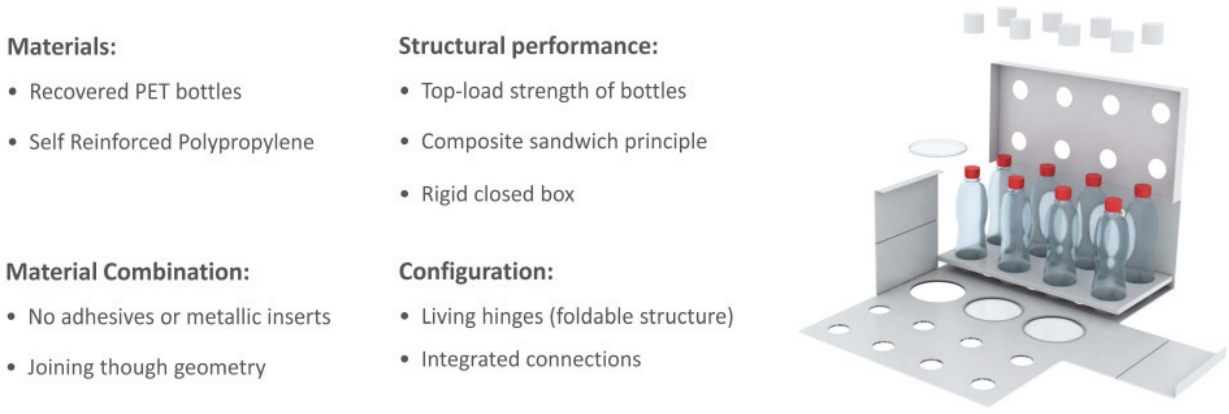

Figure 265. Decisions taken that lead to the design of a cheap, lightweight and eco-friendly building module

Acknowledgements

I wish to thank Dr.ir. F.A. Veer *(Assistent professor of Materials Science, Bouwkunde, TU Delft)*, Ir. A. Borgart *(Researcher, Blobs, Structures, Bouwkunde, TU Delft)*, Dipl.ing. F. Heinzelmann *(PhD researcher at Architectural Engineering, Bouwkunde, TU Delft),* Ir. A. de Ridder *(Docent, TU Delft)* M. Turrin *(Researcher, Informatics, Bouwkunde, TU Delft),* M. Morales Beltran *(PhD researcher, Bouwkunde, TU Delft)*, P.J. Dwarshuis *(Holland Composites Industrials)*, D. Repija *(Ducona Holland BV)*, F. Bloemhof *(Lankhorst Pure Composites bv)* G. Baardolf *(Technical Staff, BT lab, TU Delft)*, and A.L. den Breejen *(Technical Staff, BT lab, TU Delft)*, for their support, inspiration and valuable comments.

References

[1] HINTE, VAN E., NEELEN, M., VINK, J. and VOLLAARD, P. 2003. Smart Architecture. Rotterdam, 010 Publishers
[2,3] BEUKERS, A. Capita Selecta: Thin City. Amsterdam. Academy of Architecture. <http://www.lightness-studios.nl/downloads/AIRboekjeA5_e-book.pdf>
[4] SMITHERS RAPRA. Material selection for composite design. < http://www.rapra.net>
[5] CHAKRABARTI, P.R., MILLAR, D. & BANDYOPADHYAY, S. Application of Composites in Infrastructure – Part III (a brief report on research and development). <http://www.quakewrap.com/frp papers>
[6] DANIEL, A.R. 2003. Environmental Considerations to Structural Material Selection for a Bridge.
European Bridge Engineering Conference Lightweight Bridge Decks. Rotterdam.
[7,8] EIRE COMPOSITES. Thermoplastc Composites Explained. < http://www.eirecomposites.com/thermoplastic-composites-explained.html>
[9] ASHBY, M.F. 2009. Materials and the Environment Eco-informed Material Choice. Canada, Butterworth-Heinemann
[10] U.S. ENVIRONMENTAL PROTECTION AGENCY. Wastes - Resource Conservation - Common Wastes & Materials. < Wastes - Resource Conservation - Common Wastes & Materials>
[11] see [9]
[12] V-ROM INSPECTIE, MINISTERIE VAN INFRASTRUCTUUR EN MILIEU 2011. Kunststof verpakkingsafval uit huishoudens in beeld. <www.vrominspectie.nl>
[13] SUTTON, J. 2009. Why is it cheaper to make new plastic bottles than to recycle old ones? Viewed 15th December 2009. < http://engineering.mit.edu/ >
[14] WIKIPEDIA 2012. Dry Ice. < http://en.wikipedia.org >
[15] ROSENTRATER, A.K. 2006. Economics and Impacts of Ethanol Manufacture, *BioCycle*, vol. 47, no. 12, p. 44.
[16] GRANTA 2011. CES EduPack.
[17] SPERLING, L. H. 2006. Concentrated Solutions, Phase Separation Behavior and Diffusion. *Introduction to Physical Polymer Science*, New Jersey, John Wiley & Sons, Inc. p. 173.
[18] SMITHERS RAPRA. Rapra Testing for Environmental Stress Cracking. < http://www.rapra.net>
[19] MÜLLER-PLATHE, F. 1994. Permeation of polymers a computational approach, *Acta Polymerica*, vol. 45, no. 2, pp. 259-293.
[20] FAO 1995. Packaging materials. *FAO Agricultural Services Bulletin.* Rome: FAO Publications, vol. 119.
[21] MAUL, P. 2005. Fillers, Pigments and Additives for Plastics in Packaging Applications. *Barrier Enhancement Using Additives*, Pira International Conference. Brussels, Belgium. p. 1.
[22] SMITHERS RAPRA. Rapra Testing for Environmental Stress Cracking. < http://www.rapra.net>
[23] HANNAY, F. 2002. Rigid Plastics Packaging - Materials, Processes and Applications. *Rapra Review Reports,* vol. 13, no. 7, p. 17
[24] MGC 2007. Nylon-MXD6. Various Grades and Uses. <http://www.mgc.co.jp>
[25] EVATANE. Evatane® Product Range. < www.evatane.com >
[26] BRODY, A. 2004. Plastic fantastic? Viewed 15th September 2004. <http://www.packaging-gateway.com>
[27] CHEMISTRY TEXAS A&M UNIVERSITY. Gases: Elements and Compounds that are Gases at Room Temperature. <http://www.chem.tamu.edu>
[28] ROSATO, D. V., ROSATO, D. V. & ROSATO, M. G. 2001. Design Influencing Factor. *Plastics Design Handbook*. Springer - Verlag. p. 64
[29] IUPUI TESTING CENTRE. Creep Experimental Lab. <www.engr.iupui.edu>. p. 3.
[30] TRES, P. A. (2006). Designing Plastic Parts for Assembly (6th Edition). Munich, Carl Hanser Verlag
[31] BARKOULA, N.-M., T. PEIJS, et al. (2005). Processing of single polymer composites using the concept of constrained fibers. Polymer Composites 26(1): 114-120.
[32] L. M. MORGAN, B. M. WEAGER, C. M. HARE AND G. R. BISHOP, G. M. SMITH. Self Reinforced Polymer Composites: Coming Of Age. <http://www.iccm-central.org>

[33] see [30]
[34] APTIFORM. SRPET Versus SRPP. < http://www.aptiform.com>
[35] SURENDRA, A. 2004. PP is closing in on PET. Viewed 14 March 2004. <http://www.packaging-gateway.com/features/feature26/>
[36] see [7]
[37, 38] see [32]
[39] GARDINER, G. 2006. Preconsolidated fiber-reinforced thermoplastics offer short cycle times, tailored properties, recyclability and lower cost. Viewed 4 January 2006. < http://www.compositesworld.com/articles/thermoformable-composite-panels-part-1 >
[40] see [32]
[41] ALCOCKA, B., CABRERA, N.O., BARKOULA, N.-M., PEIJSA, T. 2006. Low velocity impact performance of recyclable all-polypropylene composites. Composites Science and Technology 66(11–12): 1724-1737.
[42] see [16]
[43] JONES, R. S., RILEY, D. E. A New Self-Reinforced Polypropylene Composite < http://www.speautomotive.com/SPEA_CD/SPEA2002/pdf/a01.pdf >
[44] see [16]
[45, 46] THE ENGINEERING TOOLBOX. Coefficients of Linear Thermal Expansion. <http://www.engineeringtoolbox.com>
[47] see [32]
[48] see [30]
[49] MILLIKEN. Processing TEGRIS. < http://www.milliken2.com/MFT/MFThtml.nsf/page/process.htm >

Literature

ALLEN, H. G. 1969. Analysis and design of structural sandwich panels. Oxford, Pergamon.
ANDREA MASELLI, J. D. Influence of Dissolved CO2 on the Measurement of Diet Beverages. <www.maselli-uk.com/>.
ARMSTRONG, R. B. New EVAL® EVOH Resins for Flexible Packaging, <www.eval.eu/us/home>.
ASHBY, M. F., SHERCLIFF, H. AND CEBON, D. 2007. Materials Engineering, Science, Processing and Design. Oxford: Elsevier.
ASHBY, M.F. 2005. Materials Selection in Mechanical Design (3rd Edition). Italy, Butterworth-Heinemann.
ASHBY, M.F. 2009. Materials and the Environment Eco-informed Material Choice. Canada, Butterworth-Heinemann.
AYDINCAK, I. 2007. Investigation of Design and Analyses Principles of Honeycomb Structures. MSc Thesis, Aerospace Engineering, The Graduate School of Natural And Applied Sciences of Middle East Technical University.
BITZER, T. 1997. Honeycomb Technology: Materials, Design, Manufacturing, Applications and Testing. Glasgow, Cambridge University Press.
BEUKERS, A., HINTE, E. V., 2005. Lightness: The Inevitable Renaissance of Minimum Energy Structures. Rotterdam, 010 Publishers.
BONENBERGER, P. R. 2005. First Snap-Fit Handbook - Creating Attachments for Plastic Parts (2nd Edition). Munich, Hanser Publishers.
BRODY, A. L. 2003. Barrier coatings fortify plastic bottles. Viewed 1st March 2003. <www.allbusiness.com>.
BURKE, J. 1992. Vapor Barrier Films. *WAAC Newsletter*, Western Association of Art Conservators, vol. 14, no. 2, pp. 13-17.
DEMIREL, B. 2008. *Optimisation of Petaloid Base Dimensions and Process Operation Conditions to Minimise Environmental Stress Cracking in Injection Stretch Blow Moulded Bottles*. Doctor of Philosophy, RMIT University.

ENSO Bottles, LLC 2009. Gas Barrier, Hot Fill Bottles, Carbonated Beverages.< www.ensobottles.com>.
ERHARD, G. 2006. Designing with Plastics, Munich, Hanser Publishers.
FAO 1995. Packaging materials, *FAO Agricultural Services Bulletin.* Rome: FAO Publications, vol. 119.
GRANTA 2011. CES EduPack.
HAI-JIN, W., BAI-QUAN, L. & QIAN, Y. 2009. The theory model and analytic answer of gas diffusion. *Procedia Earth and Planetary Science*, vol. 1, no. 1, pp. 328-335.
HE, M., HU, W. 2008. A study on composite honeycomb sandwich panel structure. Materials & Design 29(3): 709-713.
HEXCEL. HexWeb Honeycomb Sandwich Design Technology. < http://www.hexcel.com/ >.
IUPUI TESTING CENTRE. Creep Experimental Lab. <www.engr.iupui.edu>.
JÜRGEN, B. 2010. Chapter 16 - Multilayer oriented films. In: JOHN, R. W. & JR.A2 - JOHN R. WAGNER, JR. (eds.) *Multilayer Flexible Packaging*. Boston: William Andrew Publishing.
KNAACK, U., TILLMANN, K., BILOW, M. 2008. Imagine 02, Deflatables, Rotterdam, 010 Publishers.
LAZIC, V. L. B.-S., J. ; GVOZDENOVICB, J.J. AND SIMENDICB, B. 2010. Barrier Properties of Coated and Laminated Polyolefin Films for Food Packaging. *ACTA PHYSICA POLONICA A,* vol. 117, no.5, pp. 855-858.
LONG, F. A. & THOMPSON, L. J. 1955. Diffusion of water vapor in polymers. *Journal of Polymer Science*, vol. 15, no. 80, pp. 413-426.
MÜLLER-PLATHE, F. 1994. Permeation of polymers — a computational approach. *Acta Polymerica*, vol. 45, no. 2, pp. 259-293.
MASI, P. & PAUL, D. R. 1982. Modeling gas transport in packaging applications. *Journal of Membrane Science*, vol. 12, no. 2, pp. 137-151.
MAUL, P. 2005. Fillers, Pigments and Additives for Plastics in Packaging Applications. *Barrier Enhancement Using Additives*, Pira International Conference. Brussels, Belgium.
MOALLI, J. 2001. Plastics Failure - Analysis and Prevention. William Andrew Publishing/Plastics Design Library.
PHILLIP, W. A., RZAYEV, J., HILLMYER, M. A. & CUSSLER, E. L. 2006. Gas and water liquid transport through nanoporous block copolymer membranes. *Journal of Membrane Science*, vol. 286, no. 1-2, pp.144-152.
PINO, M., DUCKETT, R. A. & WARD, I. M. 2005. Single and mixed gas diffusion through polyethylene films. *Polymer*, vol. 46, no. 13, pp. 4882-4890.
ROSATO, D. V., ROSATO, D. V. & ROSATO, M. G. 2001. Plastics Design Handbook. Springer - Verlag.
ROTHSCHILD, D. D. 2011 Plastiki; across the Pacific on plastic, an adventure to save our oceans, California, Chronicle Books.
SIVARAMAKRISHNA, V., RASPANTE, F., PALANIAPPAN, S. & PASCALL, M. A. 2007. PET bottles seal quality testing using an on-line pressure differential detector. *Journal of Food Engineering*, vol. 80, no. 2, pp. 645-654.
SMITHERS RAPRA. Rapra Testing for Environmental Stress Cracking. < http://www.rapra.net>
SOUTH, J. T. 2001. Mechanical Properties and Durability of Natural Rubber Compounds and Composites. Doctor of Philosophy, Virginia Polytechnic Institute and State University.
SPERLING, L. H. 2006. Introduction to Physical Polymer Science, New Jersey, John Wiley & Sons, Inc.
TRES, P. A. (2006). Designing Plastic Parts for Assembly (6th Edition). Munich, Carl Hanser Verlag.
TROUGHTON, M. J. 2008. Handbook of Plastics Joining - A Practical Guide (2nd Edition), William Andrew Publishing.
VALSPAR. Valor Barrier Resins. < www.valsparpackaging.com>.
VEGT, A.K. van der. 2002. From Polymers to Plastics. Delft, DUP Blue Print.
VERMEIREN, L. H., DEVLIEGHERE, F. and DEBEVERE, J. 2003. Oxygen, ethylene and other scavengers. *Novel food packaging techniques*. Ghent University, Belgium: Woodhead Publishing Online.
WEBB, K. F. & TEJA, A. S. 1999. Solubility and diffusion of carbon dioxide in polymers. *Fluid Phase Equilibria*, vol. 158-160, pp. 1029-1034.
WRAP 2007. Raising the bar in PET bottle lightweighting. *Retailer Sector Innovation: Esterform Packaging Final Report* [Online]. [Accessed March 2007]. <www.wrap.org.uk/retail>.